AGRICULTURAL SPRAY DROPLET DISPERSION IN TURBULENT WINDFLOW

by

JEREMY CHARLES PHILLIPS

A thesis submitted to the Faculty of Engineering
of the University of Birmingham
for the degree of
DOCTOR OF PHILOSOPHY

FAST TEAM
School of Chemical Engineering
Faculty of Engineering
The University of Birmingham
September 1997

SUMMARY

Off-target contamination (or spray drift) during agricultural chemical application, arising from removal of small (diameter < 100 μm) droplets from sprays by atmospheric or vehicle-generated cross flows, is investigated experimentally. The primary requirement for realistic wind tunnel studies is identified from background review as matching the full-scale logarithmic mean velocity profile with suitable surface roughness parameters. A general calculation scheme is presented for spacing horizontal flat plates to simulate weakly-sheared mean velocity profiles. Adequate full-scale matching of logarithmic mean velocity profiles is achieved after systematic equipment modification. Comparative field and wind tunnel experiments using single nozzles show adequate agreement following the above approach, indicating that air entrained into the liquid spray stabilizes the spray to the cross flow action. Measurements within an agricultural spray in still air show that small droplets are passively transported within the entrained air field, whose characteristic turbulence length scale is too small to contribute to droplet dispersion. Wind tunnel studies employing conventional sprays show small droplet removal associated with regions where the entrained air velocity is less than the cross flow velocity, with essentially passive downwind transport. Numerical simulations of spray drift must clearly incorporate characteristics of the entrained air velocity field.

Preface and Acknowledgements

The experimental work described in this thesis is believed to be original except where stated to the contrary. No part of this work has been submitted for a degree or diploma at any other university. This dissertation is the result of my own work, and includes nothing which is the outcome of work done in collaboration. The experimental work in this thesis was carried out at the Department of Applied Mathematics and Theoretical Physics, University of Cambridge, and Silsoe Research Institute. Financial support for this work was provided by the Agriculture and Foods Research Council (now the Biotechnology and Biological Sciences Research Council) as part of grant LRG103. During this project I was registered for a higher degree on a part-time basis with the Faculty of Engineering, University of Birmingham.

Project LRG103 was supervised by Professor Julian Hunt (University of Cambridge), to whom I am indebted for many useful discussions on concepts underlying the experimental work presented here. The work in this thesis was supervised by Dr Neale Thomas (University of Birmingham) and Professor Paul Miller (Silsoe Research Institute). I would like to express my thanks to them both for their enthusiasm and patience, and the insight which they provided into this area of research. In particular I thank Neale for thorough and thought-provoking reviews of the draft of this thesis and associated publications. I am grateful to Professor Stephen Sparks and Dr Colm Caulfield (University of Bristol) for useful comments on parts of the draft of this thesis, and Rebecca Niblock for assistance with proof-reading. Technical assistance from David Cheesely and Brian Dean at DAMTP and John Power and David Baker at Silsoe Research Institute is gratefully acknowledged.

I am grateful to many colleagues for useful discussions, encouragement and support, in particular Mark Davidson, Mark Hallworth, Knud Lunde and Richard Perkins at Cambridge, and Giray Ablay, Jenni Barclay, Eliza Calder, Charlotte Gladstone, David Gower, Steve Lane, Anita Lewis, Teal Riley and Andrew Woods at Bristol.

Over the life of this thesis, many friends have provided necessary balance and perspective. Of these, Ruth Martin, Stuart Schmege, Keith Furniss, Tom Tofield, Des Haynes, the residents of [redacted], and members of the Makhno organisation deserve special recognition. I am grateful to the Phillips family for their diverse talents. Finally, Julia and Sarah are especially thanked for being both good listeners and real friends.

Nomenclature

(i) General

Wherever possible in this thesis, the nomenclature used has been that conventionally employed in the atmospheric sciences and fluid dynamics background literature. Quantities which conventionally use the same nomenclature have been retained only where their meaning is clear. Throughout the text, overbars are used to denote time averages, and primes are used to denote fluctuating quantities.

The following terms have general meaning:

x, y, z Streamwise, spanwise and vertical axes respectively,

u, v, w Streamwise, spanwise and vertical component velocities respectively,

f function,

F universal function,

t time,

T temperature.

The following subscripts have general meaning:

c - plant canopy value,

e - entrainment,

f - fluid,

g - geostrophic,

h - heat,

o - surface or initial value,

p - particle or droplet,

s - liquid sheet,

u - streamwise component,

v - spanwise component,

w - vertical component.

(ii) Roman letters

b - jet half-width (the spanwise position at which the jet velocity is half the centreline value),

C_d - drag coefficient,

C_f - friction coefficient (flow over flat plates),

d - zero-plane displacement,

d - diameter (general),

e - turbulence kinetic energy,

f - dimensionless frequency (scaled on height and mean velocity),

f_r - Coriolis parameter ($=2\Omega sin\iota$),

g - acceleration due to gravity,

G - geostrophic wind vector,

h_t - wind tunnel height,

i_u - streamwise turbulence intensity,

k_r - gauze resistance coefficient,

k_1 - constant relating spray entrainment to spreading,

K_h - thermal eddy viscosity,

K_m - momentum eddy viscosity,

l - length scale (general),

L - Monin-Obukhov length (atmospheric stability parameter),

n - frequency,

p - pressure,

Q_e - surface dissipation,

r - radius,

Re - Reynolds number,

R_f - Flux Richardson number,

R_i - Gradient Richardson number ($=\frac{K_m}{K_h}R_f$),

s - plate spacing,

S_u - streamwise velocity spectrum,

u_{cf} - cross flow velocity,

u_e - entrainment velocity,

u_j - jet or spray centreline velocity,

u_{st} - terminal (Stokes velocity),

u_* - friction velocity (surface-defined velocity scale),

U_t - velocity at wind tunnel roof,

z_c - plant canopy height,

z_o - roughness length (surface roughness-defined length scale),

z^* - aerodynamic stopping distance.

(iii) Greek letters

α - entrainment constant,

β - velocity ratio $\frac{u_j}{u_{cf}}$,

γ - density ratio $\frac{\rho_p}{\rho_f}$,

Γ - adiabatic lapse rate,

δ - empirical constant relating to spray spreading,

δ_o - jet width at nozzle,

ϵ - energy dissipation (i.e. $\frac{{u_*}^3}{\kappa z}$ for surface friction),

θ - potential temperature,

ι - latitude,

κ - von Karman constant ($\simeq 0.4$),

λ - wavelength,

μ - dynamic viscosity,

ν - kinematic viscosity,

ρ - density,

σ_u - r.m.s streamwise component velocity fluctuation,

τ - shear stress,

τ_a - aerodynamic response time,

τ_e - eddy turnover time,

Ω - Earth's rate of rotation ($=7.29 \times 10^{-5}$ s^{-1}),

Ω - twice the angular velocity of a Rankine- type vortex.

CONTENTS

CHAPTER 1. LITERATURE REVIEW

Summary

Established experimental and theoretical work on spray drift and jets in cross flows is surveyed with special reference to modelling guidelines in wind tunnel evaluation studies. Field investigations and laboratory simulations of agricultural spraying indicate that spray drift increases systematically with cross wind mean velocity typically either linearly or exponentially. Related relevant work on the deflection of single-phase jets in cross flows, in particular its dependence on cross flow velocity, is reviewed here. To a first approximation, deflection is dominantly controlled by mean momentum entrainment with wind turbulence (intensity and scale) essentially insignificant for present considerations. Established methods are reviewed for modelling representations of the mean and turbulent fields within the atmospheric boundary layer paying special attention to the logarithmic mean velocity profile appropriate for neutral atmospheres.

1. Introduction

Agricultural chemicals such as pesticides, herbicides or fungicides [Miller, 1988; Miller, 1993] are mostly applied as liquid sprays, encouraging uptake by the plant, with a view to maximizing their biological efficacy [Elliott and Wilson, 1983]. Figure 1 shows a typical agricultural boom sprayer in operation. Not all of the spray is deposited on target, that is immediately under the boom. A small fraction travels downwind as drift in the wake of the spraying vehicle and may pose [Gilbert and Bell, 1988] serious environmental engineering issues notably contamination of surrounding land and waters. For the farmer, drift represents an indirect financial penalty in terms of restriction of conditions under which chemical application may occur (see below), and only a small direct financial penalty due to the high cost of agrochemicals, with less than 2% of the applied formulation lost as airborne drift [Miller, 1993].

One generally-accepted strategy [Miller, 1988] for minimizing the environmental impact of polluting chemicals is to use the *minimum dosage* (volumetric delivery onto the crop). The use of the lowest spray volume (lowest volume of spray solution) aims to increase work rates and reduce operation costs and run-off onto soil surfaces. Spray solutions (with typical active chemical concentration up to 5%) are usually prepared in the field with the transportation of

water providing a significant contribution to the process cost [Nation, 1978]. Also, it is broadly agreed that biological efficacy increases with decreasing droplet size [Hislop, 1987]. For practical purposes, operations are usually conducted in the range 100-200 μm as a compromise between efficacy of small droplets and drift resistance of large droplets. Spray must be applied at the optimum plant growth stage so as to combat pests or disease (*optimum timeliness*), providing an operational window of typically 2-3 days [Miller, 1993]. This period can be further reduced by inappropriate atmospheric conditions (notably wind enhancing off-target drift and rain wetting the crop thus diluting the active chemical concentration) significantly limiting possiblities for the farmer who may have to spray several plant varieties within consecutive or simultaneous operational windows. Guidelines contained in the Food and Environment Protection Act 1985 [Anon, 1990] advise that application should be restricted to conditions of 'steady Force 2 (2-4 mph at the boom height) light breeze blowing away from any susceptible crops, open waters or neighbour's land' for non-convective atmospheres. Unacceptably high levels of *spray drift* (the proportion of liquid volume flux as droplets removed by a relative cross flow and airborne at a given downwind station) can occur during convective atmospheric conditions [Elliot and Wilson, 1983], so spraying operations are only recommended on days when the atmospheric boundary layer is neutrally stratified (see section 3 below). Guideline conditions do not conventionally include stable stratification because of the possiblity of accumulation of vapour produced by some (now not widely used) chemical formulations in topographic lows under these conditions [P.C.H.Miller, personal communication]. The use of smaller spray droplets and higher vehicle forward speeds in potentially windier conditions all encourage drift, so it is clearly important to understand the key mechanism of formation in order to devise practical solutions and to assess the environmental impact of drift.

Over 90% of United Kingdom arable spraying is carried out using equipment comprising a boom supporting an array of overlapping *flat-fan* nozzles [P.C.H.Miller, personal communication]. Boom lengths ranging to 24 m (although perhaps more typically 18 m) are employed with the spray applied from boom height 0.5 m above the canopy with the vehicle travelling up to 5 m s^{-1} [Miller, 1993]. As illustrated in figure 2, flat-fan nozzles deliver spray sheets with included angles of 80^o, 90^o or 110^o with elliptical cross-section and slightly out-of-plane orientation with up to 0.25 m overlap to compensate for non-uniform coverage along the spray edges. Typical liquid sheet velocities are up to 25 m s^{-1} with liquid flowrates at the nozzle up to 3.0 L/min [Miller, 1993]. As shown in figure 3, flat-fan nozzles deliver essentially planar liquid sheets whose breakup is determined by aerodynamic instability caused by shear against the surrounding air

and surface tension. Waves grow on the sheet until a critical amplitude (determined by liquid surface tension) is reached. Using an inviscid potential flow model, Clark and Dombrowski [1972] show the sheet ruptures at positions approximately corresponding to wave crests and troughs ($\frac{3}{8}\lambda$ and $\frac{7}{8}\lambda$, where λ is one wavelength) and fragments whose length scale is one half wavelength are produced. Under the action of surface tension, these fragments contract into cylindrical ligaments which are unstable, and subsequently break down into droplets. Further details of this mechanism are given by Chandrasekhar [1961, p.515] and Yarin [1993, p.252] and an analysis of liquid sheet breakup is also presented by Dombrowski and Johns [1963]. The disintegration of fluid ligaments has been studied by Hinze [1955] and Lane [1951] who consider the effect of aerodynamic drag forces and show that breakup is controlled by liquid surface tension and viscosity. Aerodynamic drag against the liquid sheet and droplets induces air entrainment into the spray, shown here in figure 4 for a typical agricultural flat-fan spray visualised using smoke released essentially passively adjacent to the spray nozzle, showing clearly the two-phase structure of droplets and co-flowing air.

Droplet size distributions are used to classify spray *quality* relative to a reference flat-fan nozzle [Doble et al., 1985] incorporating specification of geometry and operational parameters e.g. F110/1.6/3.0, which refers to (F)lat-fan spray nozzle, of spray angle $(110)^o$, producing a flowrate of (1.6) L/min at an operating pressure of (3.0) bar (see figure 5). Fine sprays provide optimum coverage of the crop, coarse sprays allow greater drift resistance, with medium sprays representing a compromise between the two. Nozzles are designed typically to produce droplet sizes from 50-400 μm with up to 8% of the spray volume in the diameter range 20-100 μm [Western et al., 1989]. Droplet volume median diameter (VMD) is one measure commonly used to characterise a polydispersed droplet size distribution [Miller, 1993]. In such a distribution, the VMD is the diameter of a spherical droplet such that 50% of the total liquid volume is in droplets of smaller diameters. The mass median diameter (MMD) is also used, being defined as the diameter of a spherical droplet such that 50% of the total liquid mass is in droplets of smaller diameters. These two measures are identical for agricultural spray formulations which employ non-volatile active ingredients, as the droplet density remains constant.

Previous studies of spray drift are reviewed here, including a summary of the analogous problem of deflection of a single- phase jet by a cross flow. Computational simulations of spray drift (not the subject of investigation here) are examined in greater detail than field and laboratory studies, technical details of which are deferred to subsequent chapters where they are employed. This is followed by a consideration of the cross wind, whose simulated conditions

must include the important characteristics of the atmospheric boundary layer. In this case, turbulence generated by wind shear over the surface dominates convective turbulence, and there is negligible buoyancy-driven flux. In particular, the basic meteorological factors governing the neutrally-stratified atmospheric boundary layer are introduced as background for simulation work reported in chapter 2. The velocity field above a crop canopy is examined, followed by wider discussion of reviewed studies and conclusions.

2. Previous Studies of Spray Drift

2.1. Field Measurements

Field measurements of spray drift are limited, as they are expensive and produce variable quality data, although previous work has established broad protocols for design [Gilbert and Bell, 1988] and sampling [Parkin and Merritt, 1988]. The primary correction to field measurements is due to wind gustiness and localised wind veering causing the airborne spray to not be completely directed at finite-sized collectors whether for dropsize or airborne flux. The role of coherence in the turbulent boundary layer flow above a plant canopy and its coupling with flow within the canopy has received some attention (see the review by Raupach and Thom [1981]), although it has yet to be fully characterised. Associated studies of single-phase jets in cross flow (see below) suggest the effect of upstream turbulence is negligible for sprays in cross flow other than for coherent structures on the scale of the spray noted here. To date, no field studies have attempted to quantify this correction, although the variable quality of field data has been used to justify increasing use of laboratory experiments and computational simulations [e.g. Miller, 1993].

Early field measurements of drifting droplet diameter were made by Byass and Lake [1977]. Using kaolin-coated glass slides and broad leaved plants as collectors, droplet impressions or diameters were measured. The mass median diameter (MMD) ranged from 99 μm at 13 m down to 60 μm at 100 m downwind of the sprayed area.

Figures 6 and 7 show measured variation of airborne spray volume versus windspeed as reported by Gilbert and Bell [1988] and by Rutherford et al. [1989]. Gilbert and Bell's [1988] fits to field data (the data are not shown in their study) emphasize the significantly enhanced drift for droplets with a volume median diameter of 100 μm, compared with droplet distributions with larger VMD (figure 6). Both studies employed dye tracer, now the established method, to label material collected on 2 mm diameter line collectors 8 m downwind of the spray boom.

Airborne spray volume flux is estimated based on fractional area of collector intercepted and rate of mass accumulation on this area compared with the rate of supply from nozzle. Further details of this method are supplied in chapter 3 but it is noted here that these dyes show no surfactant effect and that for the range of droplet diameters and velocities typical for agricultural spraying there is a non-negligible correction for collector efficiency [Gilbert and Bell, 1988]. Estimates of collector efficiency are presented for field experiments carried out as part of this study in chapter 3. Regression analysis on these datasets shows an exponential increase of airborne spray volume with windspeed with exponents ranging from about 0.1 to 0.3. Other workers [Miller, 1993; Hobson et al., 1993] have reported adequate linear regression fits over the lower half of the windspeed range of the field data presented here (figures 6 and 7).

2.2. Laboratory Measurements

Wind tunnel experiments provide a controllable environment in which to establish a reproducible baseline for comparative measurements. The earliest wind tunnel studies utilised uniform approach flow without reference to either shear or turbulence in the case of Western et al. [1989] and Western and Hislop [1991] and both studies recorded a linear dependence of airborne spray volume with cross flow velocity. Miller et al. [1989] reported the earliest study simulating mean shear, more fully reflecting the mean velocity profile immediately above a plant canopy. In contrast to the field measurements reviewed above, they employed a laser interferometric technique at a station 1 m downwind to measure drifting droplet diameters and thus infer the spanwise airborne spray flux distribution produced by a single flat-fan spray nozzle oriented across the flow. The use of a single nozzle was not intended to be representative of typical agricultural equipment configurations, but enabled the origin of drifting droplet fluxes to be identified in this fundamental study. The airborne spray volume flux is plotted for the plane 100 mm (vertical) $\times$ 400 mm (spanwise i.e. normal to the cross flow direction), 200 mm below the nozzle in figure 8. The spanwise dimension of this plane corresponds to one half-width of the spray i.e. the region over which the flow field is symmetric. The figure shows the spatial position of highest airborne droplet flux corresponds to the spray edges. Non-uniform spanwise distribution of droplet volume median diameter [Miller et al., 1989] contributes to non-uniform downwind airborne flux distribution, and this is characterised in chapter 4 for small (diameter < 100 μm) droplets which make up most of the drifting volume (see figure 6). However, the primary mechanism for production of downwind flux distribution profiles of this form is scavenging of fine droplets by edge vorticity produced from the interaction of the spray and cross flow velocity fields. Although not

yet investigated for sprays, the expectation by analogy with study of single-phase jets in cross flow [e.g. Andreopoulos and Rodi, 1984] is that spray entrained air streamlines are deflected by the cross flow bending over the spray, and cross flow streamlines are deflected around the spray (visualised in detail in chapter 5). This leads to re-orientation and generation of streamwise vorticity contained in a pair of counter-rotating vortices at the spray edges (described in detail for jets in cross flow below), illustrated schematically in figure 9.

Miller [1993] invoked vortex trapping (observed in unpublished wind tunnel experiments [P.C.H. Miller, personal communication]) and deposition of drifting droplets to explain downwind measurements of spray distribution patterns for a spray in an undefined non-laminar profile [Young, 1991]. Spray was collected at the floor (using 50 mm diameter beakers as collectors, which were recessed into a false floor) to determine deposit spatial volume distributions (*pattern nation experiments*) with the spanwise deposit profile showing a twin peak and central trough from about 0.15 m downwind of the nozzle.

To date, no studies have made a direct comparison of airborne spray volume flux or more sophisticated measures of downwind dispersion using identical equipment and sampling arrangements in field and laboratory studies. This is addressed in chapter 3, where airborne spray volume flux produced by a single static nozzle is measured under field and wind tunnel conditions to provide a comparative measure.

2.3. Numerical Simulation

The main advantages of using computational simulations to investigate spray drift as compared with field or laboratory experiments are those of lower cost and greater flexibility in prescribing initial conditions. Random-walk calculations have been used to model turbulent dispersion of droplets in cross flows [Thompson and Ley, 1983; Legg, 1983; Miller and Hadfield, 1989], with flow fields described as a Markov process in which the velocity comprises a mean value and a fluctuation component which is correlated only over consecutive time steps. The droplet is pairwise correlated over consecutive time steps in a boundary layer flow field comprising the semi-logarithmic mean velocity profile (with displacement height estimated as a fraction of the plant canopy height, as suggested by Jackson [1981]; see section 4 below). The time step defining the correlation time is selected to be shorter that the Lagrangian integral timescale of the fluctuation field whose variation with height above the surface is parameterised using standard methods. Longitudinal and vertical turbulence intensities are parameterised using standard empirical

correlations based on height and diabatic flux-profile relationships for prescribed atmospheric stability conditions (see section 3 below and appendix 1) and incorporated into the mean field in conjunction with a random component (Gaussian distribution with mean zero and standard deviation of unity). This approach appears to be satisfactory for droplets smaller than 450 μm diameter [Thompson and Ley, 1983] presumably as a consequence of the low fall velocity of these droplets being smaller than the root mean square velocity. In this regime, the *trajectory crossing* effect is negligible [Wells and Stock, 1983]. This results from a heavy particle or droplet's tendency to change its fluid surroundings due to its finite fall velocity, leading to it sampling turbulent eddies at a faster rate than the average eddy decay rate, consequently losing velocity correlation faster than a light droplet.

Simulations were run by Thompson and Ley [1983] for monodispersed droplets with diameter 50, 100, 150 and 200 μm, from a 'release height', the point where a representative droplet velocity within the spray (usually that of the VMD-sized droplet) slows to its terminal fall value. The effect of air entrainment into the spray creating a co-flowing air jet is identified as reducing the drag force on the droplets, thus increasing their *stopping distance* (the distance from the nozzle below which the difference between the droplet excess velocity and its terminal fall velocity is comparable with local vertical velocity fluctuations) compared with a single droplet. The model was used to assess the dependence on release height, windspeed and atmospheric stability. The simulation was run for 10000 monodispersed droplets, showing negligible dependence on lower boundary conditions. Results are presented here in figure 10 for simulations utilising 100 μm droplets, the threshold diameter below which airborne spray flux increases significantly (see figure 6). The results are in the form of variation of surface deposit density (expressed as droplet number per m^2) with downwind distance. Surface deposit density could be converted to a deposition flux to allow comparison with field studies, although unfortunately the simulation results presented by Thompson and Ley [1983] do not correspond to boom heights or downwind collector configurations and positions used in field studies. Increasing release height always increases airborne spray volume (see model runs for 5 m s^{-1} windspeed on figure 10). The effect of windspeed on surface deposit density is also shown in figure 10; surface deposit densities decrease in a similar manner downwind of the spray for windspeeds of 2 m s^{-1} and 5 m s^{-1} (solid lines on figure 10), typical for agricultural applications, but absolute values are an order of magnitude higher for windspeed 5 m s^{-1}. With only two windspeeds representative of agricultural spraying, the dependence of surface deposit density on windspeed cannot be determined for comparison with field studies; the model simply shows greater deposit density

corresponds to higher windspeed.

Miller and Hadfield [1989] used Thompson and Ley's [1983] model to describe far-field dispersion, and a trajectory model to describe initial droplet transport, based on an empirical model for centreline entrained air velocity within a flat-fan spray [Briffa and Dombrowski, 1966]. They simulated droplet transport due to a cross wind only in a vertical plane parallel to the boom (see figure 11) and neglected the effect of vehicle motion. Droplets were confined to the spray centreline, sampling only the vertical entrained air velocity, until their initial velocity had decreased to their fall velocities, at which point they sampled only the boundary layer flow field defined for Thompson and Ley's [1983] simulation above. The velocity of entrained air on the spray centreline (u_j) was described using the relationship

$$\frac{\delta^2}{2k_1}\ln\left(\frac{z}{l_s}\right) = \ln\left(\frac{u_s}{u_j}\right) \tag{1}$$

where

δ is an empirical constant with a value of 0.4 for water sprays in air,

z is distance below the nozzle,

l_s, u_s are length and velocity of the coherent liquid sheet,

k_1 is a constant expressing entrainment in terms of the spread of the spray perpendicular to the fan major axis.

This relationship was determined from experimental measurements of entrainment into a flat-fan spray by Briffa and Dombrowski [1966]. The exponential relationship is consistent with momentum integral constraints where the spreading of the spray depends only on centreline velocity and liquid momentum flux. k_1 was determined from photographic measurement of the spray minor axis for flat-fan sprays of various included angles, although with significant uncertainty resulting from difficulty in determining the exact position of the spray fan boundary. The mean experimental value of 0.14 was used in simulations [Miller and Hadfield, 1989], although this had to be reduced to 0.08 to produce reasonable agreement with laser interferometry measurements of droplet velocity within a typical agricultural flat-fan spray.

The switch from the vertical trajectory model to quasi-horizontal boundary layer flow took place at $4t_{st}$, where t_{st} is the droplet (Stokes) response time

$$t_{st} = \frac{\rho d^2}{18\mu} \tag{2}$$

where

ρ is the fluid density,

μ is the fluid dynamic viscosity,

d is the droplet diameter [Clift et al., 1978, p.264].

This was determined from experiments as the approximate time after which droplets are moving at their terminal fall velocity. Simulations were conducted for collectors positioned up to 6 m from the boom for response times up to $10t_{st}$, returning constant airborne spray volumes with values greater than $4t_{st}$, defining the extent of the spray near-field [Miller and Hadfield, 1989]. The model is compared with field measurements made using vertical line collectors oriented to measure airborne spray volume perpendicular to the direction of vehicle motion, shown here as figure 12. Reduction in entrained air velocity by adjustment of k_1 does improve the fit to field data, although dependence on cross flow velocity was not investigated.

The greatest uncertainties in application of these simulations arise from their simplified formulation. Far-field random walk simulations such as that presented by Thompson and Ley [1983] do not include any treatment of wind gusting and veering, which are the primary corrections to field measurements, although the trajectory crossing effect for larger droplets has now been fully incorporated into these models [Walklate, 1987]. The formulation of near-field transport provided by Miller and Hadfield [1989] has been retained in more sophisticated models [Hobson et al., 1993] despite uncertainty in values of empirical constants and lack of description of spray *structure*, the simplest formulation of which would incorporate the spatial variation of droplet size and entrained air velocity within the spray fan.

2.4. Jets in Cross Flows

Although experimental and numerical study of sprays in cross flow is limited, significant literature exists for single-phase jets in cross flow [e.g. reviews by Rajaratnam, 1976; List, 1982]. Both two-phase sprays and single-phase jets acquire momentum by entrainment of surrounding fluid, and measurements of centreline entrained air velocity within a flat-fan spray [Ghosh et al., 1991] suggest that the spray behaves as a single-phase air jet passively transporting droplets at distances from the nozzle greater than a short initial region (about 0.1 m for typical agricultural sprays). Based on these momentum considerations, broad similarities are expected for the effect of a cross flow velocity field on a spray or jet, and for their velocity field on the cross flow.

However, the primary limitation of this analogy between jets and sprays is that circular and plane air jets in cross flow are singular cases such that dependent on the ratio of jet velocity to cross flow velocity, the cross flow either flows around or completely penetrates the jet [Andreopoulos and Rodi, 1984]. For spray droplets even passively tranported by entrained airflow, the expectation is of some localised penetration of the spray sheet in regions of low entrained air velocity, even with low cross flow velocity.

Axisymmetric jets have been the subject of most attention within the literature, while flat-fan sprays of interest here show similarities to plane single-phase jets. However, irrespective of geometrical differences, the jet flow development region is characterised by a potential core bounded by a mixing layer, from which the jet spreads by entrainment of ambient fluid. Integral-momentum considerations show that the spreading of the jet scales on the square of centreline velocity (u_j) and jet half-width b (the spanwise position at which the local streamwise velocity is half the centreline value) for a plane jet and u_j^2 and b^2 for an axisymmetric jet, consistent with respectively 2-d and 3-d propagation of these jets [Rajaratnam, 1976, p.9 and p.33]. For both jets, the half-width b scales on streamwise distance from the nozzle and u_j decreases linearly with distance from the nozzle for an axisymmetric jet and as the square root of distance from the nozzle for a plane jet. Thus, the entrainment constant (α), defined by

$$u_e = \alpha u_j \tag{3}$$

where

u_e is the entrainment velocity,

u_j is the centreline velocity,

at a given streamwise position [Morton et al., 1956], has values of about 0.05 for a plane jet and 0.03 for an axisymmetric jet in still air [Rajaratnam, 1976, p.23 and p.48]. Within this simple physical framework, plane and axisymmetric jets show similar behaviour in terms of their propagation in still air. The conclusions of more sophisticated descriptions of axisymmetric jets in cross flow (see below) are also applicable to plane air jets with corrections due to geometry essentially insignificant for the physical mechanisms.

Observations of a circular jet in a cross flow (summarised by Coelho and Hunt [1989]) show that jet cross-sectional area increases due to entrainment of ambient fluid (as for still air conditions), and interaction with cross flow results in a shape change from circular through kidney-shaped to horseshoe-shaped (figure 13). Experimental observations summarised by Ra-

jaratnam [1976, p.184] suggest this process occurs for ratios (β) of jet centreline velocity (u_j) to mean cross flow velocity (u_{cf}) of less than about 4, from 1 nozzle diameter from the origin (figure 13). As the jet issues further into the cross flow, the tips of the horseshoe evolve into a vortex pair, and the jet bends over towards the cross flow direction, shown in figure 14 for β=2. An important feature of this flow field is the streamwise and vertical deflection of streamlines, and their reorientation and generation of edge vorticity, summarised here from the study of Andreopoulos and Rodi [1984], with reference to figure 14. The approach flow boundary layer contains negative spanwise vorticity, which is increased by spanwise shear as the boundary layer is deflected around the jet and re-oriented as vortex lines which are stretched around the jet to form a horseshoe vortex (similar to that observed for cross flow deflection around an obstacle). The jet flow issuing from the nozzle exhibits concentric vortex rings with the maximum vorticity at the tube walls, which is re-oriented into a region of bound vorticity on the lee side of the jet [Moussa et al., 1977] (see figure 14). This is strengthened by generation of vorticity at the interface of the initially orthogonal jet and cross flow for ratios β >0.6 [Andreopoulos and Rodi, 1984]. The secondary motion contained in the horseshoe vortex pair decays downstream under the action of turbulent stresses, providing a possible mechanism of droplet capture from a spray in regions of high vorticity and subsequent downstream detrainment.

Dimensional analysis applied to a plane jet issuing normally into a cross flow [Rajaratnam, 1976, p.207] suggests functional relationships for the deflected jet trajectory of the form

$$C_d \left(\frac{z}{\delta_o}\right) \frac{1}{\beta^2} = 2\sqrt{C_d \left(\frac{x}{\delta_o}\right) \frac{1}{\beta^2}} \tag{4}$$

where

x and z are streamwise and vertical coordinates of the jet centreline respectively,

C_d is the drag coefficient between cross flow and jet,

δ_o is the jet width at the nozzle (figure 15).

Reasonable agreement with experiments was obtained for values of C_d about 2, not excessively high for this simple formulation. Similar analysis can be applied to axisymmetric jets [Rajaratnam, 1976, p.200], although in this case, C_d must be assigned unreasonably large values (about 4) to match experimental data. Computational models have been developed [Rajaratnam, 1976, p.192], which assume this pressure drag mechanism, where the jet responds to the dynamic pressure ($C_d \rho {u_{cf}}^2$) exerted by the cross flow. Integral approaches have also been applied, modelling

the flow as a pair of contrarotating vortex filaments or tubes in a cross flow, consistent with the physical description presented above [e.g. Broadwell and Breidenthal, 1984]. Neither model matches internal (jet) and external flows, and selection of suitable entrainment parameters and coefficients and drag coefficients provide satisfactory agreement for prediction of the deflected jet trajectory, irrespective of assumptions about the mechanism of jet deflection.

In order to address these discrepancies, Coelho and Hunt [1989] conducted a comprehensive investigation of the response of a circular jet in cross flow as wind tunnel measurements of cross-section at various stations from the orifice and evaluated the extent to which 3-dimensional vortex sheet and entraining vortex sheet models could reproduce the observed behaviour. 3-dimensional solutions were obtained for a thin vortex sheet separating the irrotational internal (potential core of the jet) and external flows with turbulent entrainment simulated by allowing the vortex sheet to thicken as a mixing layer whose thickness is proportional to the entrainment rate. Coelho and Hunt [1989] conclude that the primary mechanism for deflection is addition of horizontal momentum due to entrainment, because only the entraining model produced deflection of the jet by the cross flow. The entrainment velocity was assumed proportional to the local strength of the vortex sheet, in agreement with earlier analysis for turbulent shear layers [Rajaratnam, 1976, p.184]. Pressure drag must occur because of the formation of a wake behind the jet [Coelho and Hunt, 1989], but its effect is small compared to entrainment. Asymptotic solutions in β for entraining vortex sheets are dependent on upstream turbulence levels to determine initial distortion of the jet [Coelho and Hunt, 1989], but entrainment is controlled by the local turbulence intensity in the mixing layer on the jet upstream surface. In most practical applications the jet velocity is much higher than the cross flow velocity, so the magnitude of cross flow turbulence intensity will be insignificant compared to that of the jet. The turbulence intensity level within the cross flow can thus be considered insignificant compared to the action of the mean flow in deflecting the jet.

3. Basic Meteorology of the Neutral Atmospheric Boundary Layer (ABL)

Spray drift occurs as a consequence of the action of the spraying vehicle wake or atmospheric wind, or in the absence of wind, the action of convective heat exchange at the surface. As noted earlier, agricultural chemical application is only recommended under conditions of windspeed from 1-3 m s^{-1} and neutral atmospheric stability (see below), typical of cloudy days with low winds. The static stability of the atmosphere is introduced as an indicator of whether convective

dispersion processes will be important in the spray far- field [Elliott and Wilson, 1983] i.e. outside the vehicle wake. Details of the convective contribution to turbulence kinetic energy are contained in appendix 1, which also demonstrates equations of mean motion for the neutral atmospheric boundary layer (ABL).

Agricultural spray booms are usually mounted no more than 1 m above the crop canopy, within the lowest region of the atmospheric boundary layer. Upper level (geostrophic) winds are required by bottom friction to have zero relative velocity at the surface [Plate, 1971]. Major gradients of air movement are confined near the surface, within a region of highly turbulent strong shear flow, known as a *boundary layer.* It is noted here that nearly all established fluid mechanics development and understanding of boundary layers relates to solid walls. This condition is not always well approximated for spraying operations, as some vegetative canopies (e.g. mature cereal crops) are mobile, so that there is an additional dissipative layer as the effective lower boundary condition on the airflow. However, the modification of turbulent stresses by plant motion has not been fully characterised [Raupach and Thom, 1981], so for present purposes the plant canopy is assumed to constitute a rigid, fully rough boundary to the airflow.

The ABL is usually considered as consisting of a *surface layer* characterised by well developed mixing due to mechanical turbulence generated by surface shear, extending typically to a height of 50-200 m. Mechanical turbulence dominates any convective effects in this layer defining the atmospheric stability as neutral (see below). The lowermost region of the surface layer is called the *roughness or canopy sublayer*, which is the region of flow affected by individual surface roughness elements (figure 16). Mean flow in this sublayer is very inhomogeneous and 3-dimensional in character, because it depends on the geometry and arrangement of roughness elements. Above the surface layer, in the *outer layer* (or mixed layer), convective turbulence dominates purely mechanical turbulence, a reversal of the situation within the turbulent surface layer. These regions are illustrated schematically in figure 16.

Transport of heat within the ABL determines outer layer depth and turbulence structure, which can contribute to far-field droplet dispersion at distances of a few tens of metres from the spraying vehicle, which are accessible by small droplets (see sections 2.2 and 2.3 above). Adiabatic lapse rate (Γ) is defined as the rate of cooling with height of an elemental volume of air [Oke, 1978, p.302]. Within the ABL, the hydrostatic equation is a good approximation to the vertical pressure distribution, even under strongly turbulent conditions [Nieuwstadt and

Van Dop, 1982, p.5]

$$\frac{\partial \overline{p}}{\partial z} = -\rho g \tag{5}$$

where

$\overline{p}$ is the mean pressure,

ρ is the density of air,

g is the acceleration due to gravity.

Under adiabatic conditions, an elemental volume of air cools at a constant rate. As the air volume rises, its internal pressure exceeds the local atmospheric pressure, and it expands. The only energy available for expansion (as the process is adiabatic) is thermal energy, so the air volume cools on ascent. The vertical mean pressure gradient is constant for the ABL (equation 5), so the cooling rate is constant; $\Gamma = 9.8 \times 10^{-3}$ ^{o}C m^{-1} for a dry (unsaturated) atmosphere. The environmental lapse rate (ELR) is a measure of the actual temperature gradient at a given location [Oke, 1978, p.303],

$$ELR = \frac{\Delta T}{\Delta z}. \tag{6}$$

The static stability of the atmosphere is a measure of its capability for buoyant convection. An unstable zone is characterised by ELR $>$ Γ. Displaced upwards, an air volume would initially be warmer than its surroundings and rise by buoyancy. This motion is unstable, as its temperature would always be higher than the local surroundings. A stable zone is characterised by ELR $<$ Γ. Displaced upwards, an air volume would be cooler than the surrounding air, and would sink. Displaced downwards, it would be warmer than its surroundings, and rise. Thus an equilibrium position is reached. The neutral condition is characterised by ELR $=$ Γ. After any vertical displacement, the temperature of the air volume and its surroundings are the same, so there is no tendency for the volume to rise or sink.

4. The Velocity Field Above a Crop Canopy

4.1. Mean Velocity Profile

The spray near-field lies within the surface layer (figure 16) extending from the plant canopy top (z_c) to a height where the atmospheric flow is unperturbed by the boom structure (about 1 m above z_c for typical equipment described above). This region includes the transition region

between the canopy sublayer (where the flow is affected by individual roughness elements) and the inertial sublayer (figure 16). The mean velocity profile is described by the *semi-logarithmic mean velocity profile* demonstrated in appendix 1,

$$\frac{\overline{u_z}}{u_*} = \frac{1}{\kappa} ln \left(\frac{z-d}{z_o} \right) \tag{7}$$

where

z_o = Roughness length, a representative length scale for flow over a rough surface,

$\overline{u}_z$ is mean horizontal velocity at height z,

d = zero plane displacement,

u_* = friction velocity (the appropriate surface-defined velocity scale),

κ = Von Karman constant (an empirical constant with a value of approximately 0.4).

For the purposes of this study where the velocity profile above the plant canopy is of primary interest, it is convenient to combine the effects of surface roughness (z_o and d) into a single parameter. Both these length scales simply determine the location of a virtual origin for zero mean velocity above the ground plane (z=0), reflecting drag contributions from the surface and the plant canopy. Surface influences include horizontal inhomogeneity which scales on the inter-element spacing [Mulhearn and Finnegan, 1978] and wake diffusion (enhanced turbulent diffusivity above the canopy due to element wakes) which scales on the tranverse element length scale [Raupach et al., 1980]. For dense plant canopies consisting of narrow roughness elements (typical of arable cereal crops) both contributions to displacement of the zero-plane are small. Blockage of the mean flow within the canopy provides the main contribution to zero-plane displacement which incorporates undetermined canopy features such as roughness element height. Typically, z_o, $\frac{u_*}{\kappa}$ and d are all unknown, and have to be determined by fitting the semi-logarithmic law to a velocity profile measured at only a few heights [Jackson, 1981]. To close this problem, d is given an assumed value (usually zero), although the effect of this may simply be to increase the scatter in z_o and κ [Jackson, 1981]. This approach will be followed in subsequent wind tunnel simulations (chapter 2), with the virtual origin for the mean velocity profile characterised by z_o values taken from previous field measurements [Anon, 1975].

4.2. Turbulence Profiles

Shear-generated turbulence is the only positive contribution to the turbulence kinetic energy budget (see appendix 1) in the surface layer, as there is negligible buoyancy flux [Tennekes and Lumley, 1972, p.100], particularly for neutral atmospheres typical of agricultural spraying. The streamwise turbulence intensity, $i_u = \frac{\sigma_u}{\overline{u}}$ (where σ_u is the standard deviation of the streamwise velocity fluctuations and $\overline{u}$ is the mean streamwise velocity component) referred to a local level of roughness height is always higher in canopies than above them due to strong retardation of the mean flow by blockage due to canopy elements (figure 17). Streamwise turbulence intensity is used as an indicator of 'turbulence intensity', as spanwise and vertical turbulence intensities $i_v = \frac{\sigma_v}{\overline{v}}, i_w = \frac{\sigma_w}{\overline{w}}$ are roughly proportional to streamwise turbulence intensity: $i_w < i_v < i_u$ [Shaw et al., 1974]. Cionco [1972] summarised field data, concluding that i_u increases with roughness element density: $i_u \simeq 0.4$ in arable crops; $i_u \simeq 0.6$ in temperate forests; $0.7 \leq i_u \leq 1.2$ in tropical forests. Field data [Anon, 1975] shows atmospheric turbulence length scales 3 m above typical agricultural land (roughness height $z_o \sim$ 0.01-0.1 m) are about 5 m in the streamwise direction, about 2 m in the spanwise direction and about 1.5 m in the vertical direction. Scaling on the typical boom height of 0.5 m, these eddy sizes are comparable with the spray fan width, although at only about 10 roughness heights from the surface, eddies generated by individual element wakes may provide a more significant contribution to droplet removal from the spray fan. However, the study of jets in cross flow suggests that the action of the mean flow and vorticity generated by its interaction with the spray entrained air velocity field will dominate.

Spectral properties of canopy turbulence differ substantially from those in the surface layer [Seniger et al., 1976]. Busch [1973] has shown that surface layer turbulence over short vegetation is characterised by hump-shaped spectra for velocity components, which are invariant with respect to height when plotted against a dimensionless frequency $f = \frac{nz}{\overline{u}}$, where n is the frequency in Hz (figure 18). On the high frequency side of the peak, spectra obey the Kolmogorov $-\frac{5}{3}$ power law. Above tall vegetation, turbulence spectra scale with a dimensionless frequency $f = \frac{n(z-d)}{\overline{u}}$ [Shaw et al., 1974]. Turbulence production in the canopy environment is due to both average shear and local wake mechanisms, with the addition of resonant coupling at certain frequencies in the case of waving plants. Both wake production and plant waving introduce high frequency peaks into the velocity component spectra [Raupach and Thom, 1981].

5. Discussion

In addition to providing background material for agricultural chemical application equipment and processes as a baseline for the following experimental study, this review has also focussed on the velocity field sampled by the spray in its near-field. This is recapitulated here, with an indication of approximations to the full-scale process.

In the absence of detailed description of the structure of a flat-fan spray and its response to an imposed cross flow, the best available conceptual picture is of a porous planar jet passively transporting droplets. Noting that the largest flaw in this view may be the ability of the spray to be locally penetrated by the cross flow, its interaction with the cross flow is envisaged as some form of flexure resulting in generation of streamwise vorticity. No direct evidence via wind tunnel visualisation of the action of paired vortices has been presented, although unpublished observations have been made [P.C.H. Miller, personal communication], and the mechanism has been invoked [Miller, 1993] to interpret downstream volume distribution patterns produced by single nozzles in wind tunnel studies [Miller et al., 1989; Young, 1991]. In particular, the association of this vorticity with scavenging of small droplets (diameter less than 100 μm) from the spray fan edges provides an explanation as to their predominance in the spray far-field, at distances greater than a few metres from the nozzle [Byass and Lake, 1977]. However, this could also be due to local spray penetration by the cross flow and 'stripping out' of droplets by essentially irrotational cross flow. Both these mechanisms cast doubt on the formulation of numerical simulations of the spray near field [e.g. Miller and Hadfield, 1989], since these assume point release of droplets which sample only the centreline entrained air velocity of the spray as vertical component velocity. Clearly, some characterisation of the spray internal structure is required to understand the initial dispersion mechanism.

There is also no complete description of the cross flow velocity field sampled by the spray. Recognising limitations on acceptable spray volume fluxes transported to the far-field restricting process operations to neutral atmospheres with low wind [Elliot and Wilson, 1983; Anon, 1990] the mean velocity profile is adequately described by the logarithmic mean velocity profile with accomodation of additional scatter in the roughness height due to an incomplete description of the effects of the surface on the mean flow. By analogy with jets in cross flow, it is argued here that atmospheric cross flow turbulence intensity profiles are not a requirement in wind tunnel simulations. The strength of the analogy between jets and sprays depends on entrainment controlling flexure to the cross flow; evidence presented here as figure 4 and by Ghosh et al.

[1991] provides initial support for experimental design neglecting turbulence intensity. Possibly of greater significance is the action of shear and wake (plant element and vehicle) generated vorticity in scavenging droplets from the spray edges. An additional complexity is possible resonant coupling between the cross wind and the plant canopy, which will generate small eddies which scale on the canopy element dimension [Raupach and Thom, 1981]. Atmospheric wind eddies exhibit scales of about 0.5 m, comparable with the boom height. It is also noted that to remove spray droplets by scavenging into the sub-pressure zone associated with an eddy, the eddy length scale controls local pressure conditions, limiting this mechanism to a small range of scales. Subject to lack of characterisation of the turbulence field in the vicinity of the spray, simulation of mean velocity profile only appears sufficient for wind tunnel studies.

Field studies have provided some measurements of airborne spray volume flux and droplet diameter within the spray far- field. Best estimates from field experiments suggest that airborne spray volume flux increases approximately exponentially with windspeed, with exponents about 0.1 to 0.3. Perhaps the key observation is that drift increases dramatically when the droplet size distribution is dominated by droplets with diameters smaller than 100 μm, which are the only droplets transported more than a few metres from the boom [Byass and Lake, 1977]. Wind tunnel experiments employing uniform cross flow [e.g. Western et al., 1989] report a linear increase in drift with windspeed, which may be a plausible approximation to an exponential profile. Wind tunnel experiments have been predominantly conducted as fundamental studies using single nozzles, and a particular problem has been the lack of comparative measurements of spray dispersion using field experiments, wind tunnel experiments and computational simulations.

6. Present Contribution

The first requirement of an experimental investigation of the mechanism of spray drift is to achieve reproducible wind tunnel conditions (presented as chapters 2 and 3), identified here as simulation of mean velocity profile only. In this way parameters can be measured which are currently unobtainable through field experimentation (e.g. simultaneous measurement of droplet size and velocity [Miller, 1993]). Measurement of these spray drift parameters is achieved here using a phase-Doppler anemometry technique, enabling polydispersed droplet sizes to be measured within the spray fan (chapter 4) or downwind drift field (chapter 5). The internal structure of the spray and entrained air velocity field is not yet well understood; investigation of small droplet transport within the spray is carried out in order to identify initial conditions

for droplet dispersion. These will be dependent on the particular spray geometry considered, so experiments are carried out here using conventional flat-fan spray nozzles to ensure widest current applicability of results. Observations of the interaction of a cross flow with agricultural sprays will facilitate the development of mathematical models of spray drift formation. These near-field models can then be combined with existing random-walk (far- field) type models [e.g. Thompson and Ley, 1983] to provide a more complete description of spray droplet transport by the atmospheric wind.

Since completion of the work presented in this thesis in 1993, results from experimental work extending these studies [Smith and Miller, 1994; Miller et al., 1996; Miller et al., 1997] and numerical simulations guided by the present experimental study [Ghosh and Hunt, 1994; Ghosh and Hunt, 1997] have been published. Reference to these studies in the present text is limited to the PDA measurements presented by Miller et al. [1996] using more sophisticated equipment than available during the present study and the modelling approach of Ghosh and Hunt [1994], with discussion of the other contributions deferred until chapter 6.

7. Conclusions

1. Off-target contamination (*spray drift*) resulting from agricultural chemical application poses serious environmental and engineering problems. Use of reduced volume rates of pesticides, higher vehicle forwards speeds and the requirement of optimum timeliness of chemical application are likely to enhance spray drift. Engineering solutions to minimize spray drift require identification of the mechanism of droplet dispersion in the spray near-field.

2. Wind tunnel experiments provide a reproducible environment in which to carry out spray drift measurements. Previous wind tunnel experiments are limited and have failed to make detailed comparison with field studies.

3. An appropriate methodology for spray drift experiments suggested by previous studies is use of a wind tunnel that reproduces the logarithmic mean velocity profile in the vicinity of a plant canopy. Formal comparison of airborne spray volume (spray drift) profiles with field experiments must be made to test this approach, and field experiments must conform with established protocols.

4. Wind tunnel experiments will enable measurement of spray fan and drift parameters which cannot be made in the field (such as droplet sizes and velocities downwind of the boom),

which may be important in controlling drift formation.

5. Modelling of droplet dispersion in the near-field during agricultural spraying is currently limited to empirical studies. Experimental investigation of the flow field within and around an agricultural spray is required to identify the initial droplet dispersion mechanism, which will lead to models of the spray structure.

6. Previous experimental studies of dispersion from single nozzles require extension to typical agricultural spray boom sections, up to the size limit of the wind tunnel facility.

References

Andreopoulis, J. and Rodi, W. [1984] Experimental investigation of jets in a crossflow. *J. Fluid Mech.* **138**, 93-127.

Anon [1975] ESDU Item 75001 Characteristics of atmospheric turbulence near the ground III: variation in space and time for strong winds (neutral atmosphere). *Wind Engineering sub-series I.* Engineering Sciences Data Unit, London.

Anon [1990] Pesticides: code of practise for the safe use of pesticides on farms and holdings. Part III of the Food and Environmental Protection Act, 1985. HMSO, London.

Broadwell, J.E. and Briedenthal, R.E. [1984] Structure and mixing of a transverse jet in incompressible flow. *J. Fluid Mech.* **148**, 405-412.

Briffa, F.E.J. and Dombrowski, N. [1966] Entrainment of air into a liquid spray. *A.I.Ch.E. Jnl.* **43**, 708-717.

Busch, N.E. [1973] The surface boundary layer (part 1). *Bound. Layer Meteor.* **4**, 213-240.

Byass, J.B. and Lake, J.R. [1977] Spray drift from a tractor powered field sprayer. *Pesticide Science* **8**, 117-126.

Chandrasekhar, S. [1961] *Hydrodynamic and Hydromagnetic Stability.* Clarendon Press, Oxford.

Cionco, R.M. [1972] Intensity of turbulence within canopies with simple and complex roughness elements. *Bound. Layer Meteor.* **2**, 453-465.

Clark, C.J. and Dombrowski, N. [1972] Aerodynamic instability and disintegration of inviscid liquid sheets. *Proc. Roy. Soc. Lond. A.* **329**, 467-478.

Clift, R., Grace, J.R. and Weber, M.E. [1978] *Bubbles, Drops and Particles.* Academic Press, London.

Coelho, S.L.V., and Hunt, J.C.R. [1989] The dynamics of the near-field of strong jets in crossflows. *J. Fluid Mech.* **200**, 95-120.

Doble, S.J., Matthews, G.A., Rutherford, I. and Southcombe, E. [1985] A system for classifying hydraulic nozzles and other atomisers into catagories of spray quality. *Proc. British Crop Protection Conference*, 1125.

Dombrowski, N. and Johns, W.R. [1963] The aerodynamic instability and disintegration of liquid sheets. *Chem. Eng. Sci.*, **18** 203-214.

Elliott, J.G. and Wilson, B.J.(eds.) [1983] The influence of weather on the efficiency and safety of pesticide application. The drift of herbicides. *British Crop Protection Council Occasional Publication No.3.*

Ghosh, S., Phillips, J.C. and Perkins R.J. [1991] Modelling the flow in droplet driven sprays.

In Johansson, A.V. and Alfredson, P.H. (eds.) *Advances in Turbulence 3*, 405-414, Springer-Verlag, Berlin.

Ghosh, S. and Hunt, J.C.R. [1994] Induced air velocity within droplet driven sprays. *Proc. Roy. Soc. Lond. A* **444**, 105-127.

Ghosh, S. and Hunt, J.C.R. [1997] Spray jets in a cross flow. Submitted to *J. Fluid Mech.*

Gilbert, A.J. and Bell, G.J. [1988] Evaluation of drift hazards arising from pesticide spray application. *Aspects of Appl. Biol.* **17**, 363-375.

Hinze, J.O. [1955] Fundamentals of the hydrodynamic mechanism of splitting in dispersion processes. *A.I.Ch. E. Jnl.* **1**, 289-295.

Hislop, E.C. [1987] Can we define and achieve optimum pesticide deposits? *Aspects of Appl. Biol.* **14**, 153- 172.

Hobson, P.A., Miller, P.C.H., Walklate, P.J., Tuck, C.R. and Western, N.M. [1993] Spray drift from hydraulic spray nozzles: the use of a computer simulation model to examine factors influencing drift. *J. Agric. Eng. Res.* **54**, 293-305.

Jackson, P.S. [1981] On the displacement height in the logarithmic velocity profile. *J. Fluid Mech.* **111**, 15-25.

Lane, W.R. [1951] Shatter of drops in streams of air. *Ind Eng. Chem.* **43**, 1312-1317.

Legg, B.J. [1983] Movement of plant pathogens in the crop canopy. *Phil. Trans. Roy. Soc. Lond. B* **302**, 559-574.

List, E.J. [1982] Turbulent jets and plumes. *Ann. Rev. Fluid Mech.* **14**, 189-212.

Miller, P.C.H. [1988] Engineering aspects of spray drift control. *Aspects of Applied Biology*, **17**, 377-384.

Miller, P.C.H. [1993] Spray drift and its measurement. In Matthews, G.A. and Hislop, E.C. (eds.) *Application Technology for Crop Protection*, CAB International.

Miller, P.C.H. and Hadfield, D.J. [1989] A simulation of spray drift from hydraulic nozzles. *J Agric. Eng. Res.* **42**, 135- 147.

Miller, P.C.H., Mawer, C.J. and Merritt, C.R. [1989] Wind tunnel studies of the spray drift from two types of agricultural spray nozzle. *Aspects of Appl. Biol.* **21**, 237-238.

Miller, P.C.H., Butler Ellis, M.C. and Tuck C.R. [1996] Entrained air and droplet velocities produced by agricultural flat-fan nozzles. *Atomization and Sprays*, **6**, 693-707.

Miller, P.C.H., Ganzelmeier, H., Smith, R.W. and Herbst, A. [1997] Measurements of the downwind airborne spray characteristics from hydraulic flat-fan nozzles operating in a wind tunnel. Submitted to *Crop Prot.*

Morton, B.R., Taylor, G.I. and Turner, J.S. [1956] Turbulent gravitational convection from maintained and instantaneous sources. *Proc. Roy. Soc. Lond. A.* **234**, 1-23.

Moussa, Z.M., Trischka, J.W. and Eskinazi, S. [1977] The near field in the mixing of a round jet with a cross stream. *J. Fluid Mech.* **80**, 49-80.

Mulhearn, P.J. and Finnigan, J.J. [1978] Turbulent flow over a very rough, random surface. *Bound. Layer Meteor.* **15**, 109-132.

Nation, H.J. [1978] Logistics of spraying with reduced volume of spray and higher vehicle speeds. *Proc. British Crop Protection Conf.-Weeds*, 641-647.

Nieuwstadt, F.T.M., and Van Dop, H. [1982] *Atmospheric Turbulence and Air Pollution Modelling.* D.Reidel, Dordrecht.

Oke, T.R. [1978] *Boundary Layer Climates.* Methuen, London.

Parkin, C.S. and Merritt, C.R. [1988] The measurement and prediction of spray drift. *Aspects of Applied Biology*, **17**, 351-362.

Plate, E.J. [1971] *Aerodynamic characteristics of atmospheric boundary layers.* U.S. Atomic Energy Commission, AEC critical review series.

Plate, E.J.(ed.) [1982] *Engineering Meteorology.* Elsevier, Amsterdam.

Rajaratnam, N. [1976] *Turbulent Jets.* Elsevier, London.

Raupach, M.R., Thom, A.S. and Edwards, I. [1980] A wind tunnel study of turbulent flow close to regularly arrayed rough surfaces. *Boundary-Layer Meteorology* **18**, 373-379.

Raupach, M.R. and Thom, A.S. [1981] Turbulence in and above plant canopies. *Ann. Rev. Fluid Mech.* **13**, 97-129.

Rutherford, I., Bell, G.J., Freer, J.B.S., Herrington, P.J. and Miller, P.C.H. [1989] An evaluation of chemical application systems. *Proc. British Crop Protection Conf.-Weeds*, 601-613.

Seniger, I., Mulhearn, P.J., Bradley, E.F. and Finnigan J.J. [1976] Turbulent flow in a model plant canopy. *Bound. Layer Meteor.* **10**, 423-453.

Shaw, R.H., Silversides, R.H. and Thurtell, G.W. [1974] Some observations of turbulence and turbulent transport within and above plant canopies. *Bound. Layer Meteor.* **5**, 429-449.

Smith, R.W. and Miller, P.C.H. [1994] Drift predictions in the near nozzle region of a flat fan spray. *J. Agric. Eng. Res.* **59**, 111-120.

Tennekes, H. and Lumley, J.L. [1972] *A First Course in Turbulence.* M.I.T. Press, Cambridge, Massachusetts.

Thompson, N. and Ley, A.J. [1983] Estimating spray drift using a random-walk model of evaporating drops. *J. Agric. Engng. Res.* **28**, 419-435.

Walklate, P.J. [1987] A random-walk model for dispersion of heavy particles in turbulent airflow. *Bound. Layer Met.* **39**, 175-190.

Wells, M.R. and Stock, D.E. [1983] The effects of crossing trajectories on the dispersion of particles in turbulent flow. *J. Fluid Mech.* **136**, 31-63.

Western, N.M., Hislop, E.C., Herrington, P.J. and Jones, E.I. [1989] Comparative drift measurements for BCPC reference nozzles and for an Airtec twin fluid nozzle under controlled conditions. *Proc. British Crop Protection Conf.-Weeds*, 641-648.

Western, N.M. and Hislop, E.C. [1991] Drift of charged and uncharged droplets from an experimental air assisted sprayer. *British Crop Protection Monograph no. 46: Air-assisted Spraying in Crop Protection,* 69-77.

Yarin, A.L. [1993] *Free Liquid Jets and Films: Hydrodynamics and Rheology.* Longman Scientific and Technical.

Young, B.W. [1991] A method for assessing the drift potential of hydraulic nozzle spray clouds and the effect of air assistance. *British Crop Protection Monograph no. 46: Air-assisted Spraying in Crop Protection,* 77-86.

Figures

1. A typical agricultural boom sprayer during operation. The 18 m boom of overlapping sprays (geometry as in figure 2 below) is mounted 0.5 m above the plant canopy top. The vehicle is moving at 6 mph into a light breeze (1.5 m s^{-1} at boom height). Note the region of airborne spray behind the vehicle (photograph courtesy of Silsoe Research Institute).

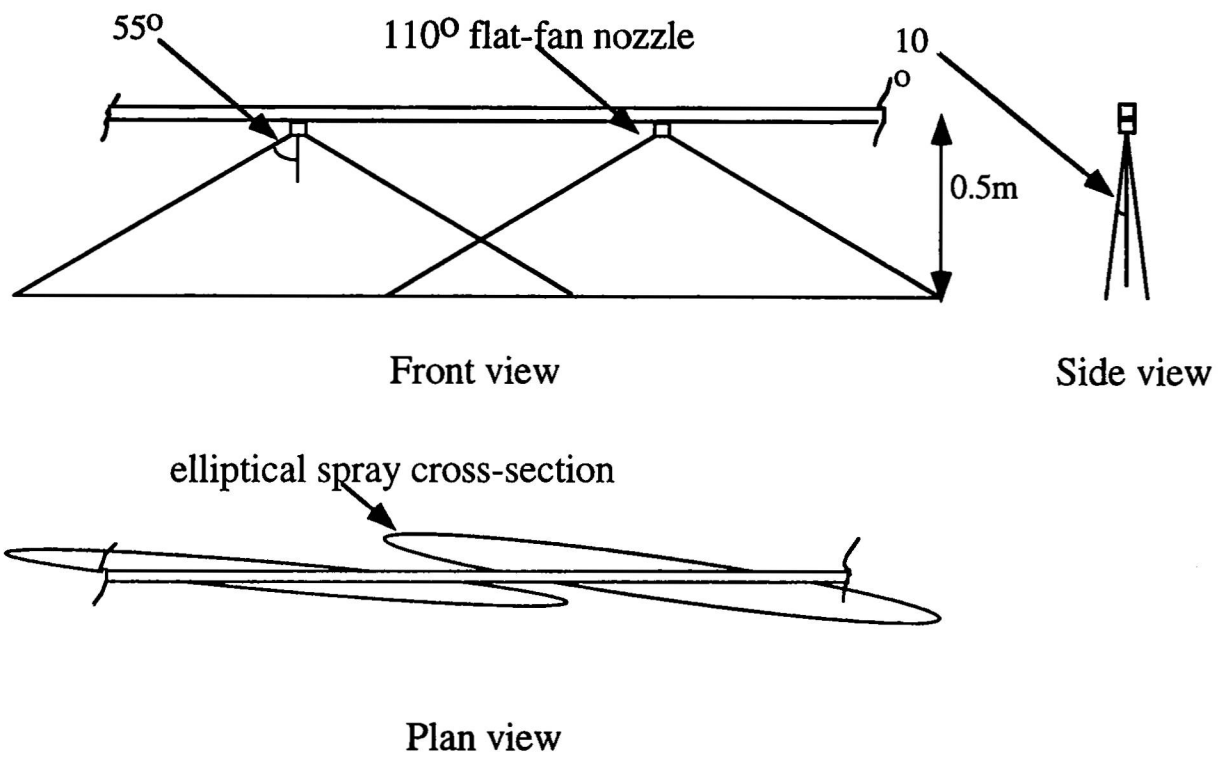

2. Typical geometry and arrangement of 110° agricultural flat-fan sprays on a boom. The front view corresponds to vehicle motion out of the page.

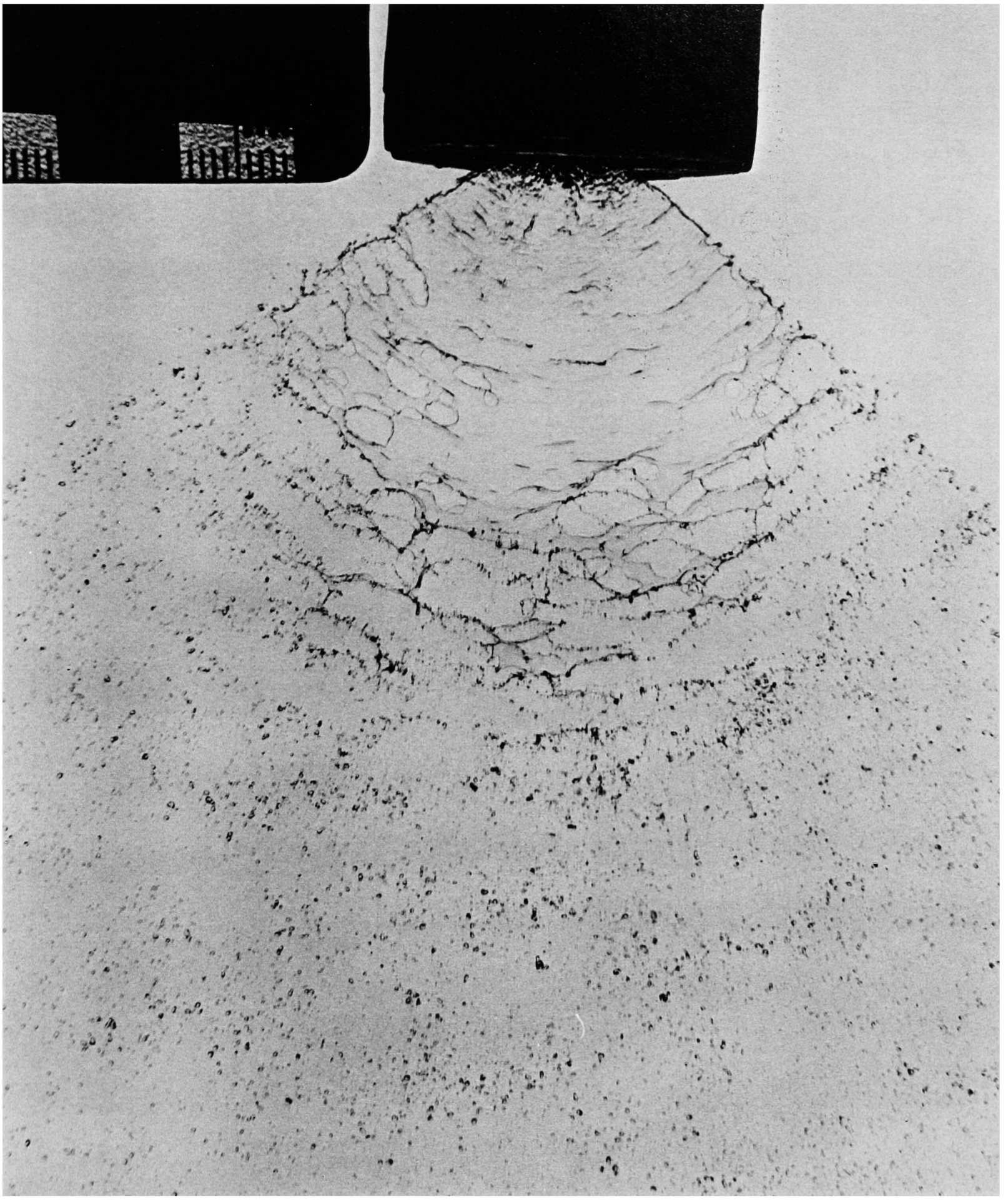

3. The break-up of a liquid sheet issuing from a flat-fan nozzle. This nozzle produces a 110° spray fan at a liquid flowrate of 1.6 L/min and pressure of 3.0 bar. The nozzle width is 36 mm, and the flash duration is 0.1 ms (photograph courtesy of Silsoe Research Institute).

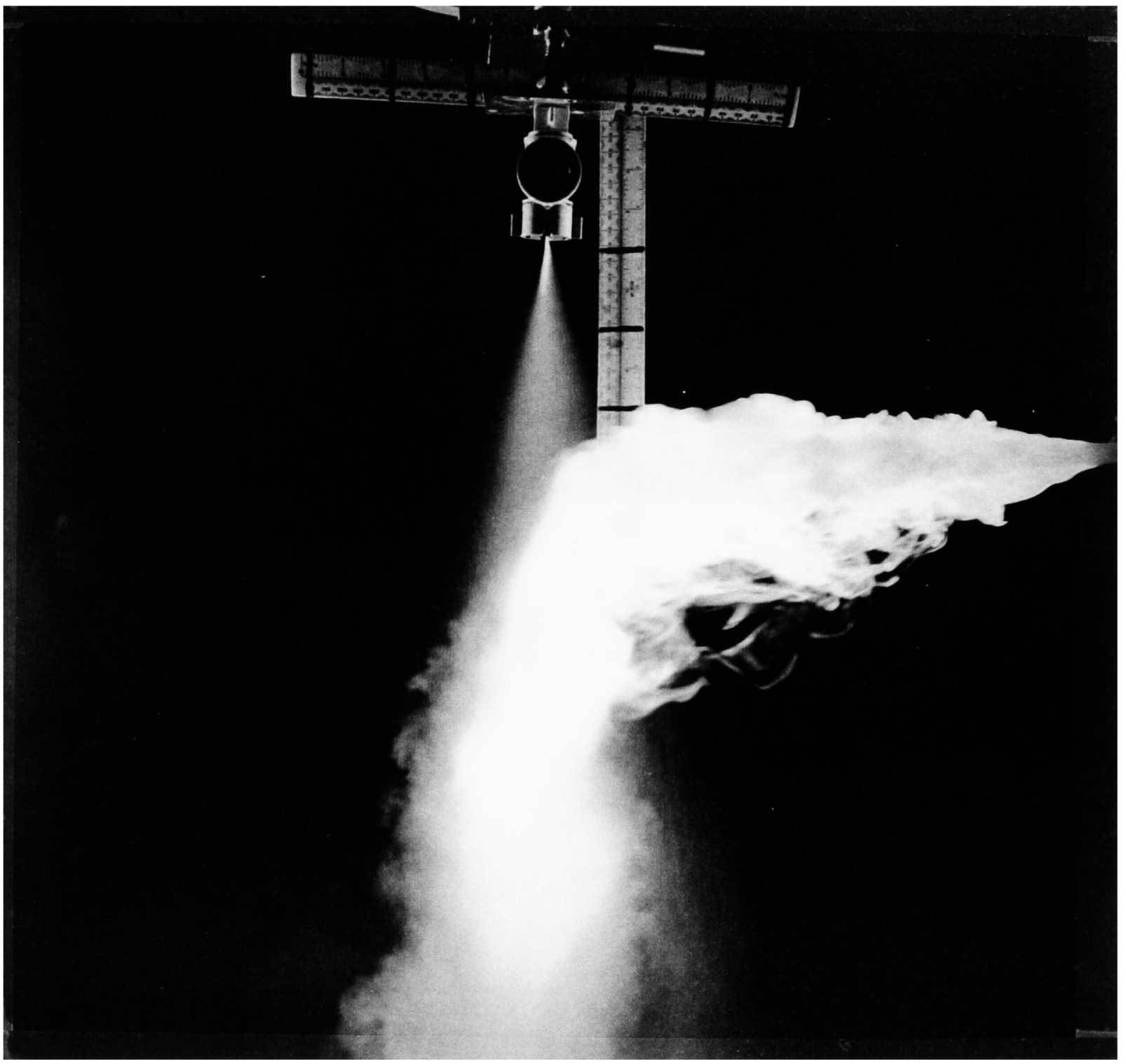

4. Entrainment of ambient air by an agricultural spray (side view) visualised by smoke. The nozzle produces a flat-fan spray with included angle of 110°, inplane angle of about 10°, operated at a nozzle pressure of 3.0 bar and flowrate of 1.6 L/min. A CFT smoke generator generator burning Shell Ondina oil was used to produce a near neutrally-buoyant release. The black lines on the ruled scales denote 50 mm intervals (photograph courtesy of Silsoe Research Institute).

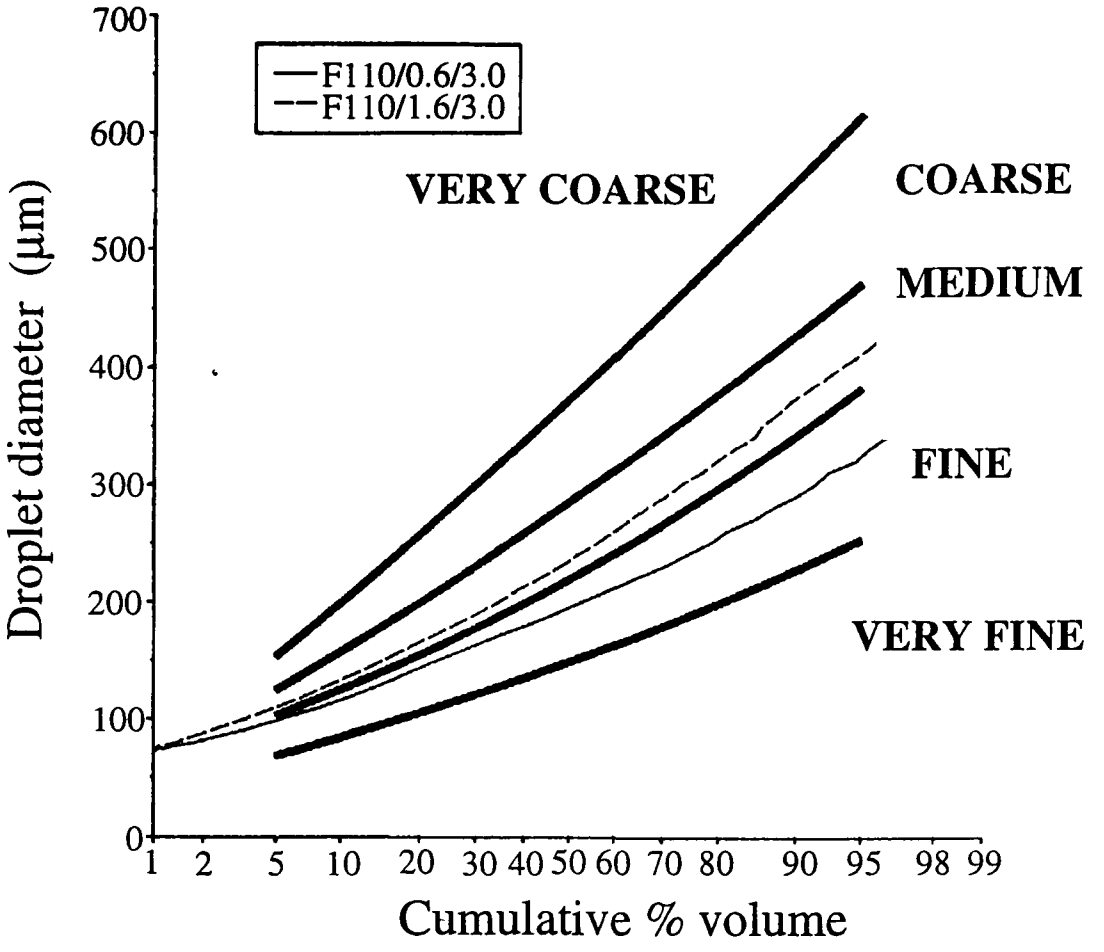

5. Cumulative droplet size distribution plot illustrating British Crop Protection Council classifications of spray quality [Doble et al, 1985]. Droplet size distributions produced by two reference flat-fan nozzles are shown: solid line, 110° flat-fan nozzle operating at 0.6 L/min and 3.0 bar (denoted F110/0.6/3.0); broken line 110° flat-fan nozzle operating at 1.6 L/min and 3.0 bar (denoted F110/1.6/3.0).

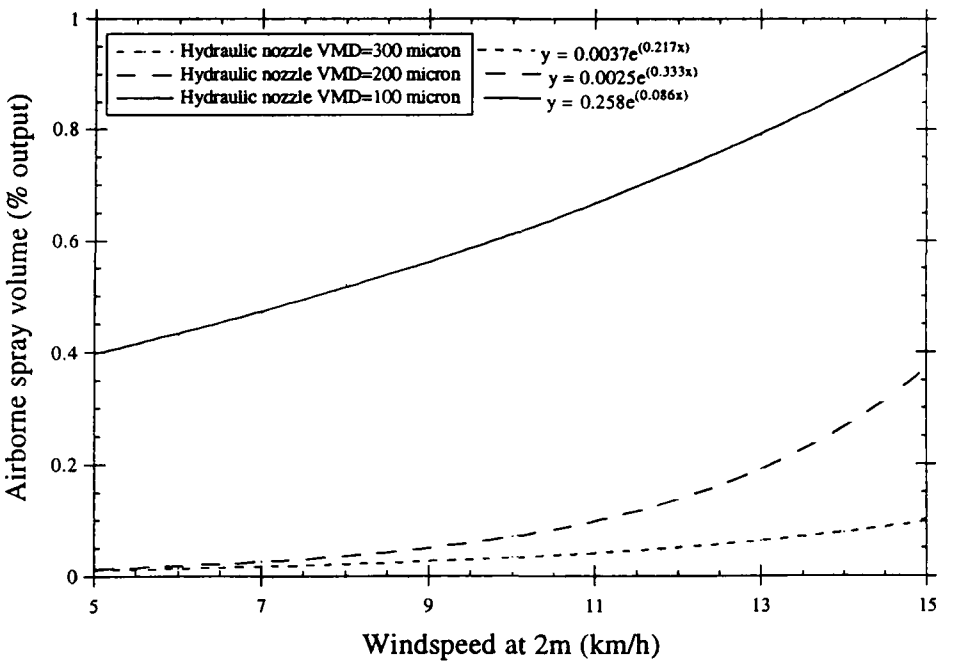

6. Variation of airborne spray volume (as % of sprayer output) with windspeed measured 8 m downwind of a spraying vehicle. The measurements are average values measured using a single 10 m vertical passive line collector, passed once by the vehicle, operating at 6 mph (after Gilbert and Bell, 1988). No data points are presented in the published data, only the exponential form fitted curves reproduced here. The equations of these curve fits are shown to the right of the legend, with y denoting airborne spray volume and x denoting windspeed at 2 m.

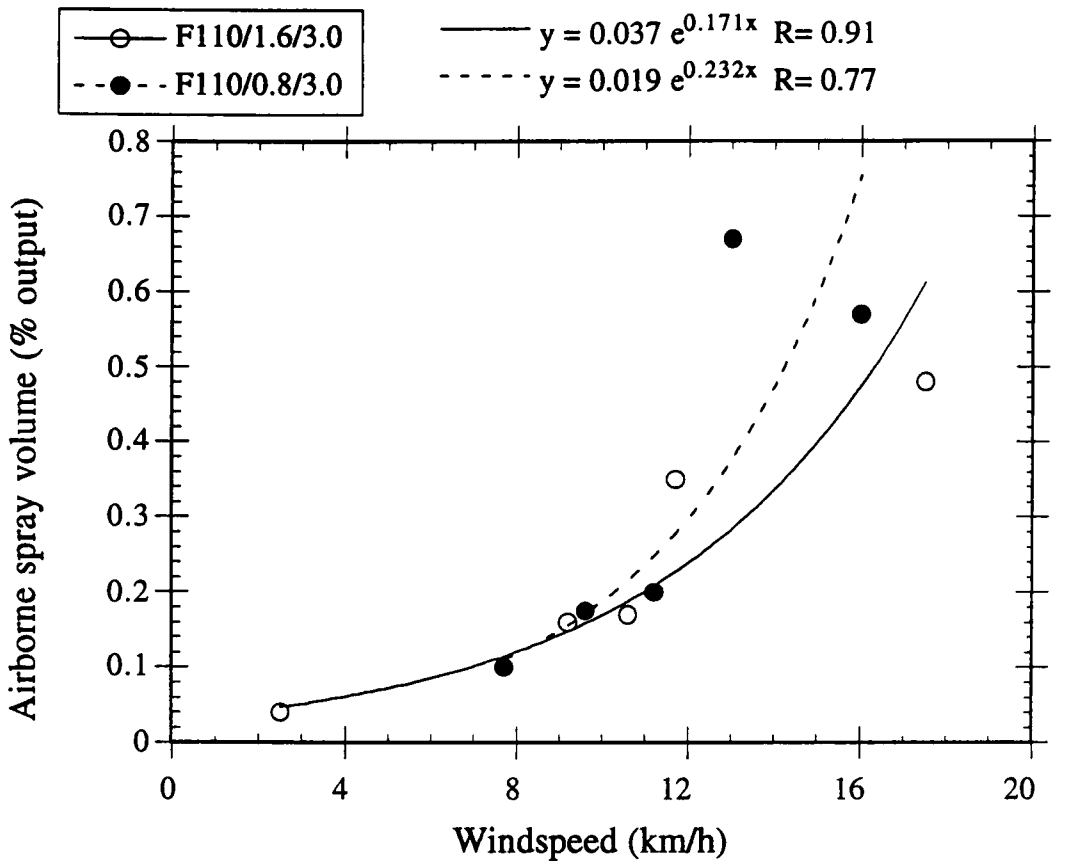

7. Variation of airborne spray volume (as % of sprayer output) with windspeed measured 8 m downwind of a spraying vehicle, operating at 6 mph. Data for two flat-fan nozzles are plotted, operated at 0.8 L/min and 3.0 bar (denoted F110/0.8/3.0) and 1.6 L/min and 3.0 bar (denoted F110/1.6/3.0). Exponential form curves have been fitted to the published data (after Rutherford et al., 1989).

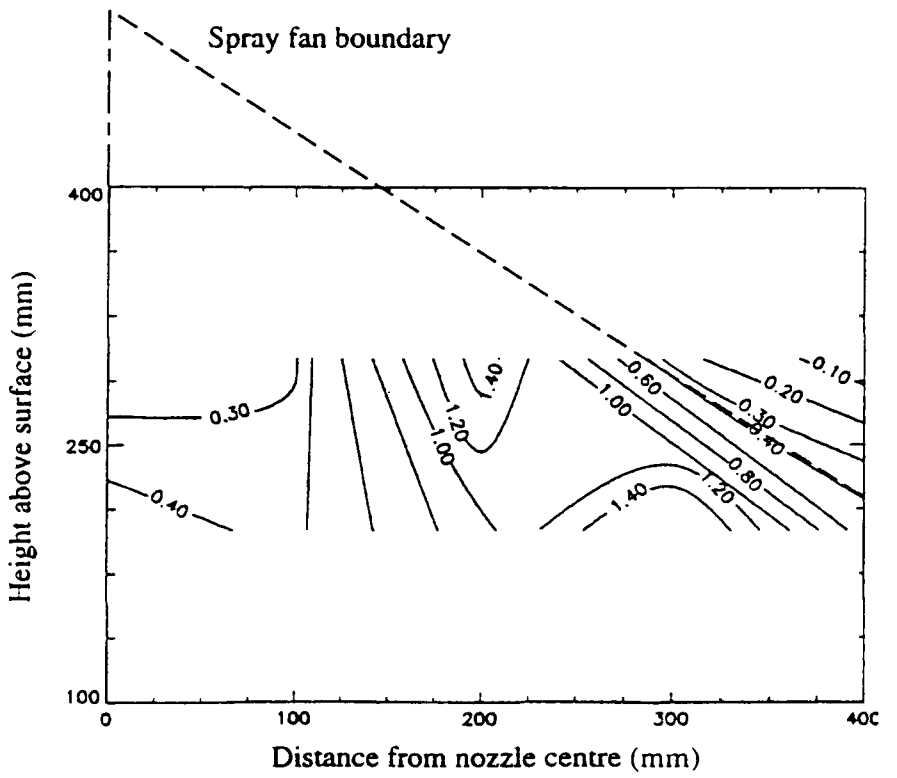

8. Spanwise contours of airborne spray volume flux (μL/mm^2 s) 1 m downwind of a single 110° flat-fan nozzle (operating at 1.6 L/min and 3.0 bar) in a 2.8 m s^{-1} wind tunnel cross flow. The spray is arranged with major axis perpendicular to the cross flow, with its boundary superimposed on the figure to show the origin of the drifting droplets. The cross flow mean velocity profile used simulates that over a plant canopy (technical details in chapter 3; figure plotted using data from Miller et al., 1989).

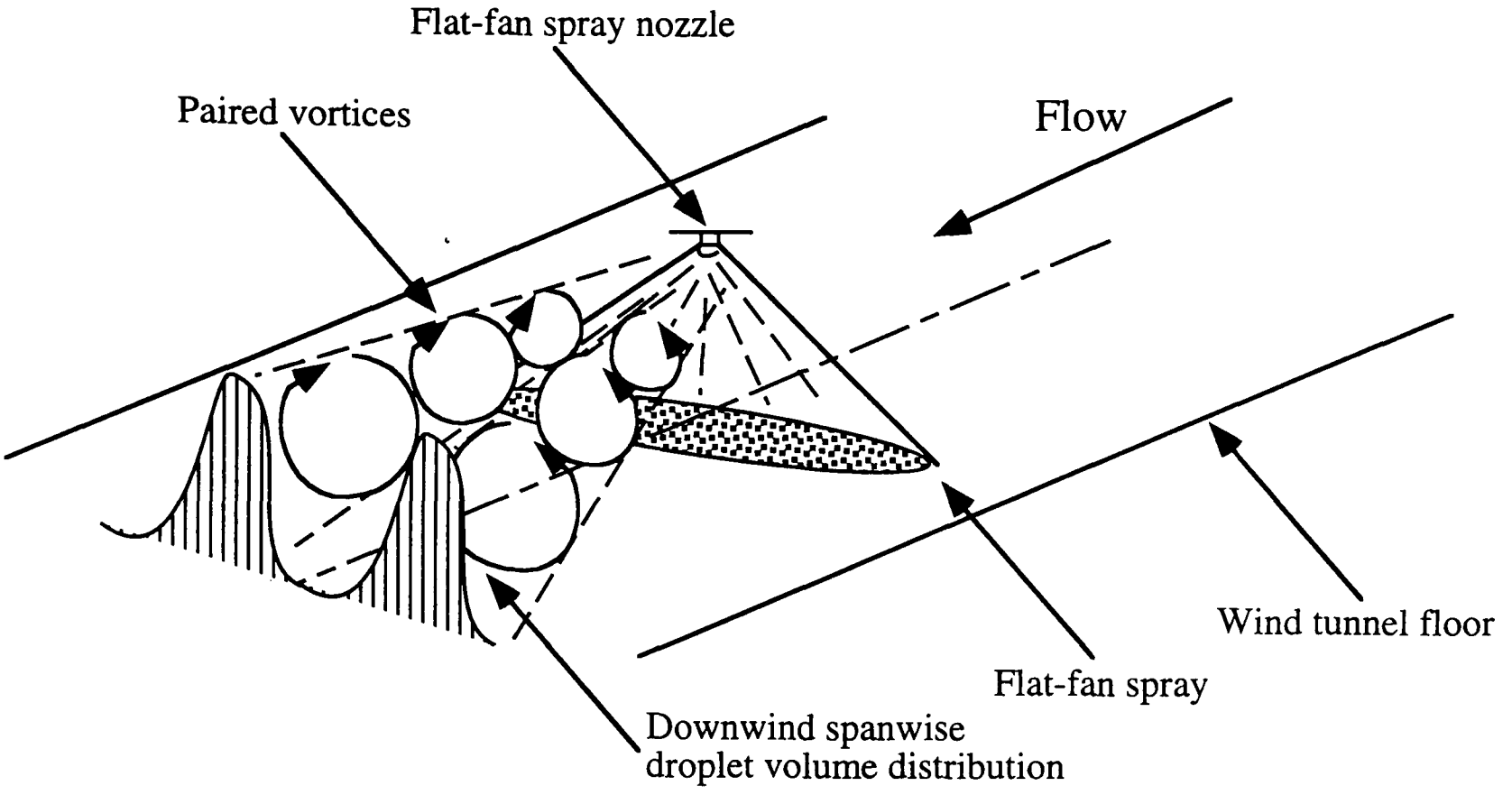

9. Schematic diagram of vortex pair production downwind of a flat-fan spray and the effect on spray drift. Paired vortices form from the interaction of the cross wind with the spray fan; these can trap and release droplets to produce spanwise profiles shown schematically here (after Miller, 1993).

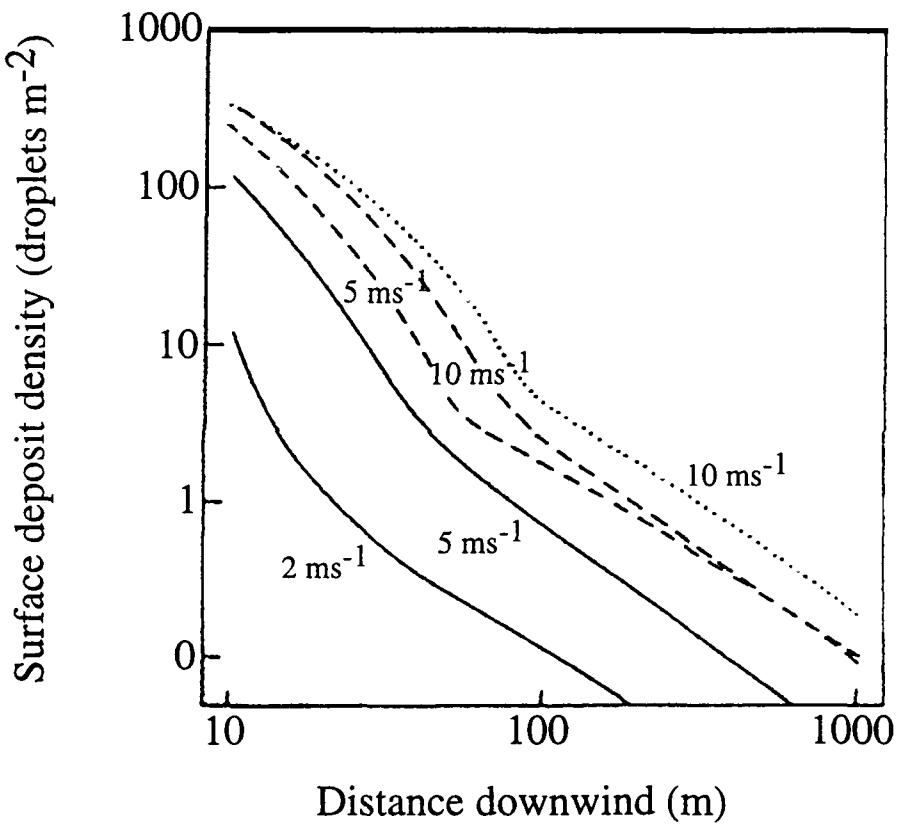

10 Predictions of downwind surface deposit density of 100 μm droplets using a random walk simulation. Dotted line, release height 1.0 m; dashed line, release height 0.5 m; solid line, release height 0.2 m (after Thompson and Ley, 1983).

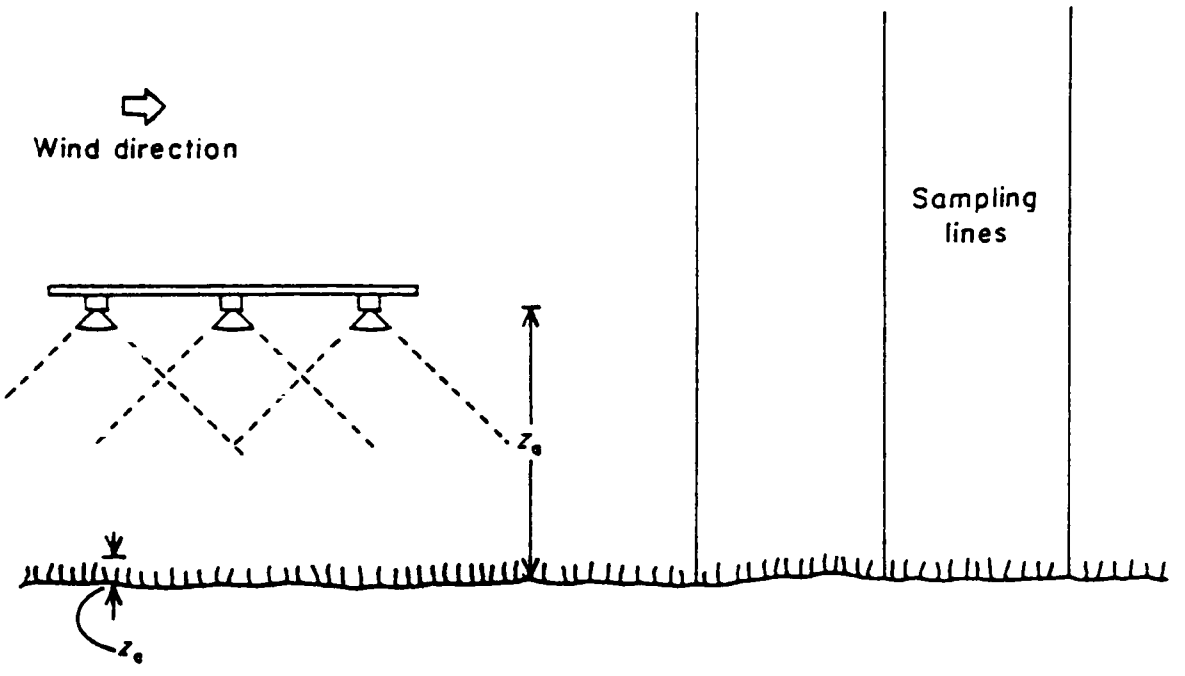

11. The spraying conditions simulated in the model formulated by Miller and Hadfield [1989]. Spraying vehicle motion, neglected in this model, would be into the page (after Miller and Hadfield, 1989).

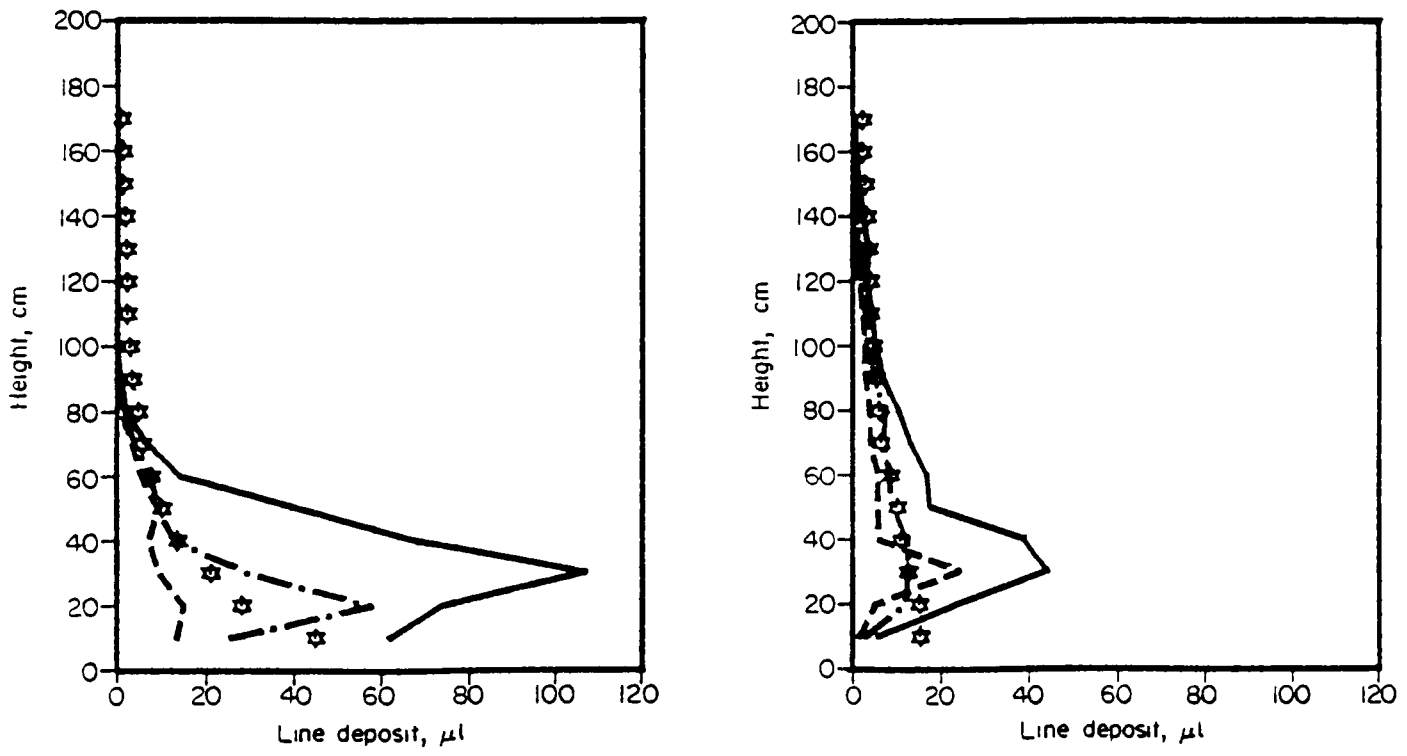

12. Measured and predicted airborne spray vertical profiles 1 m (left) and 6 m (right) downwind of a typical agricultural boom sprayer (after Miller and Hadfield, 1989). Stars, measured; solid lines, predicted with no entrained air velocity and initial liquid sheet velocity of 17 m s^{-1}; dashed lines, predicted with entrained air parameter $\frac{\delta^2}{2k_1}$=0.57 and initial liquid sheet velocity of 17 m s^{-1}; dotted and dashed lines, predicted with entrained air parameter $\frac{\delta^2}{2k_1}$=0.95 and initial liquid sheet velocity of 15 m s^{-1}.

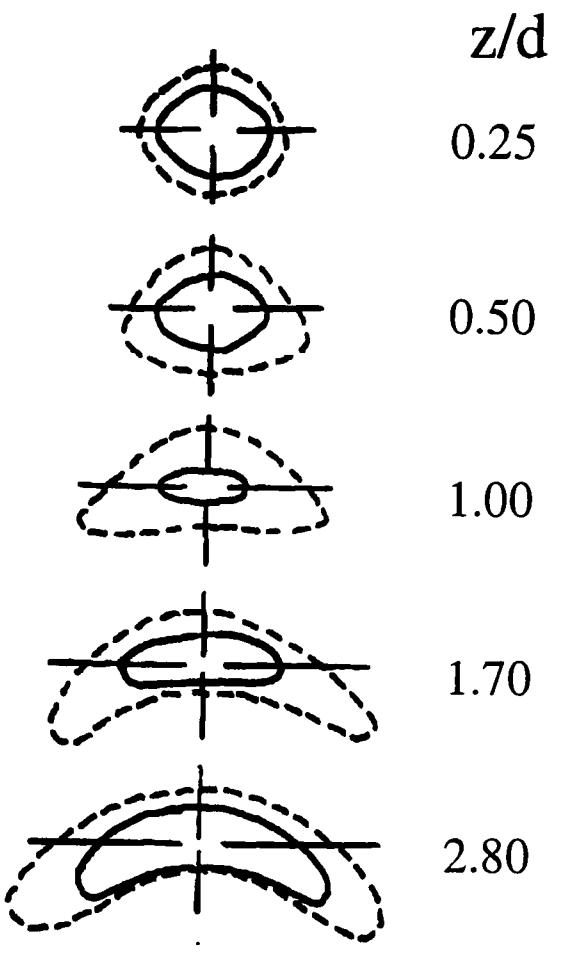

13. The development of kidney-shaped cross-section of a circular jet issuing vertically upwards into a uniform cross flow. Cross-sections were taken through the jet at vertical distances z above the origin; d is the initial width of the jet. The dashed line represents the jet edge (after Rajaratnam, 1976, p.186).

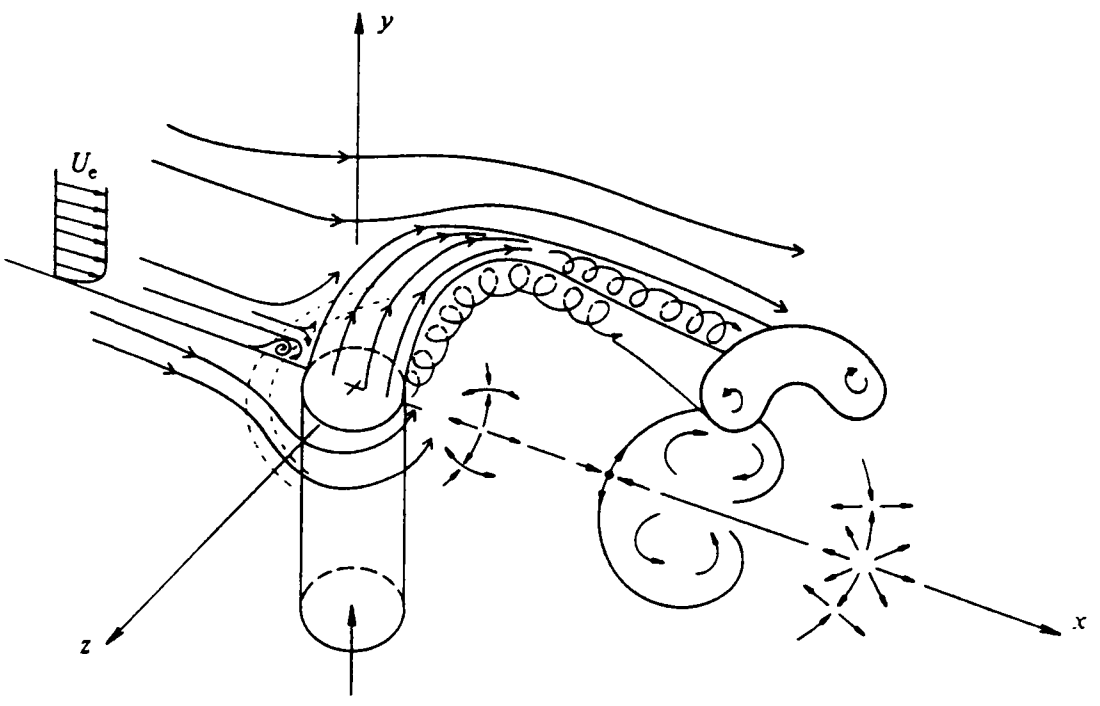

14. Flow development for a jet issuing normally into a cross flow at high (β=2) velocity ratio (after Andreopoulos and Rodi, 1984).

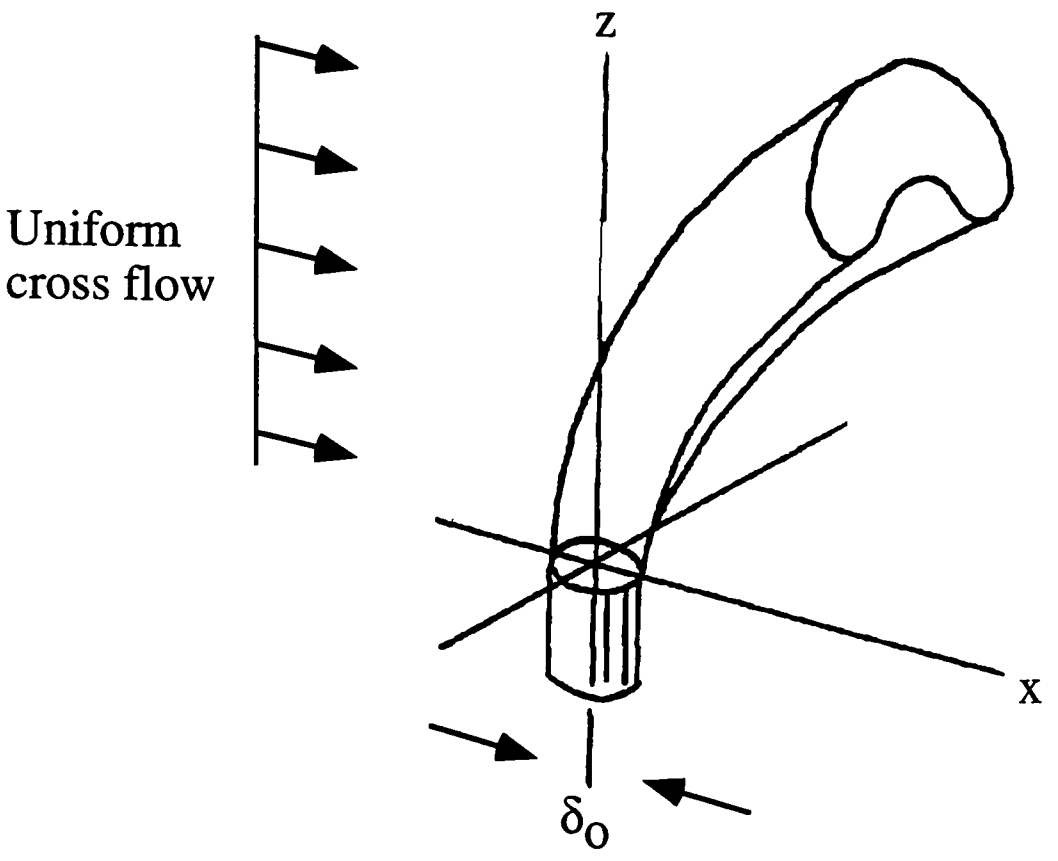

15. Definition sketch of a jet issuing normally into a uniform cross flow.

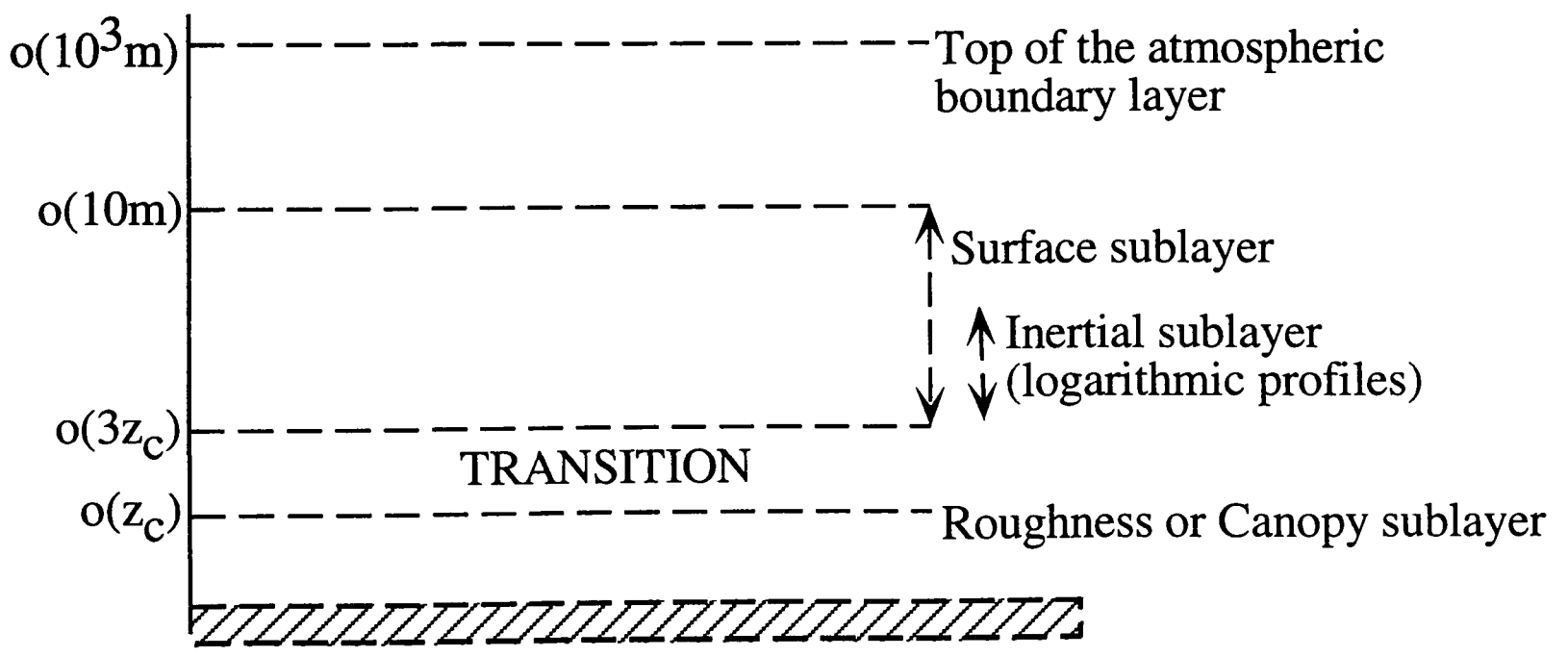

16. Definition sketch of the lower layers of the ABL over a uniform rough surface. z_c is the height of the roughness obstacles (after Plate, 1982).

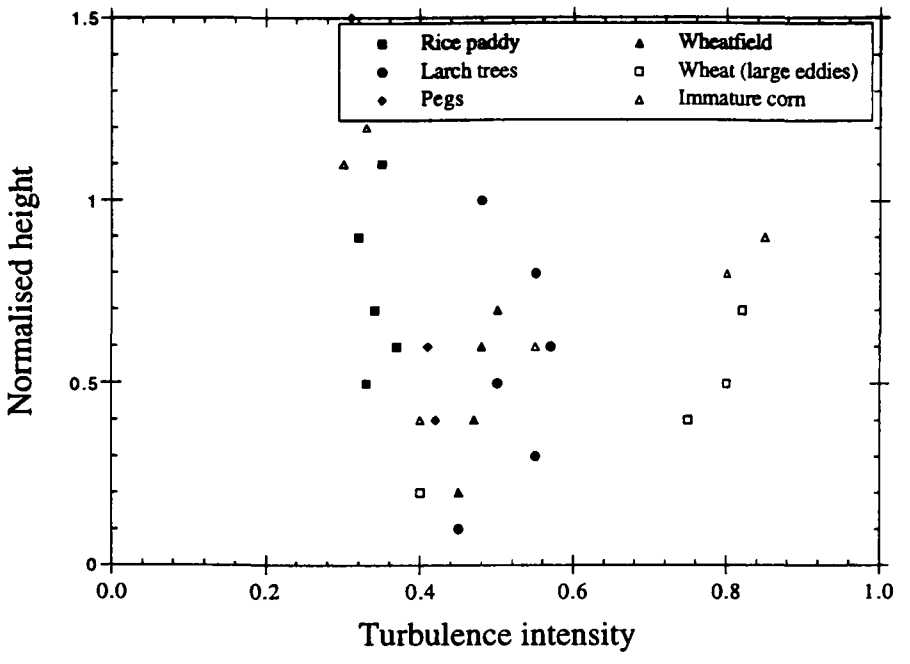

17. Intensity of turbulence in and above simple canopies and wind tunnel roughness elements. Normalised height = $\frac{z}{z_c}$ (after Cionco, 1972).

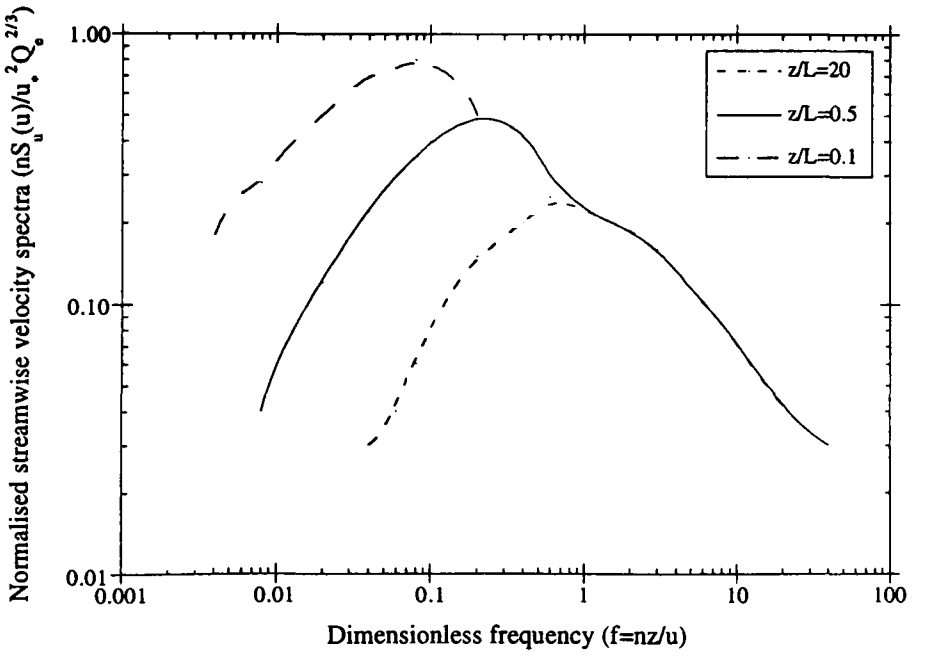

18. Longitudinal velocity spectra from field experiments normalised on friction velocity u_* and surface dissipation Q_e (after Busch, 1973). The curves correspond to measurements at different Richardson numbers z/L (see appendix 1), where z is the measurement height, and L is the Monin-Obukhov length.

Appendix 1. Turbulence Kinetic Energy and Momentum Transport within the ABL

1. Turbulence Generation in the Atmospheric Boundary Layer

The turbulence kinetic energy budget equation written for a co-ordinate system aligned with the mean wind, assuming horizontal homogeneity and no subsidence (large scale vertical motion) appears as follows [Stull, 1988 p.151],

$$\frac{\partial \overline{e}}{\partial t} = \frac{g}{\overline{\theta}}(\overline{\theta' w'}) - (\overline{u' w'})\frac{\partial \overline{u}}{\partial z} - \frac{\partial}{\partial z}(\overline{w' e'}) - \frac{1}{\rho}\frac{\partial}{\partial z}(\overline{w' p'}) - \epsilon \qquad (A1)$$

where

e = turbulent kinetic energy per unit mass,

θ = local potential temperature (the temperature of an elemental volume of air brought adiabatically to 100 kPa [Oke, 1978, p.303]),

ϵ = viscous dissipation of turbulent kinetic energy ($\epsilon = \nu\overline{\left(\frac{\partial u'}{\partial z}\right)^2}$).

The term on the left hand side of equation (A1) represents the local storage of turbulent kinetic energy. The first term on the right hand side is the buoyant production/consumption, depending on whether the heat flux $\overline{\theta' w'}$ is positive (e.g. daytime over land) or negative (e.g. at night over land). The second term on the right hand side is the shear production/loss term. Turbulence generated as a consequence of surface shear contributes essentially to the u and v component motions. The effects of this purely mechanical turbulence are concentrated near the ground, where the shear production term ($-\overline{u' w'}\frac{\partial \overline{u}}{\partial z}$) is positive. The third and fourth terms on the right hand side represent the spatial re- distribution of turbulent kinetic energy by vertical fluctuations w' and pressure-gradient fluctuations $\overline{w' p'}$. Term five on the right hand side represents the viscous dissipation of turbulent kinetic energy i.e. conversion of turbulent kinetic energy into heat.

The shear production term and hence the mechanical turbulence generation decrease rapidly with height, as a consequence of the rapid decrease with height of the velocity shear ($\frac{\partial \overline{u}}{\partial z}$). Convective turbulence production is characterised by a buoyancy term which contributes to w component motions.

Atmospheric turbulence is generated by the interaction of shear-generated and convective

turbulence. The ratio of the turbulence production terms, *the flux Richardson number,* [Nieuwstadt and Van Dop, 1982, p.23] is a measure of the local turbulence level,

$$R_f = \frac{g}{\overline{\theta}} \frac{\overline{w'\theta'}}{\overline{u'w'}} \frac{\partial z}{\partial \overline{u}} \tag{A2}$$

where,

R_f = flux Richardson number,

g = acceleration due to gravity,

θ = local potential temperature,

$\overline{w'\theta'}$ = vertical heat flux.

The vertical heat flux can be related semi- empirically to heat transfer via the eddy diffusivity, defined as

$$\overline{w'\theta'} = -K_h \frac{\partial \overline{\theta}}{\partial z}. \tag{A3}$$

The use of R_f is awkward in situations involving flow stratification, as it contains a mixture of mean gradients and eddy correlation terms. A *gradient* Richardson number (R_i) may be defined using equations (A2) and (A3) above, such that

$$R_f = \frac{K_h}{K_m} \frac{g}{\overline{\theta}} \frac{\frac{\partial \overline{\theta}}{\partial z}}{\left(\frac{\partial \overline{u}}{\partial z}\right)^2} = \frac{K_h}{K_m} R_i \tag{A4}$$

using the Boussinesq closure of the momentum conservation equations,

$$\overline{u'w'} = -K_m \frac{\partial \overline{u}}{\partial z}. \tag{A5}$$

R_i has the advantage of containing only mean quantities, although in practice it is a complicated function of height within the ABL. The Richardson number represents the ratio of convective turbulence to shear generated turbulence and is numerically zero for neutral atmospheric conditions, greater than zero for stable atmospheric conditions, and smaller than zero for unstable atmospheric conditions.

2. The Mean Velocity Profile under Neutral Atmospheric Conditions

Under conditions of neutral atmospheric stability and horizontal homogeneity, the equations for steady, unidirectional mean motion of a turbulent viscous fluid may be written as [Stull, 1988, p.203]

$$\frac{\partial \overline{u'w'}}{\partial z} = f_r(\overline{v} - \overline{v_g}) + \nu \frac{\partial^2 \overline{u}}{\partial z^2} \qquad (A6)$$

and

$$\frac{\partial \overline{v'w'}}{\partial z} = -f_r(\overline{u} - \overline{u_g}) + \nu \frac{\partial^2 \overline{v}}{\partial z^2} \qquad (A7)$$

where

$\overline{v_g}$ = y-component of the geostrophic wind velocity,

$\overline{u_g}$ = x-component of the geostrophic wind velocity,

ν = kinematic viscosity ($1.5 \times 10^{-5} m^2 s^{-1}$ for air at STP),

f_r = Coriolis parameter, $f_r = 2\Omega sin\iota$, where Ω = Earth's rate of rotation (7.29 x 10^{-5} s^{-1}) and ι = latitude.

u_g and v_g are components of the geostrophic wind vector G, such that $G = \left(\overline{u_g}^2 + \overline{v_g}^2\right)^{\frac{1}{2}}$.

Reynolds numbers ($Re = \frac{lu}{\nu}$) for atmospheric surface layer flows are typically $O(10^7)$ [Nieuwstadt and Van Dop, 1982, p.18], so the viscous term in equations (A6) and (A7) may be neglected in comparison with the Reynolds' stress (eddy transport) and geostrophic wind (pressure-gradient) terms. Thus, (A6) and (A7) can be normalised as follows,

$$-\frac{f_r z_o}{u_*} \frac{\overline{v} - \overline{v_g}}{u_*} = -\frac{\frac{d\left(\overline{u'w'}\right)}{u_*^2}}{\frac{dz}{z_o}} \qquad (A8)$$

and

$$\frac{f_r z_o}{u_*} \frac{\overline{u} - \overline{u_g}}{u_*} = -\frac{\frac{d\left(\overline{v'w'}\right)}{u_*^2}}{\frac{dz}{z_o}}. \qquad (A9)$$

The roughness height z_o is a representative length scale for flow in the vicinity of a rough surface, and u_* is an appropriate velocity scale (the friction velocity). The left hand sides of these equations are small (typically $\overline{u_g}$ = 10 m s^{-1}, $\overline{v_g}$ = 5 m s^{-1}, ${u_*}^2$ = 0.1 m^2 s^{-2} and z_o = 0.01 m [Nieuwstadt and Van Dop, 1982, p.42]) and it is reasonable to assume that the left

hand side would decrease with increasing surface Rossby number, $\left(\frac{G}{f_r z_o}\right)$, i.e. the ratio of the geostrophic pressure gradient to surface roughness. Thus, in the limit $\left(\frac{G}{f_r z_o}\right) \to \infty$, the left hand sides of equations (A8) and (A9) would vanish, and yield

$$\frac{d\left(\overline{u'w'}\right)}{u_*^2} = \frac{dz}{z_o} \tag{A10}$$

and

$$\frac{d\left(\overline{v'w'}\right)}{u_*^2} = \frac{dz}{z_o}. \tag{A11}$$

The boundary conditions are

$$\tau_x = -\rho\left(\overline{u'w'}\right) = \tau_o = \rho u_*^2 \tag{A12}$$

$$\tau_y = -\rho\left(\overline{v'w'}\right) = 0 \tag{A13}$$

at $z = z_o$, so the result that the shear stress is approximately constant for all values of $\frac{z}{z_o}$ that are not too large (up to values corresponding to $z = 20$ m [Nieuwstadt and Van Dop, 1982, p.46]) is obtained:

$$-\left(\overline{u'w'}\right) = u_*^2 \tag{A14}$$

$$-\left(\overline{v'w'}\right) = 0. \tag{A15}$$

This is the basis for the concept of a *constant stress layer* near the bottom of the ABL and it leads directly to the *surface similarity* profile

$$\frac{\overline{u}}{u_*} = f_x\left(\frac{z}{z_o}\right). \tag{A16}$$

Using the technique of asymptotic matching [Blackadar and Tennekes, 1968] for the surface layer with the transformed universal function of non-dimensional height,

$$\frac{\overline{u} - \overline{u_g}}{u_*} = F_x\left(\frac{f_r z_o}{u_*}\right) \tag{A17}$$

equation $(A18)$ is obtained

$$\frac{z}{u_*}\frac{\partial \overline{u}}{\partial z} = \eta\frac{dF_x}{d\eta} = \chi\frac{df_x}{d\chi} \tag{A18}$$

for the double limit process $\eta \to 0, \chi \to \infty$, where $\eta = \frac{z f_r}{u_*}, \chi = \frac{z}{z_o}$.

The only way to satisfy equation (A18) without producing singular or trivial results is if both η and χ approach a non-zero asymptote,

$$\frac{z}{u_*}\frac{\partial \overline{u}}{\partial z} = \frac{1}{\kappa} \qquad (A19)$$

where κ is an asymptotic number, called the *Von Karman constant.* This suggests physically that in the region where $\frac{z}{z_o}$ is large (the effects of z_o are negligible) and $\frac{zf_r}{u_*}$ is small (the effects of the Coriolis factor are negligible), the mean wind shear $\frac{\partial \overline{u}}{\partial z}$ depends only on the friction velocity u_* and the height z.

Integration of (A19) leads to the *logarithmic velocity profile,*

$$\frac{\overline{u}}{u_*} = \frac{1}{\kappa}\ln\left(\frac{z}{z_o}\right) \qquad (A20)$$

where,

z_o = Roughness length,

κ = Von Karman constant (an empirical constant with a value of approximately 0.4).

This equation appears in the main text of chapter 1 (incorporating zero-plane displacement due to surface roughness) as equation (7).

References

Blackadar, A.K. and Tennekes, H.A. [1968] Asymptotic similarity in neutral barotropic planetary boundary layers. *J. Atmos. Sci.* **25**, 1015-1020.

Nieuwstadt, F.T.M., and Van Dop, H. [1982] *Atmospheric Turbulence and Air Pollution Modelling.* D.Reidel, Dordrecht.

Oke, T.R. [1978] *Boundary Layer Climates.* Methuen, London.

Stull, R.B. [1988] *Boundary-Layer Meteorology.* Kluwer, Dordrecht.

CHAPTER 2. WIND TUNNEL VELOCITY PROFILES GENERATED BY DIFFERENTIALLY-SPACED FLAT PLATES

Summary

In principle, boundary layer flow over a flat plate at zero incidence provides an avenue for controlled deceleration of the approach flow. Interacting boundary layers between adjoining flat plates merge to provide fully-developed duct flow with controllable velocity reduction according to their length, for a given pressure drop. In this way, an array of differentially-spaced flat plates can be used to modify a uniform wind tunnel velocity field to a specified velocity profile. A one-step iterative scheme is offered to determine plate spacings for simulation of weakly-sheared flows, constrained by zero vertical pressure gradient in the downstream flow (representative of boundary layer conditions). The scheme is tested for realisation of uniform shear flow (maximum velocity variation ±10% of centreline velocity) by wind tunnel simulation, and produces reasonable results, at least comparable with previous studies. However, the scheme is sensitive to the number of plates selected such that representative atmospheric boundary layer simulation is not possible for large-scale simulations. The calculation scheme provides a platform to which elements can be added to increase the simulated range of mean shear and turbulence level by empirical determination of the frictional resistance of individual flow modification elements. This was achieved here for adequate approximation to the logarithmic mean velocity profile of the atmospheric boundary layer over typical agricultural land at full-scale using gauzes and vertical baffles.

1. Introduction

The first stage in this study of spray drift mechanisms is establishment of reproducible conditions in which to make spray drift measurements. This is achieved here by modifying a uniform wind tunnel velocity field to match similarity conditions identified in chapter 1. Despite strictly limited understanding of cross flow dynamics in the vicinity of an agricultural spray, similarity conditions for wind tunnel simulation are restricted to mean velocity profile only. Airborne spray volume flux increases exponentially with mean cross wind speed under field conditions [Gilbert and Bell, 1988; Rutherford et al., 1989] with approximately linear proportionality observed in

wind tunnel simulations using uniform cross flow [Western et al., 1989]. Recent modelling of single-phase jets in cross flow shows that jet deflection and cross-sectional shape change are independent of cross flow turbulence intensity levels [Coelho and Hunt, 1989]. The role of turbulence coherence in droplet dispersion has not been identified, and it is noted here that this provides the greatest uncertainty in establishing similarity conditions, as canopy element wakes and the vehicle wake may both contribute. Subject to this reservation, it is only necessary to simulate the logarithmic mean velocity profile in wind tunnel experiments, most conveniently conducted at full-scale. This can be written as

$$\overline{u_z} = \frac{u_*}{\kappa} \ln \frac{z}{z_o}, \tag{1}$$

where,

$\overline{u_z}$ = mean horizontal velocity at height z,

u_* = friction velocity (surface-defined velocity scale),

κ = Von Karman constant (an empirical constant with a value of approximately 0.4),

z_o = roughness length, length scale for flow in the vicinity of a rough surface.

This is the integrated form of law of the wall scaling (appendix 1, chapter 1) for the atmospheric wind. The geometry of typical arable cereal crops introduces only a small zero plane displacement, which is neglected here, as is standard practice (see chapter 1). Guidelines for agricultural spraying [Anon, 1990] suggest the safest condition for spray application is a force 2 light breeze blowing away from susceptible crops. This corresponds to a wind velocity at boom height of about 2 m s^{-1}. To reduce uncertainty in airborne spray volume measurements, wind tunnel experiments are usually conducted at higher cross flow velocities [Miller, 1988]. In this study, a logarithmic mean velocity profile corresponding to a mean velocity of 3.5 m s^{-1}, 1 m above the crop canopy (2.8 m s^{-1} at boom height) with z_o = 0.03 m (typical of agricultural land [Anon, 1978]) was simulated. The effect of neglecting zero plane displacement will increase scatter in z_o, so matching this value in wind tunnel simulations of the mean profile is considered secondary here.

As a consequence of neglecting any matching of turbulence structure (particularly in canopy element wakes), the only fluid mechanical scaling requirement is similarity of flow dynamics between field and wind tunnel. Rossby number similarity (which describes the effect of the Earth's rotation) is not required for full-scale simulation as the horizontal length scale of the

spray near-field is only approximately 5 m [Miller et al., 1989]. Convective effects described by Froude number and Prandtl number similarity do not require simulation under conditions of neutral atmospheric stability. Reproduction of flow dynamics requires matching Reynolds number between model and full-scale flows; this is usually unattainable in small-scale wind tunnel studies because of the large ratio of atmospheric length scale to wind tunnel length scale [Plate, 1982, p.578]. However, similarity of flow *regime* can be achieved for this full-scale simulation because length scales are defined by spraying equipment. The appropriate length scale for dynamic similarity is defined by the spray fan geometry, shown in figure 1 for the typical arrangement of flat-fan sprays on a boom. Considering a single spray, relevant length scales for interaction with cross flow will be the spray height (0.5 m). For a boom of overlapping sprays, these will be spray height (0.5 m) and spacing (0.5 m). For these length scales, typical Reynolds numbers at guideline spraying conditions (windspeed of 1-2 m s^{-1} at boom height [Anon, 1990]) are of order 50,000, henceforth denoted o(50,000). Therefore, the establishment of fully turbulent conditions in full-scale wind tunnel cross flows is sufficient to match field conditions.

The aim of scale simulations of the atmospheric boundary layer velocity field is to provide a boundary layer flow which adequately reproduces the full-scale characteristics and this is usually achieved by introducing an array of barriers to artificially thicken the boundary layer within a reasonable streamwise distance, supplemented by mixing devices to tune the resulting mean and turbulence profiles and even turbulence spectra [Armitt and Counihan, 1968; Counihan, 1969; Cook, 1978; Irwin, 1981]. More exotically, arrays of jets or fans have been used to achieve the same effect [Teunissen, 1975; Nishi and Miyagi, 1995], although necessarily at greater expense, both as equipment and operational costs. Recalling reservations on exact similarity requirements, adequate approximation, rather than absolute precision is deemed appropriate for the purposes of these studies. In this spirit a relatively low cost technique for generating mean velocity profiles using an array of parallel flat plates to introduce the appropriate momentum deficit is described here, which is applied to both the benchmark case of weak uniform shear flow and full-scale simulation of the logarithmic mean velocity profile.

The method described here is a variation on that presented by Lloyd [1967], who provided a design procedure based on uniform fully-developed channel flow between each pair of plates in the array. His scheme proceeds in a stepwise manner from the wind tunnel floor, specifying the spacing of each pair of plates to produce channel flow with velocity matching the required downstream profile as sole design condition, thus yielding the number of plates required. As a

variation on this approach, an alternative design procedure in terms of frictional losses associated with boundary layer development along the surfaces of each plate in the array is offered here subject to an overall constraint of zero vertical pressure gradient in the emerging downstream flow. Perhaps the most significant consideration is that the plates are thin compared with the boundary layer thickness in order to minimise discrete wake deficits in the downstream profile. As a consequence flat plates cannot produce high turbulence levels in the downstream flow by vortex shedding, limiting their application to problems with low representative turbulence levels described above. Lloyd [1967] had to add a vertical barrier to the downstream end of his flat plates to generate streamwise turbulence intensity levels above 2%.

The work reported here demonstrates extreme sensitivity to the number of plates adopted such that representative atmospheric boundary layer simulation is impractical without additional flexiblility in attaching for example variable length plates, supplementary grids or gauzes. Consequently, simulation of the logarithmic mean velocity profile at full-scale utilised supplementary grids, surface roughness elements and a horizontal barrier. On the other hand, the method is demonstrated to be an adequate approximation for weaker shear flows, requiring a smaller number of plates without risking separation of the upstream approach flow. In section 2 the design approach and calculations are outlined, and in section 3 the experimental method and instrumentation are reported, with section 4 describing the experimental results and finishing with broader discussion and main conclusions in sections 5 and 6.

2. Design Calculations

The principle is illustrated in the schematic of figure 2, the purpose here being to deliver the desired downstream velocity profile using plate spacings within an array of thin plates all of equal length as the design parameter. Neglecting hydrostatic variations, as is usual, and introducing a Fanning friction factor to describe the head loss over each surface, the mechanical energy balance over plate n (see figure 2) can be written as follows

$$\frac{p_1}{\rho} + \frac{u_1^2}{2} = \frac{p_{2n}}{\rho} + \frac{u_{2n}^2}{2} + \frac{C_f l \left(\frac{u_1+u_{2n}}{2}\right)^2}{2s_n} \tag{2}$$

where,

p_1 is the upstream static pressure at plate n,

p_{2n} is the downstream static pressure at plate n,

u_1 is the upstream uniform mean velocity,

u_{2n} is the prescribed downstream velocity at plate n,

ρ is the fluid density,

C_f is the friction coefficient for flow over plate n,

l is the plate length,

s_n is the spacing between plates n and $n+1$.

The frictional term in equation (2) is based on mean velocity over the plate length $\left(\frac{u_1+u_{2n}}{2}\right)$, assumed representative for velocity modification from u_1 to u_{2n}. The friction factor C_f is assigned according to the Reynolds number (Re) at each plate based on this mean flow velocity, following established empirical correlations for laminar and turbulent flows [Schlichting, 1968, p.122 and p.567] e.g.

$$C_f = \frac{1.328}{Re^{\frac{1}{2}}} \qquad (Re < 10^6) \tag{3}$$

Re-arranging equation (2) explicitly in terms of plate spacings

$$s_n = \left[\frac{p_1 - p_{2n}}{\rho} + \frac{{u_1}^2 - {u_{2n}}^2}{2}\right]^{-1} \frac{C_f l (u_1 + u_{2n})^2}{8}. \tag{4}$$

For present purposes u_1 is regarded as prescribed uniform approach flow, u_{2n} as prescribed (uniformly-sheared) exit flow, p_1 as prescribed uniform entry pressure, p_{2n} as unknown exit pressure, with s_n, the plate spacing, as solution variable. Clearly additional closure constraint is required to specify p_{2n}, here being the requirement of zero vertical pressure gradient in the downstream flow. For weak shear flows considered here, the mean downstream pressure defined according to $\overline{p}_2 = \frac{\sum p_{2n}}{n}$ was used as an estimate of constant downstream pressure.

An iterative argument was adopted, described in outline as follows. Starting with n plates spaced equally across the control volume (s_n assigned), the downstream exit pressure p_{2n} was calculated for each plate using equation (4) and the mean determined. This was substituted back into equation (4) in place of the local value p_{2n} to specify a new spacing for each plate in the array based on the prescribed local exit velocity u_{2n} and mean downstream pressure. Downstream exit pressures were re-calculated from equation (4), and a new mean and set of spacings determined. From equation (4) it can be seen that plate spacings are simply proportional to the inverse values of pressure and dynamic head differences, and as the latter term is prescribed, the iteration

process simply corresponds to modification of plate spacing by the factor $\frac{p_1 - p_{2n}}{p_1 - \overline{p}_2}$, calculated at each iterative step. The iteration was repeated until the plate spacings calculated for consecutive steps varied by less than 0.5%. In weak shear simulations, with shear parameter (maximum velocity variation as a proportion of centreline velocity) $< \pm 15\%$, the maximum downstream pressure variation ($\frac{p_{2n}}{\overline{p}_2}$) at each iterative step was about 10%, determined at the duct walls.

The convergence of the scheme is linear, as indicated by the proportionality of plate spacing to pressure head shown by equation (4). Convergence of the iteration scheme is characterised by approximately constant static pressure conditions both upstream and downstream of the plate array, with changes in dynamic pressure to match the prescribed shear balanced by changes in drag loss due to variation in plate spacing. In assuming this behaviour, the limitation of this technique to the simulation of weakly-sheared flows is noted, in which case the upstream static pressure remains uniform across the plate array, this depending on specification of an adequate number of plates. In principle it is possible to increase the range of flow shear simulated by using streamlined plates to minimize blockage of the approach flow, maintaining uniform upstream static pressure, and by using plate length as a variable to allow greater drag loss.

The calculation scheme was compared with that due to Lloyd [1967] for production of a weak nominally-uniform shear, characterised by shear parameter (mean velocity difference at the tunnel wall expressed as a fraction of the centreline velocity) of $\pm$ 10%. Lloyd's scheme calculates plate number explicity, and so was solved for a range of shear parameters to provide an estimate of the number of plates required for weak shear simulations (figure 3). Both schemes were solved numerically for 19 plates 305 mm long and 2 mm thick with upstream approach flow velocity of 10 m s^{-1}, yielding plate spacings shown in figure 4. The coded form of the present scheme is listed in appendix 1. The spacings calculated for the present iterative scheme show a steady increase across the wind tunnel, consistent with uniform weak shear simulation, whereas spacings calculated using Lloyd's method increase at an increasing rate near the wind tunnel top. This region is most poorly reproduced in Lloyd's original uniform shear simulation [Lloyd, 1967], with plate spacings showing similar trends at the tunnel top.

Given the difficulties of maintaining a uniform upstream pressure gradient at higher values of shear parameter required for large-scale ABL simulations, it was decided to restrict the number of plates used for ease of construction at full-scale, and attach supplementary grids and surface roughness elements to tune the resulting profile. For simulation of logarithmic mean velocity

profiles, the appropriate form is

$$u_2(z) = U_t \frac{ln\left(\frac{z}{z_o}\right)}{ln\left(\frac{h_t}{z_o}\right)} \tag{5}$$

where U_t is the velocity at the wind tunnel roof, and h_t is the wind tunnel height. This profile was simulated using the code listed in appendix 1 for 10 plates 305 mm long and 2 mm thick with upstream approach flow velocity of 10 m s^{-1}, yielding plate spacings shown in figure 5.

3. Experimental Method

3.1. Weak Uniform Shear Flow

Experiments were conducted in an 18" square section open-circuit NPL-type wind tunnel. Nominally-uniform cross flow velocities up to 15 m s^{-1} are attainable in this tunnel, the tunnel wall expressed as a fraction of the centrelinwith maximum streamwise turbulence intensity of 4% at 10 m s^{-1} measured using hot-wire anemometry. The working section length is 3 m with constant 0.46 m square cross-section, in which the plate array was located just downstream of the entry section, which contained 0.15 m thickness of 0.01 m diameter honeycomb flow straightener at its inlet. A 3-d stepper motor-driven traverse was mounted at a position corresponding to 1.3 tunnel heights downstream of the flat plate array. Plate arrays were constructed from dural plates 305 mm long and 2 mm thick (Sharpe and Fisher Ltd) using spacings calculated for the two schemes above (see figure 4). The arrays consisted of struts made from 2BA studding (British Association standard thread: 0.81 mm pitch, 12.4 threads per cm) and 2 mm dural plates, with a different set of brass spacer sleeves for the two plate spacings. A mixing grid (cell dimension 11 mm $\times$ 11 mm, bar diameter 1 mm) was added immediately downstream of the plate array to allow velocity profile relaxation. Quality of the downstream flows was gauged by measuring the mean velocity profiles using a Dantec 55P11 single hot-wire probe in conjunction with a Dantec 55M01 hot-wire anemometer mounted on the 3-d stepper motor-driven traverse 1.3 tunnel heights downstream of the plate array. The probe was traversed across the tunnel height at a spanwise position corresponding to the tunnel centreline. At each measuring station, 300 voltage readings were taken, using the ASYST data acquisition package sampling at 500 Hz. These were converted to velocity data within the ASYST package using probe calibrations against pitot-static measurements taken using a Betz manometer.

3.2. Logarithmic Mean Velocity Profile

The logarithmic mean velocity profile defined by a full-scale mean velocity of 2.8 m s^{-1} at 0.5 m and roughness length of 0.03 m was simulated initially at prototype (1:3.3) scale in the NPL-type wind tunnel and subsequently at full-scale in a 2 m × 1.5 m Eiffel-type wind tunnel. The diffuser section in the full-scale wind tunnel is 2 m wide × 1.5 m high, and 3 m in length, with 0.3 m thickness of 0.01 m diameter honeycomb flow straightener at the inlet. This channels air into the working section, which is 4 m wide × 2 m high, and 5 m in length (typical of Eiffel tunnel configuration). Equipment for velocity profile simulation was positioned at the entrance to the working section. The tunnel produces approximately uniform upstream flow, with streamwise turbulence intensity which is approximately constant over the working section, with maximum value of 2% at 1.8 m s^{-1}, measured using a Gill Instruments sonic anemometer. The tunnel discharges air through an exhaust section which has the same cross-section as the diffuser section, and is 2 m long. The airflow is drawn through the tunnel by a 1.6 m diameter 4-bladed fan, powered by a 26.6 Kw 3-phase electric motor.

A uniform upstream velocity of 10 m s^{-1} was used at prototype (1:3.3) scale, corresponding to 3.3 m s^{-1} at full-scale (based on dynamic similarity between prototype and full-scale). 2 mm thick dural plates were used and positioned as before, supported on simple right angle brackets mounted on the wind tunnel walls. Mean velocity profiles were measured on the centreline 1.3 tunnel heights downstream using a Dantec 55P11 single hot-wire probe and a 55M01 hot-wire anemometer. Anemoneter mean voltage was recorded on an RS Thirlby 1906a digital voltmeter, and converted to mean velocity data using a probe calibration made against a pitot-static tube and Betz manometer. Systematic supplementary equipment modification (based on previous wind tunnel studies) was adopted to match the initial experimental velocity profile to the desired logarithmic profile. Gauzes mounted over the upstream and downstream ends of the plate array and horizontal baffles were used to retard flow at specific heights and increase mixing in the downstream flow. The additional pressure drop due to the presence of a gauze is characterised by the gauze resistance coefficient formulated by Taylor and Batchelor [Owen and Zienkiewicz, 1957]

$$k_r = \frac{p_1 - p_{2g}}{\frac{1}{2}\rho {u_1}^2} \tag{6}$$

(symbols as above).

This coefficient can be expressed in terms of the gauze dimensions [Pankhurst and Holder, 1952],

$$k_r = \frac{1 - (1 - \frac{d}{l})^2}{(1 - \frac{d}{l})^4} \tag{7}$$

where

l = length of the gauze cell,

d = diameter of the gauze bar (see figure 6).

The effect of adding gauzes of defined blockage coefficient was investigated by incorporating the additional pressure drop due to the gauze into the Bernoulli equation (equation 4) and solving as before. Vertical baffles mounted horizontally across the wind tunnel were used to redistribute flow momentum from regions of excess velocity. The height of the baffle is related to the size of the particular velocity defect [Armitt and Counihan, 1968].

It was necessary to add artificial surface roughness as the calculation scheme described above cannot accommodate the effect of 'law of the wall' parameters roughness height (z_o) and friction velocity (u_*). Roughness elements were positioned on the wind tunnel floor downstream of the plate array to act as a momentum sink and establish the Reynolds stress profile through the boundary layer, which controls mean velocity and turbulence characteristics. Initial estimates of roughness element height and spacing were made using Cook's [1978] paper on wind tunnel simulation of the ABL, assuming that the action of gauzes near the wind tunnel floor is analogous with Cook's use of a barrier to provide the initial momentum deficit. The cardboard packing for egg boxes provided roughness elements of approximately the correct size and aspect ratio in a suitable arrangement.

The final equipment configuration is shown in figure 7. This was scaled-up geometrically to full-scale (dynamic similarity being maintained by using higher airflow velocity at prototype scale). The full-scale plate array was constructed from 6 mm plywood plates, supported at each corner by a right-angled bracket. At two points on the centreline of the plates, collars fixed to two vertical Bowden cables provided support in the manner of a biplane wing. Scaled-up floor roughness elements consisted of inverted 90 mm plastic drinking cups, glued to plywood sheets placed on the wind tunnel floor. The cups had an upper surface diameter of 40 mm, and their arrangement was identical to the eggbox roughness, with spacing (5 mm) adjusted to produce the same element density as the prototype (see figure 7).

4. Experimental Results

4.1. Weak Uniform Shear Flow

Mean streamwise velocity profiles are shown for the present iterative scheme (figure 8) and Lloyd's design calculation (figure 9). The effects of plate wakes are manifest as velocity defects in the downstream flow. Fitting trends in these data by eye suggests production of shear flows with parameter about $\pm 9\%$ for both schemes. Addition of the mixing grid enabled the downstream velocity profile to satisfactorily relax, although reducing the final shear parameter simulated. This is shown in figure 10 for the present scheme, with reduction in final shear parameter to $\pm 8.6\%$, determined using linear regression. Streamwise turbulence intensity $\left(\frac{\sqrt{\overline{u'^2}}}{\overline{u}}\right)$ was calculated from the velocity data, shown in figures 11 and 12 for the present iterative scheme and Lloyd's calculation respectively. For both schemes, the turbulence intensity level produced was around 3% over the tunnel depth, broadly in accordance with results obtained by Lloyd [1967] (recall introduction). Peak values of 10% at the walls simply indicate the presence of wall boundary layers in the upstream flow. A smoke tracer (CFT generator, Shell Ondina oil) was used to visualise flow through the plate array, shown in figure 13 for the present scheme. For both calculation schemes with and without mixing grid attachment, smoke streams followed approximately horizontal trajectories, indicating approximately zero vertical pressure gradient in the downstream velocity field.

4.2. Logarithmic Mean Velocity Profile

The velocity profile produced by the calculated plate spacings is shown in figure 14. As expected, 10 plates was too small a number to introduce a significant velocity gradient. Gauzes were added to the plate array to produce the velocity profile shown in figure 15. Two retarding grids were mounted over the upstream end of the array, with rectangular cell dimensions of 2 mm $\times$ 2 mm and 0.2 mm $\times$ 0.6 mm, and grid bar diameters of 1 mm and 0.1 mm respectively. A mixing grid was mounted over the downstream end of the array to reduce the persistence of velocity defects (figure 14) through enhanced mixing of the downstream flow. The mixing grid had a rectangular cell dimension of 11 mm $\times$ 11 mm and a grid bar diameter of 2 mm. Matching to the design logarithmic profile is improved in the region $\frac{z}{h_t} < 0.2$.

The profile produced by addition of surface roughness is shown in figure 16. A short roughness fetch was employed (1.2 tunnel heights, as opposed to a typical fetch of 4-8 tunnel heights [Cook, 1978]), but this established a satisfactory velocity profile near the wind tunnel floor. The effectiveness of the short roughness fetch suggests that simulation of surface roughness characteristics can be decoupled from simulation of mean velocity profiles above the region of surface influence with this combination of equipment. Final tuning of the velocity profile employed a vertical baffle to redistribute flow momentum from regions of excess velocity, present at $\frac{z}{h_t} = 0.2$ and 0.4 (figure 16). Two 25 mm baffles were mounted at $\frac{z}{h_t} = 0.13$, and $\frac{z}{h_t} = 0.21$, to produce the velocity profile shown in figure 17 (which shows a larger dataset than previous figures). Through systematic equipment modification, a good match to the design profile had been achieved. Data from figure 17 were replotted in log-linear form in figure 18. As a statistical test of the fit of experimental to design profiles, regression of the experimental profile on the design profile was carried out (details in appendix 2). The two were indistinguishable at the 95% confidence level, constituting acceptable matching of the design profile.

The equipment used to produce the matched velocity profile at prototype (1:3.3) scale was geometrically scaled up to full-scale and installed in the Eiffel-type wind tunnel. The velocity profile produced is shown in figure 19. Agreement to the design profile was less good than at smaller scale, but trends were adequately simulated, particularly near the floor. Transferring from an NPL-type wind tunnel (prototype scale) to an Eiffel-type wind tunnel (full-scale) was expected to introduce a variation in velocity profile produced because of the change in blockage constraint [Maskell, 1963] introduced due to the difference in tunnel cross-sectional geometries. This variation appears to include the velocity defect in the profile at $\frac{z}{h_t} = 0.6$, with additional re-distribution of flow at $\frac{z}{h_t} = 0.3$. A 0.1 m vertical baffle was inserted at $z = 0.40$ m, producing the velocity profile shown in figure 20. Additional blocking of the flow by the vertical baffles has reduced the matching of the profiles near the floor, by deflecting the flow upwards away from this region. The best-fit logarithmic curve of the same form as equation (1) to these experimental points was determined using the ASYST statistical package. This yielded z_o=0.086 m, in the range for agricultural land (z_o=0.02-0.10 m, Anon [1978]).

The final equipment arrangement is shown as figure 21. A qualitative estimate of the turbulence scale generated was obtained using smoke visualisation (figure 22). The vertical turbulence scale was approximately 0.1 m in the downstream flow. Smoke tracers were not deflected vertically (except in the vicinity of the roof-mounted traverse), indicating approximately zero vertical pressure gradient downstream of this equipment.

5. Discussion

In this study, flat plates were chosen as a means of modifying uniform flow to a given mean velocity profile in the absence of any explicit design scheme for other more common equipment configurations and with only limited understanding of the full-scale flow field. Previous application of this equipment to weak shear flow simulation [Lloyd, 1967] did not include prescription of zero vertical pressure gradient appropriate to boundary layer flows, consistent with weak shear simulation, so a new calculation scheme is offered here which incorporates approaching this condition as a design requirement. Within this framework, a simple calculation scheme is attractive. The scheme offered here consists of a single-step iteration which requires the minimum of computation. Given the limited 2-d view of flow dynamics adopted here, there will be a range of convergent solutions for the calculation scheme. For representative weak shear simulation, the mean downstream static pressure provides an estimate of a convergent solution, typically within 10% of the local downstream value at any point. Modification of plate spacing is subject to maintaining uniform upstream pressure. This condition will not hold for stronger shear, where small plate spacing will lead to blockage of the upstream approach flow. However, use of flat plates as outlined for the reference weak shear flow can be extended to higher levels of turbulence and shear by using the plates as a platform on which to mount other flow modification devices. This was achieved here for logarithmic mean velocity profiles in a more systematic manner than in previous studies [Lloyd, 1967] via empirical determination of the Fanning friction coefficient for a plate-plus-resistance gauze arrangement allowing incorporation into the iterative scheme. However, it is cautioned that maintaining constant upstream pressure is a requirement for convergence of the calculation scheme, which was achieved for prototype studies presented here. Simulation of stronger shear may be approached by allowing plate length to vary independently of plate spacing, although this is beyond the scope of this preliminary investigation.

Perhaps the biggest weakness of the present iterative scheme is not calculating the plate number required for a given shear, although the graphical correlation presented as figure 3 provides a reasonable estimate for this equipment. Although inferior to Lloyd's scheme in this respect, the present iterative scheme does explicitly simulate zero vertical pressure gradient (suitable for boundary layer applications) and appears to be more reliable in uniform weak shear simulation (figure 4). The increasing plate spacing near the tunnel top appears to be characteristic for Lloyd's design scheme [Lloyd, 1967] although it is not made clear why this is the case. The effect of plate wakes as velocity defects in the downstream flow is undesirable,

although at only 1.3 tunnel heights downstream the measuring station is closer to the array than is standard for wind tunnel flow experiments [Lawson, 1980, p.80]. As demonstrated here, any uniform grid will allow the velocity defects to relax, with grid dimensions effecting downstream distance over which this occurs. Streamlined plates would also minimize this effect.

Scale-up from prototype to full-scale was straightforward, based on dynamic similarity for all equipment components (flat plates, gauzes and roughness elements), which probably constitutes adequate matching for agricultural applications given that the effects of plant canopy and vehicle wake have been neglected. A reasonable fit to the desired mean velocity profile was produced up to the boom height (z=0.5 m). Agreement was poorest in the vicinity of the wind tunnel floor, as the region of interaction of surface defined and grid defined turbulence length scales is the most difficult to physically simulate using wind tunnel baffles [Cook, 1978]. The Reynolds number of the wind tunnel velocity field was o(2×10^4) based on a typical plate spacing of 100 mm, which was of the same order as that estimated for the field condition (see introduction). Given that real uncertainties exist in the exact form of the logarithmic mean velocity profile above elastic plant canopies [Raupach and Thom, 1981], it is concluded that the experimental velocity profile is within acceptable limits for spray drift experimentation to begin. Above the plant canopy, the mean velocity profile is taken to be logarithmic, with zero-plane displacement neglected, as is standard practice (see chapter 1). Although the effect of this is to introduce uncertainty in roughness height, the best-fit to the experimental profile yielded a value of z_o=0.086 m, within the range for agricultural land (z_o=0.02-0.10 m, Anon [1978]).

6. Conclusions

1. For wind tunnel measurements of spray drift, the only requirement is to simulate the logarithmic mean velocity profile of the atmospheric boundary layer under typical spraying conditions. Matching atmospheric turbulence intensities and length scales is not a requirement.

2. A calculation scheme has been developed to specify the spacings within an array of flat plates to simulate weak shear flows with zero vertical pressure gradient, producing results comparable to the earlier design calculation of Lloyd [1967]. The balance of dynamic head to frictional loss in flow between any pair of plates in the array allows this scheme to be extended to flat plates with turbulence generators attached via an empirically-determined friction coefficient.

3. Restriction of this method to weak shear is a consequence of requiring uniform upstream static pressure; this may be maintained for more strongly-sheared profiles by introduction of plate length as an independent variable.

4. Simulation of more strongly sheared flows, such as the logarithmic mean velocity profile of the atmospheric boundary layer at 1:3.3 scale and full-scale, has been achieved using flat plates in combination with gauzes and surface roughness elements.

5. Streamwise turbulence intensity levels produced by flat plates are comparable to those produced in other studies, although the turbulence length scale is limited by local plate spacing or mixing grid dimension. This method is best suited to simulations where the turbulence field is not atmospherically-generated, such as a spray in a crosswind.

References

Anon [1978] ESDU 82026 (superceeds 72026) Characteristics of the wind speed in the lower layers of the atmosphere: Strong winds (neutral atmosphere). ESD item 82026, E.S.D.U.

Anon [1990] Pesticides: code of practice for the safe use of pesticides on farms and holdings. Part III of the Food and Environmental Protection Act, 1985. HMSO, London.

Armitt, J., and Counihan, J. [1968] The simulation of the atmospheric boundary layer in a wind tunnel. *Atmos. Env.*, **2**, 49-71.

Coelho, S.L.V., and Hunt, J.C.R. [1989] The dynamics of the near-field of strong jets in crossflows. *J. Fluid Mech.* **200**, 95-120.

Cook, N.J. [1978] Wind tunnel simulation of the atmospheric boundary layer by roughness, barrier and mixing device methods. *J. Wind Eng. Ind. Aero.* **3**, 157-176.

Counihan, J. [1969] An improved method of simulating an atmospheric boundary layer in a wind tunnel. *Atmos. Env.*, **3**, 197-214.

Gilbert, A.J. and Bell, G.J. [1988] Evaluation of drift hazards arising from pesticide spray application. *Aspects of Appl. Biol.* **17**, 363-375.

Irwin, H.P.A.H. [1981] The design of spires for wind simulation. *J. Wind Eng. Ind. Aero.* **7**, 361-366.

Lawson, T.V. [1980] *Wind Effects on Buildings. Part 1: Design Applications.* Applied Science Publishers, U.K.

Lloyd, A.R.J. [1967] The generation of shear flow in a wind tunnel.*Q. J. Roy. Met. Soc.* **93**, 79-96.

Maskell, E.C. [1963] A theory of the blockage effects on bluff bodies and stalled wings in a closed wind tunnel. *A.R.C. R & M,* **3400**, HMSO, London.

Miller, P.C.H. [1988] Engineering aspects of spray drift control. *Aspects of Applied Biology*, **17**, 377-384.

Miller, P.C.H., Mawer, C.J. and Merritt, C.R. [1989] Wind tunnel studies of the spray drift from two types of agricultural spray nozzle. *Aspects of Appl. Biol.* **21**, 237-238.

Nishi, A. and Miyagi, H. [1995] Computer-controlled wind-tunnel for wind-engineering applications. *J. Wind Eng. Ind. Aero.* **54**, 493-504.

Owen, P.R. and Zienkiewicz, H.K. [1957] The production of shear flow in a wind tunnel. *J. Fluid Mech.* **2**, 521-531.

Pankhurst, R.C. and Holder, D.W. [1952] *Wind Tunnel Technique.* Pitman, London.

Plate, E.J.(ed.) [1982] *Engineering Meteorology.* Elsevier, Amsterdam.

Raupach, M.R. and Thom, A.S. [1981] Turbulence in and above plant canopies. *Ann. Rev. Fluid Mech.* **13**, 97-129.

Rutherford, I., Bell, G.J., Freer, J.B.S., Herrington, P.J. and Miller, P.C.H. [1989] An evaluation of chemical application systems. *Proc. British Crop Protection Conf.-Weeds*, 601-613.

Schlichting, H. [1968] *Boundary-Layer Theory.* 6th ed. McGraw-Hill, New York.

Teunissen, H.W. [1975] Simulation of the planetary boundary layer in a multiple jet wind tunnel. *Atmos. Env.* **9**, 154-174.

Western, N.M. Hislop, E.C., Herrington, P.J. and Jones, E.I. [1989] Comparative drift measurements for BCPC reference nozzles and for an Airtec twin-fluid nozzle under controlled conditions. *Proc. British Crop Protection Conference - Weeds*, 641-648.

Figures

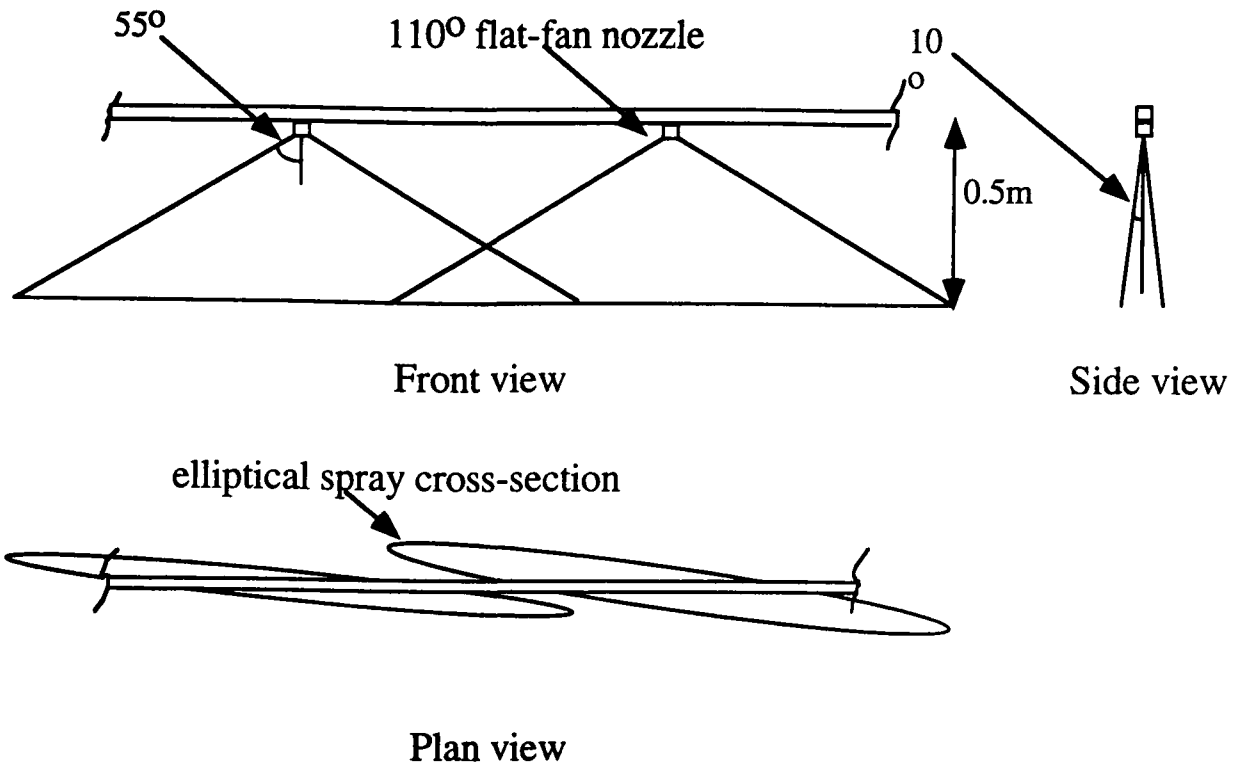

1. Typical geometry and arrangement of 110° agricultural flat-fan sprays on a boom. The front view corresponds to vehicle motion out of the page.

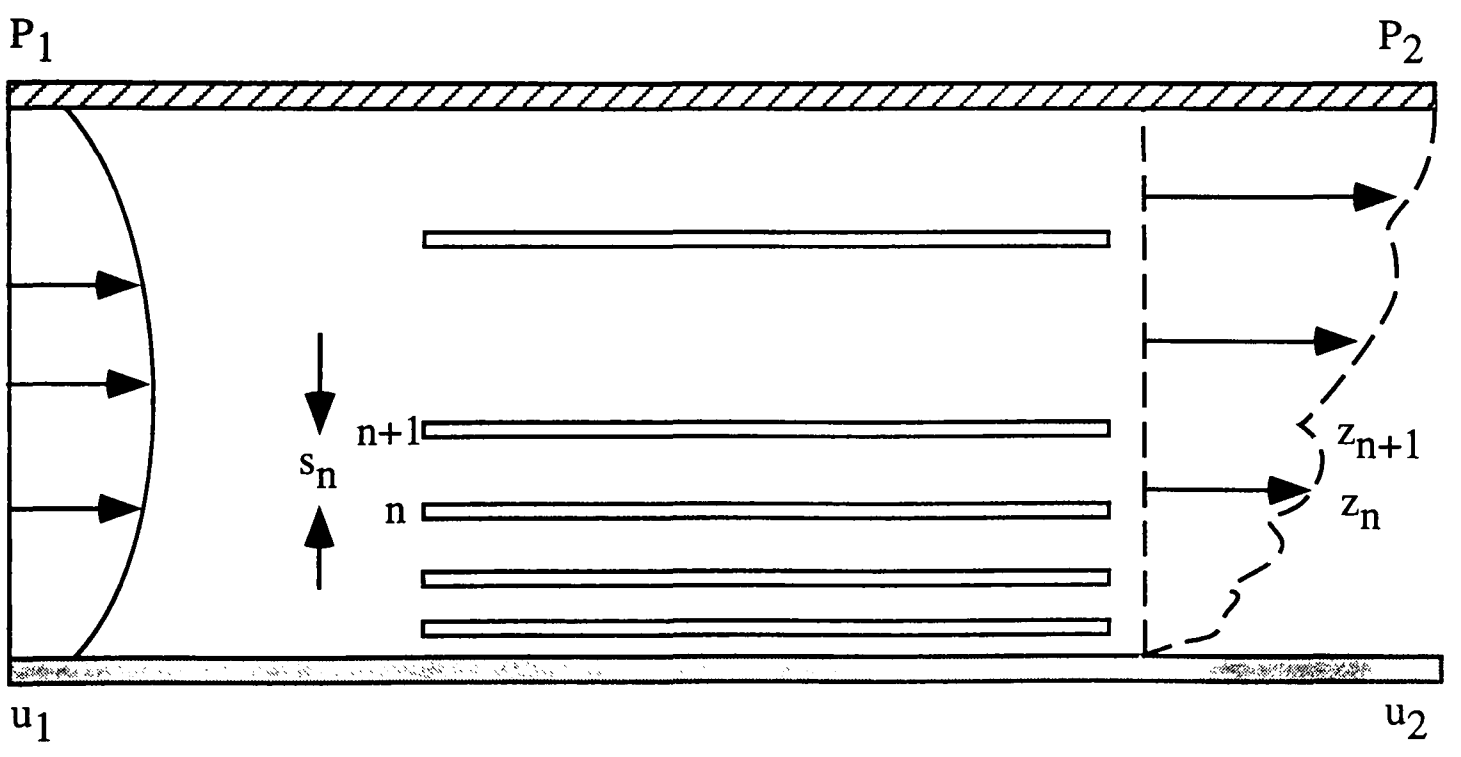

2. Schematic diagram of the array of differentially-spaced flat plates in the wind tunnel. Notation as for equation (2) in the text.

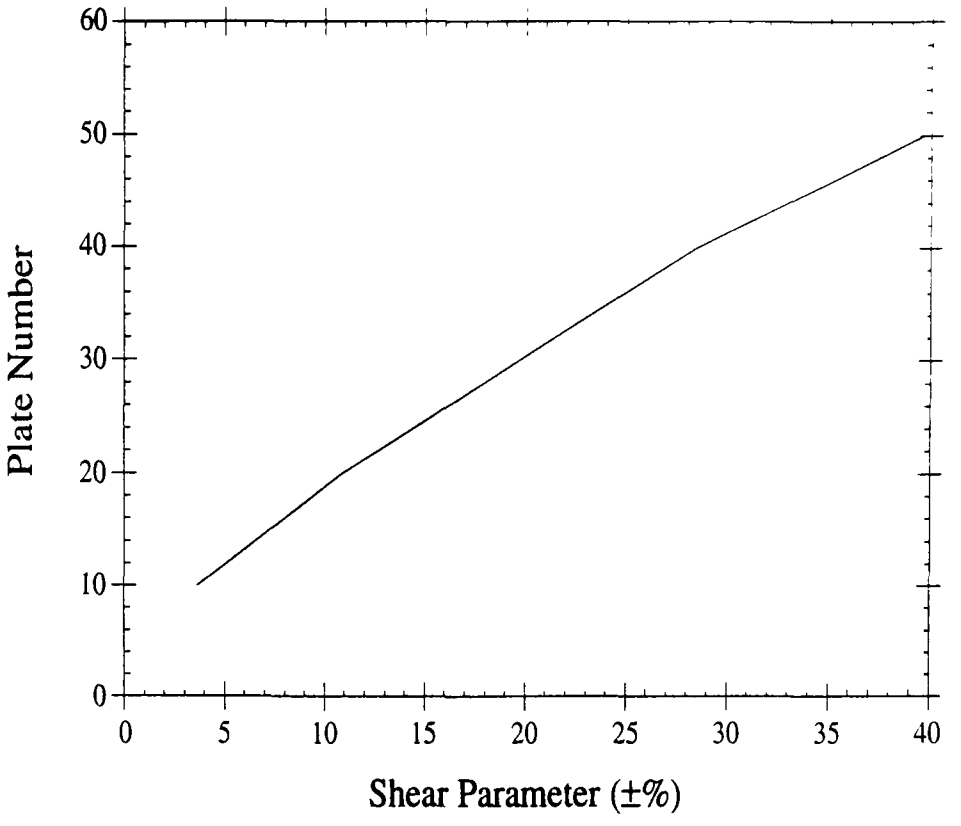

3. The number of plates required to simulate a uniform shear flow with a specified shear parameter (maximum velocity variation as a proportion of centreline velocity), calculated using Lloyd's [1967] calculation scheme.

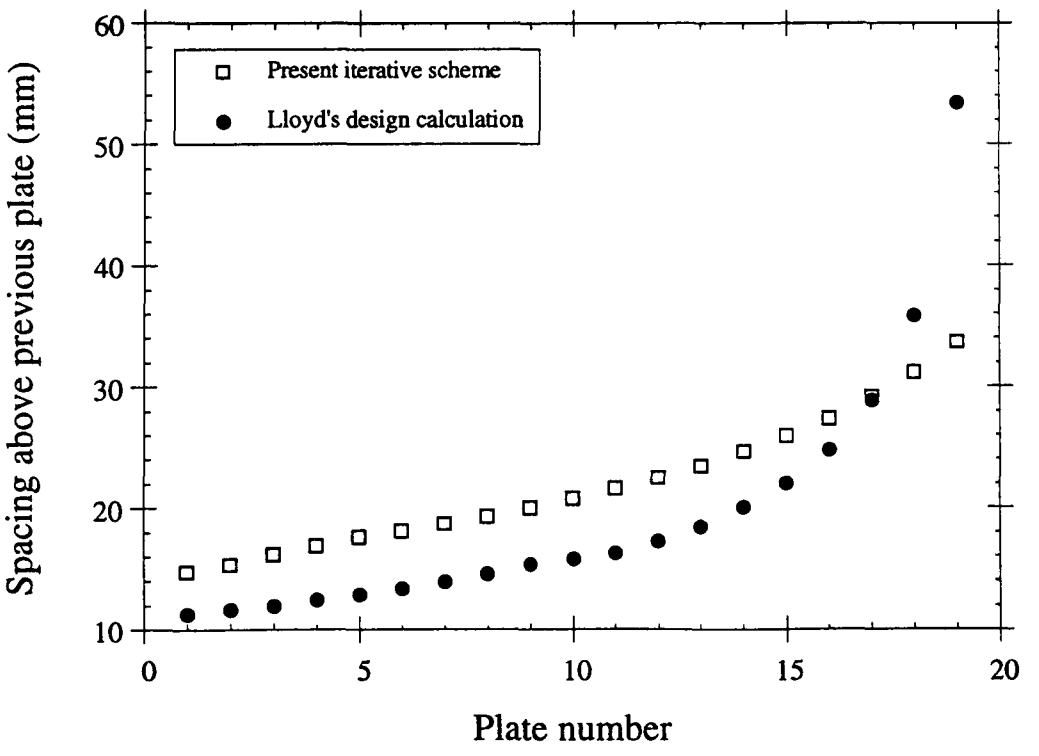

4. Comparison of plate spacings calculated using the present iterative scheme and Lloyd's [1967] scheme for simulation of weak shear flow (maximum velocity variation ±10% of centreline velocity).

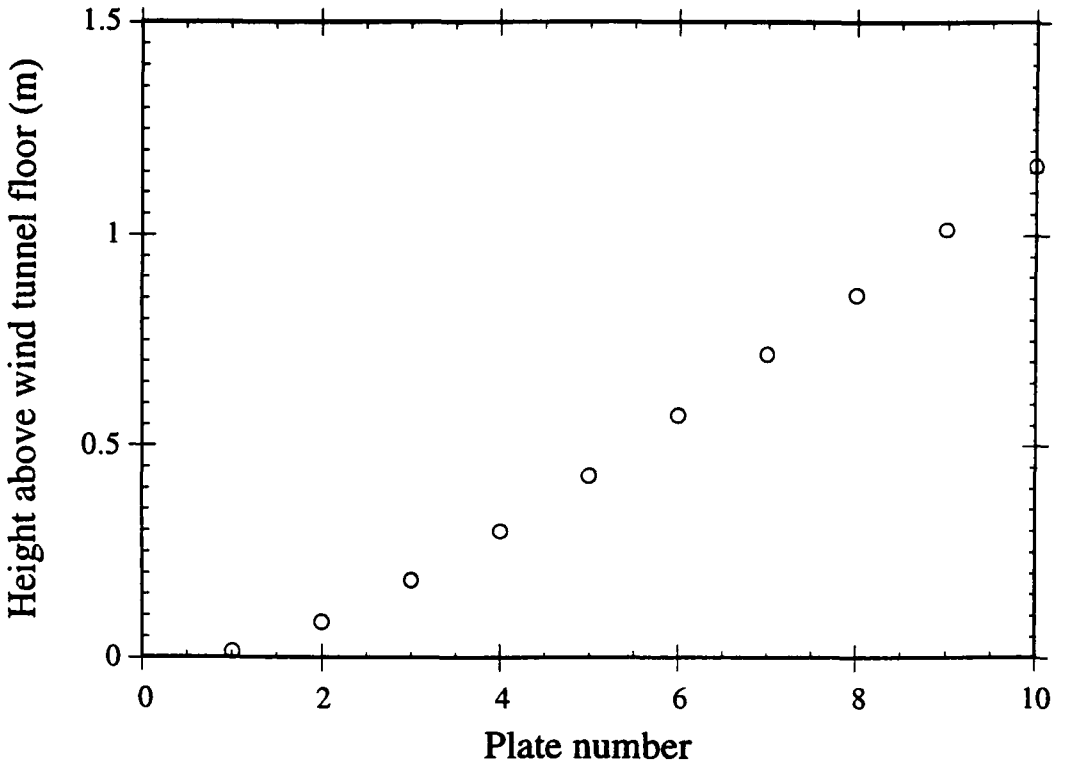

5. Spacings of an array of 10 plates for the simulation of the logarithmic mean velocity profile over typical agricultural land (z_o=0.03 m) at full-scale, calculated using the present iterative scheme.

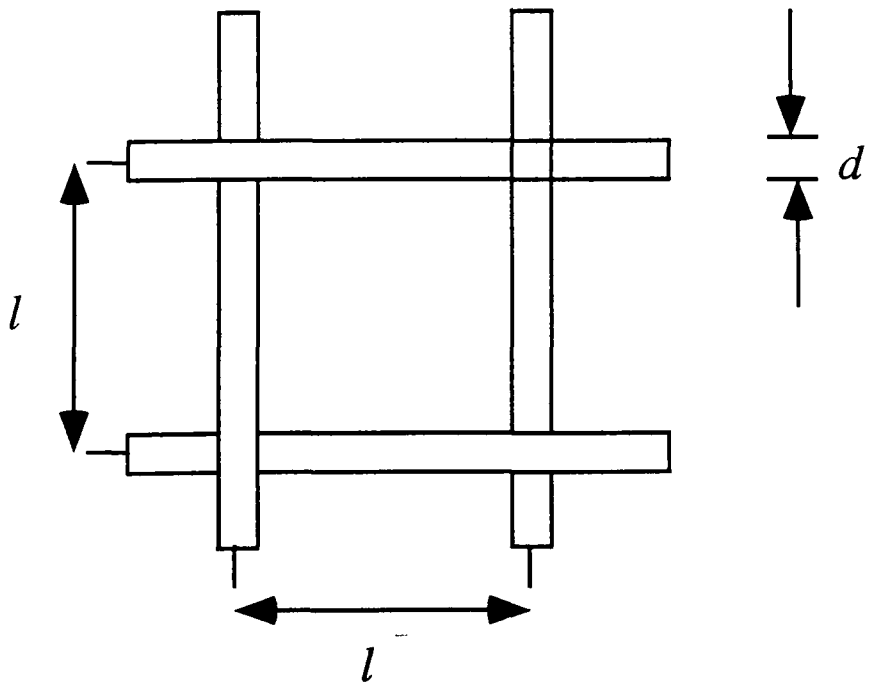

6. Definition sketch of gauze structure (after Pankhurst and Holder, 1952). l and d are the length and bar diameter respectively of the gauze cell.

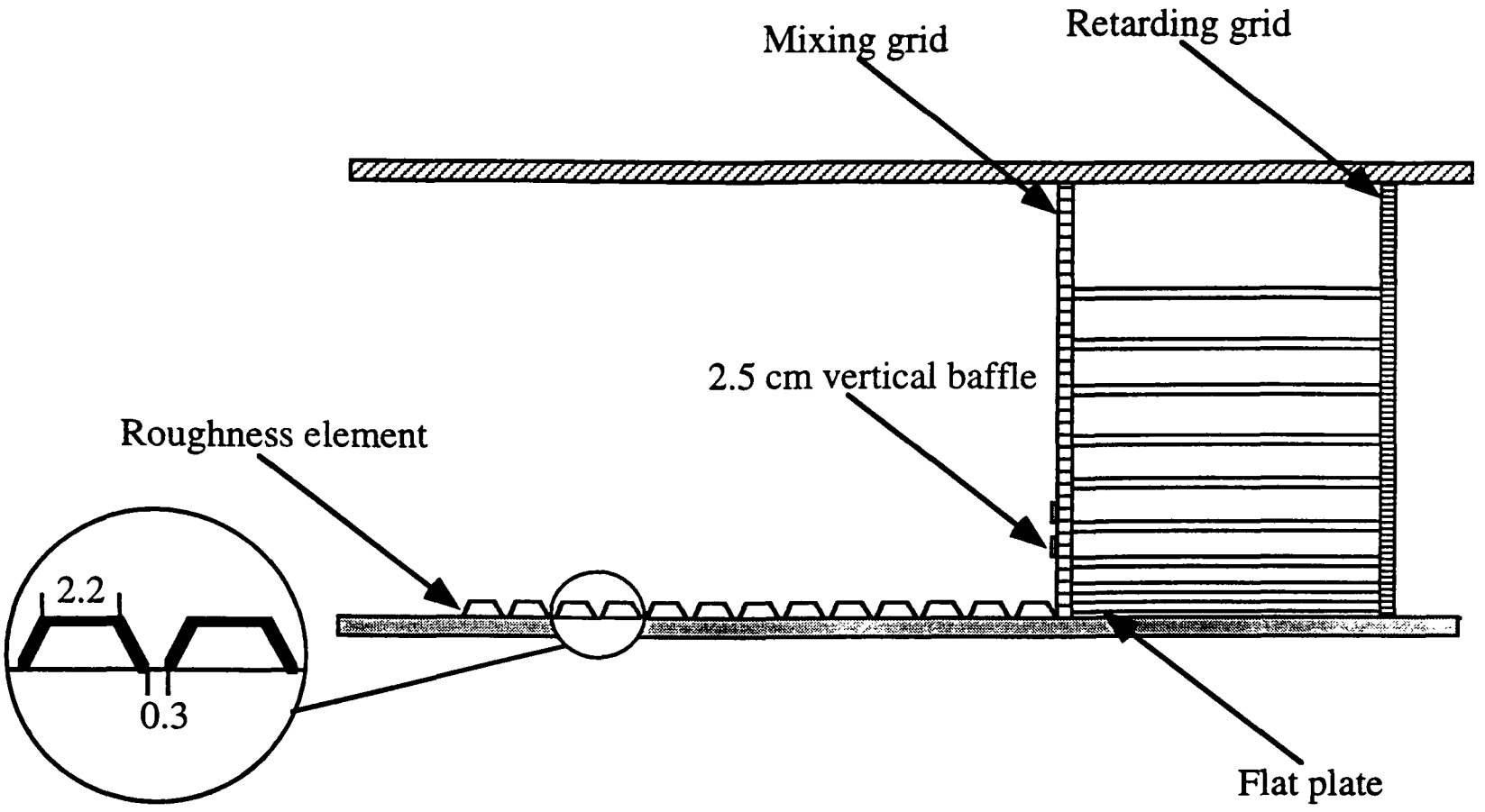

7. Final equipment arrangement for prototype scale (1:3.3) simulation of the logarithmic mean velocity profile (drawn approximately to scale, roughness element dimensions in cm). Flow direction is right to left.

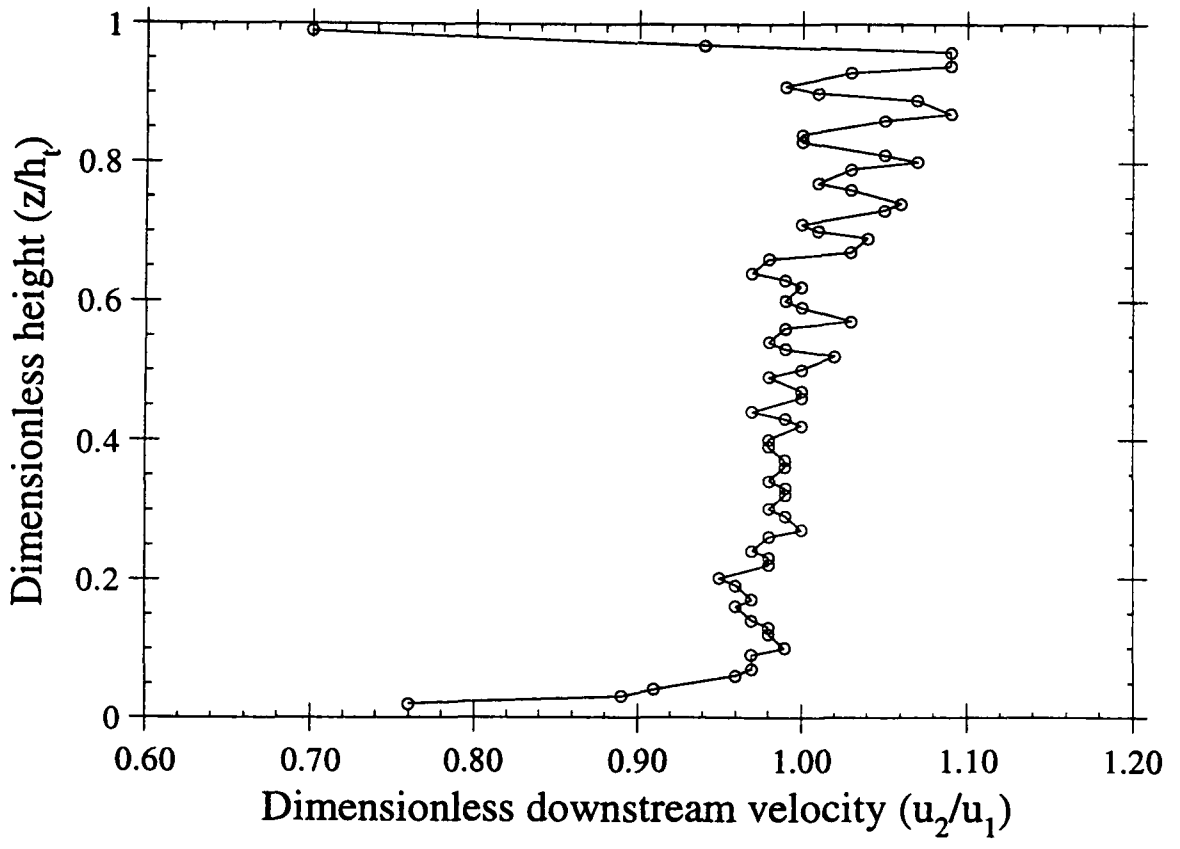

8. Mean velocity profile produced using the present iterative calculation scheme to simulate weak shear flow (maximum velocity variation ±10% of centreline velocity).

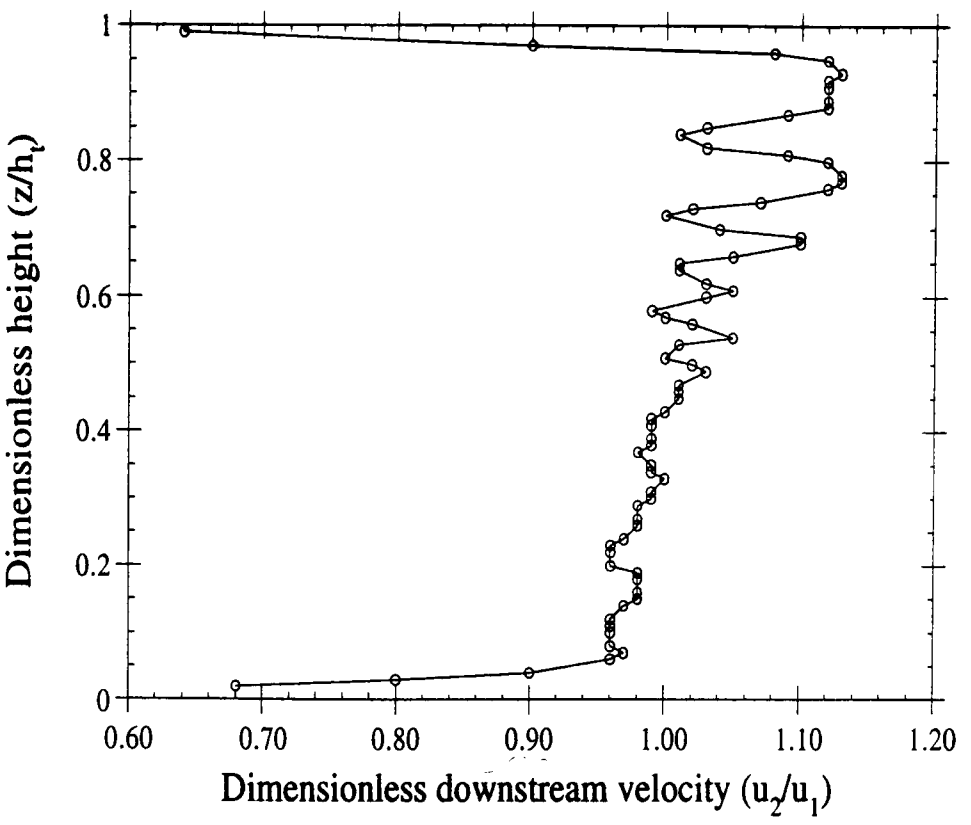

9. Mean velocity profile produced using Lloyd's [1967] calculation scheme to simulate weak shear flow (maximum velocity variation ±10% of centreline velocity).

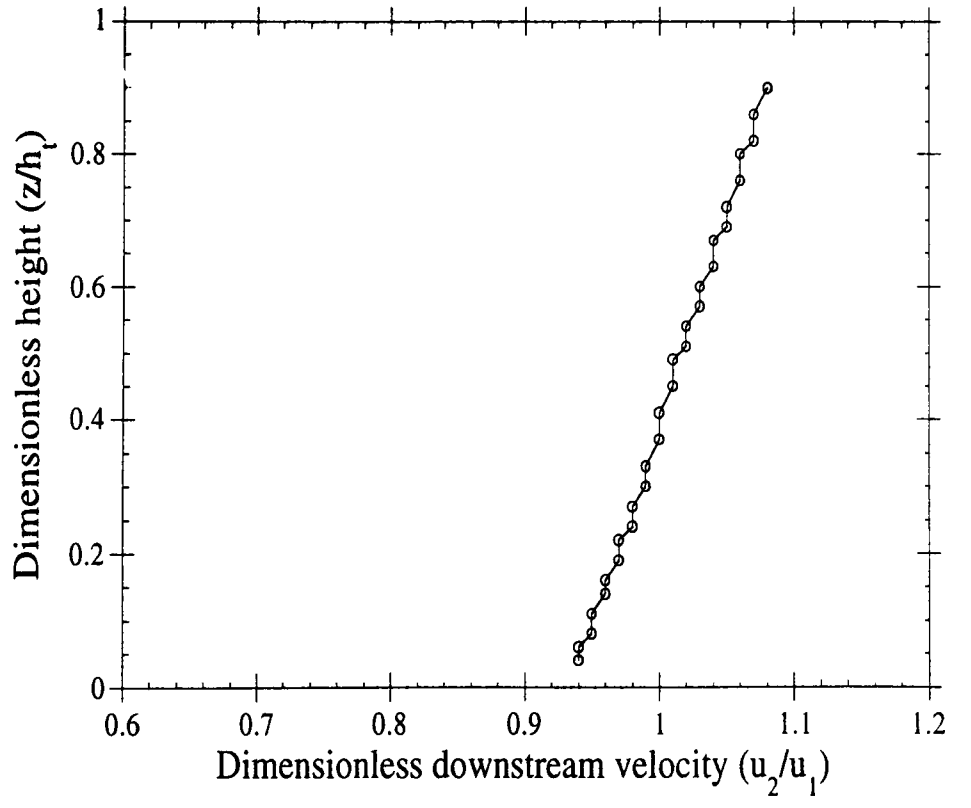

10. Mean velocity profile produced using the present iterative calculation scheme to simulate weak shear flow (maximum velocity variation ±10% of centreline velocity) with mixing grid added.

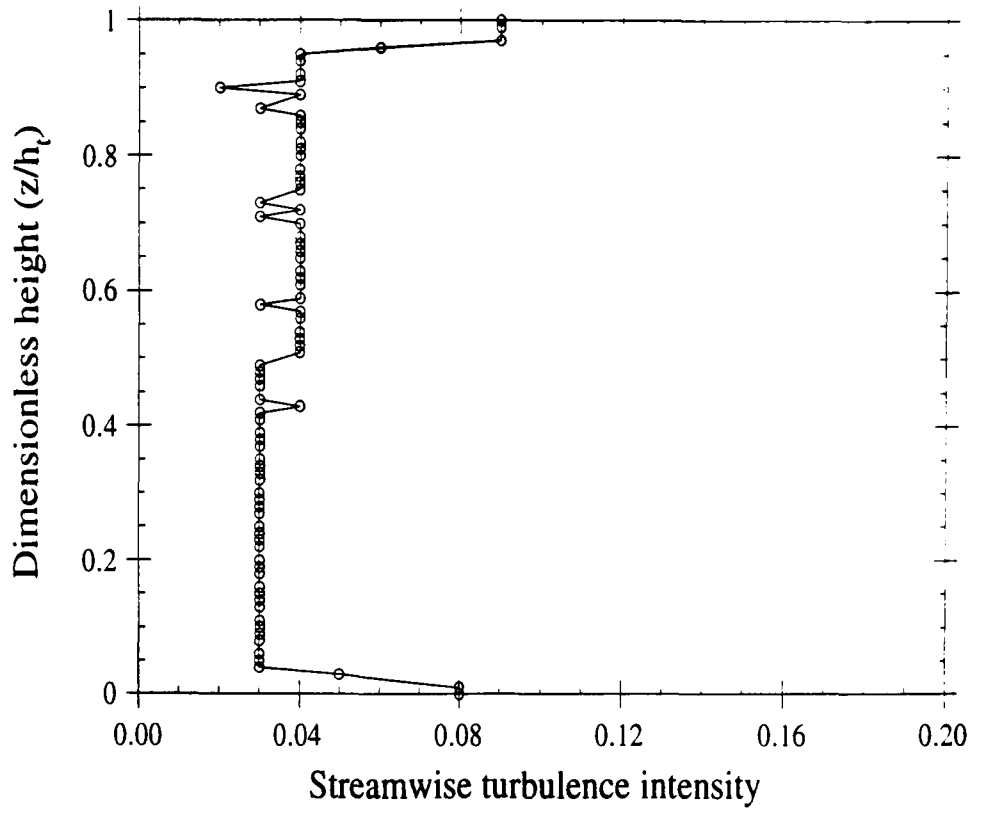

11. Streamwise turbulence intensity profile produced using the present iterative calculation scheme to simulate weak shear flow (maximum velocity variation ±10% of centreline velocity).

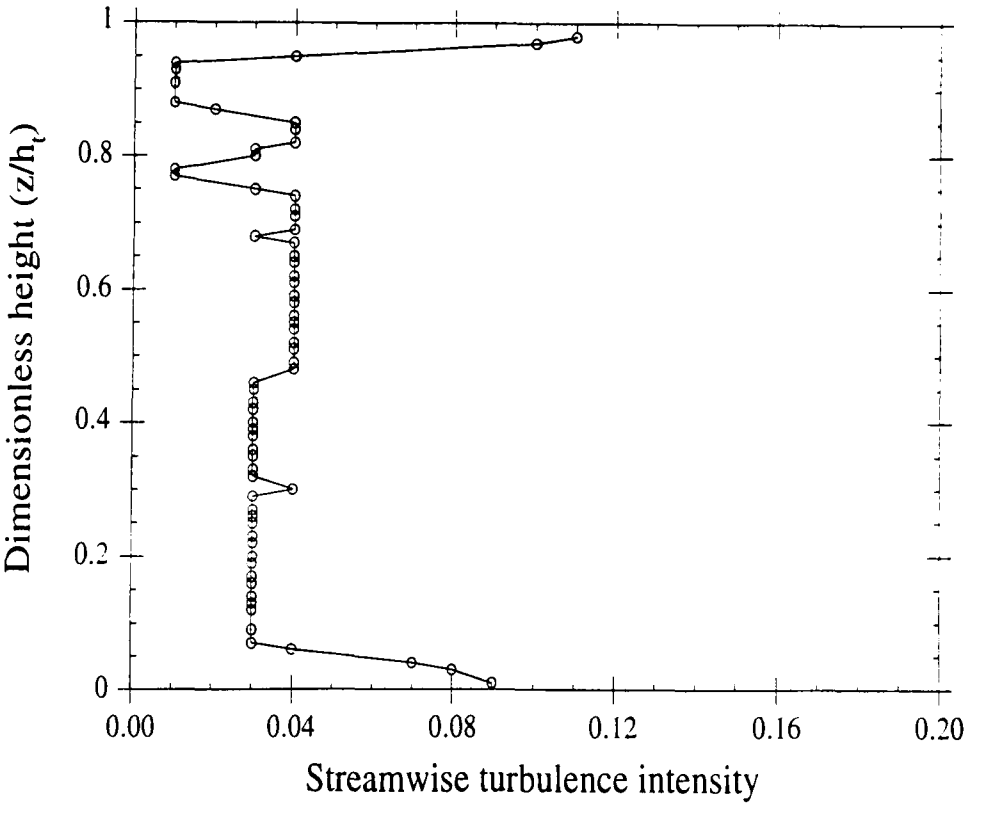

12. Streamwise turbulence intensity profile produced using Lloyd's [1967] calculation scheme to simulate weak shear flow (maximum velocity variation ±10% of centreline velocity).

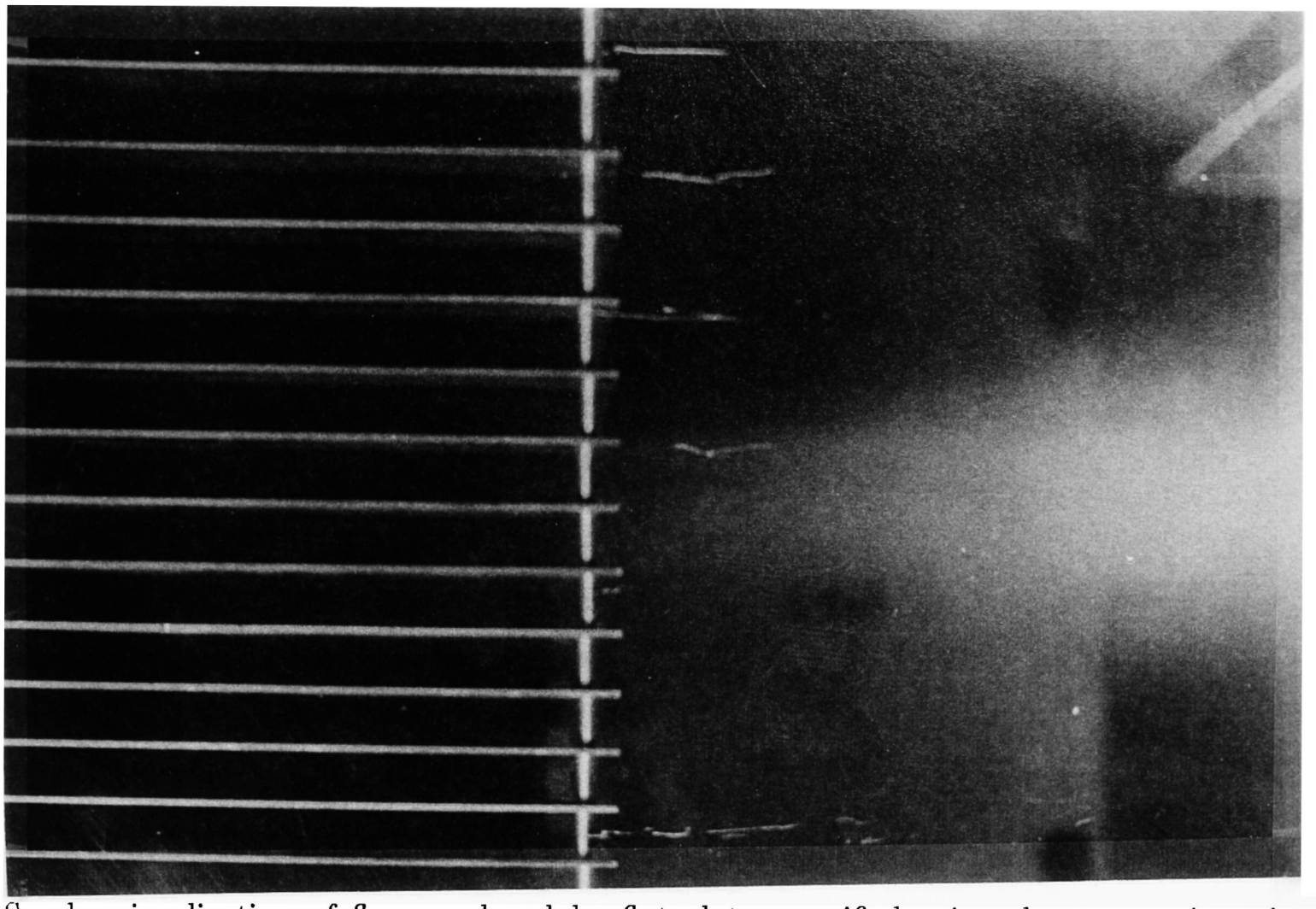

13. Smoke visualisation of flow produced by flat plates specified using the present iterative calculation scheme to simulate weak shear flow (maximum velocity variation ±10% of centreline velocity). Side view of the flat plate array in the wind tunnel with flow direction left to right, showing negligible deflection of the smoke tracer indicating approximately zero vertical pressure gradient in the downstream flow.

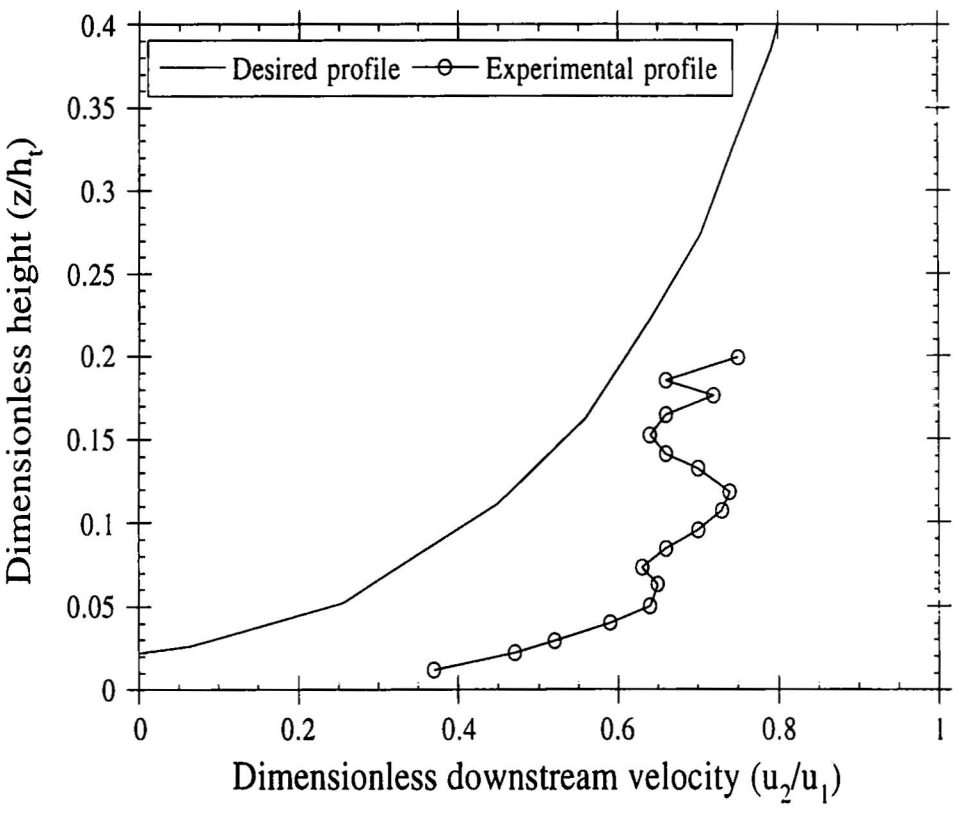

14. Mean velocity profile produced using the present iterative scheme to simulate the logarithmic mean velocity profile at prototype (1:3.3) scale. The velocity profile produced using flat plates only is shown compared to the design logarithmic profile.

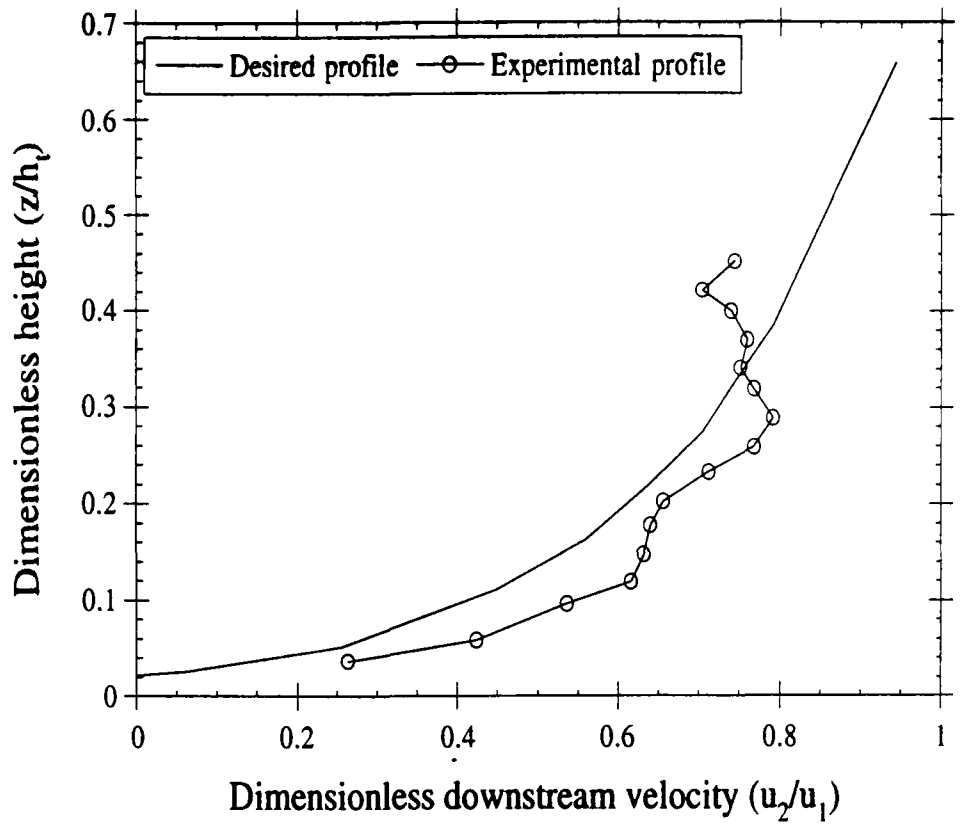

15. Mean velocity profile produced using the present iterative scheme to simulate the logarithmic mean velocity profile at prototype (1:3.3) scale. The velocity profile produced using flat plates and retarding and mixing grids is shown compared to the design logarithmic profile.

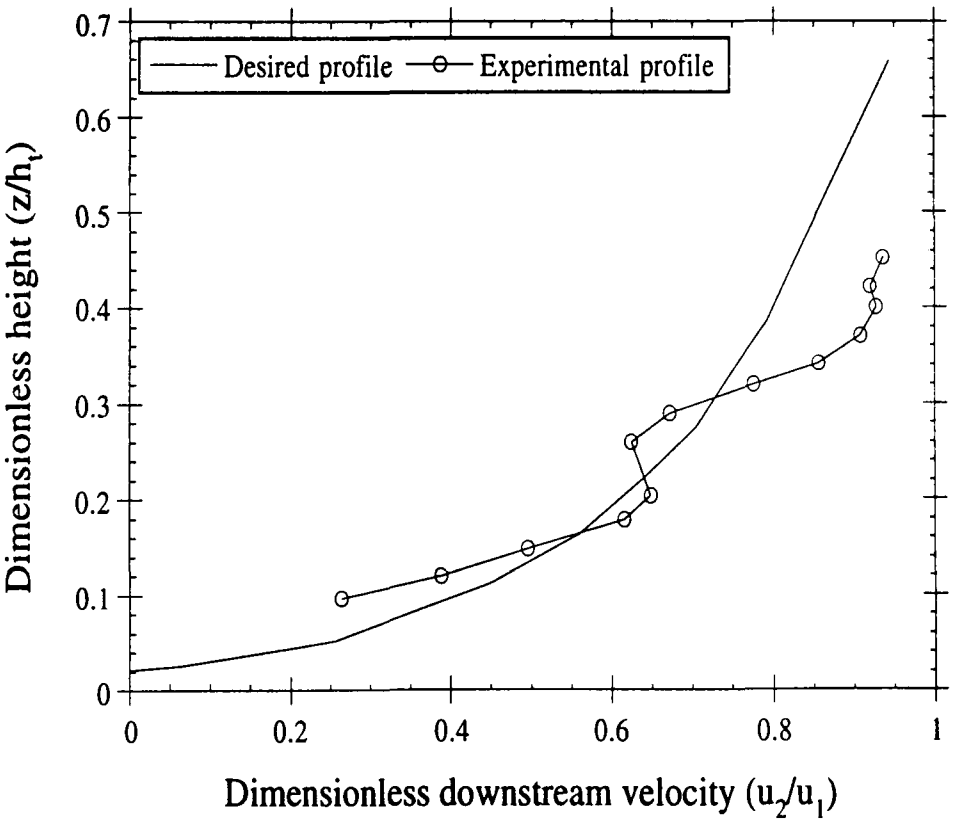

16. Mean velocity profile produced using the present iterative scheme to simulate the logarithmic mean velocity profile at prototype (1:3.3) scale. The velocity profile produced using flat plates and retarding and mixing grids and floor roughness elements is shown compared to the design logarithmic profile.

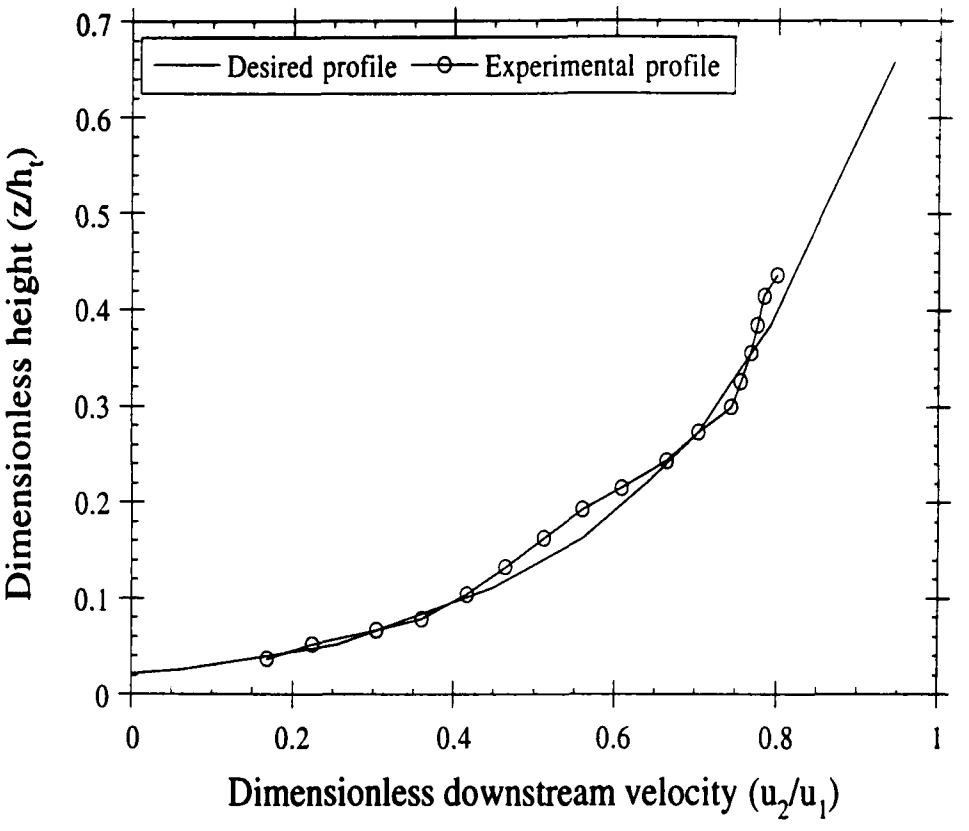

17. Mean velocity profile produced using the present iterative scheme to simulate the logarithmic mean velocity profile at prototype (1:3.3) scale. The final mean velocity profile is shown compared to the design logarithmic profile.

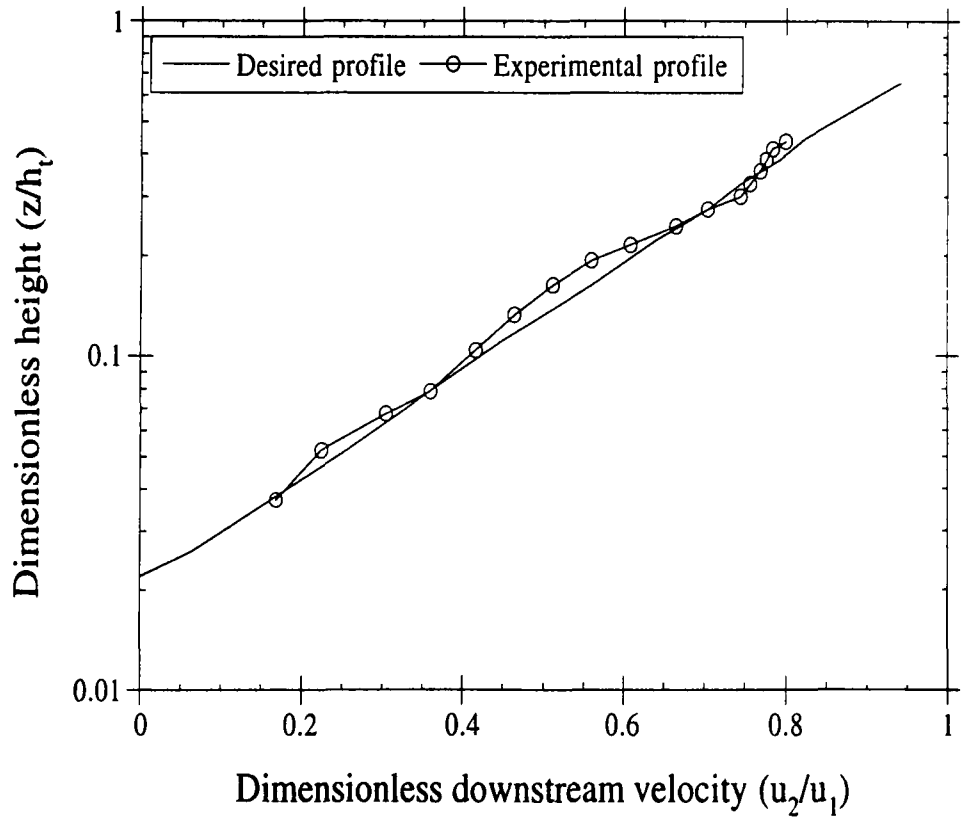

18. Mean velocity profile produced using the present iterative scheme to simulate the logarithmic mean velocity profile at prototype (1:3.3) scale. The final mean velocity profile is shown compared to the design logarithmic profile, re-plotted in log-linear form.

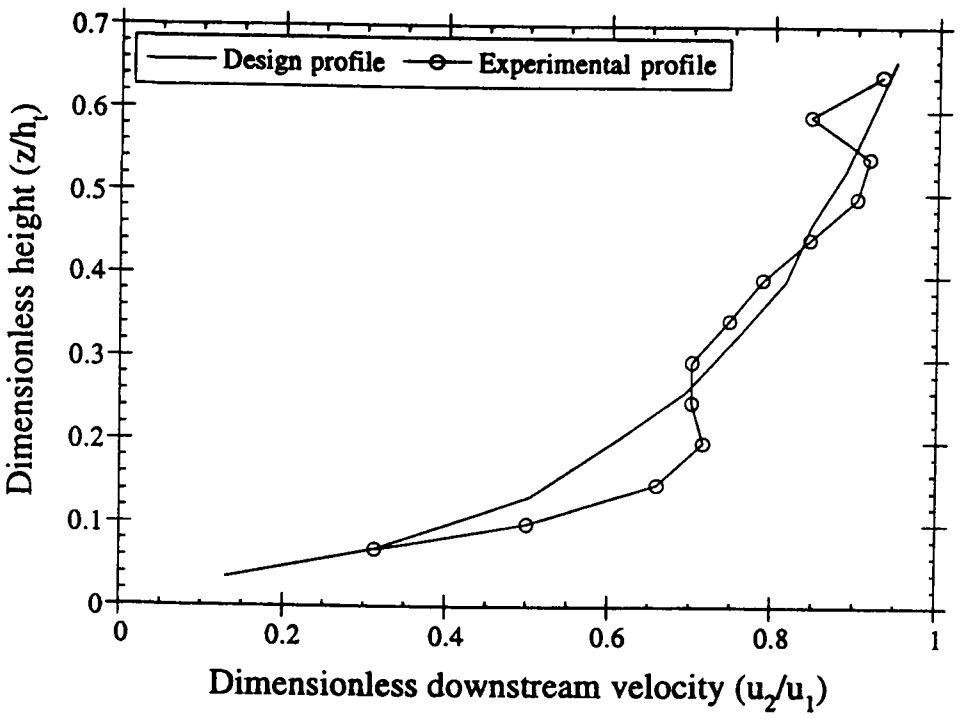

19. Full-scale simulation of the logarithmic mean velocity profile over typical agricultural land. The mean velocity profile produced using equipment scaled-up from the 1:3.3 scale simulation is shown compared to the design logarithmic profile.

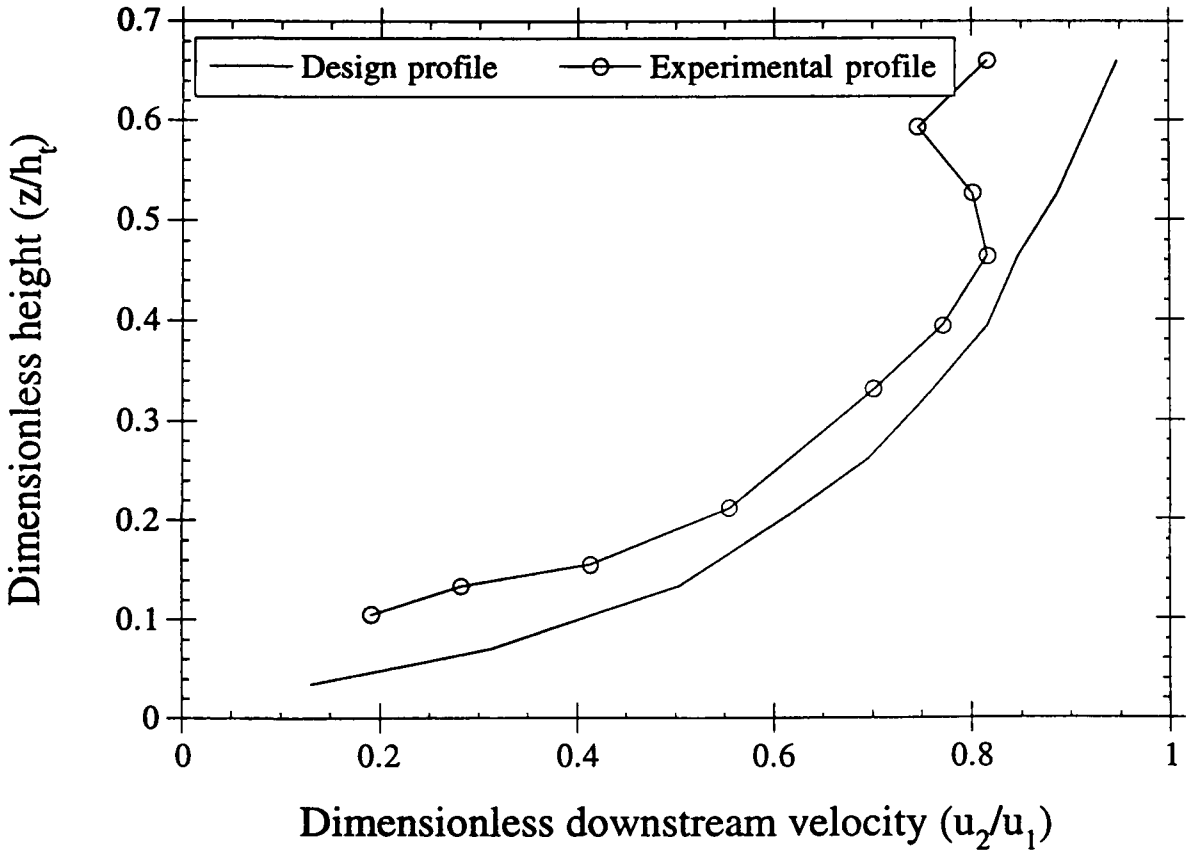

20. Full-scale simulation of the logarithmic mean velocity profile over typical agricultural land. The mean velocity profile produced using the final equipment configuration is shown compared to the design logarithmic profile.

21. Final equipment configuration for full-scale simulation of the logarithmic mean velocity profile over typical agricultural land installed in the Eiffel-type wind tunnel. Height of diffuser section is 1.5 m (photograph courtesy of Silsoe Research Institute).

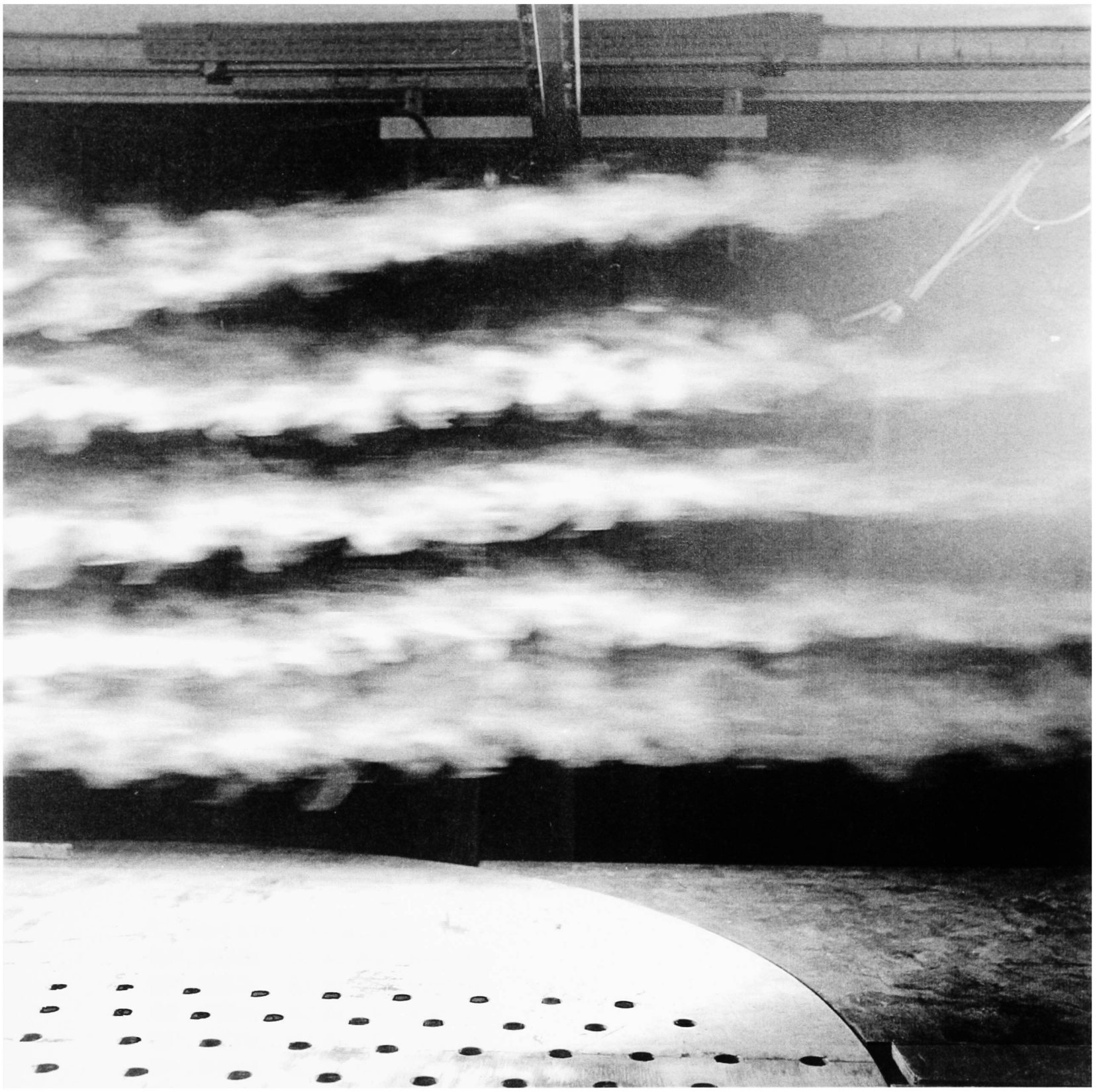

22. Smoke visualisation of the downstream vertical pressure gradient and turbulence length scale produced by the final equipment configuration for full-scale simulation of the logarithmic mean velocity profile over typical agricultural land. The flow direction is right to left, showing negligible deflection of the smoke tracer indicating approximately zero vertical pressure gradient in the downstream flow. Typical turbulence length scales in the smoke tracers are about 0.1 m. Note the effect of the roof-mounted traverse 1.5 m above wind tunnel floor, 2 m downstream of the flat plate array (photograph courtesy of Silsoe Research Institute).

Appendix 1. Coded Form of the Present Iterative Scheme

The present iterative scheme, coded into the ASYST macro language (as utilised in this study) is listed below.

```
FORGET.ALL
ECHO.OFF

\ Define arrays
DP.REAL DIM[ 50 ] ARRAY []SPOD
DP.REAL DIM[ 50 ] ARRAY []SPNW
DP.REAL DIM[ 50 ] ARRAY []PRES
DP.REAL DIM[ 50 ] ARRAY []VELC
DP.REAL DIM[ 50 ] ARRAY []CNTR
DP.REAL DIM[ 50 ] ARRAY []CDRG
DP.REAL DIM[ 50 ] ARRAY []ERRO
DP.REAL DIM[ 50 ] ARRAY []STAR
DP.REAL DIM[ 50 ] ARRAY []UPHD
DP.REAL DIM[ 50 ] ARRAY []DOHD
DP.REAL DIM[ 50 ] ARRAY []FLHD
DP.REAL DIM[ 50 ] ARRAY []PRT2
DP.REAL DIM[ 50 ] ARRAY []PRT3
DP.REAL DIM[ 50 ] ARRAY []PRT4
DP.REAL DIM[ 50 ] ARRAY []FRHD
DP.REAL DIM[ 50 ] ARRAY []SSUM
DP.REAL DIM[ 50 ] ARRAY []DDHD
DP.REAL DIM[ 50 ] ARRAY []DSHD
DP.REAL DIM[ 50 ] ARRAY []DSTH

\ Define scalars
DP.REAL SCALAR #AVIS
DP.REAL SCALAR #ARHO
DP.REAL SCALAR #GRAV
DP.REAL SCALAR #RHOG
DP.REAL SCALAR #ADEN
DP.REAL SCALAR #BFNB
DP.REAL SCALAR #BFSP
DP.REAL SCALAR #ERRO
DP.REAL SCALAR #LENG
DP.REAL SCALAR #MPRS
DP.REAL SCALAR #SPSM
DP.REAL SCALAR #UINI
DP.REAL SCALAR #WTWD
DP.REAL SCALAR #ZOLD
DP.REAL SCALAR #ZNEW
DP.REAL SCALAR #PRT1
DP.REAL SCALAR #FRST
DP.REAL SCALAR #DELP
DP.REAL SCALAR #SCND
DP.REAL SCALAR #SSTA
DP.REAL SCALAR #FACT
INTEGER SCALAR #INUM

\ Define menus
MENU JSHEAR.MENU/
```

```
\ Define constants
0.0000155 #AVIS :=
1.17 #ARHO :=
9.81 #GRAV :=
11.478 #RHOG :=


\ Initialise parameters
5.0    #UINI :=
8.0    #BFNB :=
0.305   #LENG :=
0.457   #WTWD :=

\ Set initial values
: CD.VALU.SET
      #WTWD #BFNB 1 + / #BFSP :=
      #BFNB 2 + 1 DO
                  #BFSP []SPOD [ I ] :=
      LOOP
;

\ Calculate the centreline heights above the floor
: CD.CNTR.POS
      0.0 #ZOLD :=
      #BFNB 2 + 1 DO
                  []SPOD [ I ] 2.0 / #ZOLD + #WTWD / []CNTR [ I ] :=
                  []SPOD [ I ] #ZOLD + #ZOLD :=
      LOOP
;

\ Define the velocity profile required
: CD.PROF.VEL
      #BFNB 2 + 1 DO
                  3.531 1.269 []CNTR [ I ] * + []VELC [ I ] :=
      LOOP
;

\ Calculate the drag coefficient on for each plate
: CD.DRAG.COF
      #BFNB 2 + 1 DO
                  #UINI []VELC [ I ] + 2.0 /
                  #LENG * #AVIS /
                  SQRT 1.328 SWAP / []CDRG [ I ] :=
      LOOP
;
\ Calculate the pressure distribution

: CD.PRES.DIS
      #BFNB 2 + 1 DO
         #UINI DUP * #PRT1 :=
         []VELC [ I ] DUP * []PRT2 [ I ] :=
         #UINI []VELC [ I ] + DUP * []PRT3 [ I ] :=
         #LENG []CDRG [ I ] * 4.0 []SPOD [ I ] * / []PRT4 [ I ] :=
         #PRT1 []PRT2 [ I ] - []PRT3 [ I ] []PRT4 [ I ] * - []PRES [ I ] :=
```

```
            []PRES [ I ] #GRAV  / []DSHD [ I ] :=
        LOOP
;

\ Calculate the mean pressure
: CD.PRES.MEN
        0.0 #MPRS :=
        #BFNB 2 + 1 DO
                    []PRES [ I ] []SPNW [ I ] * #MPRS + #MPRS :=
        LOOP
        #MPRS #WTWD / #MPRS :=
        #MPRS .
;

\ Calculate the spacing associated with the mean pressure
: CD.STAR.DIS
        0.0 #SSTA :=
        #BFNB 2 + 1 DO
                    #MPRS #GRAV /
                    #GRAV 2.0 *
                    #PRT1 SWAP / +
                    #GRAV 2.0 *
                    []PRT2 [ I ]  SWAP / - []FLHD [ I ] :=
                    []CDRG [ I ] #LENG *
                    #GRAV 8.0 * /
                    []PRT3 [ I ] * []FRHD [ I ] :=
                    []FRHD [ I ] []FLHD [ I ] / []STAR [ I ] :=
                    []STAR [ I ] #SSTA + #SSTA :=
                    []DDHD [ I ] []DSHD [ I ] + []DSTH [ I ] :=
        LOOP
;

\ Calculate the downstream dynamic head
: CD.DDHD.SUM
        #BFNB 2 + 1 DO
                    #GRAV 2.0 *
                    []PRT2 [ I ] SWAP / []DDHD [ I ] :=
        LOOP
;

\ Calculate the sum of star spacings and determine factor
: CD.STAR.SUM
        #SSTA #WTWD SWAP / #FACT :=
;

\ Calculate the new baffle spacing
: CD.SPAC.NEW
        0.0 #SPSM :=
        #BFNB 2 + 1 DO
                    []STAR [ I ] #FACT * []SPNW [ I ] :=
                    []SPNW [ I ] #SPSM + #SPSM :=
        LOOP
        []SPNW #WTWD * #SPSM / []SPNW :=
```

```
\ Check errors in the spacing estimate
: CD.ERRO.CAL
      0.0 #ERRO :=
      []SPNW []SPOD - []ERRO :=
      #BFNB 2 + 1 DO
                []ERRO [ I ]
                0 <> IF []ERRO [ I ] ABS #ERRO + #ERRO :=
                     THEN
      LOOP
      #ERRO .
      []SPNW []SPOD :=
;

\ Print the result to the screen
: CD.PRNT.RES
      #BFNB 2 + 1 DO
                CR []SPNW [ I ] .
      LOOP
;

\ Calculate the baffle spacing
: CD.CALC.BAF
      0 #INUM :=
      CD.VALU.SET
      BEGIN
        #INUM 1 + #INUM :=
        CD.CNTR.POS
        CD.PROF.VEL
        CD.DRAG.COF
        CD.PRES.DIS
        CD.PRES.MEN
        CD.STAR.DIS
        CD.STAR.SUM
        CD.DDHD.SUM
        CD.SPAC.NEW
        CD.ERRO.CAL
        #ERRO 0.0005 <
      UNTIL
      CD.PRNT.RES
;

\ Define menus
JSHEAR.MENU
    " Wind Tunnel Shear Layer Development" MENU.TITLE
    MENU.BLOW.UP
    0 10 20 58 MENU.SHAPE
    7 1 MENU.COLOR
    14 MENU.PROMPT.COLOR
    01 06 " The initial ambient velocity :" MENU.ITEM{ #UINI }
    02 06 " The number of baffles        :" MENU.ITEM{ #BFNB }
    03 06 " The baffle length            :" MENU.ITEM{ #LENG }
    04 06 " Wind tunnel width            :" MENU.ITEM{ #WTWD }
    06 06 " Calculate baffle spacing      " MENU.ITEM{ CD.CALC.BAF }
```

```
MENU.END

: START
      STACK.CLEAR
      NORMAL.DISPLAY
      JSHEAR.MENU MENU.EXECUTE
      NORMAL.DISPLAY
;
```

Appendix 2. Regression Analysis

Linear regression analysis was used to examine how closely the wind tunnel data fitted the design logarithmic velocity profile. The data was fitted by the logarithmic-linear relationship

$$lnz = b\overline{u} + a. \tag{A1}$$

In this analysis, it was assumed that the mean velocity has been measured without error and that the position of the hot-wire probe (z value) will show a random variation and be normally distributed about a true mean. The variance of individual z-values about their true value is the same for all mean velocity measurements.

The values of a and b are estimated from the data (chapter 2, figure 17) so that the maximum variation in z is accounted for in terms of the variation in the mean velocity. The departure from a linear relationship is assessed in terms of the sum of squares of the deviation from the values predicted by the regression equation

$$b = \frac{\text{covariance}(\overline{u}z)}{\text{variance}(\overline{u})} \tag{A2}$$

$$b = \frac{\delta\overline{u}z - \frac{(\delta\overline{u})(\delta z)}{n}}{\delta\overline{u}^2 - \frac{(\delta\overline{u})^2}{n}}. \tag{A3}$$

For the experimental and theoretical data, the values of b were 0.291 and 0.297 respectively. Although these values appear to be similar, further statistical tests were applied to see if the difference between them was significant.

The regression coefficients b_{10} (for the theoretical logarithmic profile) and b_{31} (for the experimental data) were tested against the null hypothesis

$$H_o : B_{31} - B_{10} = 0$$

$$H_1 : B_{31} - B_{10} \neq 0. \tag{A4}$$

The test statistic, t_c, was defined as,

$$t_c = \frac{b_{31} - b_{10}}{S\epsilon(b_{31} - b_{10})} \tag{A5}$$

$$t_c = \frac{b_{31} - b_{10}}{\sqrt{\frac{S\epsilon^2}{\sum(x_{31} - \overline{x_{31}})^2} + \frac{S\epsilon^2}{\sum(x_{10} - \overline{x_{10}})^2}}} \tag{A6}$$

where $S\epsilon^2$ is the variation not accounted for by regression i.e. residual variation. The value of t_c was determined from the data presented in chapter 2, figure 17, yielding t_c=-0.085. This value was compared with t-tables for $t_{\frac{\alpha}{2}}$ with α=0.05 (i.e. 95% confidence level). This gave $t_{\frac{\alpha}{2}}=\pm 2.243$ and since $t_c \geq t_{\frac{\alpha}{2}}$, the null hypothesis H_o is accepted. There is no significant difference between the experimental data and the design logarithmic velocity profile at the 95% confidence level.

CHAPTER 3. COMPARATIVE FIELD AND WIND TUNNEL MEASUREMENTS OF AIRBORNE DRIFT PRODUCED BY SINGLE STATIC FLAT-FAN SPRAYS

Summary

Field and wind tunnel measurements of airborne spray volume produced by a single static nozzle are compared. In each case, the spray major axis was aligned parallel to the cross flow, representative of the action of a cross wind perpendicular to the direction of vehicle motion. Two wind tunnel velocity fields were used, both adequately simulating the logarithmic mean velocity profile over typical agricultural land (but with different near-canopy profiles). Two spray nozzles were used, classified as producing fine and medium spray by the British Crop Protection Council scheme. Airborne spray volume (as % nozzle output) averaged through a plane 2 m by 0.5 m, 2 m downwind of the nozzle (representative of drift in the spray near-field) increases approximately exponentially with cross flow velocity, with rate increasing from medium to fine nozzles. Vertical profiles of airborne spray volume decrease approximately exponentially with height for all combinations of cross flow conditions and nozzle sizes. Good reproduction of field vertical profiles is obtained in wind tunnel simulations, suggesting a similar origin for drifting droplets hence dispersion mechanism. Droplet removal from the spray fan does not depend strongly on cross flow mean velocity profile or turbulence level, so must be controlled by droplet and entrained air velocity fields within the spray.

Wind tunnel simulations can be used to reproduce field observations of spray drift. Despite the simplified equipment configuration, these experiments provide the only direct support for the use of wind tunnels in equipment testing and classification protocols. In these schemes, uniform wind tunnel cross flows can be used for simplicity, but it is desirable to reproduce the effect of the plant canopy on the mean flow.

1. Introduction

This chapter presents a study of drift produced by a single static nozzle in atmospheric and wind tunnel cross flows, motivated for three reasons. As yet, no study has directly tested whether wind tunnel experiments (using any form of mean velocity profile) can reproduce field observations of spray drift using identical equipment configurations; this test is conducted here to assess whether simulations of mean velocity profile only (recall chapter 1) produce satisfactory reproduction of field observations. The lower compliant boundary provided by the plant canopy in the field is simulated using rigid roughness elements in the wind tunnel (recall chapter 2), so measurement of the vertical profile of airborne spray volume enables the effect of these different boundary conditions to be investigated. The vertical profile of airborne spray volume also indicates the role of the spray structure in controlling downwind drift, as the origin of regions of high concentration of airborne droplets can be identified. Comparisons are made here under guideline conditions [Anon, 1990], which recommend chemical application under neutral atmospheric conditions (see chapter 1) in a steady light breeze (2-4 mph at boom height) blowing away from susceptible crops or neighbouring land.

In a wider context, comparative measurements are important in design of agricultural spraying systems which minimise drift. Legg and Miller [1990] propose a combined approach to spray drift assessment for equipment testing and classification, based on field experiments, wind tunnel experiments and theoretical modelling, summarised as follows. Field experiments can only be used to test equipment under a limited set of spraying conditions. Wind tunnel experiments which reproduce field conditions can then provide drift mass fluxes, and drifting droplet sizes and velocities which are currently unobtainable in the field (see chapter 1). Wind tunnel experiments provide a financially attractive route to spray nozzle performance evaluation, as a wide range of simulated atmospheric conditions can be controllably investigated over short timescales compared with field experiments. Numerical simulations [e.g. Hobson et al., 1993] provide the most cost-effective and flexible technique for investigating aspects of nozzle performance in a comparative way, although the formulation of models which do not reproduce the two-phase structure of the spray is questionable (see chapter 1).

Legg and Miller [1990] suggest that a combined approach for equipment testing represents the most cost-effective route to assessment of spray nozzle performance for existing and novel equipment configurations. Such a scheme also offers the possibility of introduction of a 'driftability

index' for spraying systems (a ranking scheme which could, for example, be based on measurement of airborne spray volume at a reference station under reference conditions). This could then lead to development of an equipment classification by regulatory authorities to aid the end-user in selection of appropriate equipment to minimize spray drift fluxes produced [Parkin et al., 1994]. The development of wind tunnel configurations and numerical simulation schemes which reproduce field observations of spray drift underpin the proposal of Legg and Miller [1990]. Equipment testing protocols such as this scheme can only be adopted if reproduction of field observations of spray drift can be obtained in wind tunnel experiments.

Field measurements of airborne spray volume produced by a conventional agricultural sprayer using a boom of overlapping sprays show an exponential increase of airborne spray volume with increasing wind speed [Gilbert and Bell, 1988; Rutherford et al., 1989] with exponents ranging from about 0.1 to 0.3 (figure 1). Airborne spray volume is conventionally measured on a 10 m vertical passive line collector, sited 5-8 m downwind of a spraying vehicle moving perpendicular to the mean wind direction, that is, with spray major axis aligned with the atmospheric wind [Gilbert and Bell, 1988] (see figure 2). These measurements provide an assessment of airborne drift in the spray far-field within distances from the spray typically set aside as 'buffer zones' to prevent contamination of surrounding land [Cook, 1996]. In these studies, the sprays on the boom sample two perpendicular velocity fields: the atmospheric cross wind, with logarithmic mean velocity profile (recall chapter 1) and the relative velocity generated by the vehicle motion, which is constant with height. The latter motion provides the larger contribution to relative velocity, with typical vehicle speeds ranging from 5-8 mph [Gilbert and Bell, 1988] and guideline cross winds up to 4 mph.

Wind tunnel experiments have so far been aimed at characterisation of airborne spray volume and drifting droplet diameters produced by a single nozzle [Western et al., 1989; Miller et al., 1989]. These fundamental studies have been conducted with spray major axis perpendicular to cross flow, simulating the dominant relative velocity generated by vehicle motion. Interaction of spray entrained air and cross flow velocity fields has been postulated to generate significant edge vorticity in this orientation [Miller, 1993], with downwind deposition patterns at the ground plane attributed to action of a vortex pair scavenging small droplets from the spray fan edges [Young, 1991; Miller, 1993].

Studies of the velocity profile of the neutral atmospheric boundary layer over typical agricultural land reviewed in chapter 1 suggest that simulation of the logarithmic mean velocity profile

only is appropriate for wind tunnel measurements of spray drift. However, it is noted that probably the greatest uncertainty in the velocity field sampled during agrochemical application concerns the nature of the boundary layer arising from interaction with compliant plant canopy elements, and the efficiency of droplet capture by the plant canopy. Neither effect has received detailed attention in previous studies, although measurements of mean velocity profiles within forest and maize canopies show negligible mean wind shear within the canopy [Raupach and Thom, 1981]. Two wind tunnel configurations were employed here, both producing approximately logarithmic mean velocity profiles, the first with rigid roughness elements to simulate a roughness height typical of agricultural land, the second with a rigid false floor to simulate a high efficiency of droplet capture by plant elements. Neither of these configurations reproduces the effect of a compliant boundary, but were selected to assess the requirement of simulating canopy conditions in future studies.

In order to conduct comparative field and wind tunnel measurements using identical equipment with the specific objectives outlined above, a simplified experimental configuration must be selected to reconcile the differences in typical field and wind tunnel experiments. With only a unidirectional velocity field available in the wind tunnel, field measurements must be conducted either with static spraying equipment or zero atmospheric cross wind. It was decided to use the static configuration (spray major axis aligned with cross wind), in order to test the wind tunnel simulation of the logarithmic mean wind profile (chapter 2) against field measurements. Although the mean wind contribution is typically of the same order or smaller than that due to vehicle motion, it provides the primary transport of airborne spray to collectors 5-8 m downwind used in previous field studies, with which it would be useful to make comparison. However, in comparative measurements using identical equipment, the collector configuration must be selected to be suitable for wind tunnel experiments. In this study, an array of collectors corresponding to the wind tunnel width was used, situated at a downwind position corresponding to the end of the wind tunnel working section. A practical advantage of this configuration is that the spray is narrow compared to the collector array width, minimising the effect of wind veering in the field. As the sprays on a conventional boom are aligned streamwise in this orientation, it was decided to use a single nozzle for simplicity. Approach flow perturbation due to spray fan geometry and generation of edge vorticity are expected to be negligible, so measurement of downwind airborne spray volume flux using passive line collectors was considered appropriate.

The experimental method is described in section 2, including details of use of passive line collectors, the method-of-choice for airborne spray volume flux measurements (recall chapter 1).

The experimental results are presented in section 3, with broader discussion and conclusions in sections 4 and 5.

2. Experimental Method

2.1. Field Experiments

The geometry of the 110^o flat-fan spray used is shown in figure 2. The spray produced is elliptical in cross-section, and has an included angle of 110^o and an in-plane angle of 10^o. Experiments were carried out using 2 different flat-fan nozzles (Lurmark 110-015 and 110-04), producing droplet size distributions with volume median diameter (VMD) of 195 μm and 238 μm respectively (figure 3), measured 350 mm below the nozzle using a Dantec phase-Doppler anemometer (see chapter 4 for equipment specification). The dropsize distribution from these nozzles was classed as *fine* and *medium*, respectively, under the British Crop Protection Council (BCPC) scheme based on cumulative size distribution [Doble et al., 1985] (see figure 3). These nozzles were selected as they were significantly different in the proportion of small (diameter <100 μm) droplets they produced. The proportion of total spray volume in droplet diameters <100 μm was approximately 7% for the fine nozzle and 2.5% for the medium nozzle (see figure 3).

Field measurements of the airborne spray volume produced by a single static flat-fan nozzle were made under typical spraying conditions. The arrangement of experimental equipment in the field is shown in figure 4. The orientation of the spray major axis parallel to the mean wind direction was consistent with the action of an atmospheric cross flow perpendicular to the direction of spraying vehicle motion, although it is again emphasised that this was a fundamental comparative study rather than a realistic simulation of the action of the atmospheric wind and vehicle motion on a single spray. Airborne spray volume measurements were made directly using a spray solution of 0.1% tracer dye (Orange G, Merck Plc), with the addition of 0.1% non-ionic surfactant (Agral, Zeneca Agrochemicals Plc) to give spray behaviour typical of agricultural pesticide tank mixes. The dye was deposited on an array of 5 horizontal *passive line* collectors, made from 3.0 m lengths of 1.98 mm polyethene tubing, and positioned from the canopy top to 0.5 m above the canopy top at 0.1 m intervals. The collector frame consisted of a central 2.0 m section positioned perpendicular to the spray major axis, with additional 0.5 m end sections angled towards the nozzle such that the distance from the spray centreline to the mid-point of each face of the array was 2.0 m (figure 4).

Angled end sections were used to attempt to minimize airborne spray not intercepting the collector array due to localised wind veering.

The collection efficiency of a cylindrical collector can be estimated using graphical correlations presented by May and Clifford [1967] for droplet impaction at high Reynolds numbers. Phase-Doppler anemometry measurements of the velocity of drifting spray droplets 2 m downwind of a spray boom in uniform 2.0 m s^{-1} cross flow suggest drifting droplets have streamwise velocities greater than or equal to the cross flow velocity, and a typical VMD of 95 μm with 12% of the airborne spray volume in droplet diameters less than 52 μm (chapter 5 of this thesis). The efficiency of impaction is 1.0 for 67 μm or larger droplets moving at 2 m s^{-1} [May and Clifford, 1967]. This falls to 70% for droplets less than 52 μm in diameter, suggesting a typical impaction efficiency of about 97% in these experiments.

The volume of original dye solution deposited on the line collectors was analysed using a Philips PU 8710 spectrophotometer following the method of Gilbert and Bell [1988]. Line collectors were sectioned into 30-40 mm lengths to enable dye recovery in test-tubes, using deionized water as the solvent. The optical absorbance of dye recovered was measured at 480 nm and compared with a calibration curve produced using known dye concentrations. This technique has an estimated resolution of 0.5 μL (a background absorbance level due to the presence of dust) and estimated dye recovery of 95% [Gilbert and Bell, 1988; Sharpe, 1974], thus reducing the overall collection efficiency to about 92%. Orange G dye concentrations exhibit slight reduction on exposure to ambient light, although this is typically below the resolution limit of the analysis method [Gilbert and Bell, 1988]. Dye volume deposition on each collector was calculated, and using the duration of each experimental run and the spray flowrate, spray deposition was expressed as a proportion of the spray output.

Field experiments were carried out at Silsoe Research Institute, between 15th October and 11th November, 1991. The single static nozzle was positioned in the approximate centre of the field, at least 100 m from the field edges. Under prevailing wind conditions, an uninterrupted upwind fetch of 400 m of short grass and stubble to a height of approximately 0.1 m was available. Prior to each experimental run, nozzle flowrate was determined by collecting spray at the nozzle using a large diameter measuring cyclinder for 60 s. This was compared with manufacturers data to ensure that the nozzle was operating correctly. BCPC nozzle pressures were set using a pressure transducer (Druck SC10, calibrated to $\pm$0.1 bar) mounted at the nozzle and spray operation was controlled

using an electronic timer connected to a solenoid operating a stop valve at the nozzle. The duration of the experiment was varied for each run to ensure that sufficient dye volume was deposited at the collector (visually assessed in the field). Low dye concentrations reduce the precision of the analysis technique as a resolution limit is approached (see above), whereas excessive dye deposition results in dye dripping from the line collectors, introducing an unsystematic experimental error. Typically, experimental runs lasted between 10 s and 30 s (increments of 5 s) depending on meteorological conditions.

During each experimental run, meteorological data were sampled at the field site, using a 10 m pneumatic mast (Clark Ltd.), positioned at a transverse distance of 20 m from the spray nozzle, relative to mean wind direction. Mean wind velocity was measured at five heights up to 10 m, using Vector Instruments cup anemometers. Mean wind direction was determined using a Vector Instruments wind vane positioned 10 m above the surface. Wet and dry bulb temperatures were sampled at heights of 1 m and 5.5 m. Wind velocity and temperature data were recorded onto magnetic tape, using a Micro-Data 8 channel data logger (sampling rate 10 Hz). Gradient Richardson numbers (equation A4, appendix 1, chapter 1) and averaged logarithmic-form mean wind profiles (equation 1 below) were calculated using the the VAX VMS system at Silsoe Research Institute running software written in-house by C.R.Tuck.

2.2. Wind Tunnel Experiments

The wind tunnel used for this study was the Silsoe Research Institute 2 m $\times$ 1.5 m Eiffel-type wind tunnel. The diffuser section is 2 m wide $\times$ 1.5 m high, and 3 m in length, with 0.3 m thickness of 0.01 m diameter honeycombe flow straightener at the inlet. This channels air into the working section, which is 4 m wide $\times$ 2 m high, and 5 m in length (typical of Eiffel tunnel configuration). Equipment for velocity profile simulation was positioned at the entrance to the working section. The tunnel produces approximately uniform upstream flow, with streamwise turbulence intensity which is approximately constant over the working section, with maximum value of 2% at 1.8 m s^{-1}, measured using a Gill Instruments sonic anemometer. The tunnel discharges air through an exhaust section which has the same cross-section as the diffuser section, and is 2 m long. The airflow is drawn through the tunnel by a 1.6 m diameter 4-bladed fan, powered by a 26.6 Kw 3-phase electric motor.

An array of differentially-spaced flat plates (specified using the method described in chapter 2) was used as a shear generator to produce an approximately logarithmic mean velocity profile at full-scale in this wind tunnel,

$$\overline{u_z} = \frac{u_*}{\kappa} \ln \frac{z}{z_o} \tag{1}$$

where,

$\overline{u_z}$ = mean horizontal velocity at height z,

u_* = friction velocity (surface-defined velocity scale),

κ = Von Karman constant (an empirical constant with a value of approximately 0.4),

z_o = roughness length, length scale for flow in the vicinity of a rough surface.

10 plates were used (with spacings shown in figure 5) with the addition of an upstream retarding grid of cell dimension 6 mm × 6 mm with grid bar diameter 3 mm and a downstream mixing grid of cell dimension 32 mm × 32 mm with grid bar diameter 6 mm (see figure 6a). The velocity profile produced by this configuration is shown in figure 7 and is characterised by a mean velocity of 2.75 m s^{-1}, 0.5 m above the surface, and roughness length of 0.086 m, within the typical range for agricultural land (0.02 m - 0.10 m [Anon, 1978]). The velocity profile was non-developing from 2-5 m downstream (the region occupied by the spray and line collectors), with turbulence length scales of approximately 0.05 m produced by the mixing grid.

Experiments were also conducted using velocity profile generating equipment first reported by Miller et al. [1989] to reproduce characteristics of the mean velocity profile in the vicinity of a plant canopy top [Raupach and Thom, 1981] (referred to as the *canopy* profile to distinguish it from the *logarithmic* profile described above). This comprises a false floor only, with the upper surface covered in a layer of plastic simulated grass to minimize splash, which also acted to increase the surface roughness. This configuration was intended to simulate the droplet capture characteristics of a plant canopy, with the rough wall boundary layer on the upper surface producing a weakly-sheared mean velocity profile. The false floor was elevated 0.2 m above the wind tunnel floor, with a 0.5 m horizontal aperture immediately under the spray nozzle to simulate spray droplet penetration into the plant canopy (see figure 6b). The velocity profile produced is approximately logarithmic with significant velocity reduction in the vicinity of the false floor (see figure 7).

Wind tunnel experiments were carried out at three cross flow velocities, 2.0 m s^{-1}, 2.5 m s^{-1}

and 3.0 m s^{-1} at the nozzle height, representative of guideline conditions for agricultural chemical application (see introduction). The arrangement of spray nozzle and passive line collectors in the wind tunnel reproduced the field experiment configuration in terms of downstream position (2 m) and height (up to 0.5 m in 0.1 m intervals) of the line collectors (figure 8). The angled end sections of the collector array used in the field experiments (see figure 4) were not required as preliminary tests showed that no dye was deposited outside the central 2 m section and the upstream cross flow was unidirectional. Airborne spray volume measurements were made directly using a spray solution of 0.1% Fluoroscein dye (Merck Plc), with the addition of 0.1% non-ionic surfactant (Agral, Zeneca Agrochemicals Plc). Fluoroscein dye was selected in preference to Orange G dye for the wind tunnel experiments as it degrades less on exposure to artificial light, although its inherent sensitivity to ultra-violet light makes it unsuitable for field experiments.

Determination of dye concentration followed similar methodology to the field experiments, although fluorimetry was the analytical technique used, following Sharpe [1974]. The fluoroscein dye was recovered in 0.1 M NaOH solution, and its concentration determined using a Turner fluorimeter fitted with a 7-60 primary filter, calibrated against known dye concentrations. This method yields the same precision as for water-based dyes used in the field experiments; an estimated resolution of 0.5 μL and dye recovery of 95% [Sharpe, 1974; Gilbert and Bell, 1988].

3. Experimental Results

3.1. Field Studies

Field experiments were carried out on 5 days characterised by cloudy conditions, with wind velocities ranging from 1.7 m s^{-1} to 4.3 m s^{-1} at the boom height, wider than the range of guideline atmospheric conditions for agricultural chemical application (recall introduction). A sample plot of the meteorological data acquired during the experiments carried out on 29/10/91 is presented as figure 9, with mean wind velocity at 4 heights up to 10 m and temperature at 3 heights up to 5 m plotted in log-linear form. The gradient Richardson number (equation A4, appendix 1, chapter 1) was calculated directly because sufficient meteorological data was acquired up to 10 m to approximate local temperature and velocity gradients (see figure 9). A value of 0.05 was obtained,

corresponding to moderately stable to neutral atmospheric stability [Plate, 1982, p.447], in line with guideline conditions. Richardson numbers for the other field days were calculated as -0.035, -0.060, -0.004 and -0.013, corresponding to neutral atmospheric stability. Mean crosswind velocity measurements confirmed that the velocity profile was approximately logarithmic (figure 9), with displacement height neglected and roughness height z_o estimated as 0.01 m from

$$z_o = 0.1 z_c \tag{2}$$

where

z_c is the height of the plant canopy [Thompson and Ley, 1983], in this case 0.1 m.

An ensemble plot of the field experiment data is shown in figure 10. Here and subsequently, field airborne spray volume data show no error bars for precision, as experimental replicates of mean cross flow conditions in the field with which to estimate a standard error for the mean could not be obtained. The average airborne spray volume (as % output) through the collector plane 2 m $\times$ 0.5 m, 2 m downwind of the spray has been calculated using the experimental data measured at 0.1 m vertical intervals up to 0.5 m. Averaged airborne spray volume data are expressed as a proportion of the nozzle output to allow comparison between the two nozzle sizes used, and have been plotted against mean wind velocity at 0.5 m. Airborne spray volume 2 m downwind of the spray boom increased with wind speed for both nozzle sizes used; in addition, the rate of increase of airborne spray volume with wind speed increased from medium to fine nozzles, as previously observed by Rutherford et al. [1989]. Variability of field experiment results was due primarily to crosswind variations such as wind gusts and localised wind veering, although the latter effect should be minimized by the large ratio of collector to spray width in this orientation, and the addition of angled end sections to the collector array.

Least squares regression analysis was carried out on the averaged field data (figure 10). The form of the increase of airborne spray volume with windspeed was best reproduced by an exponential function, although regression coefficient values (0.85 and 0.71) were too low to indicate more than an approximate trend. Figures 11 and 12 show averaged field data replotted on log-linear axes for fine and medium nozzles respectively, compared with field data of Gilbert and Bell [1988] and averaged wind tunnel data with estimates of standard error of the mean (see section 3.2 below). Gilbert and Bell [1988] present exponential form curve fits to field measurements 8 m downwind constituting a standard measuring protocol. Averaged field data acquired in these experiments show the same form, although the droplet size distribution sampled 2 m downwind includes larger droplets with

appreciable settling velocities which will be collected at the plant canopy at downwind distances less than 8 m. The absolute values of airborne spray volume measured at 2 m are correspondingly higher (figures 11 and 12).

3.2. Wind Tunnel Studies

Wind tunnel experiments were repeated three times at crossflow velocities of 2.0 m s^{-1} and 3.0 m s^{-1} to provide standard errors plotted as error bars on figures 11-17. Standard error of the mean for the logarithmic profile was 17% and 10% for the medium spray at 2.0 m s^{-1} and 3.0 m s^{-1}, respectively, and 3% and 11% for the fine spray at 2.0 m s^{-1} and 3.0 m s^{-1} respectively. Standard error of the mean for the canopy profile was 17% and 10% for the medium spray at 2.0 m s^{-1} and 3.0 m s^{-1}, respectively, and 7% and 10% for the fine spray at 2.0 m s^{-1} and 3.0 m s^{-1}, respectively.

Vertical profiles of airborne spray volume are plotted for the fine nozzle in 2.0 m s^{-1} and 3.0 m s^{-1} cross flow in figures 13 and 14, and for the medium nozzle in 2.0 m s^{-1}, 2.5 m s^{-1} and 3.0 m s^{-1} cross flow in figures 15 to 17, with cross flow velocity measured at the boom height. Field data from runs where the mean cross flow velocity was approximately equal to the wind tunnel mean velocity are also plotted for comparison. Figure 13 shows airborne spray volume produced by the fine spray in a 2.0 m s^{-1} cross flow. The data generally form smooth curves indicating systematic decrease of airborne spray volume with height, with least squares regression showing best agreement to an exponential function. The field data show a reduced value of airborne spray volume at the lowest collector (positioned approximately at the plant canopy top) as compared with wind tunnel experiments, probably due to droplet capture by the canopy. Individual plant size and shape and local plant density and plant waving [Raupach and Thom, 1981] all introduce unsystematic variation into the flow field in this region. Figure 14 shows airborne spray volume produced by the fine spray in a 3.0 m s^{-1} cross flow. The logarithmic profile simulation significantly over-predicts field measurements except at 0.4 m, suggesting that the downstream velocity field produced by this equipment is a poor reproduction of field velocity profiles at this cross flow velocity. The canopy profile simulation reproduces the form of the field vertical profile of airborne spray volume, although under-predicting measured values by about 50%. Least squares regression shows an exponential form for decrease of airborne spray volume with height, with this fitting only applied up to 0.4 m for the logarithmic profile simulation where the data form a smooth curve. The validity of this approach is questionable, but is of little consequence since this simulation provides very poor reproduction of field data.

Figure 15 shows the vertical profile of airborne spray volume produced by the medium nozzle in a 2.0 m s^{-1} cross flow. Both wind tunnel simulations reproduce field measurements, although showing greater decrease of airborne spray volume with height compared with field data. All datasets are adequately described by exponential decrease of airborne spray volume with height. Figure 16 shows the same nozzle in a 2.5 m s^{-1} cross flow, with all datasets showing similar trends to those in figure 15. Figure 17 shows the medium nozzle in a 3.0 m s^{-1} cross flow. The logarithmic profile simulation produces over-prediction of field data as for the fine nozzle at this cross flow velocity, and the canopy profile simulation produces slightly greater over-prediction, inconsistent with experiments using the fine nozzle.

In general, both logarithmic and canopy profile simulations show reasonable agreement with field observations, with reasonable correlation of these data to exponential decrease of airborne spray volume with height (regression coefficient values generally greater than 0.97 for the curve fits). The logarithmic profile simulation shows reasonable agreement with field data except near the plant canopy top, although over-prediction of airborne spray volume is apparent for 3.0 m s^{-1} crossflows (figures 14 and 17). The canopy profile simulation generally under-predicts airborne spray volume over its vertical range.

4. Discussion

The agreement between field and wind tunnel profiles of airborne spray volume is adequate, considering the less than perfect reproduction of the logarithmic and canopy-defined mean velocity profiles. Neither simulation is superior in terms of overall reproduction of field observations; the canopy profile simulation provides a better match to averaged drift data, the logarithmic profile simulation shows slightly better matching of measured deposit vertical profiles. Standard error calculations for wind tunnel experiments suggest a higher scatter under controlled conditions than initially expected. It is unclear why the standard errors are larger for the logarithmic profile simulation compared with the canopy simulation. Although the logarithmic profile equipment produces turbulence scales of about 0.1 m in the downstream flow, the mean flow velocity is sufficiently high and the duration of the experimental runs is sufficiently long that the effect of local fluctuation will be smoothed out. With only three experimental runs to provide a standard error estimate, unsystematic error in one run could explain this variation. Further work is required to clarify this point. Unfortunately, none of the previous published wind tunnel studies provide any assessment of data precision for comparison.

Despite only limited difference in the form of the velocity profiles used, it is clear that airborne spray volume profiles are relatively insensitive to the mean velocity profile, particularly at the higher collectors. The implication of these observations is that spray entrained air velocity field, rather than cross flow profile or turbulence field, controls droplet dispersion in the near-field. An investigation of entrained air velocity profiles within a flat-fan spray is made in chapter 4 of this thesis. Consistent with present observations, later wind tunnel studies (chapter 5) employ a uniform wind tunnel velocity profile for simplicity. The observed decrease of airborne spray volume with increasing height in field and wind tunnel velocity fields is consistent with the concept of the spray becoming increasingly 'porous' to the action of the cross flow with distance from the nozzle, as it spreads and weakens. In the present experimental configuration with the spray major axis aligned with the cross flow, the spray presents a streamlined resistance to the approach flow; caution must be exercised with these concepts until a similar study has been undertaken for the spray major axis orientated perpendicular to cross flow direction, simulating the relative cross flow due to vehicle motion which provides a greater contribution than that due to the atmospheric wind (recall introduction). With the spray major axis perpendicular to the cross flow, the effect of the spray as a porous bluff body may be significantly modified due to generation of edge vorticity [Miller, 1993], which may provide the dominant contribution to initial droplet dispersion.

Both simulations show poorer reproduction of field airborne spray volume measurements near the plant canopy top. Real uncertainties exist relating to the form of the mean velocity profile in this region [Raupach and Thom, 1981] due to the mobility of the flow boundary. This produces coupling of flow with the motion of plant elements and generation of turbulent coherent structures (eddies) scaled on this motion [Raupach and Thom, 1981], leading to preferential trapping of certain droplet size ranges (particularly small droplets) as has been observed for shear layers bounding turbulent air jets [Chung and Troutt, 1988]. However, at the windspeeds used here the field airborne spray volume in this region is adequately approximated by wind tunnel simulation results, suggesting that solid surfaces may be able to reproduce compliant boundary deposition, but this is not exactly matched by equipment selected here. Flow blockage by the false floor employed in the canopy profile simulation results in greater droplet deposition within 2 m of the spray than is observed in the field, whereas its absence in the logarithmic simulation results in lower droplet deposition than the field condition. The compliant boundary effects in the field clearly enhance droplet deposition on the canopy for the medium spray in the higher crosswind, which is underpredicted by both equipment configurations. Results from the two equipment configurations used here suggest that

the flow in the near-canopy region could be tuned in wind tunnel simulations to match a reference field condition for comparative measurements. Future wind tunnel simulations should therefore concentrate on matching flow in the vicinity of the plant canopy top, at the expense of simulating mean shear to which the spray is less sensitive. However, adequate reproduction of field data obtained here suggests that either velocity profile defined in this study could be satisfactorily used in the wind tunnel experimentation part of equipment testing protocols [Legg and Miller, 1990]. Further work is required to improve the quality of wind tunnel simulations, but reasonable matching of field observations and reproducibility are encouraging.

5. Conclusions

1. Wind tunnel experiments can adequately reproduce field measurements of airborne spray volume produced by a single static flat-fan spray under typical spraying conditions. Field experiments show exponential increase of airborne spray volume with windspeed with increasing rate from medium to fine nozzles. Adequate matching to field vertical profiles of airborne spray volume which show an exponential decrease with height was also achieved in wind tunnel simulations.

2. Under wind tunnel conditions, droplet removal from flat-fan sprays is not strongly dependent on cross flow velocity profile, so must be controlled by droplet and entrained air velocity fields within the spray fan. Thus, cross flow turbulence level does not influence droplet dispersion. Wind tunnel measurements of drifting droplet parameters can be made using uniform cross flow for simplicity.

3. Improved matching to field data can be obtained by accurate reproduction of the effects of the plant canopy on the mean flow. A necessary pre-cursor to this is detailed characterisation of the velocity field in the vicinity of a compliant plant canopy.

4. Reproduction of field airborne spray volume profiles in wind tunnel experiments suggests that the protocol for field equipment testing and classification advanced by Legg and Miller [1990] is feasible.

References

Anon [1978] ESDU 82026 (superceeds 72026) Characteristics of the wind speed in the lower layers of the atmosphere: Strong winds (neutral atmosphere). ESD item 82026, E.S.D.U.

Anon [1990] Pesticides: code of practice for the safe use of pesticides on farms and holdings. Part III of the Food and Environmental Protection Act, 1985. HMSO, London.

Chung, J.N. and Troutt, T.R. [1988] Simulations of particle dispersion in an axisymmetric jet. *J. Fluid Mech.* **186**, 199-222.

Cook, R.J. [1996] The potential impact of buffer zones in agricultural practice. In *Buffer Zones - Their Processes and Potential in Water Protection*, Samara Pub. Ltd., 12-13.

Doble, S.J., Matthews, G.A., Rutherford, I. and Southcombe, E. [1985] A system for classifying hydraulic nozzles and other atomisers into catagories of spray quality. *Proc. British Crop Protection Conference*, 1125.

Gilbert, A.J. and Bell, G.J. [1988] Evaluation of drift hazards arising from pesticide spray application. *Aspects of Appl. Biol.* **17**, 363-375.

Hobson, P.A., Miller, P.C.H., Walklate, P.J., Tuck, C.R. and Western, N.M. [1993] Spray drift from hydraulic spray nozzles: the use of a computer simulation model to examine factors influencing drift. *J. Agric. Eng. Res.* **54**, 293-305.

Legg, B.J. and Miller, P.C.H. [1990] Drift assessment using measurements and mathematical models. Paper 901593 presented to *The American Society of Agricultural Engineers* Winter Meeting, Chicago.

May, K.R. and Clifford, R. [1967] The impact of aerosol particles on cylinders, spheres, ribbons and discs. *Annals of Occupational Hygiene* **10**, 83-95.

Miller, P.C.H., Mawer, C.J. and Merritt, C.R. [1989] Wind tunnel studies of the spray drift from two types of agricultural spray nozzle. *Aspects of Appl. Biol.* **21**, 237-238.

Miller, P.C.H. [1993] Spray drift and its measurement. In Matthews, G.A. and Hislop, E.C. (eds.) *Application Technology for Crop Protection*, CAB International.

Parkin, C.S., Gilbert, A.J., Southcombe, E.S.E. and Marshall, C.J. [1994] British Crop Protection Council scheme for the classification of pesticide application equipment by hazard. *Crop Protection* **13**, 281-285.

Plate, E.J.(ed.) [1982] *Engineering Meteorology.* Elsevier, Amsterdam.

Raupach, M.R. and Thom, A.S. [1981] Turbulence in and above plant canopies. *Ann. Rev. Fluid Mech.* **13**, 97-129.

Rutherford, I., Bell, G.J., Freer, J.B.S., Herrington, P.J. and Miller, P.C.H. [1989] An evaluation of chemical application systems. *Proc. British Crop Protection Conf.-Weeds*, 601-613.

Sharpe, R.B. [1974]. Spray deposit measurement by fluorescence. *Pesticide Science* **5**, 197-209.

Smith, R.W. and Miller, P.C.H. [1994] Drift predictions in the near nozzle region of a flat fan spray. *J. Agric. Eng. Res.* **59**, 111-120.

Thompson, N. and Ley, A.J. [1983] Estimating spray drift using a random-walk model of evaporating drops. *J. Agric. Engng. Res.* **28**, 419-435.

Western, N.M., Hislop, E.C., Herrington, P.J. and Jones, E.I. [1989] Comparative drift measurements for BCPC reference nozzles and for an Airtec twin fluid nozzle under controlled conditions.*Proc. British Crop Protection Conf.-Weeds*, 641-648.

Young, B.W. [1991] A method for assessing the drift potential of hydraulic nozzle spray clouds and the effect of air assistance. *British Crop Protection Monograph no. 46: Air-assisted Spraying in Crop Protection,* 77-86.

Figures

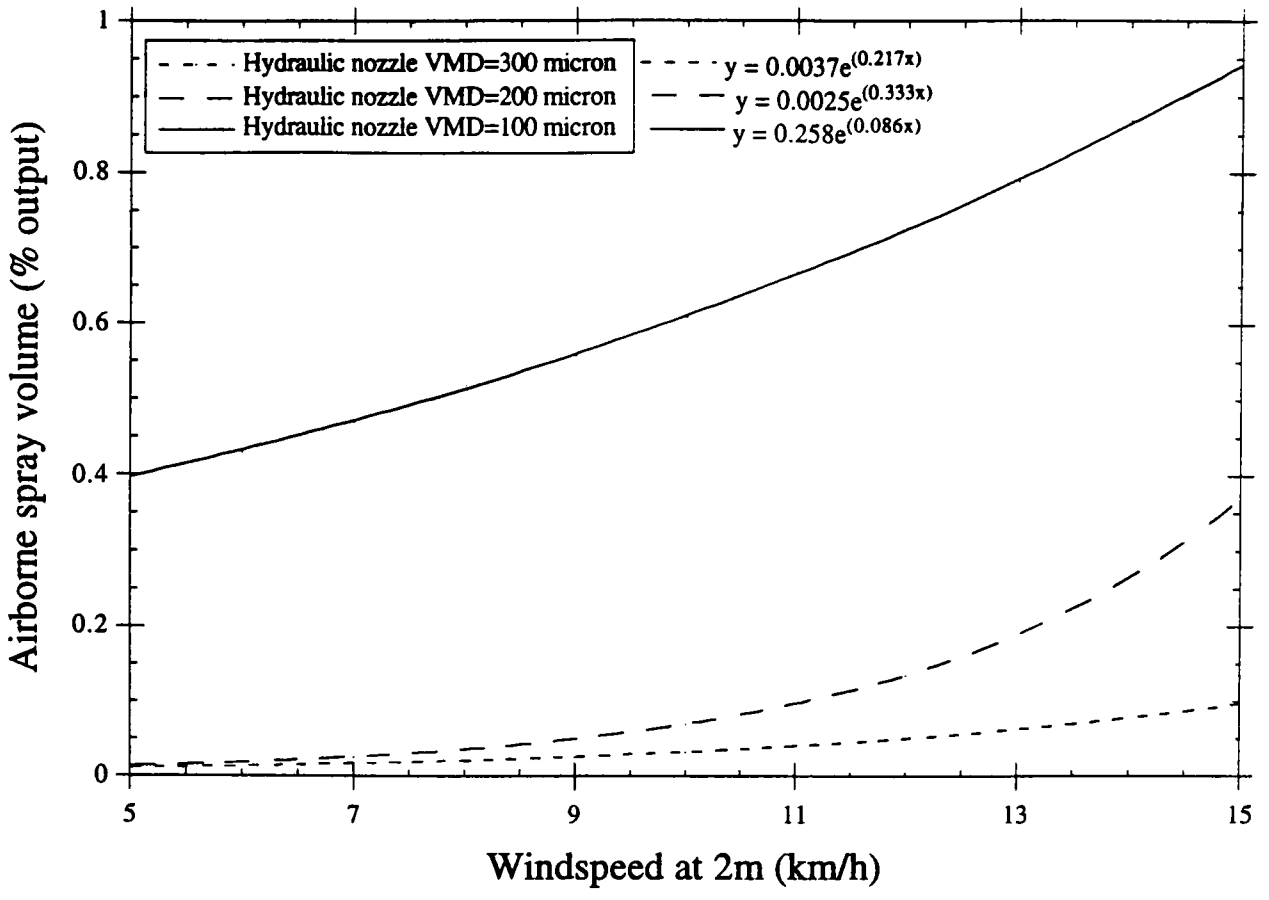

1. Variation of airborne spray volume (as % of sprayer output) with windspeed measured 8 m downwind of a spraying vehicle. The measurements are average values measured using a single 10 m vertical passive line collector, passed once by the vehicle, operating at 6 mph (after Gilbert and Bell, 1988). No data points were presented in the published data, only the exponential form fitted curves reproduced here.

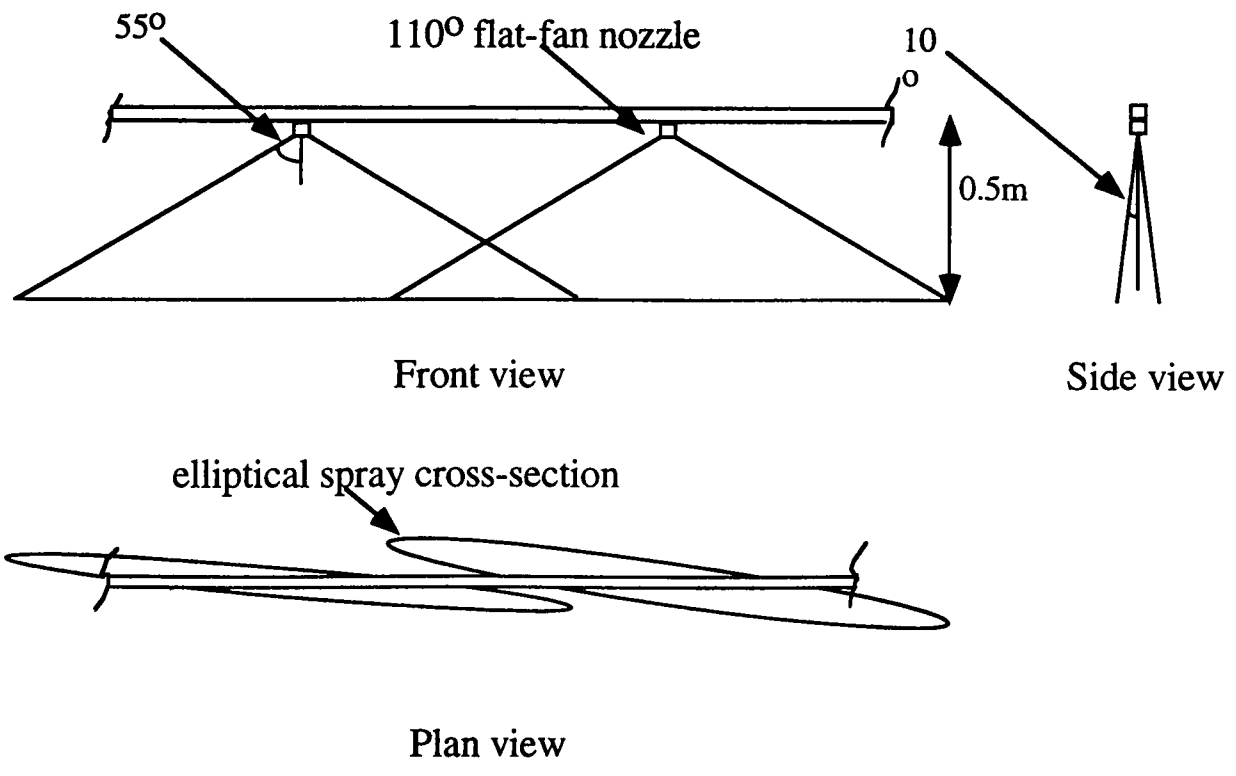

2. Typical geometry and arrangement of 110° agricultural flat-fan sprays on a boom. The front view corresponds to vehicle motion out of the page.

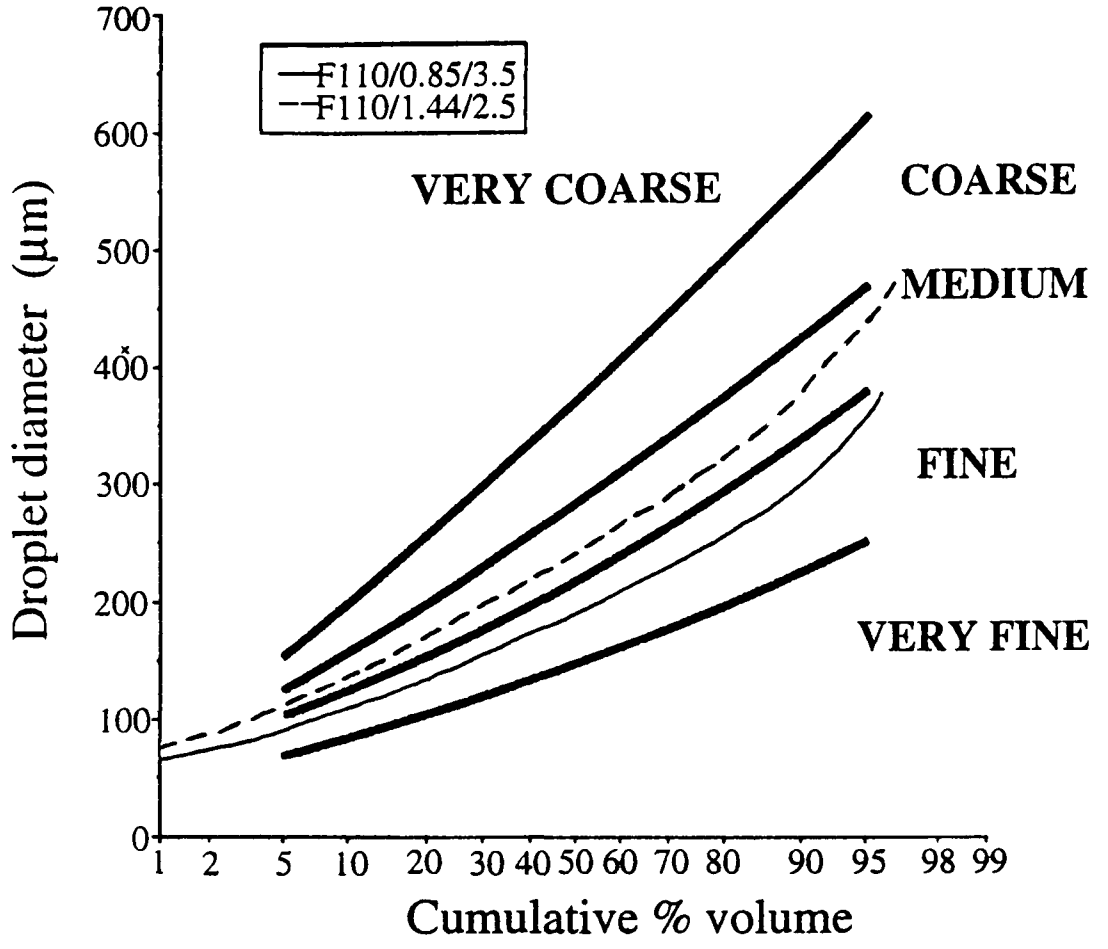

3. Cumulative droplet size distribution plot showing performance of the fine (denoted F110/0.85/3.5) and medium (denoted F110/1.44/2.5) nozzles compared with the British Crop Protection Council classifications of spray quality [Doble et al, 1985].

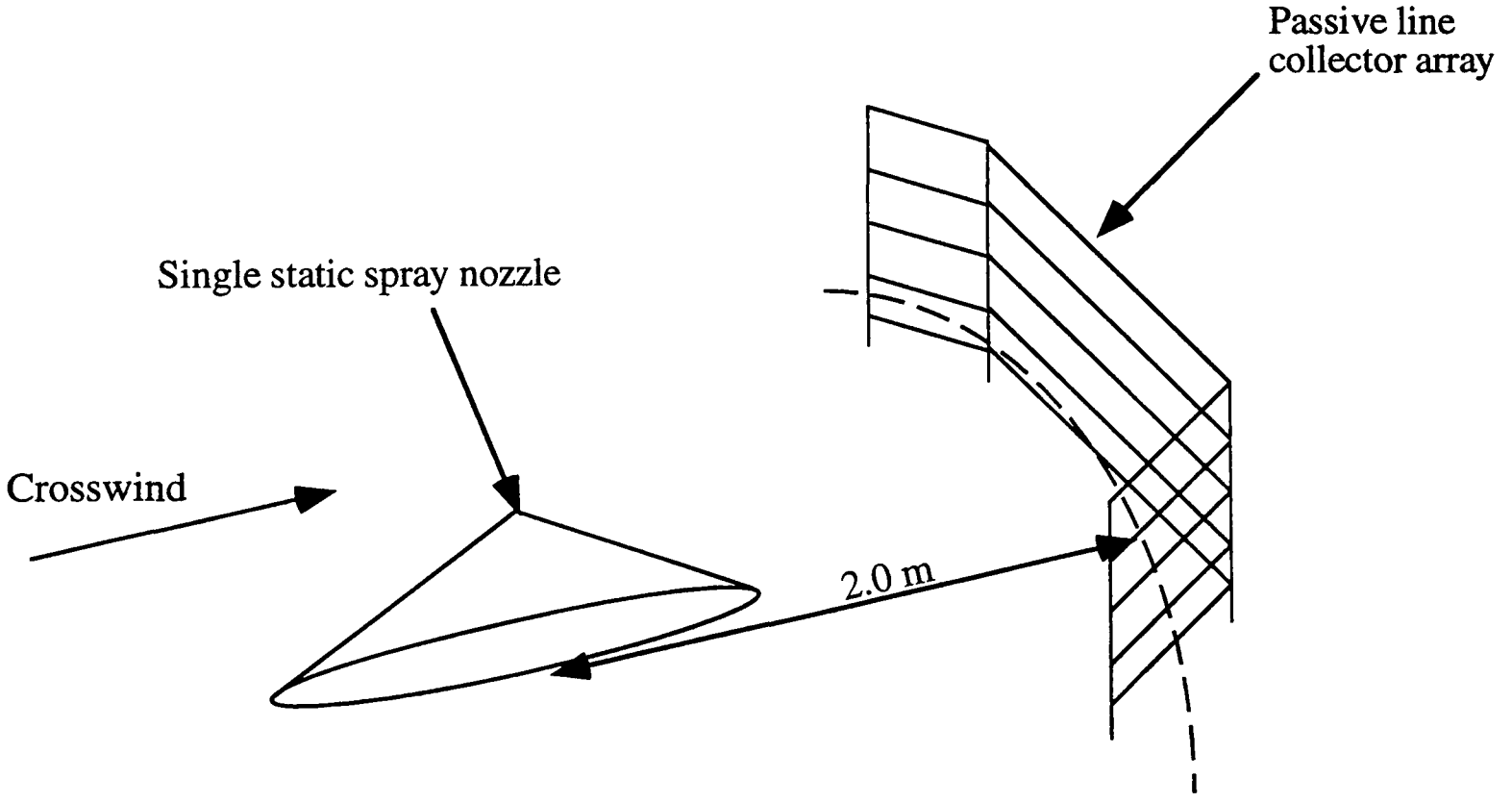

4. The equipment configuration for field experiments using a single static flat-fan nozzle.

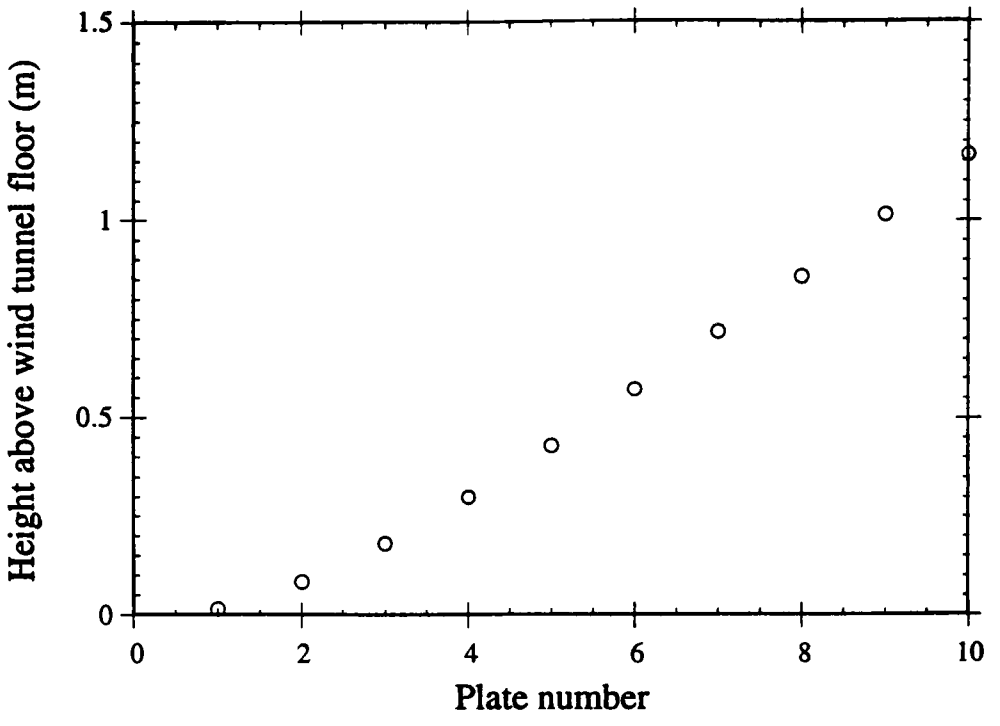

5. Spacing of flat plates used as the basis for the logarithmic profile simulation described in the text. Calculation of plate spacings and subsequent equipment selection is described in chapter 2.

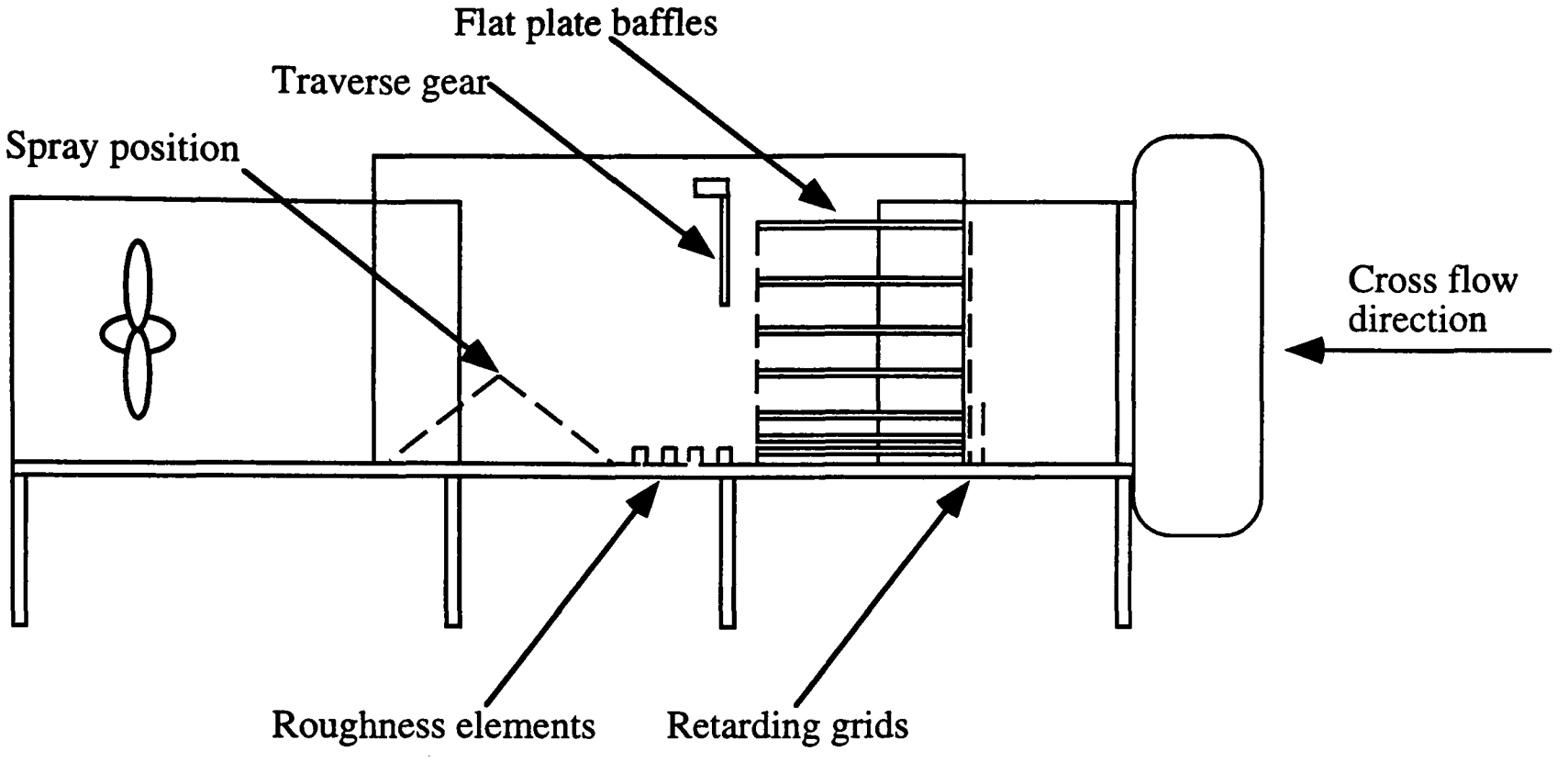

(a)

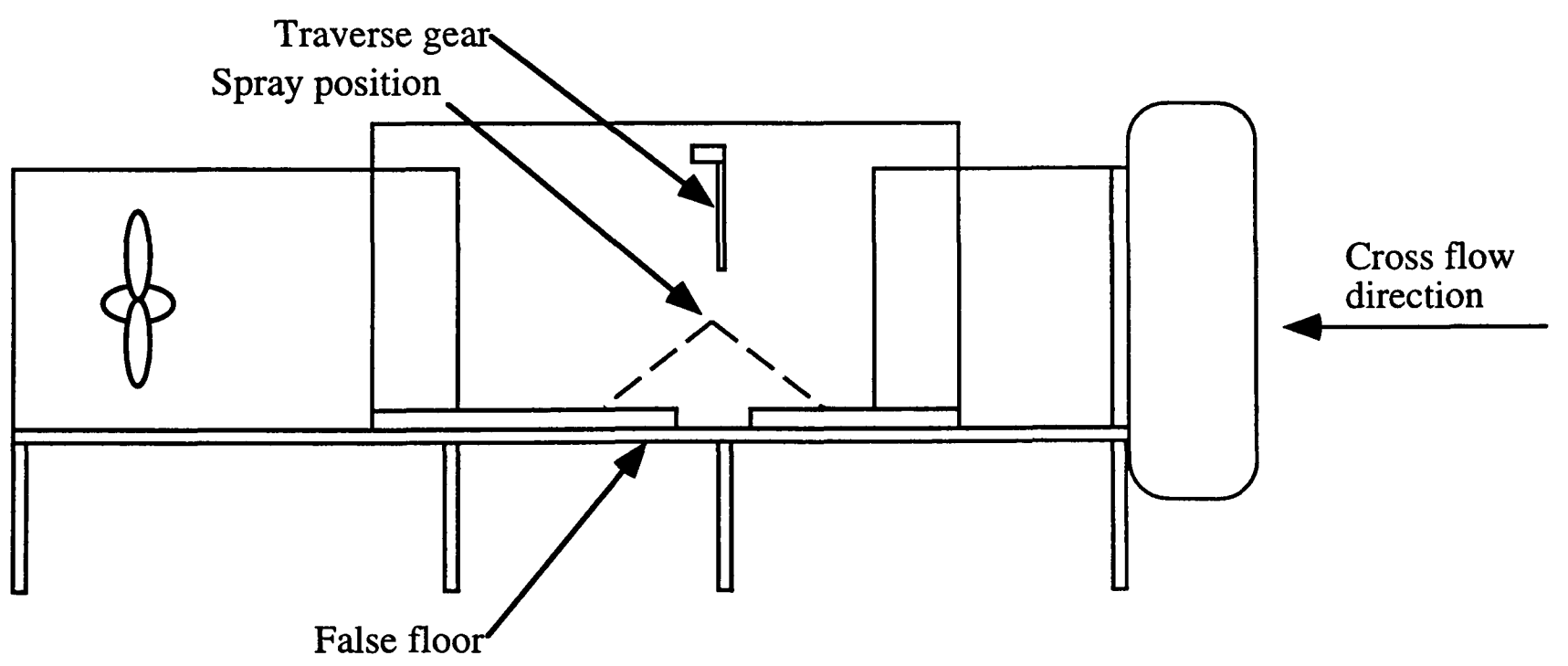

(b)

6. Schematic diagrams of the wind tunnel simulation equipment: (a) logarithmic profile; (b) canopy profile.

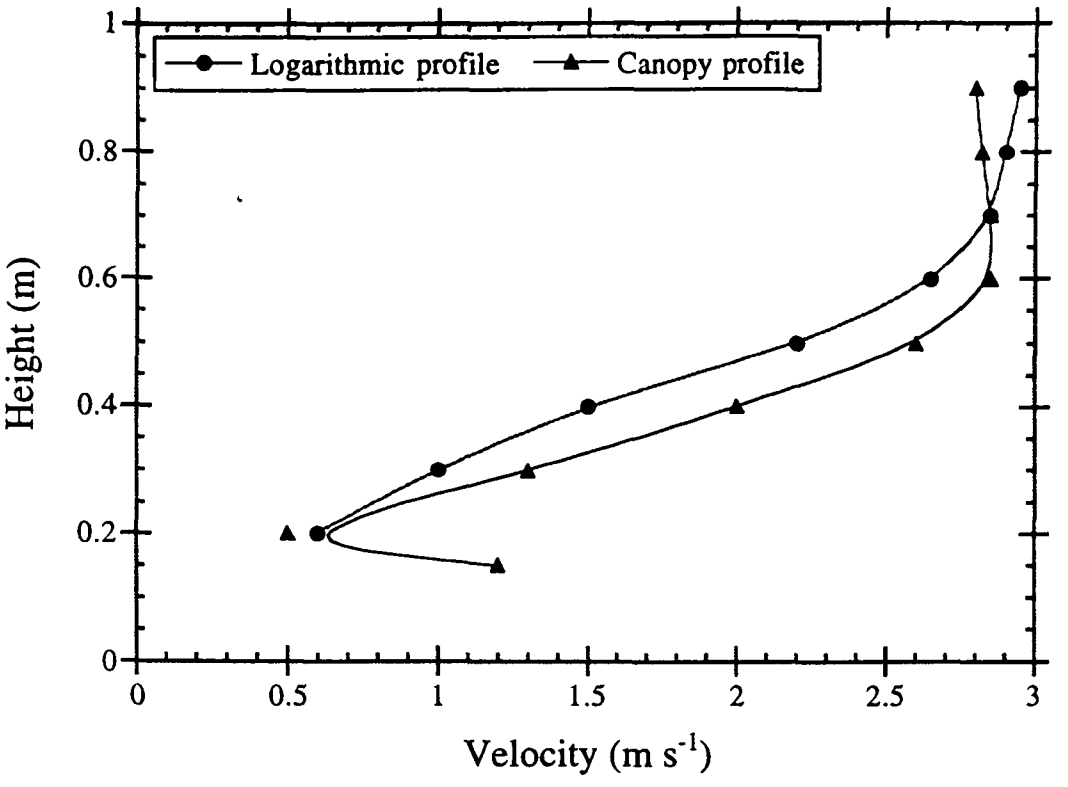

7. The mean velocity profiles produced by the wind tunnel simulation equipment.

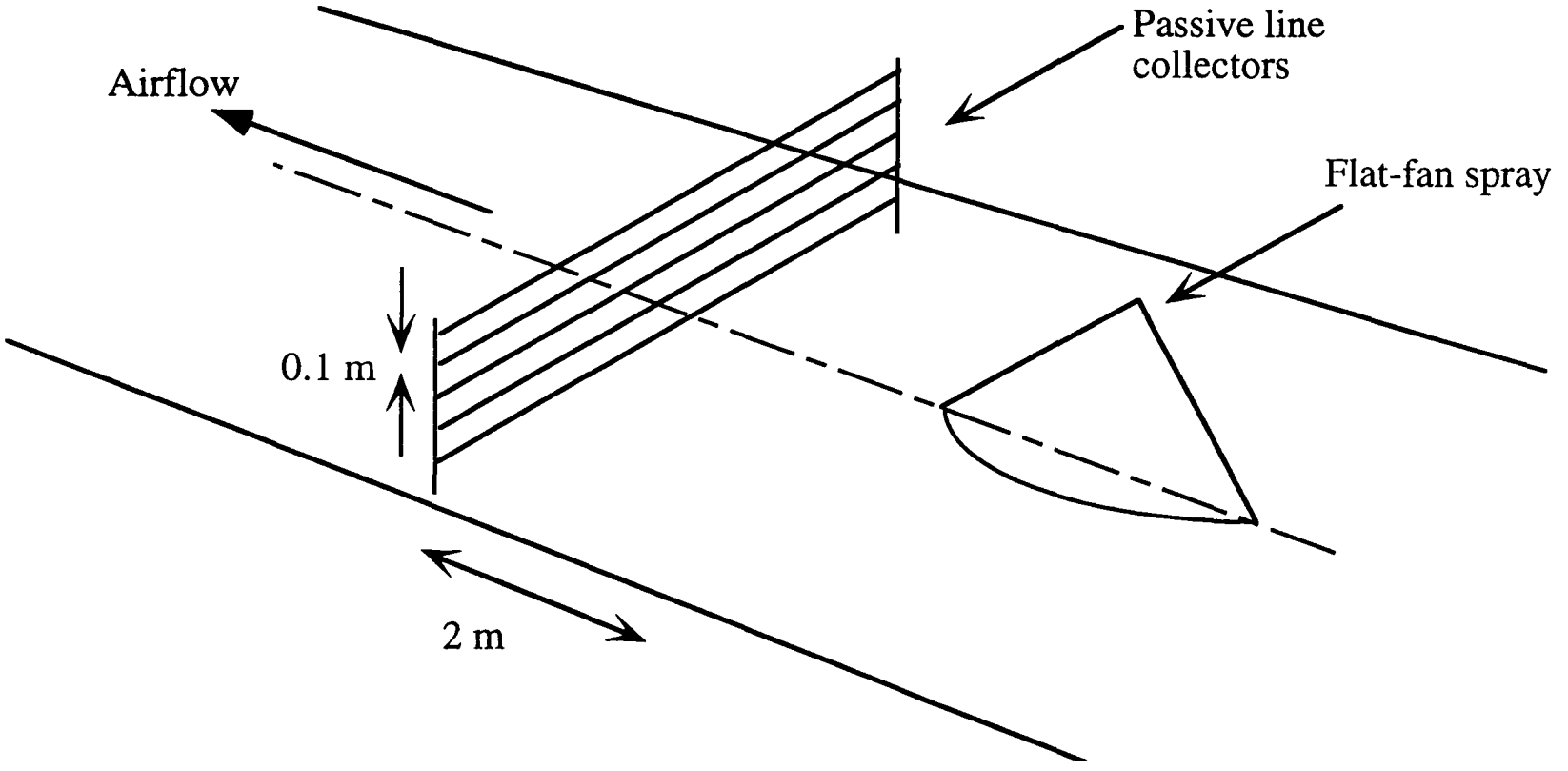

8. The equipment configuration for wind tunnel experiments analogous to field experiments using a single static flat-fan spray.

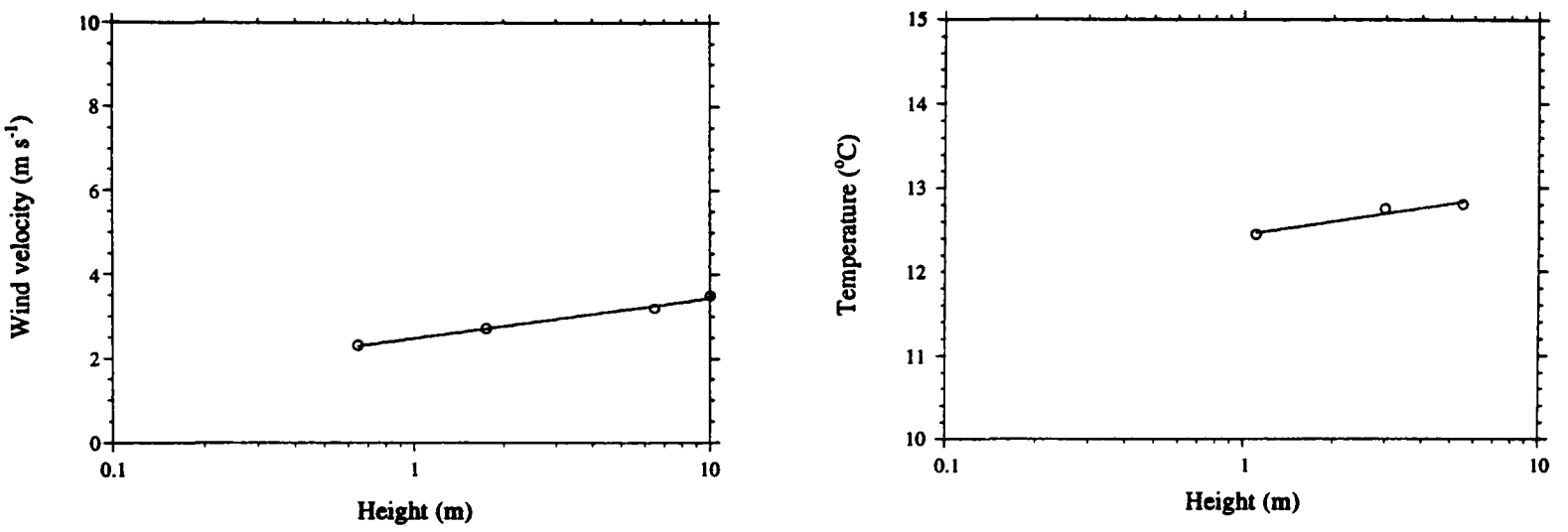

9. Vertical profiles of mean windspeed (left) and temperature (right) acquired during field experiments on 29/10/91.

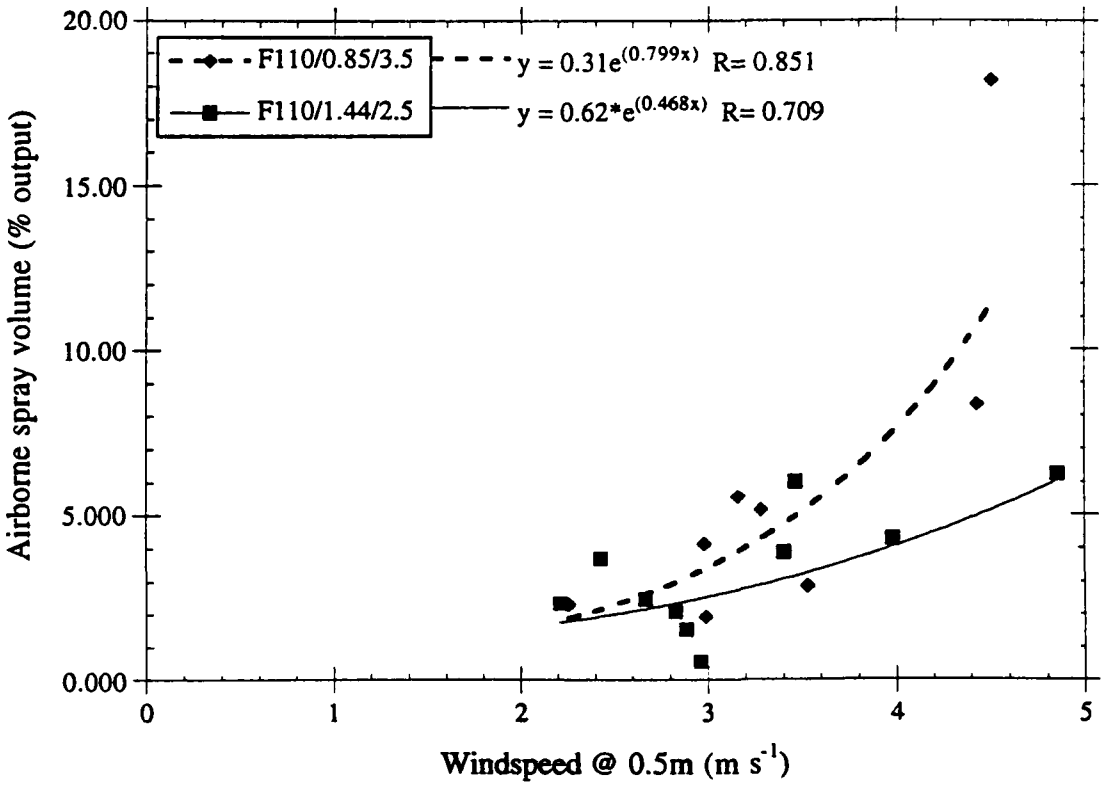

10. The variation of airborne spray volume with windspeed measured in field experiments using single static flat-fan nozzles. The fine nozzle is denoted F110/0.85/3.5 and the medium nozzle is denoted F110/1.44/2.5. Each data point represents airborne spray volume averaged over the collector array.

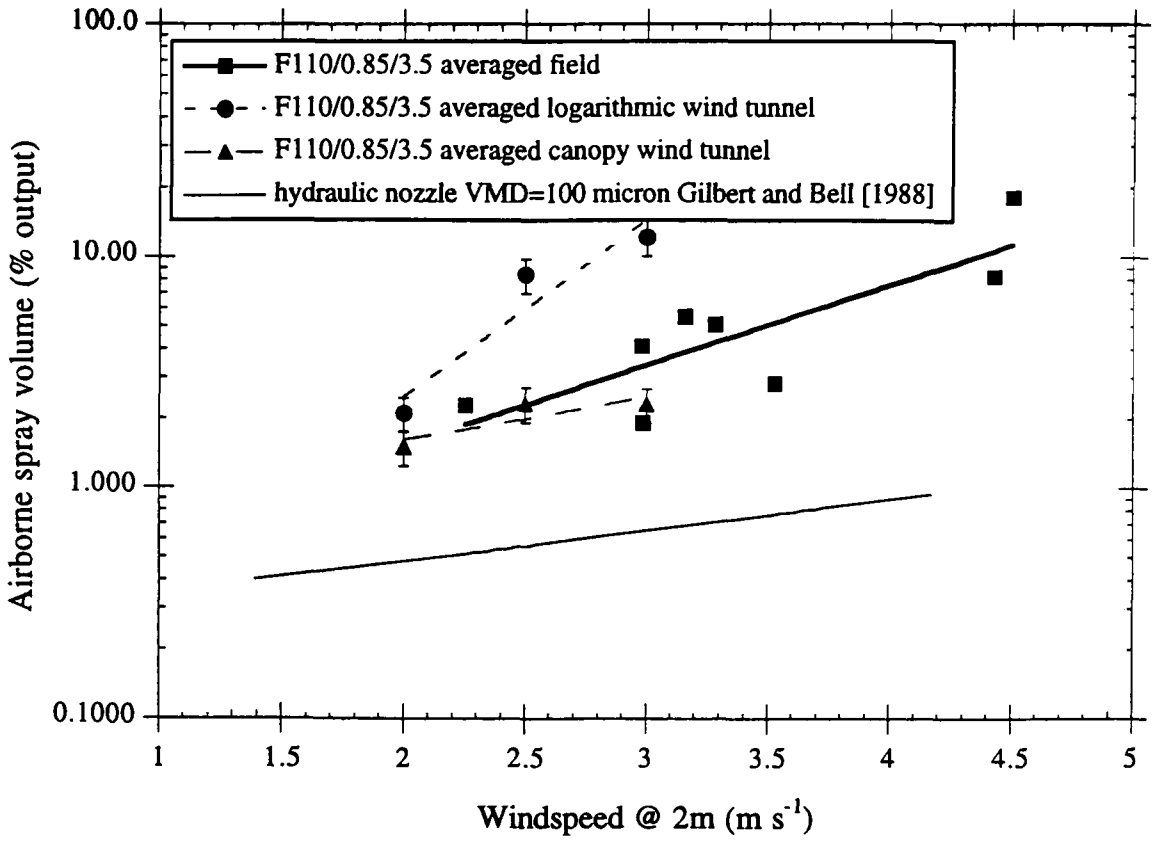

11. The variation of airborne spray volume with windspeed measured in field experiments using the fine nozzle (denoted F110/0.85/3.5). Each data point from the present experiments represents airborne spray volume averaged over the collector array. Gilbert and Bell [1988] presented curve fits to field data measured using a single vertical 10 m passive line collector, 8 m downwind of a conventional boom sprayer.

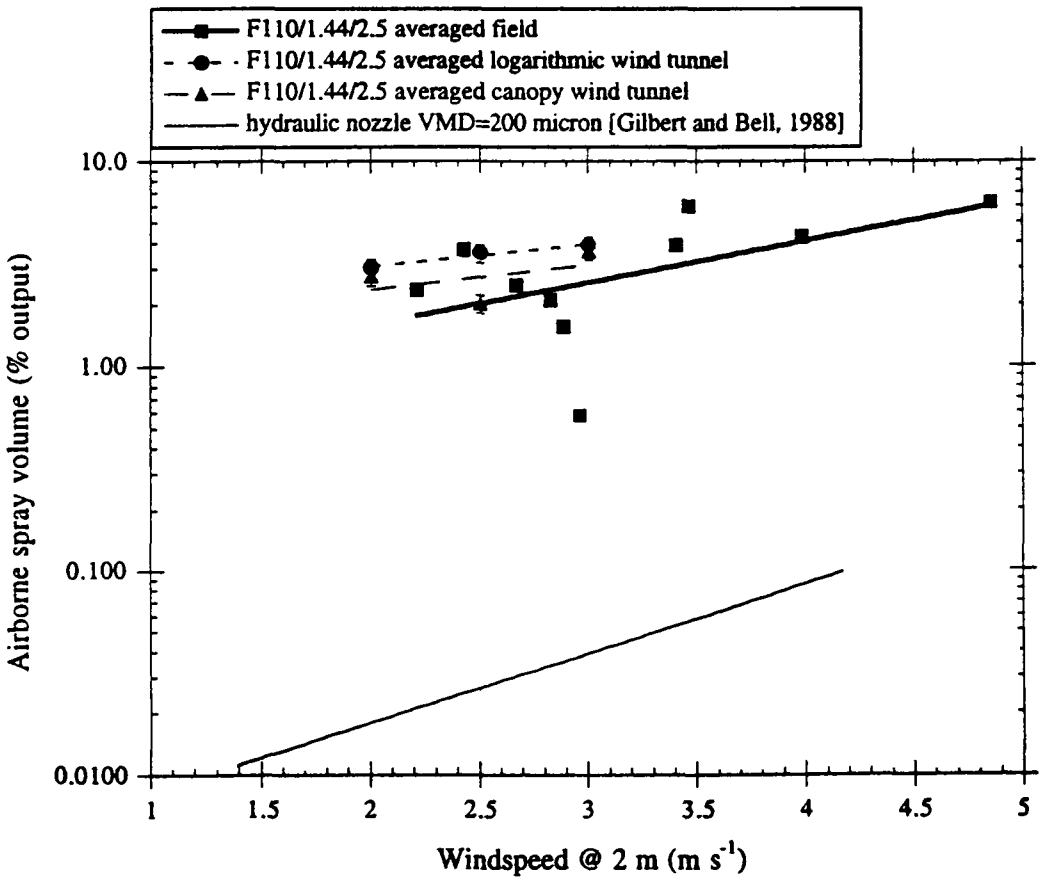

12. The variation of airborne spray volume with windspeed measured in field experiments using the medium nozzle (denoted F110/1.44/2.5). Each data point from the present experiments represents airborne spray volume averaged over the collector array. Gilbert and Bell [1988] presented curve fits to field data measured using a single vertical 10 m passive line collector, 8 m downwind of a conventional boom sprayer.

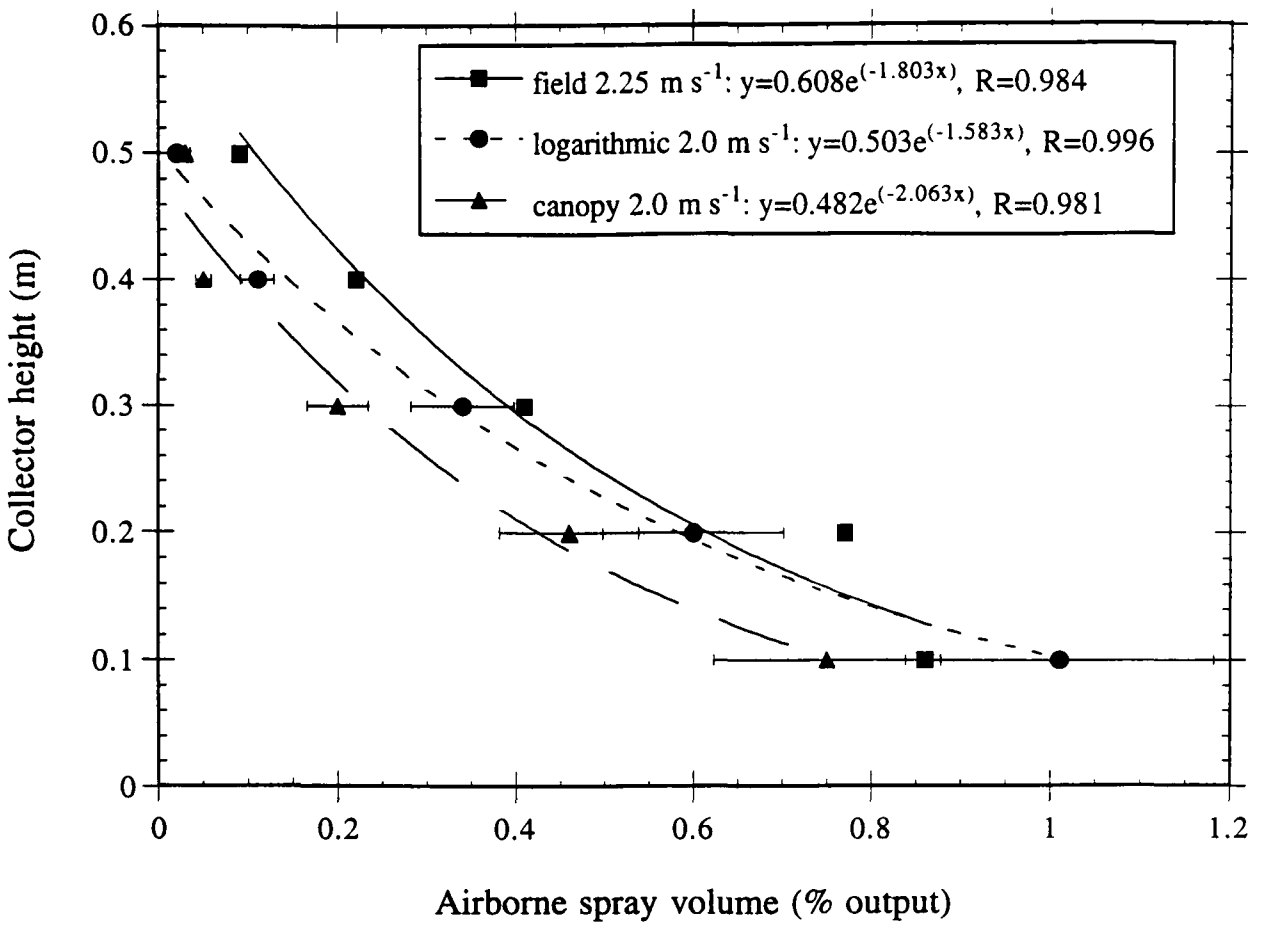

13. Comparison of the vertical profile of airborne spray volume produced by the fine nozzle in a 2.0 m s^{-1} crossflow in field and wind tunnel experiments. Exponential form curves have been fitted to the experimental data.

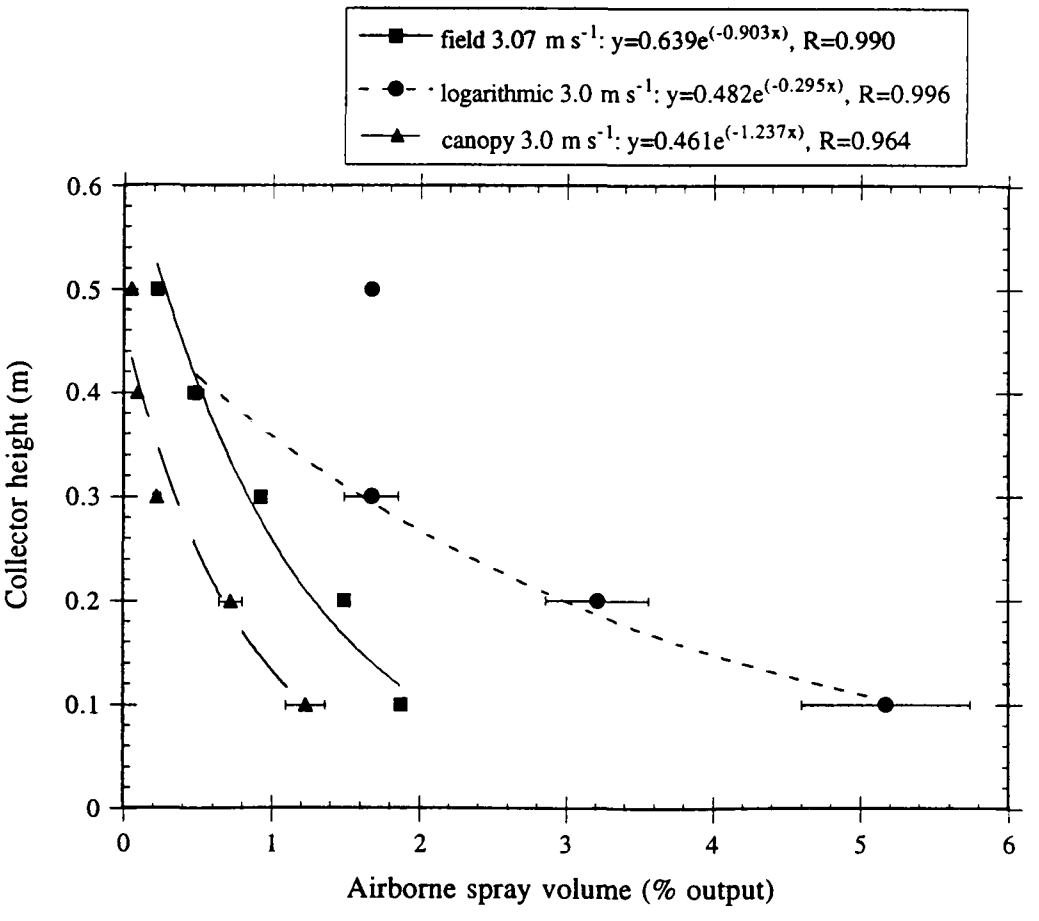

14. Comparison of the vertical profile of airborne spray volume produced by the fine nozzle in a 3.0 m s^{-1} crossflow in field and wind tunnel experiments. Exponential form curves have been fitted to the experimental data.

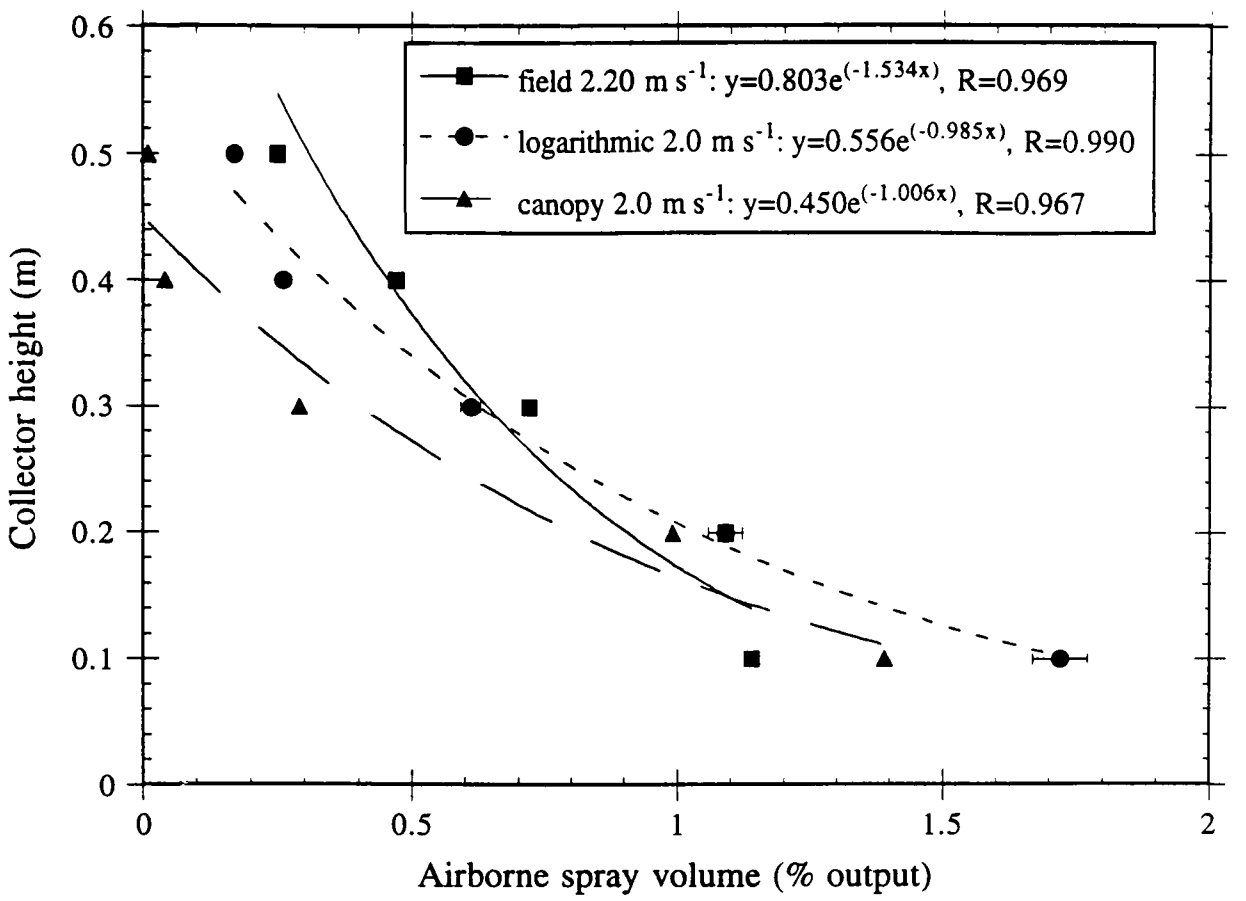

15. Comparison of the vertical profile of airborne spray volume produced by the medium nozzle in a 2.0 m s^{-1} crossflow in field and wind tunnel experiments. Exponential form curves have been fitted to the experimental data.

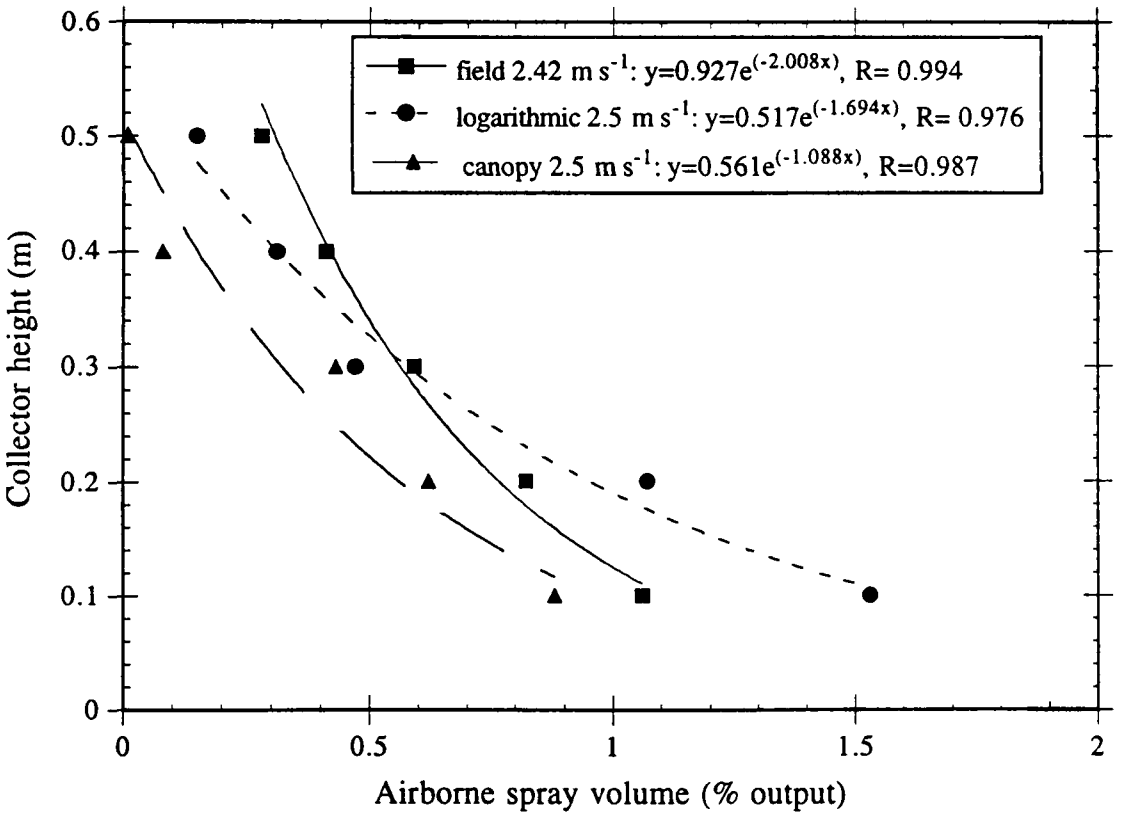

16. Comparison of the vertical profile of airborne spray volume produced by the medium nozzle in a 2.5 m s^{-1} crossflow in field and wind tunnel experiments. Exponential form curves have been fitted to the experimental data.

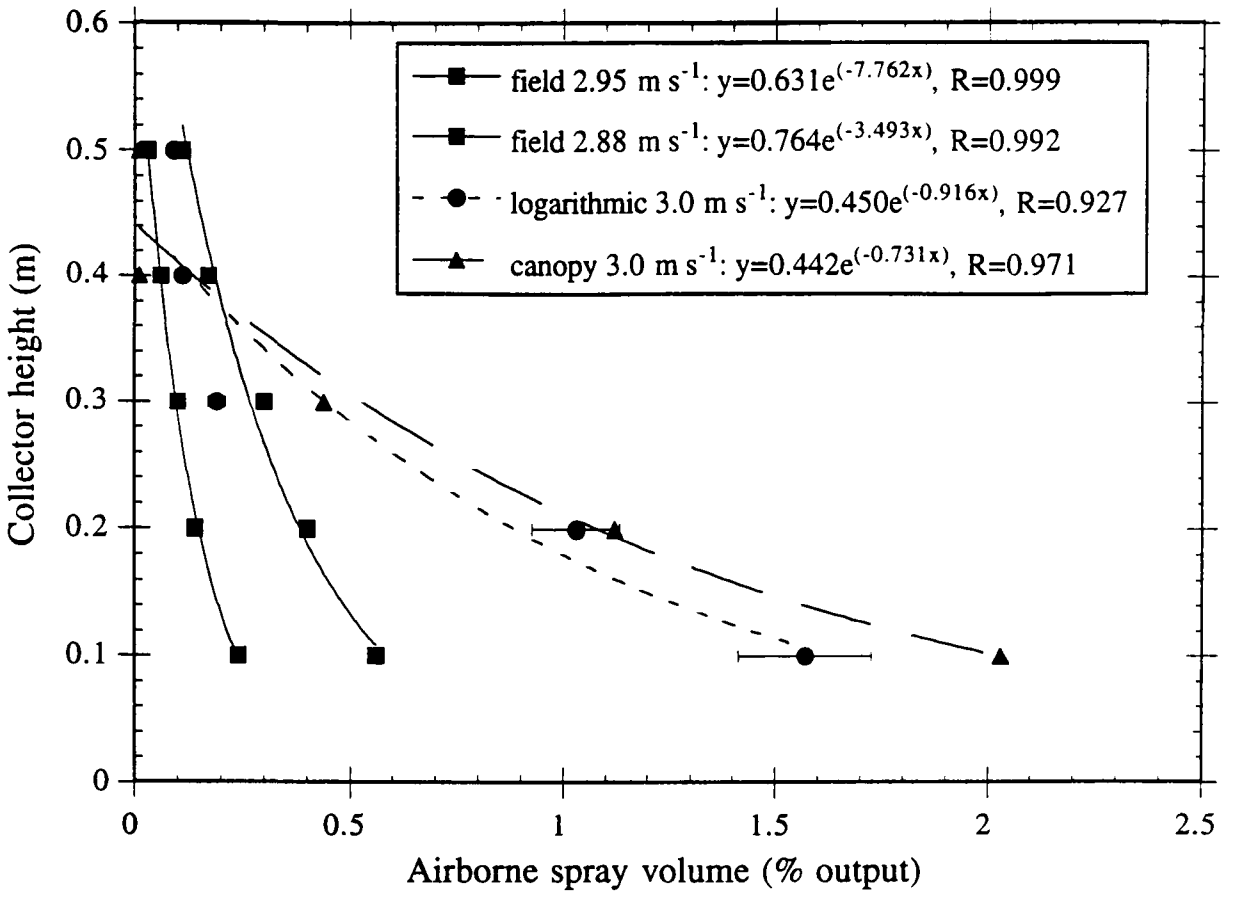

17. Comparison of the vertical profile of airborne spray volume produced by the medium nozzle in a 3.0 m s^{-1} crossflow in field and wind tunnel experiments. Exponential form curves have been fitted to the experimental data.

CHAPTER 4. SPRAY DROPLET AND JET PARTICLE DISPERSION IN STILL AIR

Summary

Measurements of small droplet (diameter < 100 μm) and entrained air transport within a typical agricultural spray, and particle dispersion from a horizontal single-phase planar air jet, both in still air, were conducted as associated background studies to the title-theme of this thesis: spray droplet dispersion in a cross flow. Within the spray, phase-Doppler anemometry (PDA) measurements were taken to determine the decrease of entrained air velocity with distance below the nozzle extending to estimates of small droplet and entrained air interaction at two positions close to the nozzle. The centreline entrained air velocity (estimated using 50 μm diameter droplets as seeding) decreases as the reciprocal of the streamwise distance from the nozzle, from a distance comparable with the *stopping distance* of the volume median diameter-sized droplet. Small droplets are concentrated at the spray centreline with trajectories close to vertical. Their velocity decreases to that of the entrained air between 100 mm and 200 mm below the nozzle. Small droplets correspond to the size fraction measured as downwind drift in previous cross flow studies, and below this initial region they are passively transported by the entrained air flow. Smoke visualisation indicates the absence of large eddies (scaling on the spray width) as observed in single-phase jets generated by the mean shear field. The passage of large droplets (diameter > 300 μm) with high energy density probably disrupts large eddy formation.

A complementary study of particle transport in a horizontal single-phase air jet showed that particle dispersion was controlled by the action of turbulent coherent structures on the jet edges. Flow visualisation experiments using dense tracers (soap-film bubbles filled with dense gas to give a prescribed fall velocity) visualised transient particle-turbulent eddy interactions. Previous numerical simulations suggest that this 'trapping' process occurs when the particle aerodynamic response time is approximately equal to the turbulent eddy turnover time. This scaling is consistent with experimental observations presented here.

1. Layout

This chapter describes two experimental studies: a preliminary characterisation of small droplet (diameter < 100 μm) transport and entrained air velocity within a typical vertical agricultural flat-fan spray; and measurements of dispersion of particles released into a horizontal planar single-phase jet. Both studies contribute associated background information as initial conditions for numerical simulation studies and fundamental transport mechanisms in shear flows. Accordingly, this chapter presents each study separately, with measurements in sprays described in section 2 and measurements in single-phase jets in section 3. Within each section, the study is sub-divided into experimental method, results and brief discussion. A discussion of the implications of these studies to the wider problem of droplet dispersion in a cross flow is provided in section 4 with conclusions in section 5.

2. Droplet and Entrained air Profiles within a Flat-fan Spray in Still Air

2.1. Introduction

A flat-fan spray is produced by forcing liquid (typically a dilute solution) through an elliptical nozzle under pressure [Lefebvre, 1980]. Aerodynamic drag of the liquid sheet issuing from the nozzle against surrounding air induces air *entrainment* into the liquid spray, such that the entrained air and liquid momentum fluxes are approximately equal in the resulting two-phase spray [Ghosh et al., 1991]. Disintegration of the liquid sheet into droplets is controlled by aerodynamic drag forces and liquid surface tension and viscosity, with an initial instability characterised by wave formation on the sheet (described in chapter 1). Droplet and entrained air velocity decrease with distance from the nozzle as the spray spreads. Typical agricultural sprays produce droplet size distributions with diameters ranging from 20-400 μm [Miller, 1993], and within the spray, the entrained air velocity has values which do not exceed the velocity of the large (typically diameter > 300 μm) droplets [Miller et al., 1996]. *Prima facie* expectations are that the large droplet motion (not investigated here) provides continued forcing of the entrained air by aerodynamic drag and that the distribution of these droplets may therefore control the turbulence structure within the spray.

Previous experimental studies of entrainment into flat-fan sprays have been limited to measurement of the entrainment velocity field outside the spray [Briffa and Dombrowski, 1966]. Here, the entrainment velocity field generated by continuity acts perpendicular to the spray

edges and forces smaller droplets towards the spray centreline, as qualitatively observed by Lee and Tankin [1984]. The absence of systematic measurements can be attributed to difficulties of using intrusive techniques such as hot-wire and hot-film anemometry because of probe damage by droplets and fluctuating heat transfer coefficients depending on whether the film is wetted, respectively. Non-intrusive techniques such as laser-Doppler anemometry cannot be applied to a polydispersed droplet diameter range, because of the dependence of Doppler frequency of scattered light on both the size and velocity of the scattering particle. However, the technique of phase-Doppler anemometry [Bachalo and Houser, 1984] has become available which permits non-intrusive simultaneous measurement of droplet size and velocity by spatial resolution of the phase of scattered light. Further details of the technique and equipment specification are provided by Bachalo and Houser [1984].

Although the phase-Doppler anemometer has become an established instrument in the investigation of sprays (in still air), two effects have been identified as potentially leading to incorrect droplet diameter measurement: the *trajectory or Gaussian beam effect* [Sankal et al., 1992] and the *slit effect* [Durst et al., 1994]. Both effects arise when the PDA is set up to measure refractively scattered light, as is typical for sprays. The Gaussian beam effect refers to the non-uniform light intensity distribution within the incident light beams, which results in discrepancies between the position of the true edge of the measuring volume and that calculated by the measurement software. The slit effect refers to the inability to measure the fundamental refraction frequency using conventional PDA due to the location of apertures within the detection optics; this is typically inferred from higher order refracted frequencies. Both effects can be minimised using Doppler burst discrimination by correlating measurements at two photodetectors. However, errors introduced into measurements of volume flux can be substantial, even if errors in diameter measurement relate to only a small percent of the sampled droplets, because of the third power dependence of volume flux on diameter. As these errors remain non-calculable, caution should be exercised when using PDA to measure volume fluxes, even with care in the layout and alignment of equipment [Tropea et al., 1995; Brenn et al., 1995].

Recent theoretical modelling of droplet-driven sprays [Ghosh et al., 1991] has made analogies with dynamics of single-phase jets. The 1-d analysis presented by Ghosh et al. [1991] for centreline entrained air velocity in a droplet-driven spray in still air adopts Taylor's entrainment principle [Morton et al., 1956], which relates the entrainment velocity to the jet velocity field via an entrainment coefficient, α,

$$u_e = \alpha u_j \tag{1}$$

where

u_j is the jet centreline velocity at a given height,

u_e is the entrainment velocity at this height.

Momentum-integral constraints and comparison with experiments yield a value α=0.11 for a droplet-driven spray [Ghosh et al., 1991], compared with α=0.05 for a plane air jet [Rajaratnam, 1976, p.48].

Results from field experiments and numerical simulations [Byass and Lake, 1977; Gilbert and Bell, 1988; Hobson et al., 1993] show that droplets with diameters <100 μm are removed from the spray fan by atmospheric wind. Computationally it is necessary to define initial conditions for estimating the downwind distribution. Detailed numerical simulations and experimental observations of single-phase jets in cross flows [Coelho and Hunt, 1989] show that entrained horizontal momentum controls jet deflection by the cross flow. Experimental work described elsewhere (chapter 3) suggests that the vertical component of momentum due to entrainment compensates for the cross flow horizontal momentum associated with downwind droplet removal, always recognising that spray flexure due to cross flow dynamic pressure will be important. Behaviour of entrained air within the spray will assist understanding of these scavenging mechanisms.

2.2. Experimental Method

The PDA was operated in forward scatter mode, in an orientation to measure the vertical velocity component of droplets in an agricultural flat-fan spray directed downwards with major axis vertical. PDA equipment consisted of a 400 mW Spectra-Physics argon-ion laser source, which produced collimated beams which intersected at an included angle of 60^o, to create a measuring volume with a major axis (vertical) of 1.6 mm and minor axes 0.6 mm. Doppler bursts were detected using Dantec 57X10 600 mm receiving optics, tuned to provide the greatest resolution for droplets in the diameter range 0-350 μm. Signals were processed using a Dantec 58N10 signal processor and Dantec acquisition software running on an HP286 IBM-PC compatible (figure 1). The Doppler frequency of the detected signal was first high-pass filtered at 40 MHz to resolve the direction of droplet motion through the measuring volume (upwards or downwards), thus enabling rejection of signals from droplet reflection (or 'splash') from the floor. Both the frequency and phase of the detected signal were band-pass filtered (4 MHz) and amplified, to remove the signature of beam intensity variation across the measuring volume. These filter values

corresponded to the manufacturer's recommendation for this droplet diameter range. The raw experimental data consisted of a time series of droplet sizes and associated transit times (the time for droplets to cross the measuring volume). This time series was subsequently processed using software written in-house at Silsoe Research Institute to sort the droplet size data into selectable ranges, and to display the number frequency in each size range, the cumulative spray volume that this accounted for, and to calculate the mean droplet velocity within this range.

Experiments were carried out in a partitioned area of the laboratory with a floor area of 3 m $\times$ 3 m, with the equipment configuration illustrated in figure 2. The partition walls extend up to 2.5 m in height, and above these a Unislide motorised 2-dimensional horizontal traverse is mounted. Maximum traverse dimensions are 1.1 m $\times$ 1.1 m and the stepper motors are controlled using an IBM-PC compatible microcomputer. This traverse enables horizontal positioning of the spray nozzle relative to the phase-Doppler anemometer measuring volume, with the height of the spray nozzle set manually to enable 3-dimensional positioning of the measuring volume within the spray. The spray was mounted vertically 0.6 m above the floor to allow measurements down to the nominal ground plane for agricultural spraying (0.5 m below the nozzle) [Miller, 1993]. The spray major axis (spanwise dimension) was aligned with the diagonal of the partitioned area (see figure 2), with the spray centreline (vertical axis) positioned at the centre of the partitioned area. The maximum spanwise traverse of the spray was 0.2 m (see below), corresponding to a minimum distance from the partition wall of 1.2 m, compared with 1.34 m for the spray positioned centrally. A 0.3 m diameter extractor fan mounted on the chamber wall (see figure 2) was used to purge air from the chamber (airflow velocity of about 0.1 m s^{-1}) to minimize droplet recirculation flows set up by the entrained air within the spray impinging on the chamber floor. The flat-fan spray nozzle used in these experiments was a Lurmark 110-02 operated at 3 bar pressure, producing a flowrate of 0.6 L/min. The droplet size distribution produced by this nozzle is shown in figure 3. It is classified as *fine* under the British Crop Protection Council scheme based on cumulative size distribution [Doble et al., 1985].

The spatial distribution of volume flux transported in small (0-100 μm diameter) droplets, their velocity and the entrained air velocity was measured 100 mm and 200 mm below the nozzle. Small droplets are representative of the size fraction measured as downwind drift in field experiments [Byass and Lake, 1977]. The measuring stations were selected to provide information in the region of establishment of entrained air profiles within the spray, and to determine the spatial distribution of small droplets in this region. The sampling region was restricted to one side of the spray to avoid excessive data acquisition. At each measuring station

below the nozzle, the origin for the measurement plane was located on the spray centreline. This position was determined from entrained air velocity measurements made on two perpendicular traverses corresponding to the spray major and minor axes, with the centreline corresponding to the 2-d maximum. Symmetry checks made during this process by also sampling larger droplet (diameter $> 300\mu$m) vertical flux confirmed that the spray was symmetrical about the centreline. The measuring positions for both vertical stations are shown in figure 4, related by simple geometrical scaling. 100 mm below the nozzle, the horizontal plane traversed had a width of 9 mm, and a length of 150 mm. At this vertical station, the spray half-width had dimensions 17.5 mm $\times$ 145 mm, so the sampled region corresponded to a view of the spray which has been halved along its length, and the central two quarters of its width selected (figure 4). 200 mm below the spray nozzle, the spray half-width had dimensions 35 mm $\times$ 290 mm. The horizontal plane traversed had width 32 mm but was only extended to 150 mm along the spray major axis, as beyond this position, only a very low flux of small droplets was observed. 100 mm below the nozzle, 6 measurements were taken along the spray major axis at each of 3 positions across the spray major axis, a total of 18 positions, and 200 mm below the nozzle, 4 measurements were taken along the spray major axis at each of 3 positions across the spray major axis, a total of 12 positions. The measurement grid is shown in figure 4.

Entrained air velocity was also measured on the spray centreline (vertical axis) at 13 stations down to 600 mm below the nozzle. At each station, the spray was traversed across the PDA measuring volume in two perpendicular directions as before to locate the spray centreline. At each vertical station 5000 droplets were measured for their sizes and velocities, with data rates varying from 2.1 KHz (50 mm below the nozzle) to $\sim$20 Hz (600 mm below the nozzle). 50 μm diameter spray droplets (diameter range 45-55 μm) were taken to be representative of the entrained air velocity. The aerodynamic response time (τ_a) of these droplets is 7.3×10^{-3} s [Clift et al., 1978, p.266],

$$\tau_a = \frac{d^2\,(2\gamma + 1)}{36\nu} \tag{2}$$

where

d is the droplet diameter,

γ is the ratio of droplet to fluid density ($\frac{\rho_p}{\rho_f}$),

ν is the fluid kinematic viscosity.

A short response time means that high frequency components of the fluctuating air velocity can

be followed by 50 μm diameter droplets. Initial experiments were conducted using smaller (15-25 μm diameter) droplets generated by the nozzle, whose response time was 2×10^{-4} s; however, electronic noise generated by the PDA photodetectors was significant when measuring very small droplet diameter ranges, and the number of small droplets produced by the spray nozzle was insufficient to provide reliable statistics. Similar problems were encountered by Miller et al. [1996] in making PDA measurements over this droplet diameter range.

The characteristic turbulent eddy size within the spray could not be measured using the PDA (as only 1-dimensional velocity measurements could be made with the equipment used) or conventional thermal anemometry (recall introduction) so a qualitative picture of the turbulence structure was obtained using flow visualisation techniques. Shell Ondina oil smoke produced by a CFT smoke generator was released essentially passively into the entrainment velocity field around the spray. The smoke was entrained into the spray, and flow patterns were recorded using a Mamiya 645 4.5×4.5 format camera on Ilford HP5 400 ASA black-and-white film.

2.3. Experimental Results

The liquid volume flux transported in small droplets 100 mm below the nozzle is shown in figure 5. The volume flux distribution is approximately uniform across the spray width within the central portion of the spray (spanwise distances up to about 60 mm at this height). Asymmetry at greater spanwise distances reflects local variation in small droplet volume flux produced by the particular nozzle used. The spanwise profile shows a systematic decrease from the spray centre to its edge, with the appearance of an approximately Gaussian profile. Similar spanwise volume flux profiles are observed 200 mm below the nozzle (figure 6). The volume flux in small droplets on the axis varies from 0.24 μL/mm^2 s at the centre to 0.16 μL/mm^2 s at the edge of the sampled region, and shows significant asymmetry across the spray width. Outside the sampled region, the volume flux of small droplets is almost zero. Numerical integration of the small droplet profiles shown in figures 5 and 6 suggested that over the measured region, the total volume flux transported by small droplets 100 mm and 200 mm below the nozzle was approximately equal.

The vertical velocity of 50 μm diameter droplets (representative of entrained air velocity) and small droplets (0-100 μm diameter) 100 mm below the nozzle is shown in figure 7. The velocity profiles show a peak on the spray centreline, decreasing along the spray major axis from the origin. Asymmetry across the spray width is observed in the profiles, probably associated with local variation in liquid sheet breakup produced by the particular nozzle measured, and

consistent with asymmetry in the small droplet volume flux measurements at this vertical station (figure 5). Vertical velocity profiles 200 mm below the nozzle are shown in figure 8. The profiles show the same general form as those measured 100 mm below the nozzle, although exhibiting less asymmetry across the spray, indicative of relaxation of velocity differences and establishment of the fully-developed spray. Small droplets show a significant decrease in vertical velocity between the two measuring positions, and 200 mm below the nozzle their velocity has decreased to the entrained air velocity.

The vertical profile of centreline air velocity below the nozzle is shown in figure 9 in log-log form. The data appear to fit a linear relationship (on logarithmic axes), corresponding to power law decrease of velocity as approximately z^{-1} where z is the vertical distance below the nozzle. The profile shows an initial rate of decrease less than z^{-1} based on an initial measurement 25 mm below the nozzle. However, this position is comparable to the liquid sheet breakup length for a typical agricultural spray [Miller et al., 1996], so the entrained airflow in this region is not characteristic of the fully-developed two-phase spray.

An instantaneous picture of smoke patterns within the flat-fan spray is shown in figure 10 (exposure time 0.001 s). There are no large-scale flow patterns visible in the smoke within the spray, suggesting that scales of turbulence are small. The turbulence structure of the entrained air velocity field within a flat-fan spray is qualitatively different from that within a single-phase planar jet, where turbulence scales of the order of the jet half-width exist [Townsend, 1976. p.223]. A plausible explanation for the observation of no large-scale structure within the spray is that the motion of large droplets disrupts any coherence within the entrained air velocity field, in line with *prima facie* expectations (recall introduction).

2.4. Discussion

Entrained air profiles and small droplet transport in the region of two-phase spray development within a typical agricultural flat-fan spray were revealed using phase-Doppler anemometry, the main elements of which are summarised as follows. Experimental measurements of entrained air velocity show a peak on the spray centreline and decrease towards the spray edges, similar to Gaussian profiles observed within single-phase air jets. This confirms that both measurement stations (100 mm and 200 mm below the nozzle) were within the fully-developed two-phase spray. The initial measurement position for the centreline entrained air measurements (25 mm below the nozzle) was comparable to the liquid sheet breakup position, with measurements

in the region of sheet breakup showing that the decrease of centreline entrained air scales as $z^{-\frac{1}{2}}$, where z is the distance from the nozzle. In this region the entrained air decreases in the same manner as the geometrically equivalent single-phase jet, a planar (fully 2-d spreading) jet. The initial position at which the entrained air decreases linearly with distance below the nozzle (this behaviour typical of the spray down to 500 mm below the nozzle) at about 80 mm below the nozzle (figure 9) is equivalent to the (Stokes) *aerodynamic stopping distance* of the VMD diameter (195 μm) droplet for this spray nozzle,

$$z_* = \frac{d}{2}\frac{\rho_p}{\rho_f} \tag{3}$$

where

d= droplet diameter,

ρ_f is the density of surrounding fluid,

ρ_p is the density of liquid droplet.

The lower rate of decrease of centreline entrained air velocity below this region presumably reflects the reduced forcing of the large droplets (which have velocities significantly in excess of the entrained air velocity [Miller et al., 1996]) on the entrained airflow within the fully-developed spray, as compared with drag against the coherent liquid sheet. The observation that the region of spray development is of equivalent length to the VMD droplet stopping distance offers the plausible possibility that entrainment of air into a polydispersed spray may be characterised by the behaviour of the VMD diameter droplet, although much further testing with other spray nozzles and qualities is required. For present purposes it provides confirmation that the measuring station 100 mm below the nozzle is located within the fully-developed two-phase flow near to its origin. Small droplets show their peak concentration within the spray at the centreline and exhibit vertical trajectories in this region. These droplets have short aerodynamic response times (0.04 s for a 100 μm diameter water droplet in air), so can respond to the action of the entrained air velocity field and migrate towards the spray centreline. Between 100 mm and 200 mm below the nozzle, the small droplet velocity decreases to that of the entrained air. This suggests that the small droplets are passively transported by the entrained air field maintained by larger droplet motion.

3. Particle Transport in a Plane Air Jet

3.1. Introduction

In the second half of this chapter, an experimental study of the interaction of dense particles with turbulent coherent structures (eddies) is presented. Previous experimental studies of agricultural sprays in cross flows (the subject of this thesis) have suggested that vortex pair formation resulting from interaction of a vertical spray with a horizontal cross flow (by analogy with single-phase jets in cross flow) leads to localised 'trapping' and subseqent dispersion of droplets (recall chapter 1). However, to date, no direct experimental observations of this process have been published. *Prima facie* expectations are that this process may also be important in the vicinity of the spraying vehicle wake (drifting droplets interacting with vehicle and boom structure wakes) and in the far-field (settling droplets interacting with plant canopy generated turbulence). The role of the plant canopy as a compliant lower boundary with associated coupling between velocity fields within and above the canopy (recall chapter 1) suggests that droplet-coherent structure interaction may control droplet deposition onto the crop.

Dense particles were released into a horizontal turbulent plane air jet to investigate the role of turbulent coherent structures (eddies) in particle dispersion. Experimental data were compared against predictions made using a random flight model for particle transport in air jets [Perkins et al., 1991]. The model velocity field was constructed from experimental velocity and turbulence intensity profiles measured here (see below), with integral timescales to describe the effect of particle inertia subject to standard approximations (full details in Perkins et al. [1991]). The experimental concentration distribution as a function of downstream position was used as a measure of whether the model was correctly predicting particle transport by the jet. A single-phase air jet was chosen as its velocity field can be simply measured using hot-wire anemometry and compared with previous characterisations [Bradbury, 1965; Rajaratnam, 1976, p.21]. Numerical models have identified trapping of dense particles by turbulent eddies in axisymmetric air jets [Yule, 1980; Chung and Troutt, 1988], which occurs when the particle aerodynamic response time is approximately equal to the eddy turnover time [Chung and Troutt, 1988]. This behaviour was observed experimentally in the present study.

3.2. Experimental Method

The plane air jet was produced by a 30 W centrifugal blower discharging through a horizontal slot of dimensions 0.2 x 0.01 m (figure 11). Vertical velocity profiles were measured at various downstream sections through the jet, using a DISA 55M01 hot-wire anemometer and an RS Thirlby 1906a digital multimeter. The hot-wire anemometer signal was linearised using a DISA 55M25 lineariser, necessary for measurement of turbulence intensity in the free shear layers which bound a plane jet, where streamwise intensities are typically 20% [Bradbury, 1965]. The hot-wire anemometer was calibrated in-situ against an Airflow Developments 4 mm pitot-static tube connected to a Betz manometer before and after each experiment (figure 12).

A patternation experiment (figure 13) was devised as a means of investigating particle transport within the jet. Particles of two different diameters were introduced into the plane air jet via a vibrating hopper to minimize cohesion between particles. This was positioned above the jet centreline, with particles collected in 30 trays (width 50 mm) mounted on the jet base, below the centreline. Particles were discharged slowly (approximately 10 g/min) to prevent them simply falling through the jet in a narrow stream; particle concentrations in the jet were correspondingly low so the effect of particles on the flow can be neglected. At the end of each experiment, the mass of particles in each tray was measured, to determine the 1-dimensional deposition concentration distribution along the jet.

Two sizes of quartz particle were employed, with volume median diameters (VMD's) of 86 μm (mean diameter 81 μm; standard deviation 43 μm) and 244 μm (mean diameter 241 μm; standard deviation 37 μm). Particle diameters were measured using an AMS optomax V image analyser by Dr A.B. Pandit (University of Cambridge). The particle density was 2.5×10^3 Kg m^{-3}, determined by density bottle analysis [Anon, 1985, P.41]. Terminal fall velocities for these particles are 0.34 m s^{-1} for 86 μm diameter and 2.4 m s^{-1} for 244 μm diameter. These velocities were calculated using a standard method for flow past a sphere outside the Stokes flow regime, which employs graphical correlations between particle Reynolds number (defined as $\frac{u_r d}{\nu}$ where u_r is the relative velocity between particle and fluid, d is the particle diameter and ν is the fluid kinematic viscosity) and drag coefficient, appropriate for Reynolds numbers less than 500 [Douglas et al., 1993, p.371]. The equation of motion for a droplet at terminal fall velocity in this regime is given by

$$C_d Re^2 = \frac{4}{3}\frac{d^3(\rho_p - \rho_f)\rho_f g}{\mu^2} \tag{4}$$

where

C_d is the drag coefficient,

Re is the particle Reynolds number,

d is particle diameter,

ρ_p is the particle density,

ρ_f is the fluid density,

g is the acceleration due to gravity,

μ is fluid viscosity,

with ρ_p=2.5×10^3 Kg m^{-3} (quartz), ρ_f=1.22 Kg m^{-3} (air), μ=1.8×10^{-5} Kg m^{-1} s^{-1} (air) [White, 1979, p.27]. The jet exit velocity for experiments using 244 μm diameter particles was 13.5 m s^{-1}, and that for the 86 μm diameter particles was 6.6 m s^{-1}, giving jet exit Reynolds numbers of 8300 and 4800 respectively. Jet exit Reynolds number is defined as $(\frac{u_o \delta_o}{\nu})$ where u_o is the exit velocity, δ_o is the nozzle width, ν is the kinematic viscosity of air. Air velocity measurements were made through the horizontal plane air jet by taking vertical traverses at 5 downstream stations (x=143 mm, 283 mm, 423 mm, 563 mm and 703 mm).

These data were used as input to a random flight model with which to compare the measured downstream concentration distribution. Full details are provided by Perkins et al. [1991] with only a brief summary presented here. The motion of the particles was modelled considering buoyancy and drag forces only, neglecting lift and pressure gradient forces (small compared with drag and buoyancy) and history effects (negligible for $\gamma < 10^3$ [Clift et al., 1978, p.67]). The fluctuating velocities sampled by a fluid element in the turbulent velocity field were modelled as a stochastic process derived from the Langevin equation, as used to compute dispersion in a range of turbulent flows [van Dop et al., 1985; Luhar and Britter, 1989]. This was modified to include correlations between streamwise and spanwise fluctuating velocities following Legg and Raupach [1982]. Lagrangian integral timescales were estimated and modified for sampling by particles rather than fluid elements using standard approximations [Corrsin, 1963; Hunt and Nalpanis, 1985].

Flow visualisation experiments were carried out on particles released into the jet. Stroboscopy using 35 mm photography provided adequate visualisation of the 244 μm diameter particle trajectories, which were smooth as expected for particles with relatively high inertia. However, visual observations of 86 μm diameter particle trajectories showed vortical motion on

the jet edges requiring a large object plane to characterise the motion. Using photographic techniques, a resolution limit is reached such that the ratio of particle size to width of object frame is less than the ratio of film grain size to width of the image plane i.e. above a critical width of flow field visualised or length of particle trajectory, particle images become smaller than the film grain size. This was the case for 86 μm diameter particles over the region of interest here, so larger diameter soap-film bubbles prescribed with the terminal fall velocity of 86 μm diameter quartz particles (0.46 m s^{-1}) were used as particle trajectory tracers. Typically, these bubbles are filled with helium to provide neutrally-buoyant flow tracers, but when filled with common laboratory gases can be given a prescribed fall velocity. It was found that air-filled soap bubbles (fall velocities in the range 0.4-0.6 m s^{-1}) provided adequate matching to the fall velocity of 86 μm diameter quartz particles. A helium bubble generator (Sage Action Inc.) fitted with a low-speed head (flows up to 20 m s^{-1}) was modified for this purpose. Bubbles produced had diameters of approximately 2 mm. Clearly, mismatch in particle and flow tracer diameters (the objective here) means that at any jet cross-section, the number of tracer bubbles accomodated in the jet will be much lower than the number of quartz particles.

3.3. Experimental Results

Air velocity measurements were made for fan speeds corresponding to jet exit velocities of 6.6 m s^{-1} and 13.5 m s^{-1}, with the resulting velocity profiles normalised on these velocities. The mean velocity profile (figure 14) was fitted to a curve of the form suggested by Goertler [Schlichting, 1968, p.605],

$$u = u_j \left[1 - \tanh^2\left(\frac{By}{x}\right)\right] \tag{5}$$

where u_j is the jet centreline velocity, and x and y are the streamwise and spanwise distances from the jet origin. B is an empirical coefficient whose value has been determined from experiments as 7.67 [Rajaratnam, 1976, p.23].

Turbulence intensity profiles were normalised in the same manner as for the mean velocity profiles, and fitted as the sum of two Gaussian profiles, as suggested by previous measurements using a plane turbulent jet [Bradbury, 1965],

$$\frac{\overline{u'^2}}{{u_c}^2} = a_1 \left[\exp\left(a_2(\frac{y}{x} - a_3)^2\right) + \exp\left(a_2(\frac{y}{x} + a_3)^2\right)\right] \tag{6}$$

where the coefficients a_1 =0.0604, a_2 =-131, a_3 =0.0880 were obtained by S.Ghosh (University of Cambridge), who used a non-linear least-squares scheme. There is significant scatter in the

experimental data (figure 15), but individual datasets exhibit the twin peaked profile. It is clear that the 'noisy' air jet used in these experiments does not provide an ideal basis for comparison with results of model predictions.

The results of the patternation experiment compared with numerical simulations (using the above fits to velocity measurements as input) are shown in figure 16. There was good agreement between the model and observed behaviour for 244 μm diameter particles for both the mean and variance of the concentration distributions. The spread in the distribution must be due to interaction between particles and turbulence so close agreement suggests that the model must adequately simulate this. However a considerable discrepancy was observed between model and experimental results for 86 μm diameter particles (figure 16). The random flight model over-predicted by a factor of approximately 2 the position of maximum concentration, and indicated a much larger spread than was observed experimentally. The 86 μm diameter particles are clearly responding to turbulence in a different way to the simple parameterisation used in the random flight model. A contribution to the larger dispersion of these particles observed in the experiments must be due to the higher turbulence intensities measured as compared with the fitted profile used in the model (see figure 15). In addition, it is unlikely that the sharp peak in the concentration distribution is due to any external mean flow induced by entrainment. Visual observations of the experiments suggested that particles were being 'ejected' from the jet by large-scale eddies, an interaction the model cannot reproduce as it does not simulate the spatial structure of the velocity field.

Observations of the trajectories of 244 μm diameter particles and 'heavy' air-filled soap film bubbles are presented as figures 17 and 18. 244 μm diameter particles show smooth trajectories associated with particles of relatively high inertia (figure 17). The bubbles produced streaklines which clearly show interactions with coherent structures (figure 18). The bubbles appear to have been drawn into a region of accelerating flow and imparted with angular velocity due to that eddy. Other dense tracer bubbles demonstrate another form of particle-structure interaction: bubbles enter the region behind an eddy where flow retardation takes place. Streaklines in figure 18 indicate tracer motions which follow the jet axis until interaction with a coherent structure causes an abrupt fall from the jet under gravity. Dense tracer bubbles appeared to fall vertically from the jet after detrainment. If these tracers had been interacting with an external upstream return flow induced by entrainment, the tracer trajectories would have shown upstream deflection. The discrepancy between experimental and random flight model results was attributed to particle-coherent structure interaction.

3.4. Discussion

Patternation and flow visualisation experiments suggested that 86 μm diameter particles were removed from the plane air jet by interaction with turbulent coherent structures. The observation that dense particles are 'flung out' of a jet by turbulent coherent structures was also made in discrete vortex simulations of an axisymmetric air jet by Chung and Troutt [1988]. They show that this interaction can occur when the particle aerodynamic response time (τ_a) is approximately equal to the eddy turnover time (τ_e). Aerodynamic response times of 86 μm and 244 μm diameter particles are approximately 0.05 s and 0.48 s respectively (equation 2). An estimate of the eddy turnover time (τ_e) can be made as follows. A typical eddy has radius approximately equal to the jet half-width, b, and velocity approximately half the jet centreline velocity, u_j [Perkins et al., 1991]. Thus

$$\tau_e \sim \frac{4\pi b}{u_j}. \tag{7}$$

The release position for 86 μm diameter particle experiments was 150 mm downstream of the jet nozzle, and here, τ_e ~0.05 s. This is approximately equal to the 86 μm diameter particle aerodynamic response time, so it is likely that dense tracer bubbles were abruptly detrained from the jet by particle-coherent structure interaction. The release position for 244 μm diameter particles was 80 mm from the jet nozzle, at which point τ_e ~0.03 s. The aerodynamic response time for a 244 μm diameter quartz particle is approximately 0.48 s, so particle-coherent structure interaction does not occur. The experimental observations and above scalings satisfactorily explain the over-prediction of the random flight model which does not incorporate turbulence *structure*.

Flow visualisation using dense tracer bubbles provide observations of particle-coherent structure interaction which are consistent with numerical modelling studies by Perkins and Hunt [1986]. For a rotational (Rankine-type) vortex (figure 19), there exists a critical trajectory which separates a region of closed trajectories; light particles released within this region remain trapped, light particles released outside this region can never enter. Perkins and Hunt [1986] show that this region can only exist if

$$\left| \frac{\Omega r_o}{2u_t} \right| \leq 1 \tag{8}$$

where

r_o=the radius at which the maximum velocity occurs,

Ω=twice the angular velocity at radius r_o,

u_t=fall velocity of particle.

A dense particle with its own inertia and trajectory will never be *trapped* in a single vortex because of its inertia, but could still experience transient interactions with turbulent coherent structures, if its response time is sufficiently short. Two modes of interaction are envisaged. The particle trajectory could intersect the high-shear region around the coherent structure and be accelerated around the recirculating region (figure 19). The particle trajectory could also intersect the low-shear region and be decelerated by the recirculating flow. This would arrest particle motion in the streamwise direction, and it would subsequently fall from the jet under gravity, or be detrained with an upstream component of velocity imparted by the local vorticity. These processes are visualised as transient particle-structure interactions, rather than 'trapping' processes and are consistent with observations of abrupt detrainment of 86 μm diameter particles and dense tracer bubbles from the plane air jet in these experiments.

4. Implications for Sprays in Cross Flows

Fundamental measurements of the entrained air velocity within a flat-fan spray and particle transport in plane air jets reveal aspects of spray structure and particle motions which are relevant to the title theme of this thesis, droplet dispersion from sprays in cross flows. However, it must be cautioned that, for the case of sprays in cross flow, spray flexure to the action of the cross flow pressure and entrained air fields may significantly modify the entrained air field within the spray, as is the case for single-phase jets in cross flow (recall chapter 1). As an intermediate stage to measurements of entrained air within a spray fan in a cross flow, present data may be used to provide improved estimates of initial conditions for numerical simulations.

Typically agricultural sprays are directed vertically downwards from nozzles mounted 0.5 m above the plant canopy top. In still air, the fully-developed two-phase spray extends from about 0.08 m below the nozzle to the canopy. From about 0.2 m below the nozzle, the small (diameter 0-100 μm) droplets which make up the downwind drift fraction in an atmospheric cross flow [Byass and Lake, 1977; Gilbert and Bell, 1988] are passively transported by the entrained air velocity field. This mode of transport suggests that the entrained air within the spray fan acts to stabilise the spray against dispersion of small droplets. The role of entrained air resisting droplet removal from the spray fan is further investigated in chapter 5, which presents measurements of drifting droplet parameters downwind of sprays oriented perpendicular to the cross flow

direction. Observations of approximately Gaussian profiles of entrained air velocity along the spray fan major axis suggest that it is insufficient to parameterise the effect of entrained air as the mean centreline value as employed in previous numerical simulations [Miller and Hadfield, 1989; Hobson et al., 1993]. This approximation may not even be sufficient with the spray major axis aligned with the cross flow, as entrained air profiles also decrease from the centreline perpendicular to the spray major axis.

Comparison of experimental measurements of particle dispersion in a plane air jet with predictions from a random flight model suggested interaction of particles with turbulent coherent structures, visualised using air-filled helium tracer bubbles. Eddy length scale measurements within sprays (not possible with the equipment used here) are required to determine whether this is an important transport mechanism in regions of high small droplet concentration within the spray. Observations suggest this interaction occurs when the particle (or droplet) response time is approximately equal to the eddy turnover time [Chung and Troutt, 1988], and this scaling could also be applied to droplet transport in the vicinity of agricultural sprays to assess the range of spray boom or plant canopy generated turbulence length scales which could trap and disperse drifting droplets. This characterisation requires the measurement of drifting droplet sizes and velocities in the drift field downwind of typical agricultural spraying equipment, investigated in chapter 5.

5. Conclusions

1. Spray drift results from the transport of droplets smaller than about 100 μm. Within the fully-developed two-phase spray, these droplets migrate to the spray centreline due to the action of entrained air, and have trajectories that are parallel with the spray centreline. Droplet velocities relax to the entrained air velocity at a distance below the nozzle which is dependent on their inertia. For small droplets (diameter < 100 μm), this occurs between 100 mm and 200 mm below the nozzle. Below this region, small droplets are essentially passively transported by the entrained air velocity field.

2. Below an initial flow establishment region, the centreline entrained air velocity decreases as z^{-1}, where z is the distance from the nozzle. The rate of decrease within the equivalent single-phase planar jet scales as $z^{-\frac{1}{2}}$. The length of the flow establishment region is approximately equal to the stopping distance of the VMD-sized droplet. The turbulence structure of entrained air flow within an agricultural spray is visually different from that of

a single-phase air jet, with only small scales of turbulence apparently present. These observations require confirmation with direct measurement of eddy length scales (not available in this study).

3. Within the fully-developed two-phase spray, the entrained air mean velocity profiles are approximately Gaussian at measuring stations 100 and 200 mm below the nozzle. It may therefore be insufficient for numerical simulation purposes to parameterise the entrained air velocity field using the centreline value only.

4. The action of turbulent coherent structures in dispersion of particles from a plane air jet has been identified. Transient interactions between particles and coherent structures occur when the particle response time is approximately equal to the eddy turnover time, as previously observed in numerical simulation studies [Chung and Troutt, 1988].

References

Anon [1985] *Physics Students Guide 1 - Nuffield Advanced Science.* Longman, U.K.

Bachalo, M.D. and Houser, W.J. 1984. Phase/Doppler spray analyser for simultaneous measurements of droplet size and velocity distributions. *Optical Eng.* **23**, 583-590.

Bradbury, L.J.S. [1965] The structure of a self-preserving turbulent plane jet. *J. Fluid Mech.* **23**, 31-64.

Brenn, G., Dominik, J., Durst, F., Tropea, C. and Xu, T.-H. [1995] Phase-Doppler arrangements with minimised Gaussian Beam effect and slit effect. Proc. 20th Anniversary Meeting of Phase-Doppler Anemometry, Erlangen, Germany.

Briffa, F.E.J. and Dombrowski, N. [1966] Entrainment of air into a liquid spray. *A.I.Ch.E. Jnl.*, **43** 708-717.

Byass, J.B. and Lake, J.R. [1977] Spray drift from a tractor powered field sprayer. *Pesticide Science* **8**, 117-126.

Chung, J.N. and Troutt, T.R. [1988] Simulations of particle dispersion in an axisymmetric jet. *J. Fluid Mech.* **186**, 199-222.

Clift, R., Grace, J.R. and Weber, M.E. [1978] *Bubbles, Drops and Particles.* Academic Press, London.

Coelho, S.L.V., and Hunt, J.C.R. [1989] The dynamics of the near-field of strong jets in crossflows. *J. Fluid Mech.* **200**, 95-120.

Corrsin, S. [1963] Estimation of the relation between Eulerian and Lagrangian scales in large Reynolds number turbulence. *J. Atmos. Sci.* **20**, 115-119.

Doble, S.J., Matthews, G.A., Rutherford, I. and Southcombe, E. [1985] *Proc. British Crop Protection Conference*, 1125.

Dombrowski, N. and Johns, W.R. [1963] The aerodynamic instability and disintegration of liquid sheets. *Chem. Eng. Sci.*, **18** 203-214.

Douglas, J.F., Gasiorek, J.M. and Swaffield, J.A. [1993] *Fluid Mechanics.* 3rd ed., Longman, U.K.

Durst, F., Tropea, C. and Xu, T.-H. [1994] The slit effect in phase-Doppler anemometry. Proc 2nd International Conference on Fluid Dynamics Measurement and its Application,

Beijing, China.

Ghosh, S., Phillips, J.C. and Perkins R.J. [1991] Modelling the flow in droplet driven sprays. In Johansson, A.V. and Alfredson, P.H. (eds.) *Advances in Turbulence 3*, 405-414, Springer-Verlag, Berlin.

Gilbert, A.J. and Bell, G.J. [1988] Evaluation of drift hazards arising from pesticide spray application. *Aspects of Appl. Biol.* **17**, 363-375.

Hobson, P.A., Miller, P.C.H., Walklate, P.J., Tuck, C.R. and Western, N.M. [1993] Spray drift from hydraulic spray nozzles: the use of a computer simulation model to examine factors influencing drift. *J. Agric. Eng. Res.* **54**, 293-305.

Hunt, J.C.R. and Nalpanis, P. [1985] Saltating and suspended particles over flat and sloping surfaces. I. Modelling concepts. Proc. International Workshop on the Physics of Blown Sand, Aarhus, Denmark.

Lee, S.Y. and Tankin, R.S. [1984] Study of a liquid spray (water) in a non-condensable environment (air). *Int. Jnl. Heat and Mass Trans.* **27**, 351-361.

Legg, B.J. and Raupach, M.R. [1982] Markov-chain simulation of particle dispersion in inhomogeneous flows: mean drift induced by a gradient in Eulerian velocity variances. *Bound. Layer Met.* **24**, 3-13.

Lefebvre, A.H. [1980] Airblast atomization. *Prog. Energy Combust. Sci.* **6**, 233-261.

Luhar, A.K. and Britter, R.E. [1989] A random walk model for dispersion in inhomogeneous turbulence in a convective boundary layer. *Atmos. Env.* **23**, 1911-1924.

Miller, P.C.H. [1993] Spray drift and its measurement. In Matthews, G.A. and Hislop, E.C. (eds.) *Application Technology for Crop Protection*, CAB International.

Miller, P.C.H. and Hadfield, D.J. [1989] A simulation of spray drift from hydraulic nozzles. *J Agric. Eng. Res.* **42**, 135-147.

Miller, P.C.H., Butler Ellis, M.C. and Tuck C.R. [1996] Entrained air and droplet velocities produced by agricultural flat-fan nozzles. *Atomization and Sprays*, **6**, 693-707.

Morton, B.R., Taylor, G.I. and Turner, J.S. [1956] Turbulent gravitational convection from maintained and instantaneous sources. *Proc. Roy. Soc. Lond. A.* **234**, 1-23.

Perkins, R.J. and Hunt, J.C.R. [1986] Particle Transport in Turbulent Shear Flows. *Report to SERC.*

Perkins, R.J., Ghosh, S. and Phillips, J.C. [1991] In Johansson, A.V. and Alfredson, P.H. (eds.) *Advances in Turbulence 3*, 93-100, Springer-Verlag, Berlin.

Rajaratnam, N. [1976] *Turbulent Jets.* Elsevier, London.

Sankal, S.V., Inenaga, A. and Bachalo, W.D. [1992] Trajectory dependent scattering in phase-Doppler anemometry: minimising and eliminating sizing error. Proceedings 6th International Symposium of Application of Laser Technology to Fluid Mechanics, Lisbon, Portugal.

Schlichting, H. [1968] *Boundary-Layer Theory.* 6th ed. McGraw-Hill, New York.

Townsend, A.A. [1976] *The Structure of Turbulent Shear Flow* (2nd ed.) Cambridge University Press.

Tropea, C., Xu, T.-H., Onofri, F., Grenhan, G., Haugen, P. and Stiegelmeier, M. [1995] Dual mode phase-Doppler anemometer. Proceedings of 4th Conference on Optical Particle Sizing, Nuremburg, Germany.

van Dop, H., Nieuwstadt, F.T.M. and Hunt, J.C.R. [1985] Random walk models for particle displacements in inhomogeneous unsteady turbulent flows. *Phys. Fluids* **28**, 1639-1653.

White, F. [1979] *Fluid Mechanics.* McGraw-Hill Kogakusha, Tokyo.

Yule, A.J. [1980] Investigations of eddy coherence in jets. In *The Role of Coherent Structures in Modelling Turbulence and Mixing* (ed. J.Jiminez), 188-207, Springer-Verlag, Berlin.

Figures

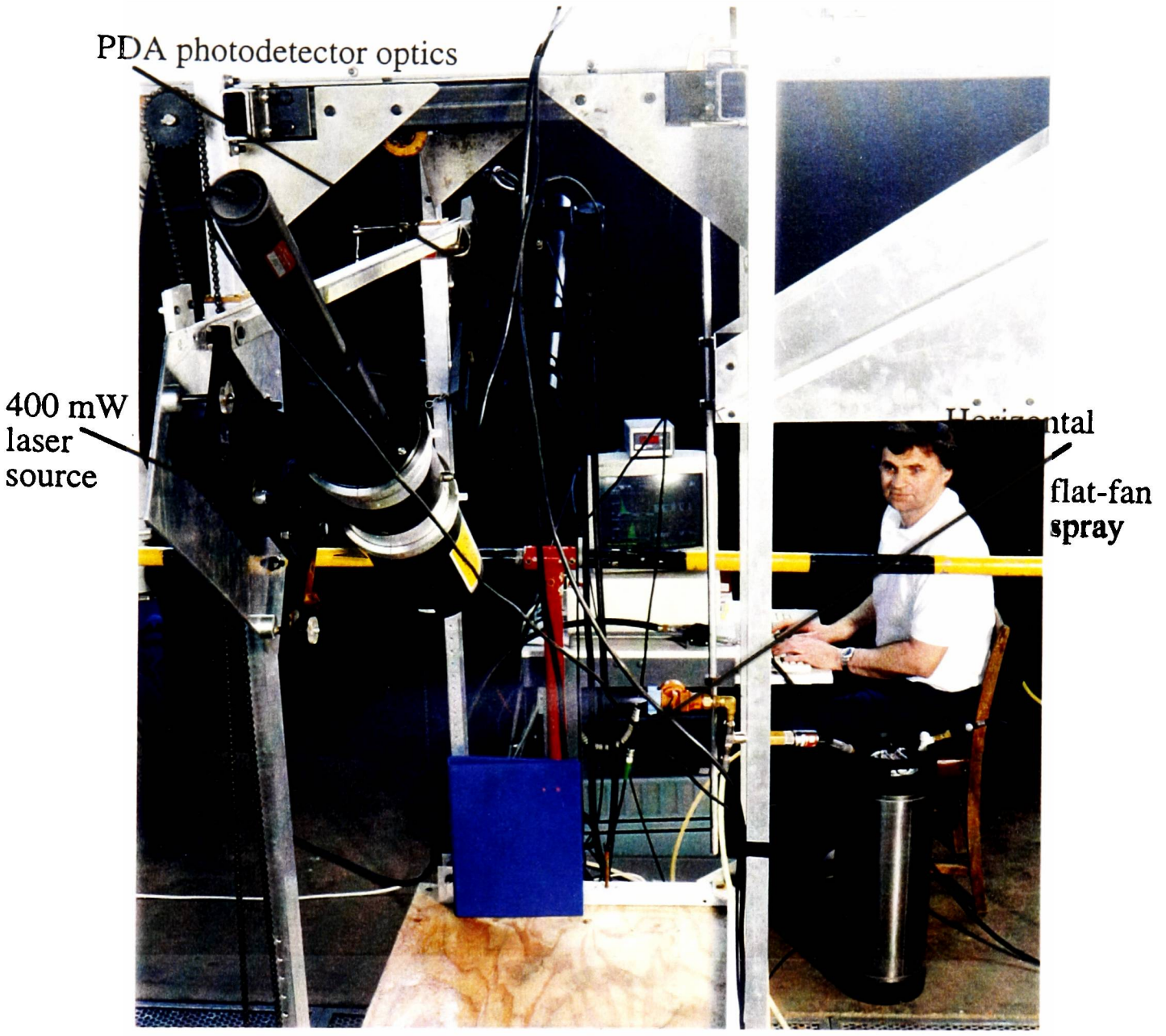

1. The Dantec phase-Doppler anemometer aligned to measure horizontal velocity component. The equipment shown is mounted in a chain-driven cradle to allow simultaneous traversing of laser source (near side) and detection optics (far side) (Photograph courtesy of Silsoe Research Institute).

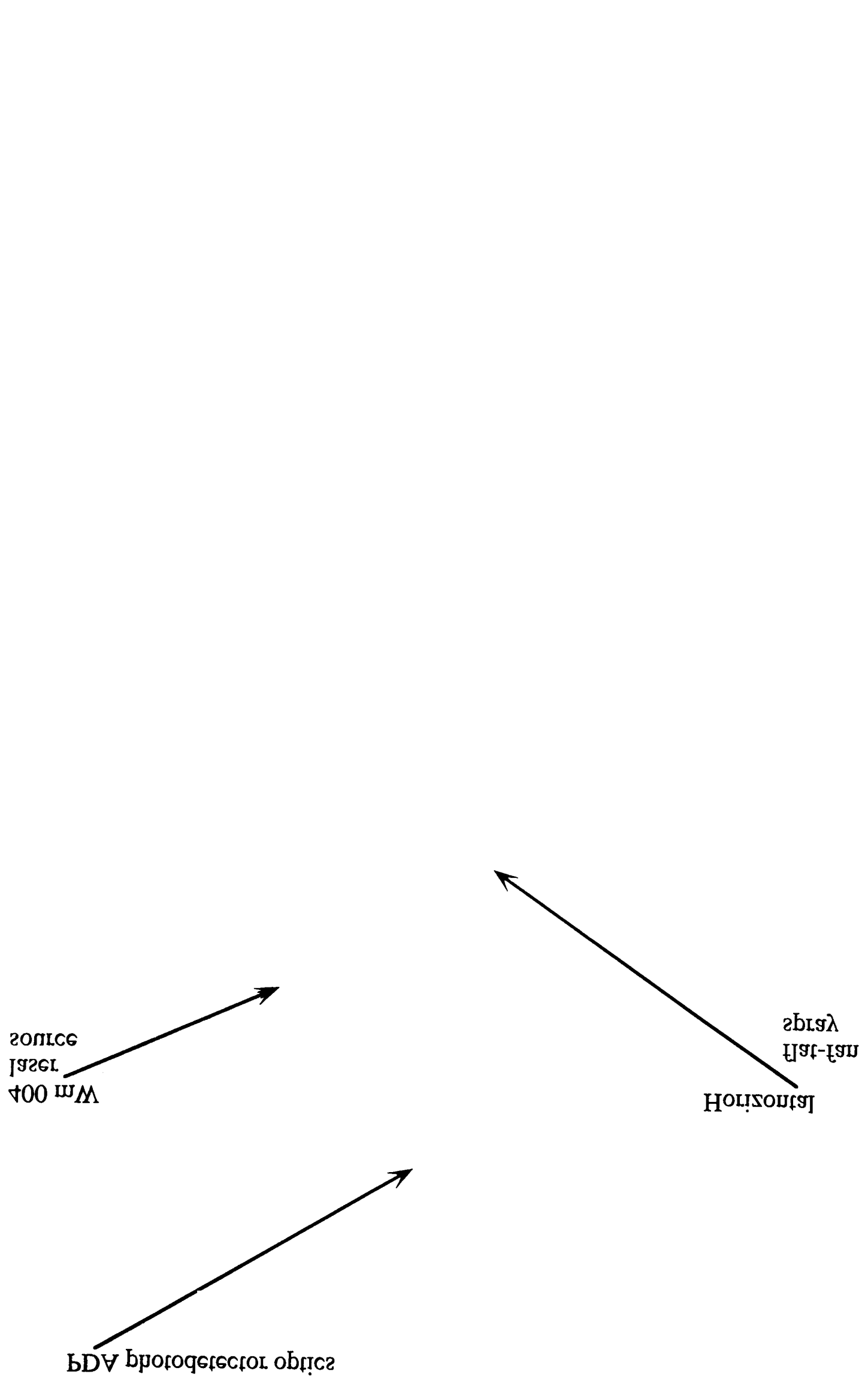
Horizontal
flat-fan
spray
800 nm
laser
source
PDA photodetector optics

Figures

1. The Dantec phase-Doppler anemometer aligned to measure horizontal velocity component. The equipment shown is mounted in a chain-driven cradle to allow simultaneous traversing of laser source (near side) and detection optics (far side) (Photograph courtesy of Silsoe Research Institute).

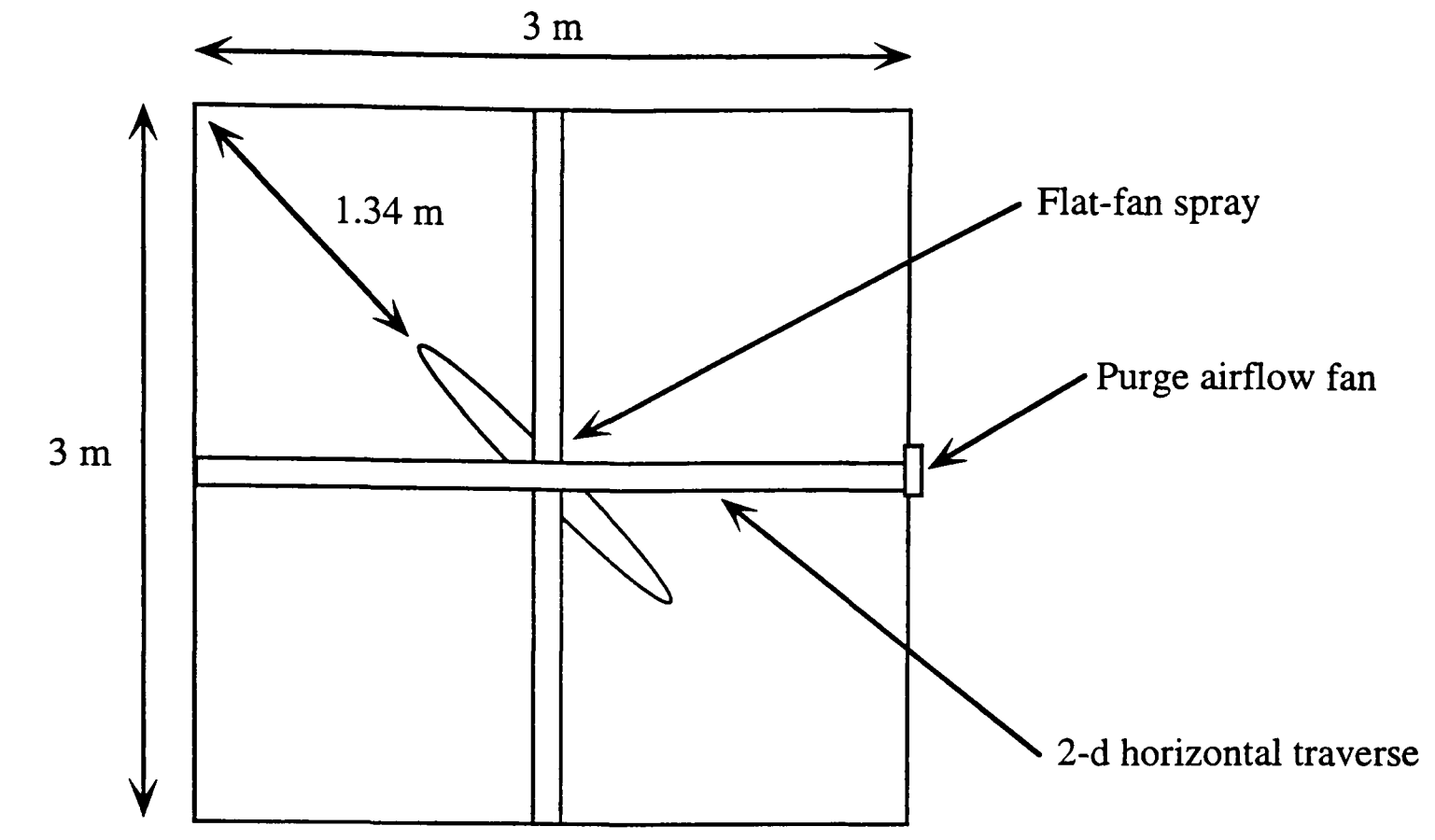

2. Schematic diagram of the flat-fan spray enclosed in a nominally still air environment (drawn approximately to scale).

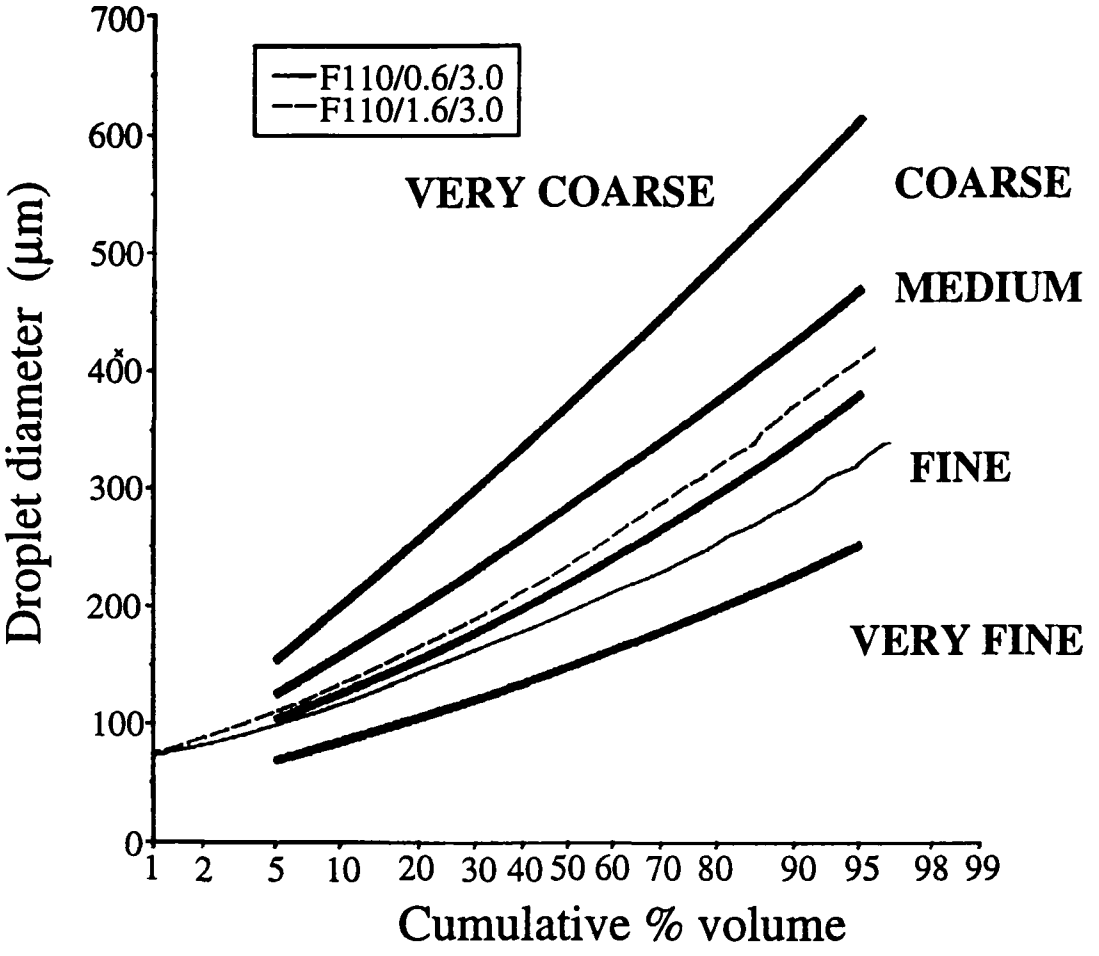

3. The droplet size distribution produced by F110/0.6/3.0 (used here) and F110/1.6/3.0 spray nozzles. The classification curves plotted correspond to the British Crop Protection Council divisions of spray quality [Doble et al, 1985].

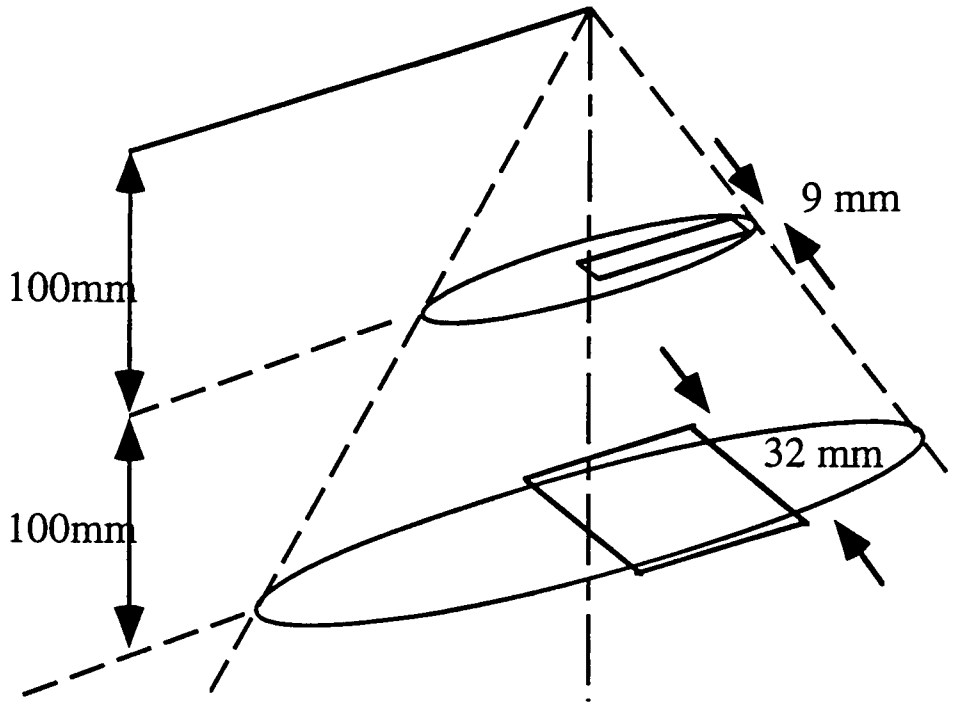

Measurement grid 100 mm below the nozzle

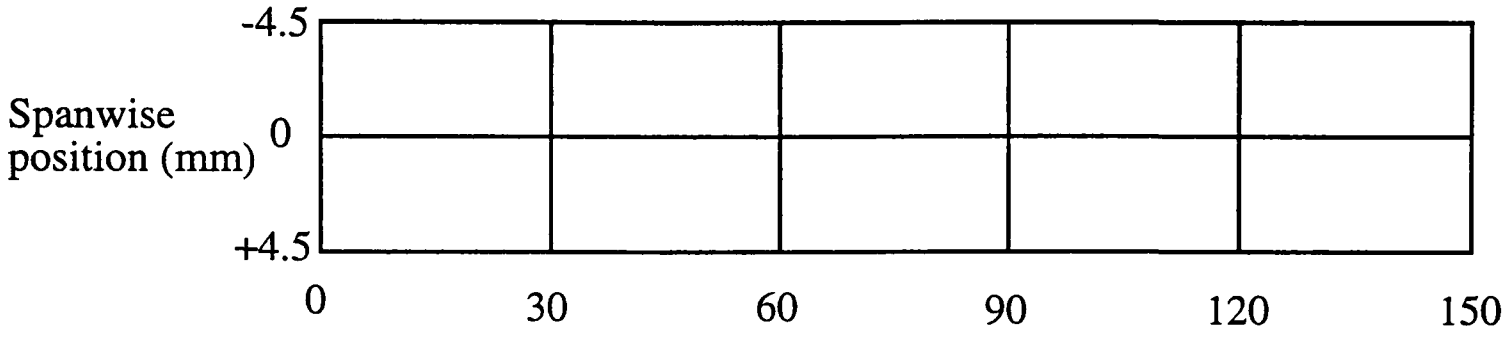

Distance along the major axis (mm)

Measurement grid 200 mm below the nozzle

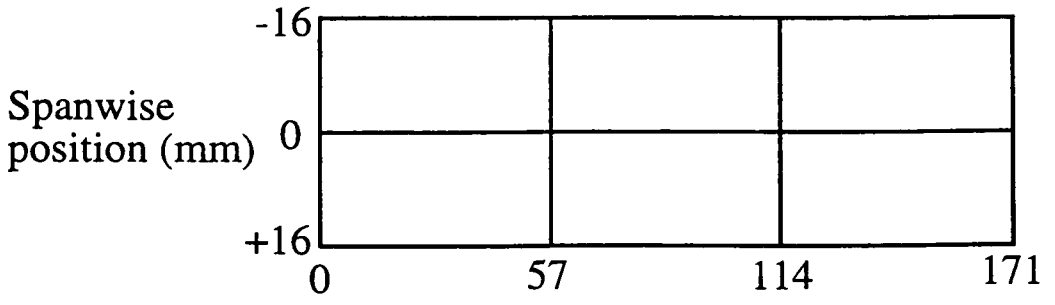

Distance along the major axis (mm)

4. Spanwise traverse positions used for phase-Doppler anemometer measurements within the flat-fan spray in still air.

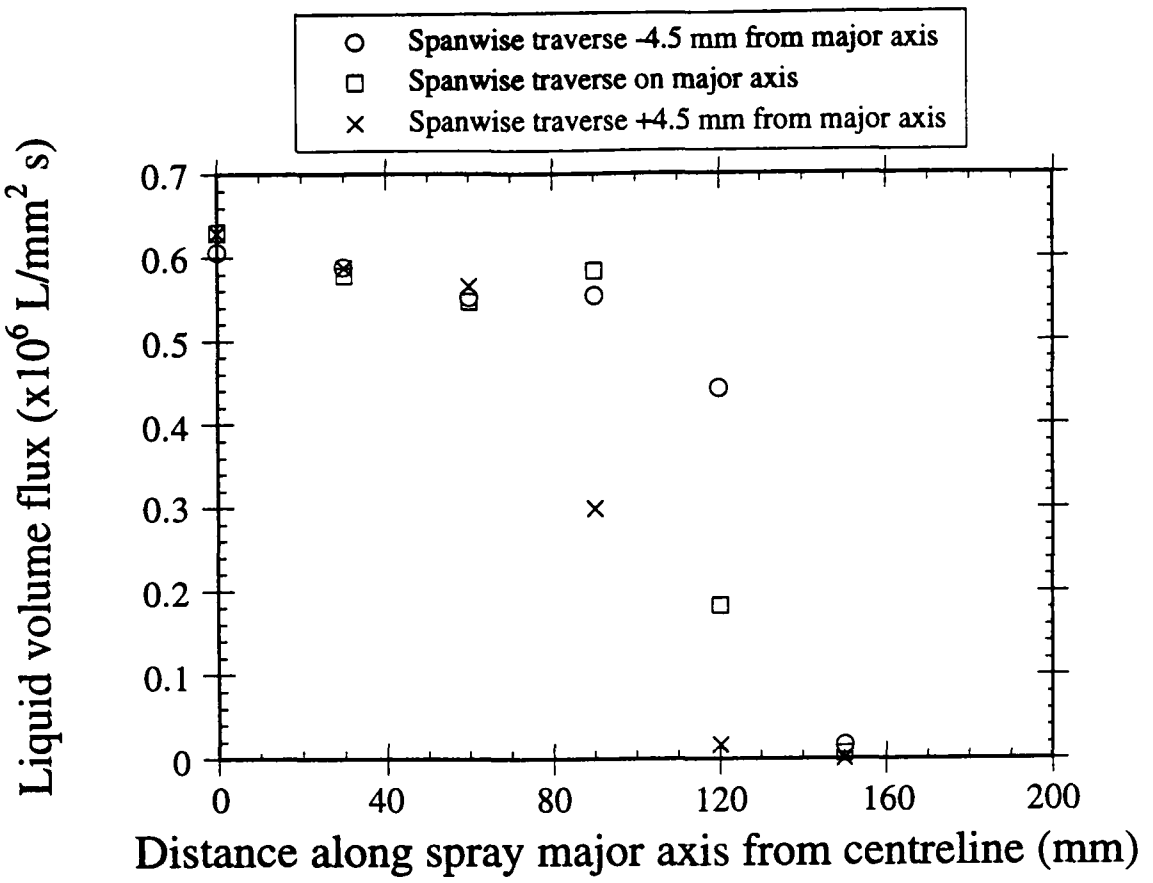

5. The liquid volume flux transported in small (diameter 0-100 μm) droplets 100 mm below the nozzle in an F110/3.0/0.6 flat-fan spray.

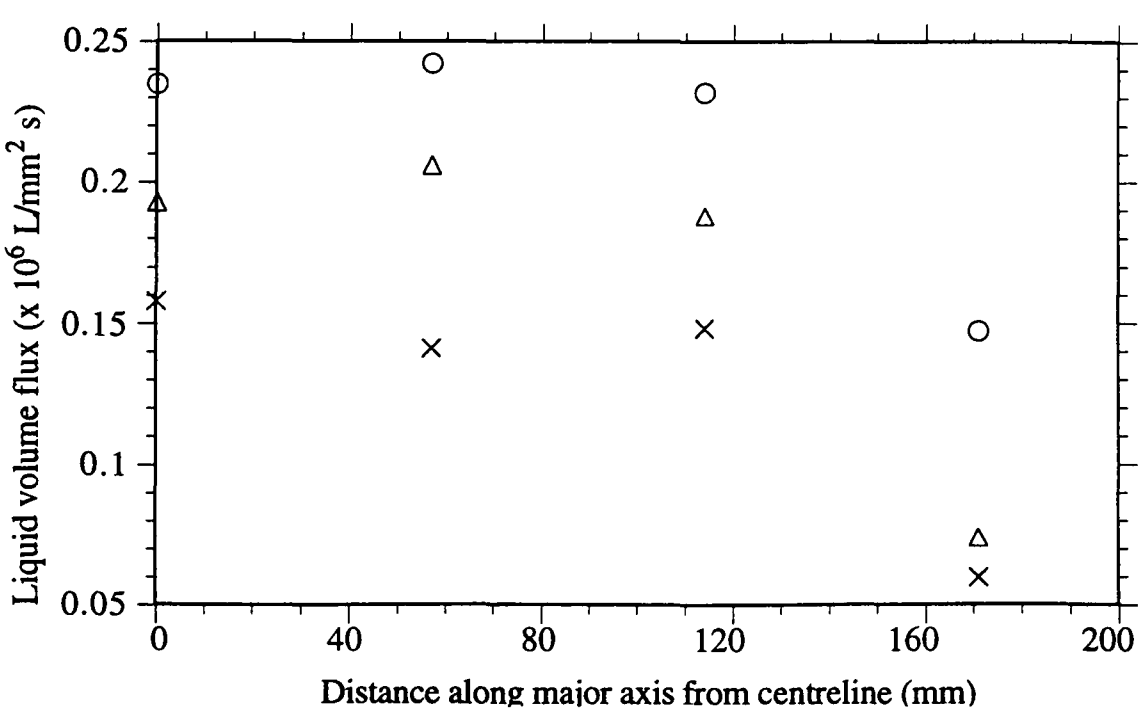

6. The liquid volume flux transported in small (diameter 0-100 μm) droplets 200 mm below the nozzle in an F110/3.0/0.6 flat-fan spray.

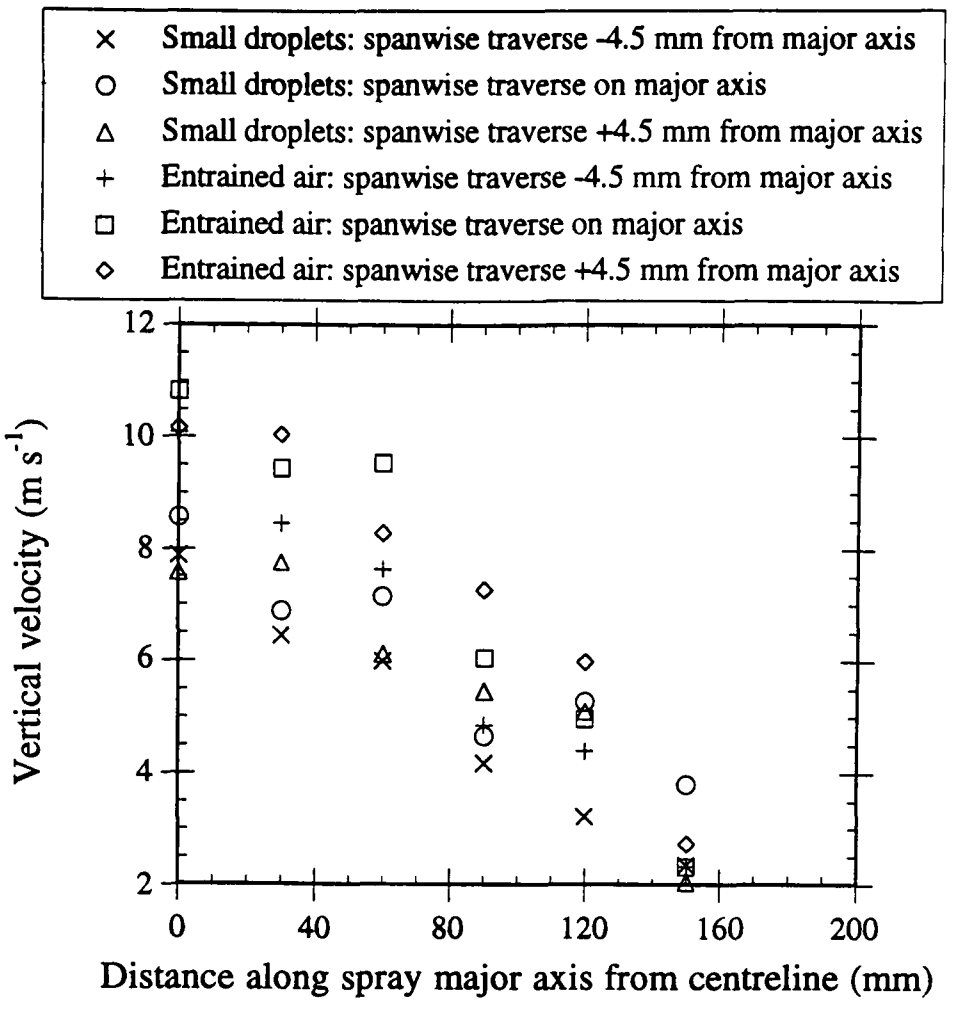

7. The vertical velocity of entrained air (45-55 μm diameter droplets) and small (diameter 0-100 μm) droplets 100 mm below the nozzle in an F110/3.0/0.6 flat-fan spray.

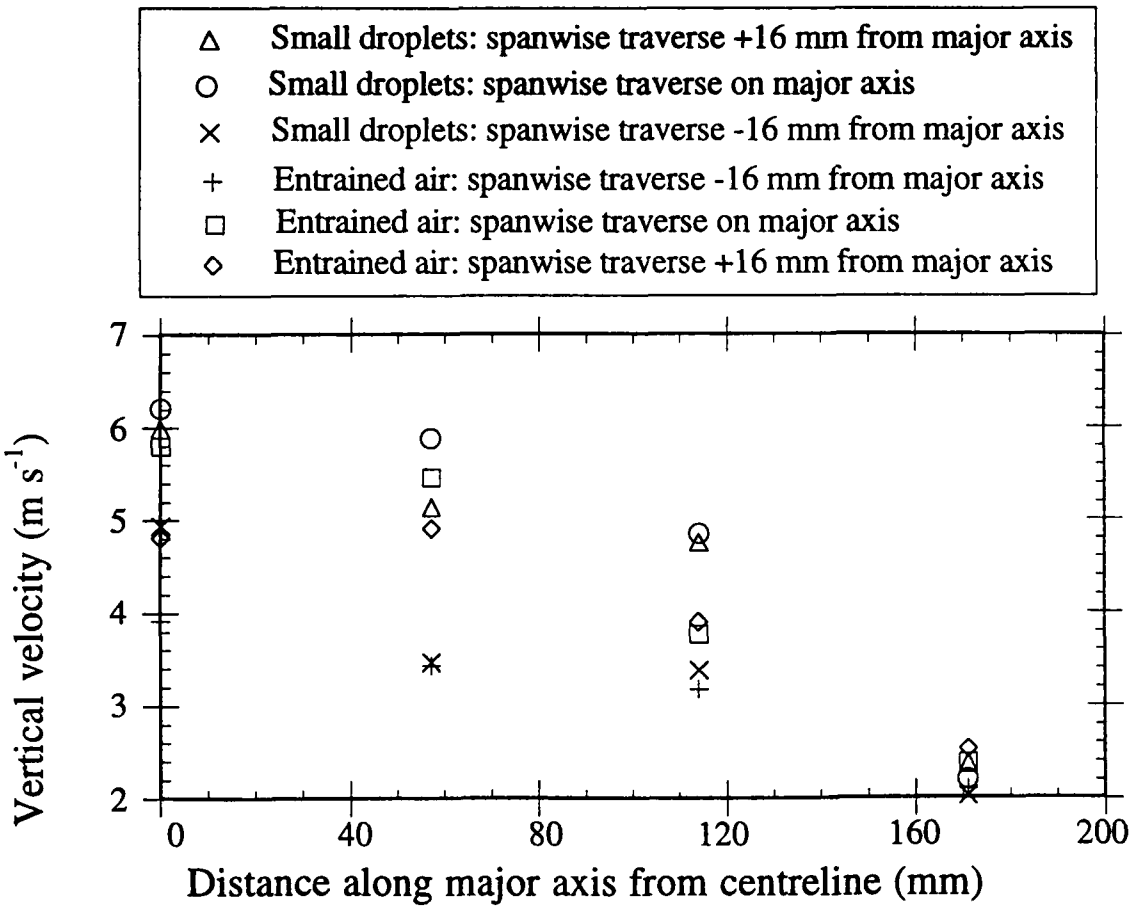

8. The vertical velocity of entrained air (45-55 μm diameter droplets) and small (diameter 0-100 μm) droplets 200 mm below the nozzle in an F110/3.0/0.6 flat-fan spray.

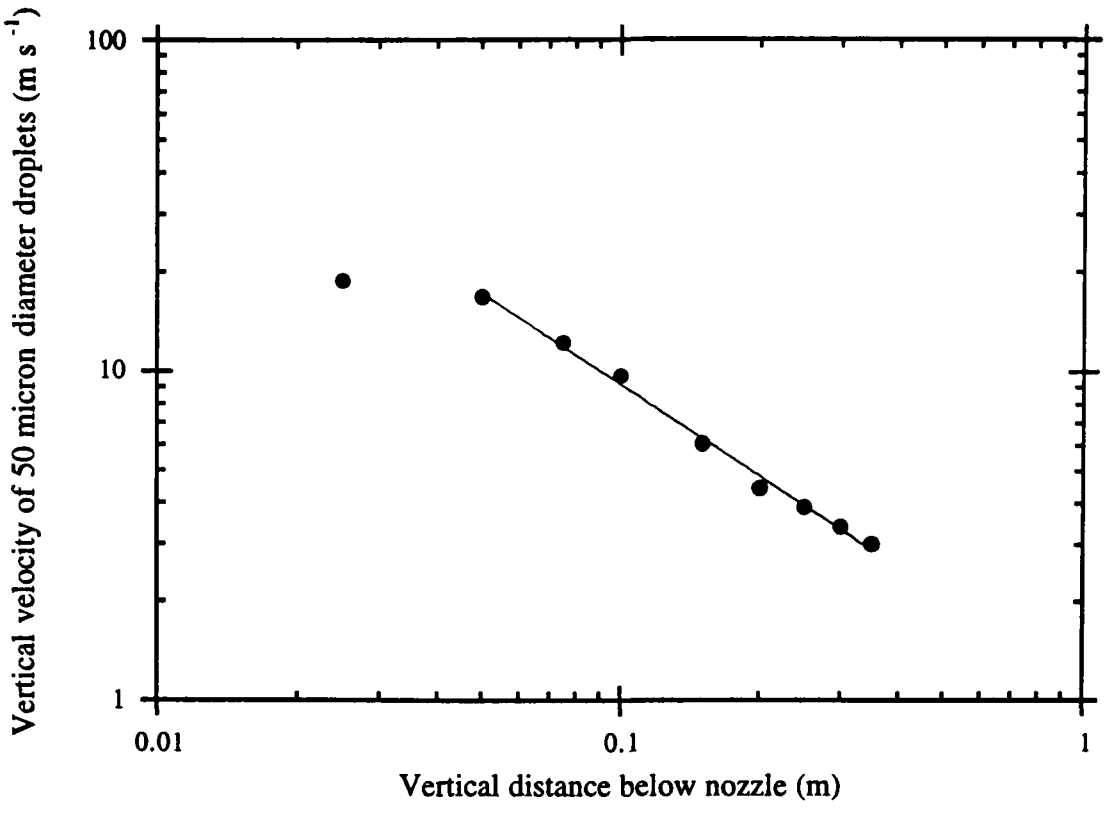

9. The decrease of centreline entrained air velocity with distance below the nozzle measured using phase-Doppler anemometry in an F110/3.0/0.6 flat-fan spray. The curve fit is a power law corresponding to a linear decrease of entrained air velocity with distance from the nozzle (regression coefficient 0.994).

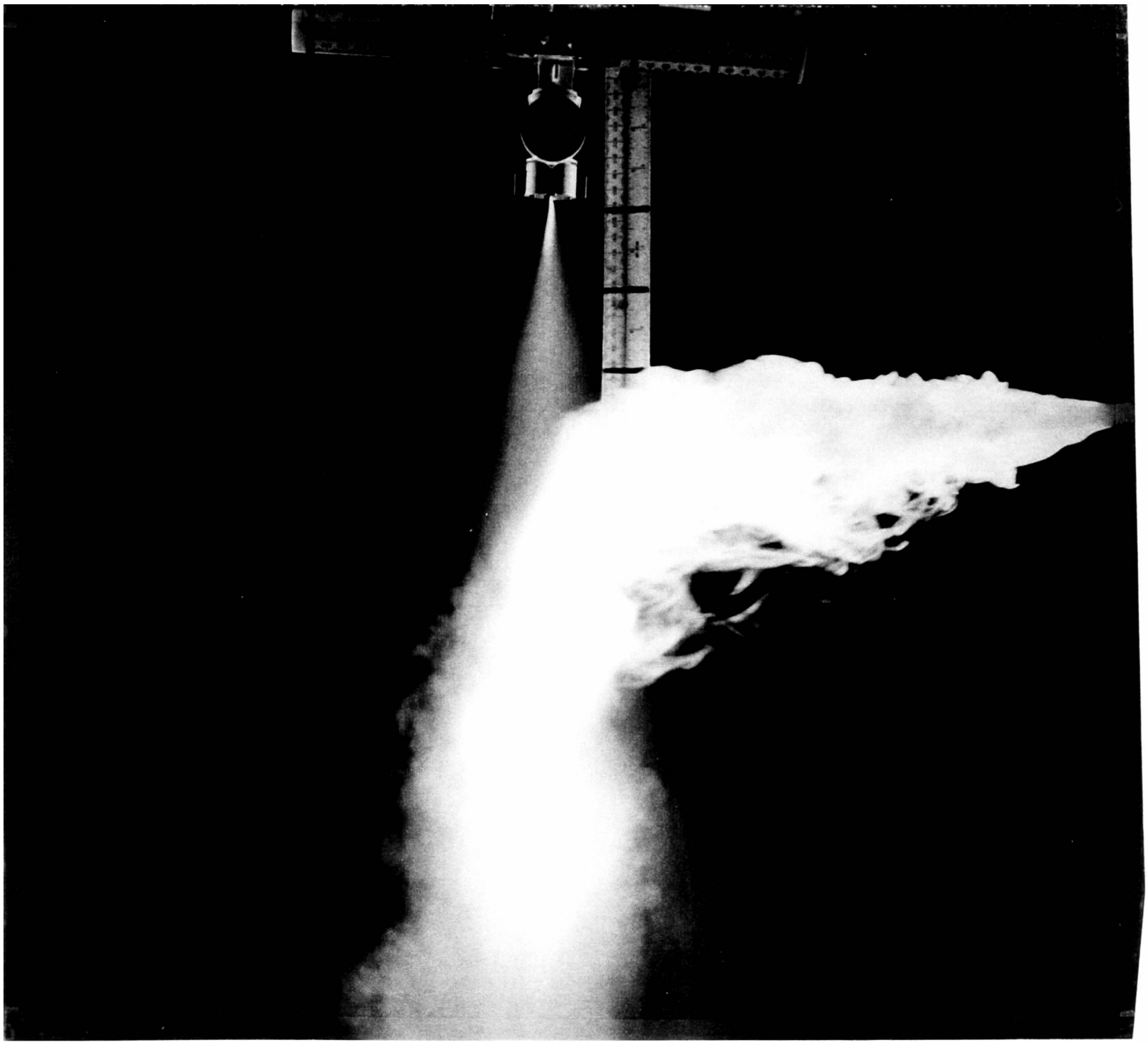

10. Entrainment of ambient air by an agricultural spray (side view) visualised by smoke. The nozzle produces a flat-fan spray with included angle of 110°, inplane angle of about 10°, operated at a nozzle pressure of 3.0 bar and flowrate of 0.6 L/min. A CFT smoke generator generator burning Shell Ondina oil was used to produce a near neutrally-buoyant release. The smoke visualises the entrainment velocity field perpendicular to the spray boundary before entering the spray (photograph courtesy of Silsoe Research Institute).

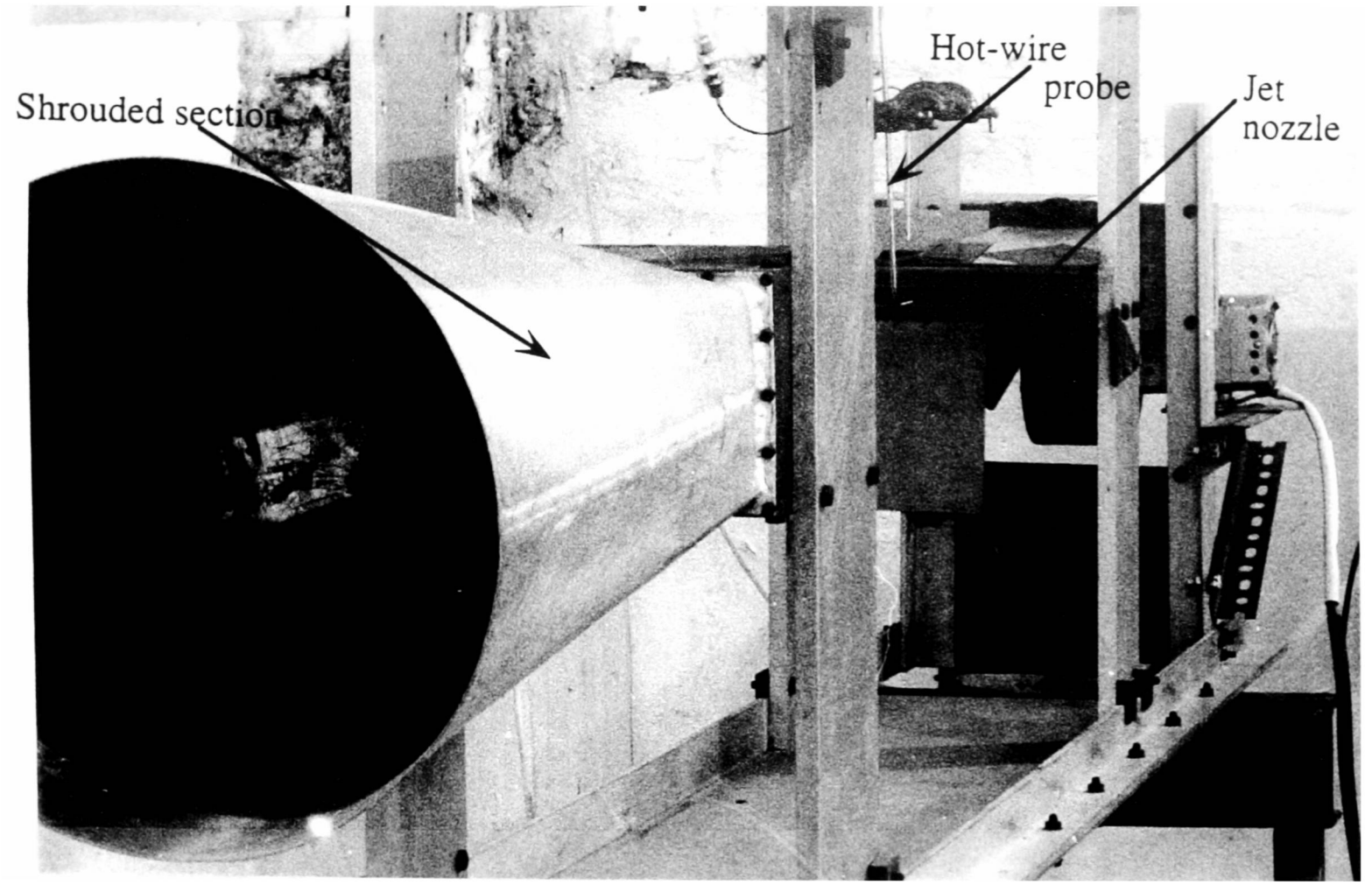

11. The plane air jet used in the patternation and flow visualisation experiments. The jet is viewed from off-axis looking towards the nozzle; the hot-wire probe is visible at the nozzle centre. The shrouded expanding section was a remnant of the former use of the jet to study dust control using air curtains and was removed prior to any experimental work being undertaken.

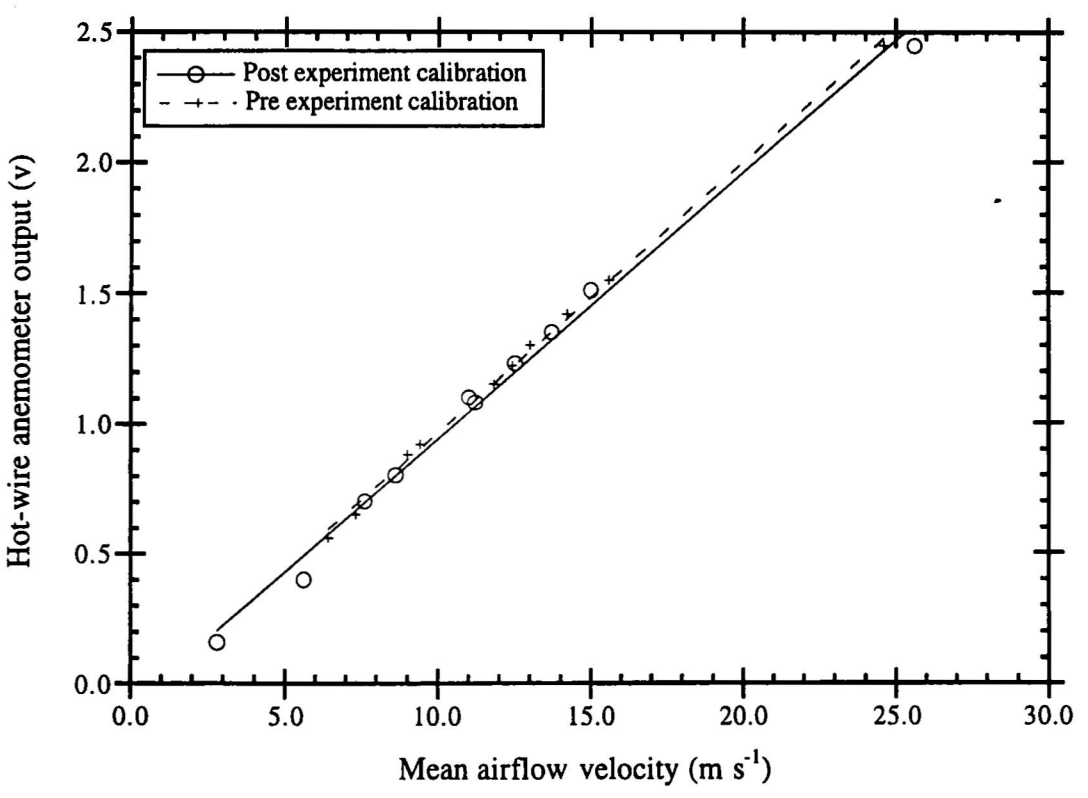

12. Calibration curves for the linearised hot-wire anemometer used in plane air jet experiments.

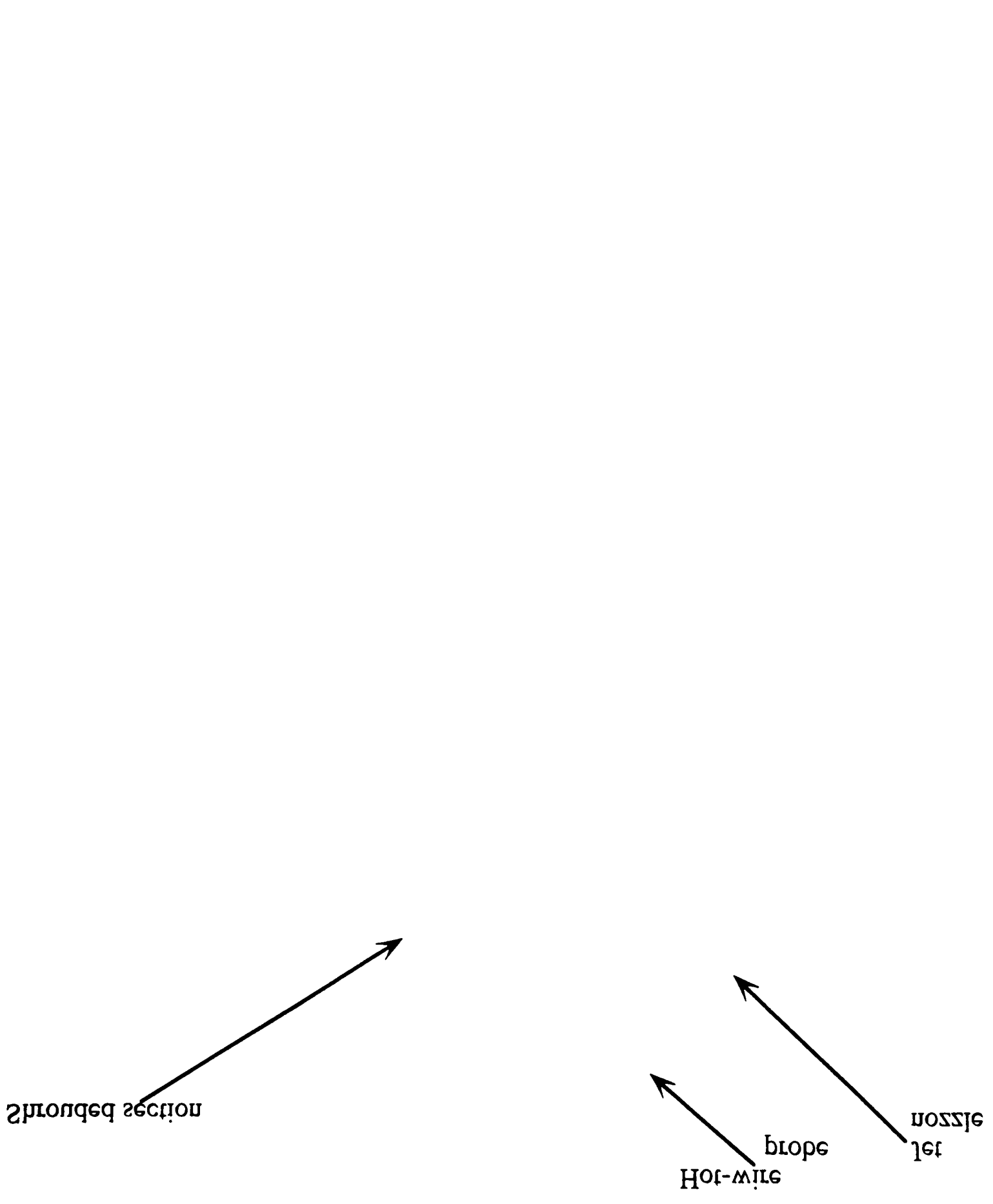
Stranded section
Hot-wire
probe
Jet
nozzle

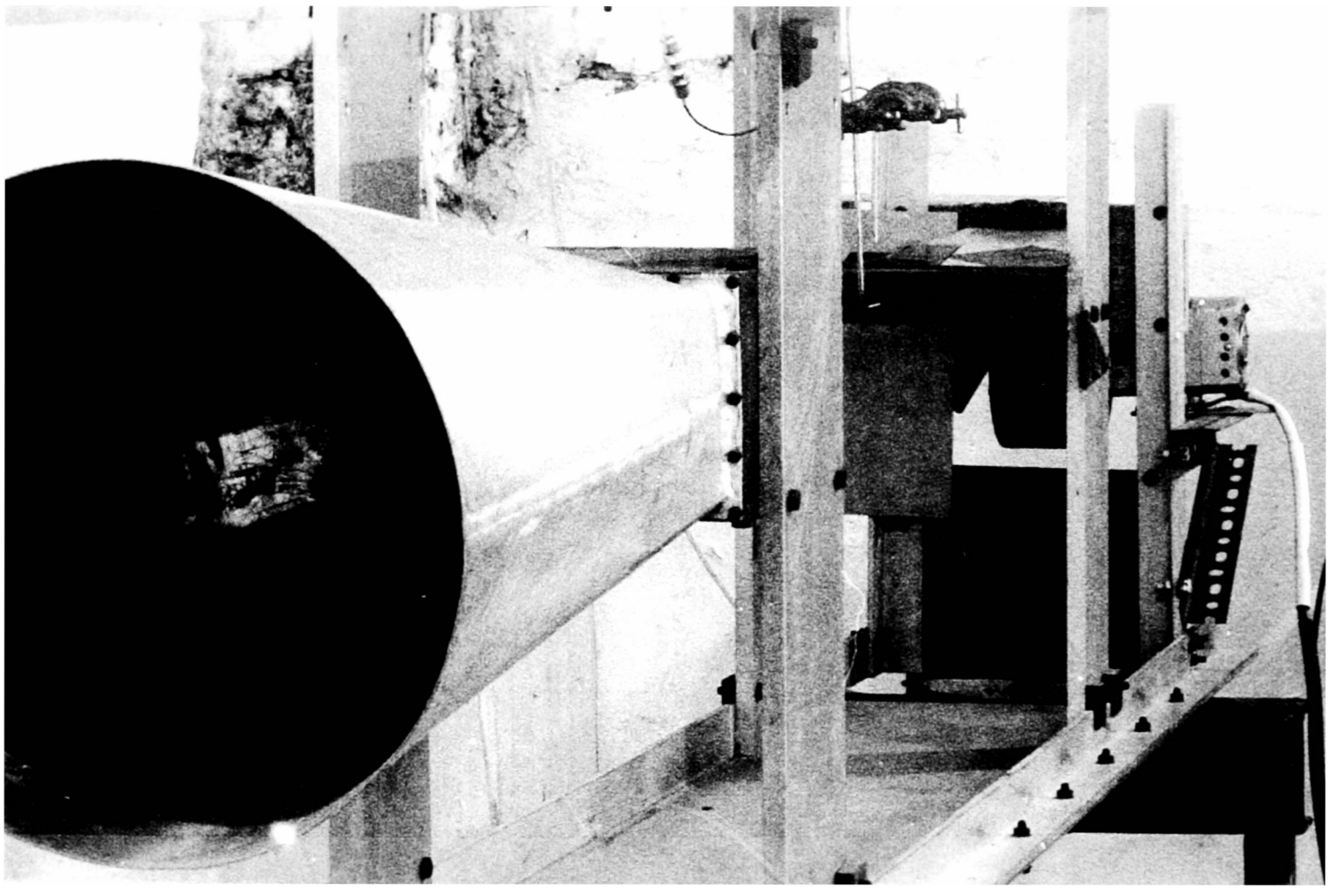

11. The plane air jet used in the patternation and flow visualisation experiments. The jet is viewed from off-axis looking towards the nozzle; the hot-wire probe is visible at the nozzle centre. The shrouded expanding section was a remnant of the former use of the jet to study dust control using air curtains and was removed prior to any experimental work being undertaken.

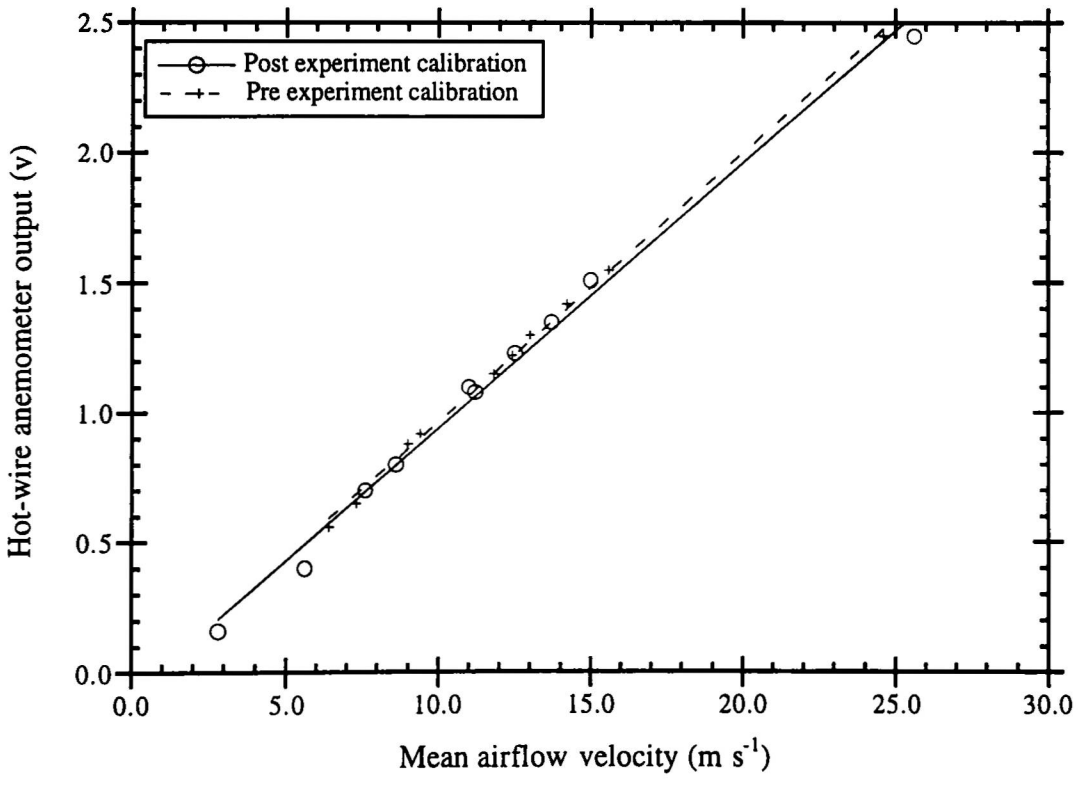

12. Calibration curves for the linearised hot-wire anemometer used in plane air jet experiments.

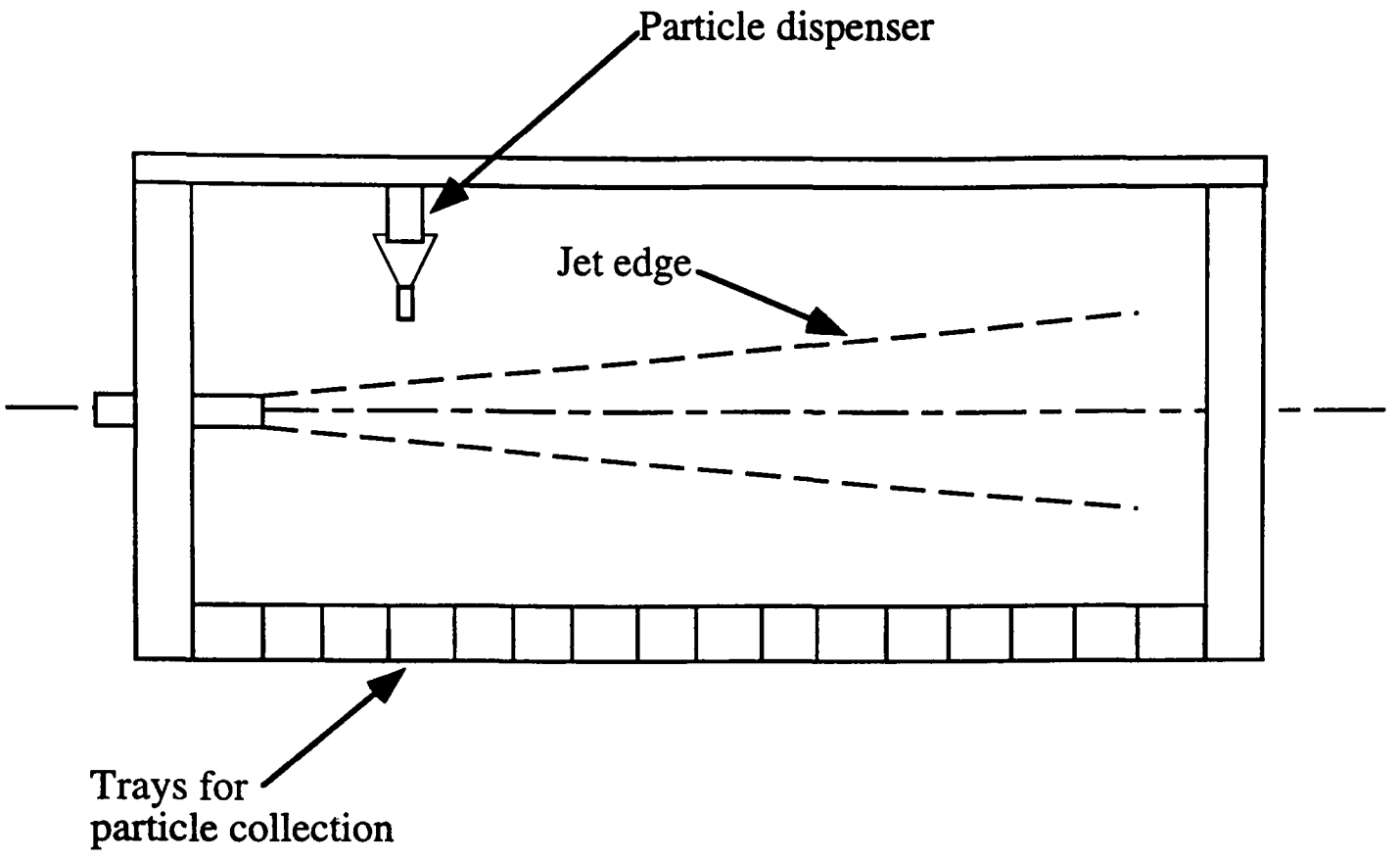

13. Schematic diagram of the equipment used in the patternation experiments. Dense particles were released from the particle dispenser and fell through the air jet under gravity, and were collected along the jet base.

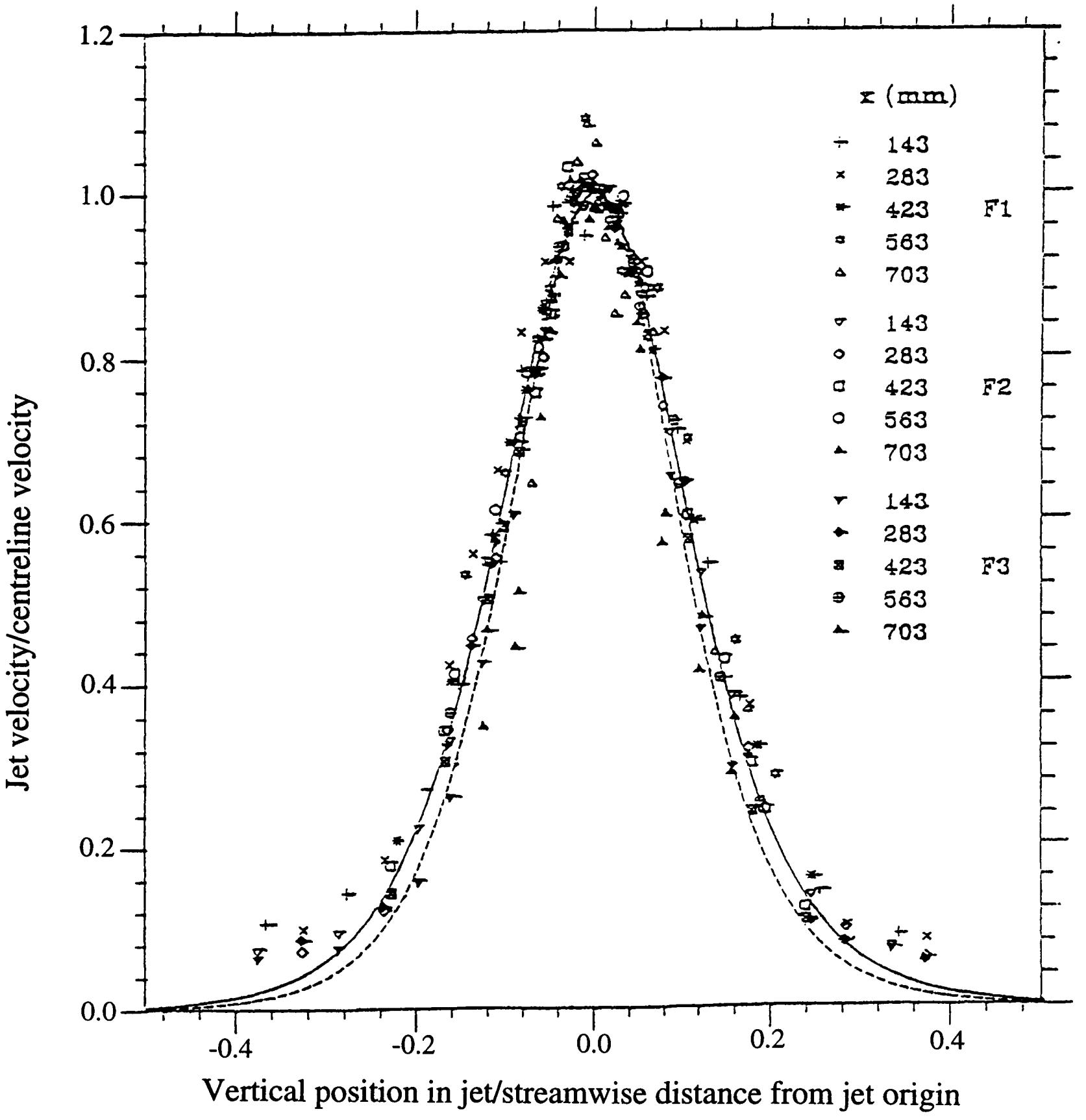

14. The mean velocity profiles measured in the plane air jet. Data is plotted from three experiments (F1, F2, F3) in which the mean velocity was measured at five downstream positions (x).

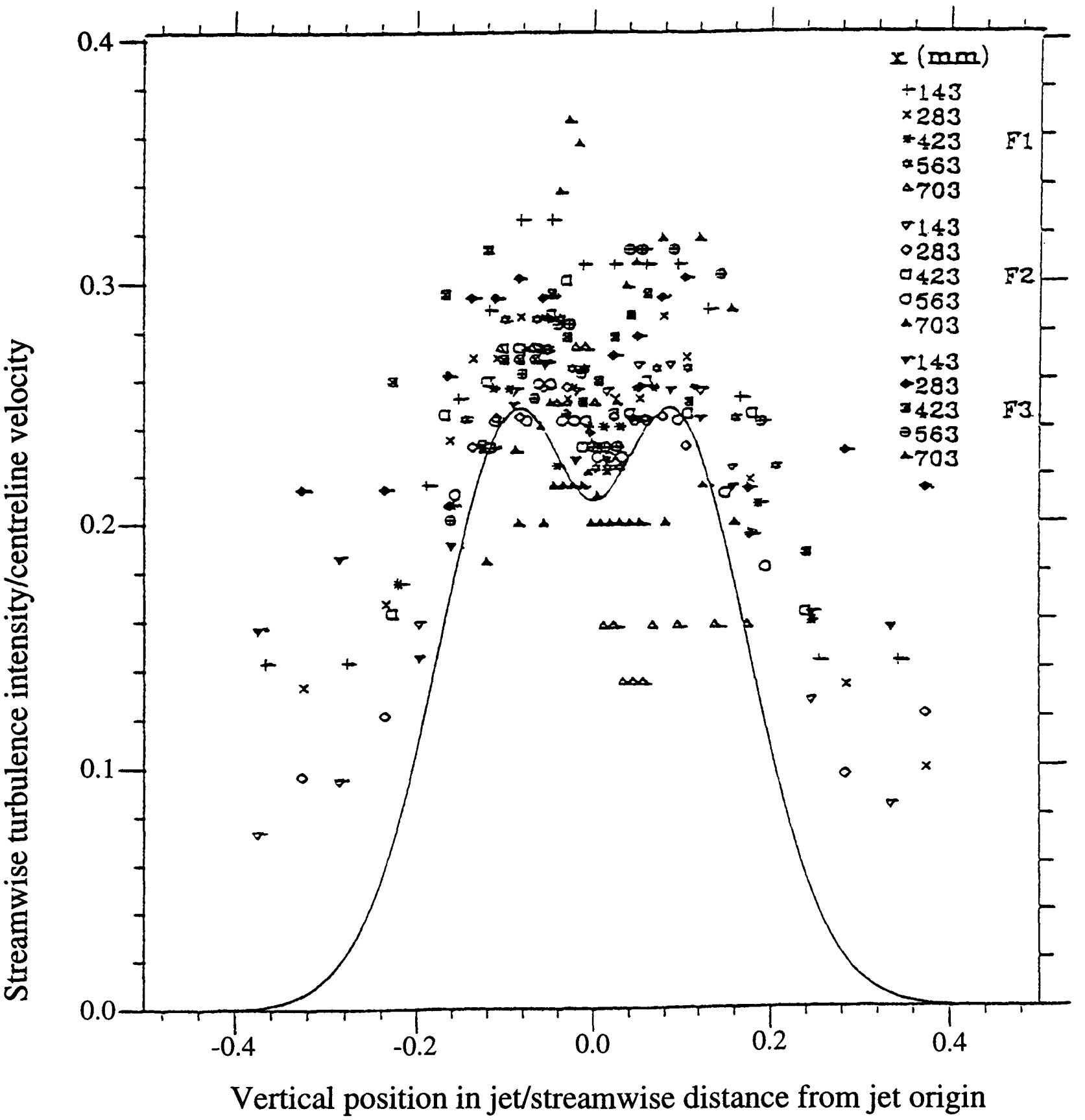

15. Streamwise turbulence intensity profiles measured in the plane air jet. Data is plotted from three experiments (F1, F2, F3) in which the turbulence intensity was measured at five downstream positions (x).

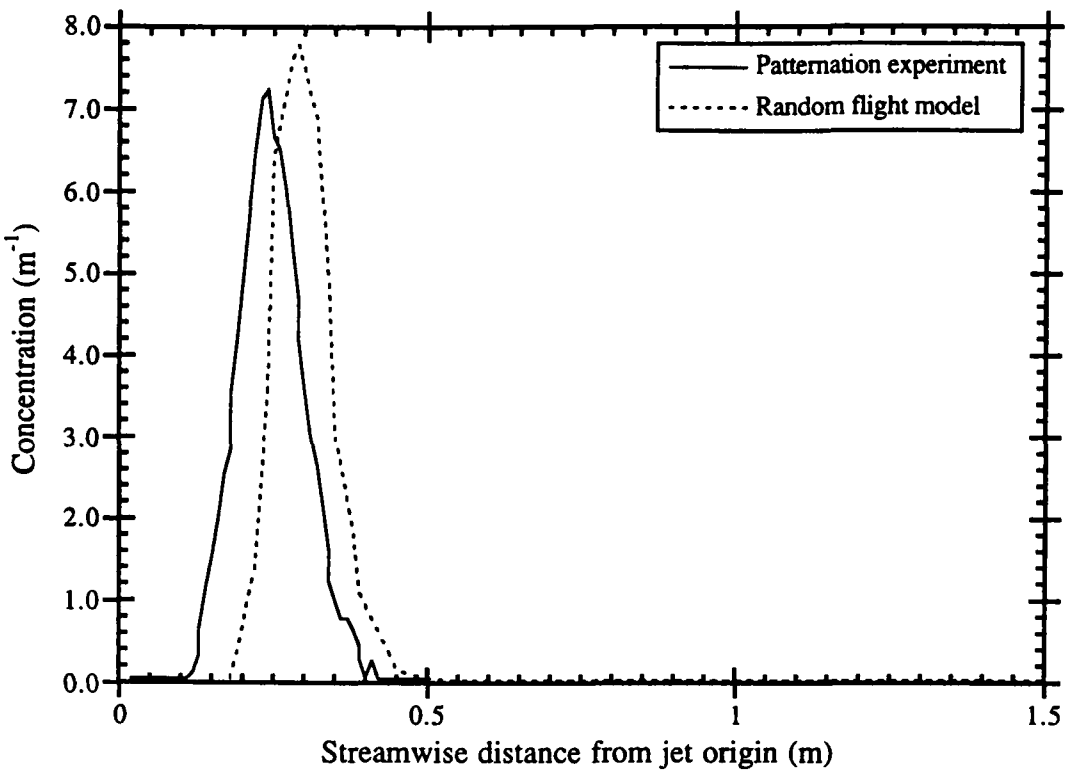

(a)

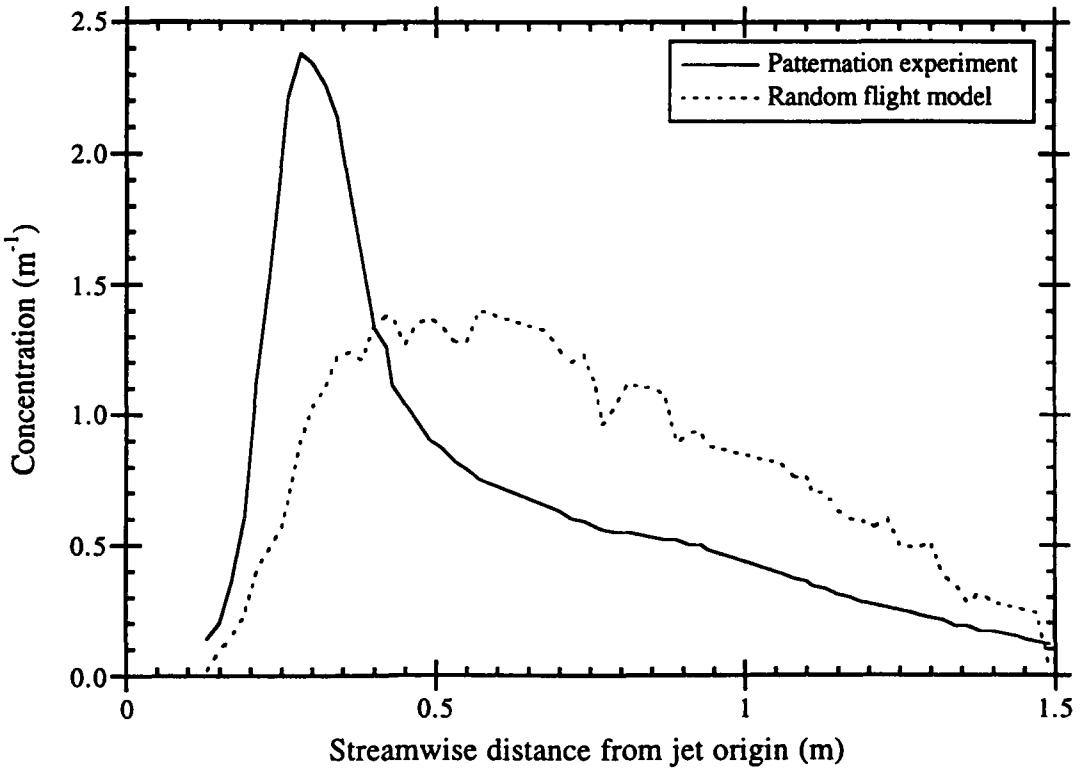

(b)

16. Comparison between the particle concentration of (a) 244 μm and (b) 86 μm particles measured at collectors below the plane jet in patternation experiments and numerical results obtained using a random flight model (after Perkins et al., 1991).

17. The trajectories of 244 μm quartz particles in the plane air jet (flow direction right to left) photographed with a strobe speed of 160 Hz. The grid illuminated behind the jet has dimensions of 5 cm × 5 cm, and the tufts on the right of the image visualise the jet width.

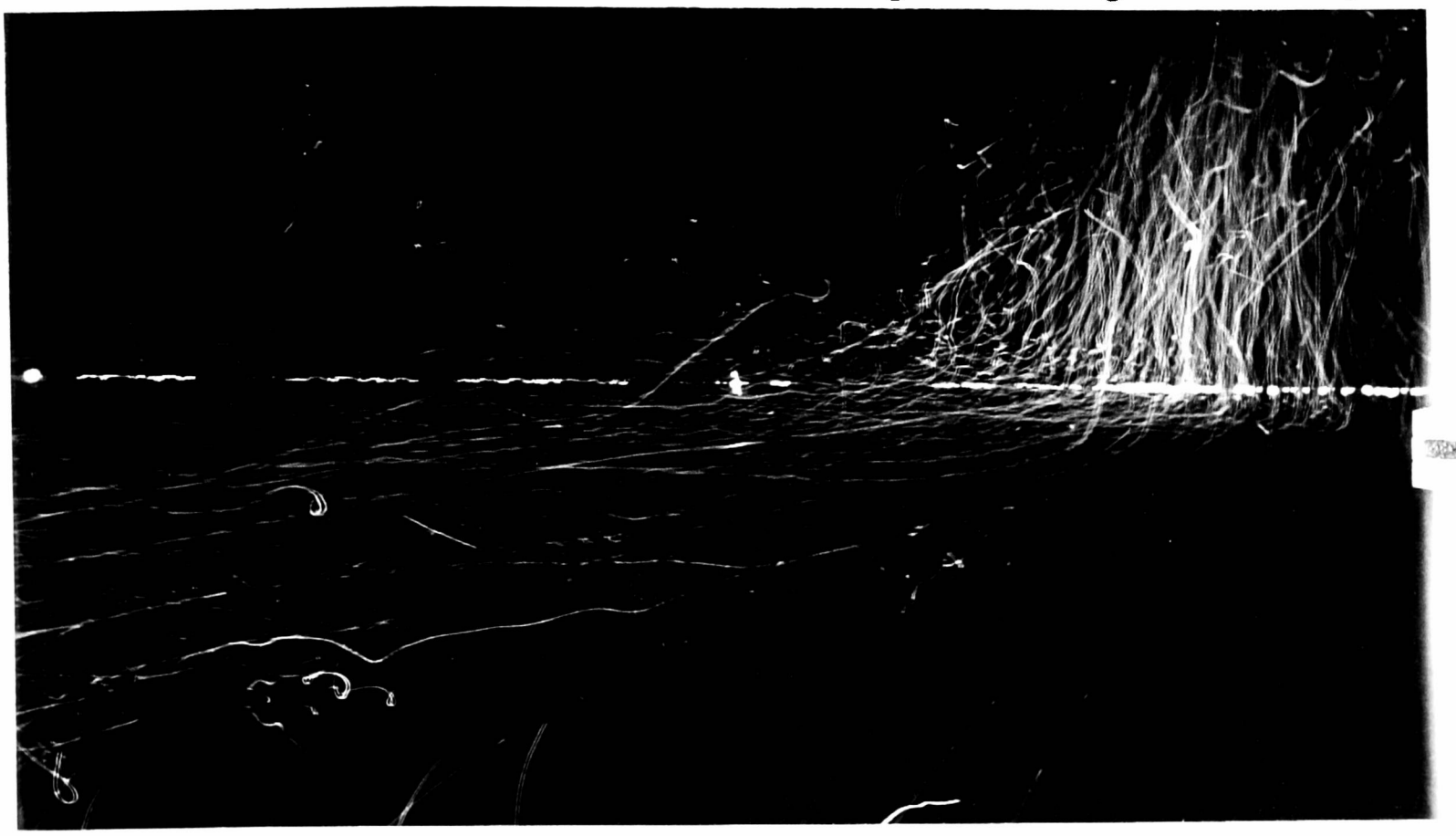

18. The trajectories of 86 μm quartz particles visualised by the motion of tracer bubbles with a diameter of approximately 2 mm and a fall velocity in the range 0.4-0.6 m s^{-1}. The jet nozzle is visible on the extreme right of the image (flow direction right to left); exposure time was 1 s.

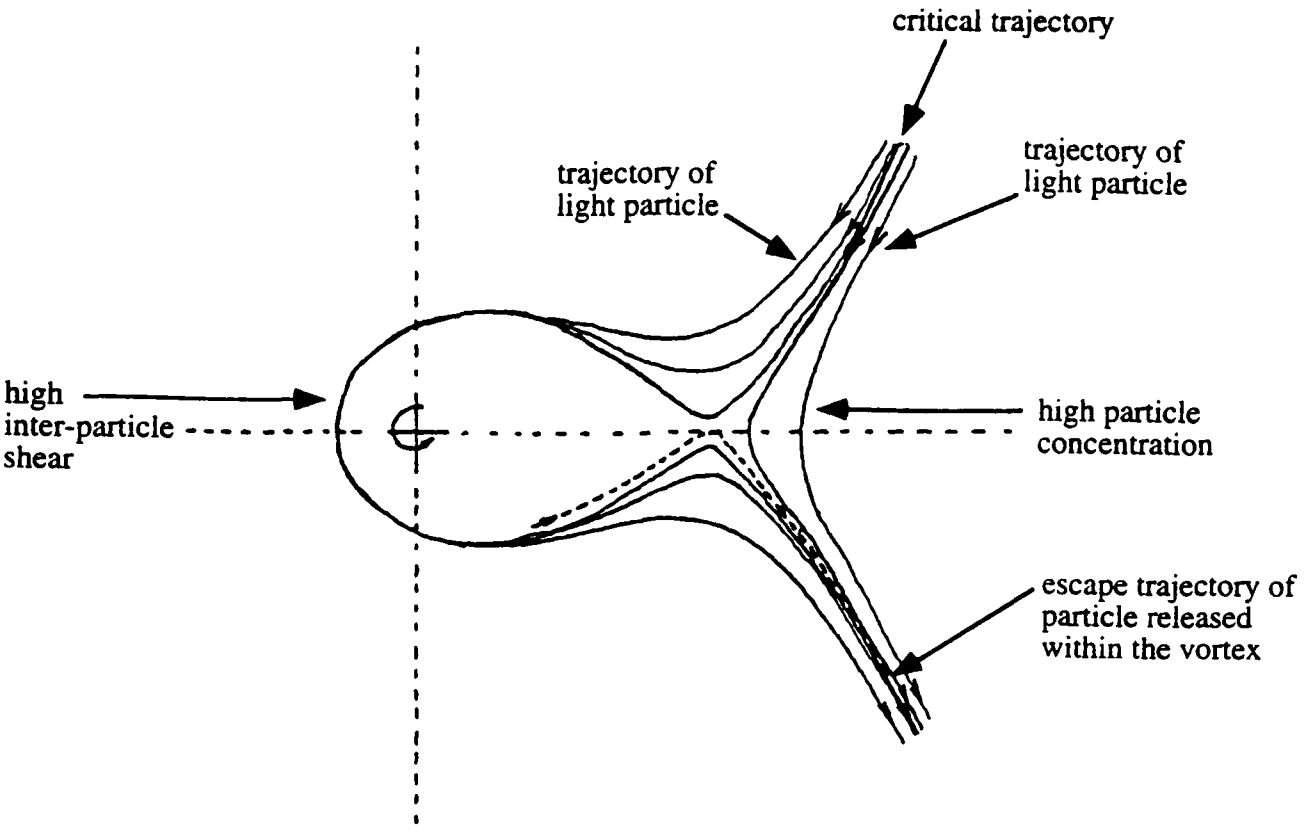

19. Schematic diagram of a Rankine vortex showing possible light particle trajectories for transient interaction with the vortex (after Perkins and Hunt [1986]).

CHAPTER 5. AIRFLOW AND DROPLET MOTIONS PRODUCED BY THE INTERACTION OF SPRAYS AND CROSS FLOWS

Summary

Flow visualisation and measurement of airborne droplet parameters are presented for a boom section supporting three flat-fan nozzles in a simple wind tunnel cross flow, conditions representative of agricultural spraying operations. Observations confirm *prima facie* expectations that the ratio of cross flow air velocity to entrained air speed is the key parameter determining removal and distribution of drifting droplets. Two experimental conditions were studied: *weak and moderate cross flows*, in which the ratio of cross flow velocity to spray entrained air speed is respectively less and greater than unity. In strong cross flow, the cross flow velocity is greater than the maximum velocity in the spray, and the spray does not form, with droplets from the nozzle carried directly downwind. Under weak cross flow, the downwind spray field consists of regions associated with flow around and through the structure of individual fans which act as sinks for cross flow momentum, with the flow accelerated between the fans and around the edges of the boom. On the other hand under moderate cross flow, the spray is penetrated everywhere across its width, with residual spanwise variations associated with varying porosity.

All measurements were taken 2 m downwind of the boom using passive line collectors and a phase-Doppler analyser. For weak cross flows, maximum droplet concentrations were identified with droplet removal and capture from the edges of adjoining fans. Under moderate cross flows, they were associated with scavenging of fine droplets from the interior of the fans. Overall the drifting fraction possess volume median diameters (VMD) of about 100 μm and these droplets were transported essentially passively.

Clearly, numerical simulations of spray drift must reproduce the near-field interaction of spray entrained air and cross flow velocity fields observed here. Input conditions to far-field random walk simulations are not necessarily those of mean upstream velocity and nozzle droplet size distribution from the complete spray.

1. Introduction

Over 90% of United Kingdom arable chemical applications are carried out using a series of overlapping agricultural flat-fan sprays supported by a simple boom [P.C.H.Miller, personal communication]. Droplets are generated by hydraulic pressure nozzles with initial velocities of typically 20-25 m s^{-1} and at liquid flowrates of up to 3.0 L/min. Spray nozzles are mounted at 0.5 m intervals along a boom which may be 24 m or more long, with individual spray fans overlapping to provide a constant spanwise spray volume distribution at the spray target. The boom is usually suspended 0.5 m above the crop, on a vehicle moving at up to 5 m s^{-1} [Miller, 1993]. The interaction of typical agricultural spraying equipment with a simple wind tunnel cross flow is investigated in this chapter. Previous experimental work in chapters 2 and 3 shows that wind tunnels provide a controlled environment which is capable of reproducing field measurements of airborne spray volume produced by a single, static nozzle.

Measurements using tracer dyes to provide estimates of the airborne spray flux have been made downwind of agricultural crop sprayers under field conditions [Gilbert and Bell, 1988; Rutherford et al., 1989] and from single nozzles in uniform wind tunnel cross flow [Western et al., 1989; Miller et al., 1989; Western and Hislop, 1991] and in wind tunnel simulations of the logarithmic mean velocity profile over typical agricultural land (chapter 3). These studies report approximately proportionate increases of airborne spray volume with cross flow velocity, for conditions ranging from weak to moderate cross flow regime. Field measurements of droplet sizes have been obtained by direct capture of the spray [Byass and Lake, 1977] and in wind tunnels using laser optical array spectrometry [Miller et al., 1989], in both cases finding that the drift volume comprises droplets with diameters smaller than 100 μm.

Flat-fan sprays are formed by the breakup of a thin coherent liquid sheet issuing from the nozzle (see figure 1). The propagation of the liquid sheet is resisted by surface tension of the liquid and aerodynamic drag against the air, which lead to formation of rapidly growing wave instabilities at the sheet surfaces, analysed by Clark and Dombrowski [1972]. Disintegration occurs when the wave amplitude reaches a critical value; fragments of the sheet are torn off and rapidly contract into unstable ligaments by surface tension, and drops are produced as ligaments break down according to varicose instability [Dombrowski and Johns, 1963]. Formation of spanwise ligaments gives the disintegrating sheet a ribbed appearance (figure 1). The aerodynamic drag against the liquid sheet induces a co-flowing *entrained* airflow, which has been characterised by Briffa and Dombrowski [1966] using double flash photography to measure

the velocity of 28.8 μm diameter lycopodium particles introduced into the entrainment field at positions outside a flat-fan spray. Experimental measurements made within spray fans using phase-Doppler anemometry (chapter 4) show that centreline entrained air velocity decreases linearly with distance from the nozzle, from a distance numerically equal to the aerodynamic stopping distance of the VMD-sized droplet, defined as $z^* = \frac{\rho_p}{\rho_f}\frac{d}{2}$, where ρ_p is the droplet density, ρ_f is the air density, d is the droplet radius [Clift et al., 1978]. This corresponds to about 0.1 m for agricultural flat-fan sprays. Profiles of entrained air and small (diameter<100 μm) droplet volume distribution show approximately Gaussian profiles across the major fan axis, with a maximum on the spray centreline (chapter 4). Lee and Tankin [1984] used droplet capture at spanwise positions along the spray axis to show qualitatively that these small droplets 'migrate' towards the spray centreline following the entrained air field. Associated theoretical analysis [Ghosh and Hunt, 1994] suggests that droplets with diameters smaller than about 100 μm are passively transported within entrained airflow at distances from the nozzle greater than the stopping distance of the VMD-sized droplet.

Complementing experimental studies of agricultural sprays in cross flows, simulations have been undertaken using random walk simulations as superimposed sources of droplets spaced equivalent to nozzles arranged on a conventional boom, so as to represent droplet transport in cross flowing shear turbulence [Miller and Hadfield, 1989; Hobson et al., 1993]. Results broadly in agreement with experimental observations were returned with appropriate selection of empirical entrainment parameters. Such simulations in no way incorporated representation of the geometrical structure of spray within the fan or the entrained air flows. The first systematic attempt to incorporate spray *structure* was described by Ghosh and Hunt [1994], guided by the spray behaviour reported herein, in particular relating to the distinction between weak and moderate cross flow velocities as defined previously.

Previous wind tunnel simulation of field measurements of airborne spray volume (chapter 3) suggests that droplet removal from the spray is controlled by the entrained air velocity field and depends only weakly on cross flow velocity profile. In these experiments, a uniform cross flow was used for simplicity. Entrained air velocity varies spatially within the spray, so it is characterised here by the maximum entrainment velocity into the spray, a measure of the strength of the spray relative to the cross flow. The maximum entrained air velocity within the spray is approximately the coherent liquid sheet velocity [Miller, 1993]. Sprays are self-similar flows with an entrainment constant of about 0.11 [Ghosh et al., 1991], so the maximum entrainment velocity into an agricultural flat-fan spray is about 2.5 m s^{-1}. Two cross flow

conditions were investigated: weak cross flow, where cross flow velocity is less than the maximum entrainment velocity into the spray; and moderate cross flow, where cross flow velocity is greater than the maximum entrainment velocity into the spray. Agricultural chemicals from ground-based sprayers are typically applied only in weak cross flows [Anon, 1990] and never under in strong cross flows.

The studies reported here were carried out using a wind tunnel employed in earlier investigations (chapters 2 and 3). Spanwise heterogeneity was assessed using flow tracers, supplemented with collector deposit measurements of the drifting volume fraction and phase-Doppler measurements of volume fractions, sizes and streamwise component velocities of drifting droplets. The experimental techniques used are described in section 2, the results obtained are presented in section 3, with discussion of the implications of these experimental observations for numerical simulation studies and conclusions in sections 4 and 5.

2. Experimental Method

An array of three overlapping flat-fan nozzles was employed here each delivering spray with included angles of 110^o inplane and about 10^o cross-plane, as illustrated in figure 2 also showing the 5^o offset nozzle-to-nozzle to avoid interactions between adjoining spray fans. At the nominal ground plane 0.5 m below the array each fan has approximately elliptical cross-section with dimensions 1.5 m by 0.1 m. Two sets of nozzles were employed respectively delivering sprays classified as *medium* and *fine* according to the British Crop Protection Council [Doble et al., 1985], the former rated at 1.6 L/min (VMD 240 μm) the latter rated at 0.6 L/min (VMD 195 μm) both as measured 0.35 m below the nozzle and with the supply set at 3 bar pressure. As shown in figure 3 the nozzles respectively produce 15% and 27% spray volume in droplets less than 150 μm diameter, the size fraction comprising much of the drift [Miller et al., 1989] in cross flow winds of 2 m s^{-1}. The experiments were conducted in a 1.5 m $\times$ 2 m open circuit (Eiffel) wind tunnel (described in chapter 2), with working section length 5 m and the floor covered in a layer of plastic simulated grass to minimize splash. Nominally uniform cross flow was employed which in the present study ranged from 0.75 m s^{-1} to 3.5 m s^{-1} (weak to moderate cross flows) as measured by a vane anemometer (Solatron Ltd.). Streamwise component turbulence intensity measured with a sonic anemometer (Gill Instruments) was approximately uniform over the working section, with maximum values of 2% at 1.8 m s^{-1} and 4% at 3.5 m s^{-1}.

Side view photographs (Canon A-1 35 mm camera; 135 mm lens, and Ilford HP5 ISO 400 film) were used to illustrate the patterns of airflow interacting with the spray structure as

visualised by neutrally-buoyant helium filled soap bubbles (Sage Action Inc.) with diameters 1 to 2 mm at a rate of about 50 per second. Bubbles were introduced 2 m upstream of the boom at locations ranging from 0.2 to 0.5 m above the floor (by vertical traverse of the bubble generator head) and up to 0.7 m from the tunnel centreline (by spanwise translation of the boom). A Spectra-Physics 5 W argon-ion water-cooled laser mounted above the tunnel delivered sheet lighting (3 mm thick) by passage through a 5 mm diameter cylindrical glass lens following reflection off an inclined front silvered plane mirror (figure 4a). The light sheet, symmetrically deployed across the tunnel was inclined at 45^o to the horizontal (see figure 4a).

Airborne spray volume flux was measured using passive line collectors [Gilbert and Bell, 1988] which operate with an implicit collection efficiency because the droplets have to penetrate the boundary layer formed by the cross flow over the collector surface. This efficiency is estimated from correlations [May and Clifford, 1967] for impaction at high Reynolds number, such that for 2 mm collectors as used here the impaction efficiency approaches unity for droplet diameters greater than 67 μm in 2 m s^{-1} cross flow and 52 μm in 3.5 m s^{-1} cross flow. Spray solution of 0.1% tracer dye (Orange G, Merck Plc) and 0.1% ionic surfactant (Zeneca Agrochemicals Plc) was collected over 15 s injection intervals controlled by an electronic timer governing a solenoid valve on the supply pipe to the nozzles. As indicated on figure 4b five horizontal line collectors (1.98 mm diameter polythene tubing) spanned the wind tunnel 2 m downstream of the boom at 0.1 m intervals to 0.5 m above the wind tunnel floor and the dye deposited on 100 mm segments of the collectors was recovered in water (10 mm cut segments shaken in test tubes) and its concentration measured using a Philips PU 8710 spectrophotometer calibrated against standard solutions [Gilbert and Bell, 1988]. The mass fraction as drift is thus recovered as a proportion of the total spray flowrate measured by a calibrated gauge in the supply line.

Droplet sizes as volume median diameters (VMD) were measured using a phase-Doppler analyser (PDA, Dantec Ltd.) incorporating a 400 mW argon-ion laser source and with effective sampling volume 0.19 mm (streamwise), 0.19 mm (spanwise) and 4.17 mm (vertical). Detailed specification of this equipment and its operation in forward scatter mode as used here has been described by Bachalo and Houser [1984] and in chapter 4. In particular in this study it was operated for maximum resolution within the droplet diameter range 0 to 250 μm. As illustrated in figure 4c the laser source and photodetector array were mounted on a vertical traverse located 2 m downstream of the boom with spanwise measurements achieved by traversing the spray boom as above. Recent studies have highlighted shortcomings in use of phase-Doppler anemometry to measure droplet or particle fluxes [Tropea et al., 1995; Brenn et al., 1995]. Consideration

of these is deferred to the discussion, but it is noted here that the precision of PDA estimates of airborne flux reported is low, with a manufacturers' claimed precision of only ±70% for the equipment used here.

The study was conducted initially for bubble tracer visualisation of the flow patterns under conditions of weak (0.75 m s^{-1}) and moderate (3.0 m s^{-1}) cross flow. Passive line collectors (recovered as 100 mm spanwise lengths) were employed to measure the spanwise distribution of airborne spray flux under the same cross flow regimes, although using higher cross flow velocities (2.0 m s^{-1} and 3.5 m s^{-1} respectively) to produce recoverable drift volumes. The PDA was used to provide comparative measurements of airborne spray flux (subject to uncertainties outlined above) and droplet volume median diameters and droplet and airflow velocities at cross flow velocities of 2.0 m s^{-1} and 3.5 m s^{-1}. All measurements were made at the reference station 2 m downstream of the boom.

3. Experimental Results

3.1. Bubble Tracer Visualisation of Flow Patterns

Representative images of the interaction of the approach flow with the spray fans are shown for the fine spray in weak (0.75 m s^{-1}) and moderate (3.0 m s^{-1}) cross flows in figures 5 and 6, taken at spanwise stations located on the central nozzle centreline (figures 5a, 5b, 6a, 6b) and at the mid-plane between nozzles (figure 5c). The field of view in figures 5 and 6 is shown schematically in figure 7. The light sheet illuminates a slice through the spray (visible as a vertical section in the extreme left of figure 5 and more centrally in figure 6) and its image on the tunnel floor appears as the horizontal line at the bottom of the figures. The tracer bubble source is situated just out of view on the right side of figures 5 and 6.

Tracer bubbles in figure 5a (released 0.4 m above the floor in weak cross flow) indicate the extent of the upstream influence of the spray fans demonstrating entrainment trajectories into the spray sheet where they are accelerated rapidly downwards and upstream blockage where they are accelerated upwards over the top of the spray boom. Tracer bubbles released 0.2 m above the floor (figure 5b) show more pronounced evidence of the upstream recirculation due to blockage of the approach flow illustrated by upstream deflection of spray entrained air near the tunnel floor. The recirculation flow appears to be of apparently uniform extent as indicated in figure 5c for bubbles released 0.2 m above the floor on the mid-plane between nozzles. The air

and re-entrained fine droplets entering this zone escape by spanwise migration, exiting around the edges of the spray sheet.

In contrast to the pronounced upstream disturbance illustrated in figure 5 for weak approach flow, with moderate cross flow the bubble tracers go through the spray field even in regions of highest spray entrained air velocity, as shown in figure 6a for bubbles released 0.4 m above the floor on the spray centreline. This pattern is confirmed for tracers released closer to the floor, for example figure 6b (release height 0.2 m) and also for spanwise release positions away from the centreline (not shown here), both corresponding to regions of weaker entrained air velocity.

Figures 5 and 6 show a wide range of bubble streak lengths, with maximum about 0.2 m for weak cross flow (figure 5) and about 0.5 m for moderate cross flow (figure 6) in regions where lateral deflection due to blockage of upstream flow is small, although most streaks are significantly shorter. For 0.5 s exposure time the maximum streak lengths expected were 0.37 m and 1.75 m respectively for unperturbed weak and moderate cross flow velocity used here, if the bubbles remained within the light sheet for the full exposure. However, bubble diameters of 1-2 mm are comparable with the sheet width of 3 mm, hence only a very small spanwise velocity component is required to displace the bubbles from the light sheet. For this reason, the combination of bubble diameter and light sheet thickness made airflow velocimetry by measurement of streak lengths unreliable.

3.2. Deposition Estimates of the Airborne Spray Flux

Figures 8 and 9 show airborne volume flux contours (μL/cm^2 s) as collector deposition 2 m downstream for the fine spray nozzle in weak (2.0 m s^{-1}) and moderate (3.5 m s^{-1}) wind. Preliminary experiments using 0.75 m s^{-1} cross flow produced very low drift fluxes at the collectors (typically less than 0.2 μL/cm^2 s everywhere) which increased uncertainties in the dye concentration estimates (see below), so a higher cross flow velocity of 2.0 m s^{-1} was selected within the weak cross flow regime. The horizontal field of view spans the interval between adjacent spray centrelines, positioned at 0 mm and 500 mm, with the position 0 mm corresponding to the boom centre. Slight asymmetries in interpolated data may reflect reduced blockage by the edge fan as compared to the central fan. Data were acquired at heights to 0.5 m and spanwise positions from -100 mm to 600 mm relative to the boom centre with the outermost values used to provide boundary values for the cubic spline interpolation routine used here. The averaged value of airborne flux calculated for each 100 mm section was assigned to the spanwise position of the centre of the section for use in this routine, and this may introduce small unsystematic

error. However, the key observations here are those of airborne flux shapes relative to the spray fan geometry, with the edge loci of the undistorted fans superposed as dotted lines. No error estimates are included on these figures, but collector precision is considered as follows. The impaction efficiency of passive line collectors, estimated from graphical correlations [May and Clifford, 1967], approaches unity for droplet diameters greater than 67 μm in 2 m s^{-1} cross flow and 52 μm in 3.5 m s^{-1} cross flow. PDA measurements of drifting droplet diameter (section 3.4 below) suggest that 12% of droplets have diameters less than these threshold values with their impaction efficiency reduced to about 70% [May and Clifford, 1967], yielding an overall impaction efficiency estimate in the drift field of about 97% for both cross flow conditions. Dye recovery and spectroscopic analysis have a precision of about 95% [Gilbert and Bell, 1988], leading to an overall precision of about 92% for airborne flux measurements.

In figure 8, the maximum airborne spray flux fraction is located midway between the nozzles at about 0.2 m above the floor, appearing to have originated from spray fan edges, whereas for stronger cross flow figure 9 shows rearrangement of the contours with the maximum located close to the centreline of the central fan and with contours much more nearly horizontal, reflecting the substantially increased underflow noted in section 3.1. With larger droplets (figure 10, showing contours for the medium spray nozzle in weak wind), the maximum drift is also located midway between nozzles but nearer the floor and is substantially reduced as compared with the fine spray, such that the maximum airborne spray flux contour is about 70% of that measured for the fine spray in weak cross flow.

3.3. PDA Measurements of Airborne Spray Flux

The volume fraction flux estimates from collector deposits described above can be directly compared with volume fraction distributions retrieved from PDA measurements of droplet size and velocity. Figure 11 shows the contours for fine spray in weak cross flow and whilst the shapes are broadly comparable with those shown in figure 8 using collector deposits, the magnitudes are substantially larger here, with peak values approximately twice those measured using line collectors. Figure 12 shows the contours for medium spray in weak wind and is to be compared with figure 10 obtained under the same conditions using line collectors. For both fine and

medium nozzles in weak cross flow the peak airborne spray flux relative to the fan geometry is located at a similar downstream position, although the shape of the flux distribution about the peak differs, with a more pronounced peak associated with PDA measurements. This is attributed to differences in interpolation using spanwise average values located at the centre of the line collector sections and associated loss of detail, as compared with point measurements through a measuring volume with spanwise length 0.19 mm using the PDA. In any case, both measurement methods show peak airborne spray flux associated with droplet removal from the fan edges in weak cross flow and from the fan centrelines in moderate cross flow. The ratio of airborne flux measured for medium to fine sprays in weak cross flow using PDA is about 0.7, in line with the ratio estimated for the deposition measurements. The higher values of airborne spray flux recorded using the PDA are consistent with shortcomings in calculations of flux from droplet size and velocity measurements discussed below.

3.4. PDA Measurements of Droplet Sizes and Velocities

Figure 13 shows droplet volume median diameters measured 2 m downwind of fine sprays in weak cross flow. It can be seen that the bigger droplets (diameter 100 μm or so) are scavenged from the edges of the fans consistent with the 'ribbing' structure of liquid sheets and also nearer to the wind tunnel floor probably associated with gravitational settling. The streamwise velocities associated with droplets in diameter classes 50 ($\pm$ 5) μm and 100 ($\pm$ 5) μm are shown in figures 14 and 15. Subject to reservations on slip speed (0.07 m s^{-1} and 0.25 m s^{-1} respectively, calculated from Stokes law [Clift et al., 1978, p.35]) the velocity contours shown on figure 14 for 50 μm diameter droplets are representative of the cross flow streamwise component velocities of airflow downstream of the fan, in which case the small transverse displacements of these contours with respect to the fan loci suggest a small spanwise component of mean flow interpreted here as due to enhanced blockage of the approach flow by the central spray fan, and consistent with previous figures. Disregarding the slight differences between figures 14 and 15 augmented by interpolation bias, drifting 100 μm diameter droplets appear to be passively transported in the cross flow velocity field.

Despite *prima facie* expectations that the flow would accelerate through the gaps between adjoining fans, the evidence in figures 14 and 15 is slight. More obviously, at heights of 0.3 m and above the droplet velocities are about 2 m s^{-1}, comparable with that of the approaching mean flow which suggests that any disturbance produced by the spray sheet has relaxed at the station 2 m downstream of the boom. It is worth remarking that peak mass fluxes were measured at

these heights which would be consistent with enhanced transport within a shear layer separating upper relatively unperturbed airflow and accelerated underflow, although more work is needed to clarify and characterise these aspects.

4. Discussion

The experimental study reported here provides considerably more detail than previous wind tunnel studies of sprays in cross flow (recall introduction), with extension of existing use of passive line collectors to spanwise distribution of airborne spray flux relative to spray fan geometry and introduction of phase-Doppler anemometry to provide droplet sizes and droplet and airflow velocities in the drift field. Although the phase-Doppler anemometer has become an established instrument in the investigation of sprays (in still air), a number of situations have been identified in which the measured size distribution of droplets and especially the measurement of flux may be in significant error despite care in the layout and alignment of equipment [Tropea et al., 1995; Brenn et al., 1995]. The magnitude of such errors can be substantial because even if errors in diameter measurement relate to only a small percent of the sampled droplets, the third power dependency of volume on diameter results in proportionally larger errors in flux. Two effects have been identified as potentially leading to incorrect size measurement: the *trajectory or Gaussian beam effect* [Sankal et al., 1992] and the *slit effect* [Durst et al., 1994]. Both effects arise when the PDA is set up to receive refractively scattered light, as is typical for sprays, but instead receives sufficient reflectively scattered light to change the phase/diameter ratio from its expected value, introducing systematic, yet non-calculable experimental error.

Discussion of these errors and methods by which they can be minimised is outside the scope of this chapter; here it is relevant to note that the discrepancy in measured airborne fluxes from passive line collectors and PDA is within the manufacturers' claimed precision. It is emphasized again that these measurements show broad agreement for shapes of airborne flux distributions within the simple framework of zones defined by the relative strength of cross flow and entrained air velocity fields. The explicit linking of downwind dispersion to spray fan geometry in principle allows extension to other spray technology applications, particularly those carried out in nominally still air with undesirable weak cross flow (surface treatment, spray painting).

Figure 16 is a schematic of the overall picture deduced from these studies, main elements of which are as follows. In weak wind, the approach flow is entirely entrained into the spray jet which thus acts as a momentum sink. Ground interaction between the upstream deflected

spray and the flow boundary layer under the approach wind result in a recirculating zone akin to that found with bluff bodies and porous bluff bodies [Coelho and Hunt, 1989]. Hang-up of the fines in the upstream recirculating flows might be expected, as has been investigated by Chung and Troutt [1988] and Perkins et al. [1991]. The precise nature of this interaction has not been investigated here, although the blocking effect in regions of highest entrained air velocity associated with spray centrelines is apparent in the airborne flux profiles 2 m downwind (figures 8 and 11) which show peak values associated with droplet removal from regions of lower entrained air velocity (spray fan edges). It is inferred that the accompanying transverse flows exit downstream via these regions, with increased droplet removal (see figure 16) and there is no large-scale underflow anywhere across the face of the spray sheet. Downwind spanwise distributions of droplet diameter and airflow and droplet velocity (figures 13 to 15) support this view, although all showing slight variation in location of maxima within the region of lower entrained airflow, attributed to interpolation bias. In moderate cross flow (of less interest for agricultural applications) tracer studies indicate that the spray entrained airflow essentially acts only to provide a downwards perturbation momentum to the approach flow, such that cross flow streamlines can pass through the spray even in regions of high entrained air velocity (spray fan centrelines). Peak airborne spray flux is associated with droplet removal in the vicinity of the spray centreline, the location of most of the 'driftable' (diameter 100 μm or smaller) droplets within the spray.

It is inferred that increasing cross flow velocity from weak to moderate increases the region of cross wind penetration from the spray fan edges to the entire spray width, with spanwise airborne droplet distributions then reflecting droplet distributions within the spray. Observation of higher airborne flux from fine nozzles as compared to medium nozzles in the same cross flow (figures 8 and 10) is also indicative of preferential droplet removal based on lower entrained airflow generated by fine nozzles. These observations support the framework developed by Ghosh and Hunt [1994], and extended based on these studies [Ghosh and Hunt, 1997], although their characterisation in terms of spray porosity has not been explored here. The downwind droplet size distribution shows a maximum VMD of about 100 μm, consistent with the maximum droplet size passively transported by entrained airflow within the spray [Ghosh and Hunt, 1994] and in line with previous field and wind tunnel studies (recall introduction).

Previous numerical models of droplet dispersion [Miller and Hadfield, 1989; Hobson et al., 1993] used the spray droplet diameters and exit velocities measured in stationary ambient as initial conditions for release from each nozzle on the spray boom. The near-field was simulated

using a trajectory model incorporating aerodynamic drag with a simple random walk following establishment of equilibrium slip. The present findings show clearly that momentum interactions between the spray and wind substantially modify this near-field behaviour, resulting in very different effective initial conditions for the far-field dispersion.

Experimental observations made here require extension to detailed characterisation of spray porosity to the cross flow. This can only be achieved by measurement of entrained air velocity within the spray in a cross flow, and cross flow velocity immediately upstream of the spray, which is significantly modified from uniform approach flow due to blockage by the spray. Phase-Doppler anemometry using suitable seeding for airflow provides a viable technique for these measurements, resolving the entrained airflow to vertical component velocity and cross flow to horizontal component velocity, although interaction between the airflow velocity fields will not be fully revealed until 2 or 3-dimensional velocity measurements are made.

5. Conclusions

1. Droplet dispersion from flat-fan sprays has been identified with droplet removal from fan edges under weak cross flow conditions and with scavenging of smaller droplets from the fan interior under moderate cross flow conditions. Spray entrainment of air and the wind provide key scales of velocity for characterising near-field behaviour and thus downstream drift.

2. Under weak cross flow conditions which are typical for agrochemical application, the drifting droplets have volume median diameters of about 100 μm consistent with field observations and appear to be essentially passively transported within a shear layer between accelerated underflow and unperturbed approach flow.

3. Realistic input conditions to random walk models may thus be significantly different from those of unperturbed upwind approach flow, casting doubts on the predictions from previous such models.

4. The experimental observations of zones of penetration of the spray by the cross flow associated with regions of low entrained air velocity within the spray requires further characterisation utilising multicomponent air and droplet velocity measurements.

References

Anon [1990] Pesticides: code of practise for the safe use of pesticides on farms and holdings. Part III of the Food and Environmental Protection Act, 1985. HMSO, London.

Bachalo, M.D. and Houser, W.J. [1984] Phase/Doppler spray analyser for simultaneous measurements of droplet size and velocity distributions. *Optical Eng.* **23**, 583-590.

Brenn, G., Dominik, J., Durst, F., Tropea, C. and Xu, T.-H. [1995] Phase-Doppler arrangements with minimised Gaussian Beam effect and slit effect. Proc. 20th Anniversary Meeting of Phase-Doppler Anemometry, Erlangen, Germany.

Briffa, F.E.J. and Dombrowski, N. [1966] Entrainment of air into a liquid spray. *A.I.Ch.E. Jnl.* **23**, 708-719.

Byass, J.B. and Lake, J.R. [1977] Spray drift from a tractor powered field sprayer. *Pesticide Science* **8**, 117-126.

Chung, J.N. and Troutt, T.R. [1988] Simulations of particle dispersion in an axisymmetric jet. *J. Fluid Mech.* **186**, 199-222.

Clark, C.J. and Dombrowski, N. [1972] Aerodynamic instability and disintegration of inviscid liquid sheets. *Proc. Roy. Soc. Lond. A* **329**, 467-478.

Clift, R., Grace, J.R. and Weber, M.E. [1978] Bubbles, Drops and Particles. Academic Press, San Diego.

Coelho S.L.V. and Hunt, J.C.R. [1989] The dynamics of the near-field of strong jets in cross flows. *J. Fluid Mech.* **200**, 95-120.

Doble, S.J., Matthews, G.A., Rutherford, I. and Southcombe, E. [1985] A system for classifying hydraulic nozzles and other atomisers into catagories of spray quality. *Proc. British Crop Protection Conference*, 1125.

Dombrowski, N. and Johns, W.R. [1963] The aerodynamic instability and disintegration of viscous liquid sheets. *Chem. Eng. Sci.* **18**, 203-214.

Durst, F., Tropea, C. and Xu, T.-H. [1994] The slit effect in phase-Doppler anemometry. Proc 2nd International Conference on Fluid Dynamics Measurement and its Application, Beijing, China.

Ghosh, S., Phillips, J.C. and Perkins R.J. [1991] Modelling the flow in droplet driven sprays. In Johansson, A.V. and Alfredson, P.H. (eds.) *Advances in Turbulence 3*, 405-414, Springer-Verlag, Berlin.

Ghosh, S. and Hunt, J.C.R. [1994] Induced air velocity within droplet-driven sprays. *Proc. Roy. Soc. Lond. A* **444**, 105-127.

Gilbert, A.J. and Bell, G.J. [1988] Evaluation of drift hazards arising from pesticide spray application. *Aspects of Appl. Biol.* **17**, 363-375.

Hobson, P.A., Miller, P.C.H., Walklate, P.J., Tuck, C.R. and Western, N.M. [1993] Spray drift from hydraulic spray nozzles: the use of a computer simulation model to examine factors influencing drift. *J. Agric. Eng. Res.* **54**, 293-305.

Lee, S.Y. and Tankin, R.S. [1984] Study of a liquid spray (water) in a non-condensable environment (air). *Int. Jnl. Heat and Mass Trans.* **27**, 351-361.

May, K.R. and Clifford, R. [1967] The impact of aerosol particles on cylinders, spheres, ribbons and discs. *Annals of Occupational Hygiene* **10**, 83-95.

Miller, P.C.H. [1993] Spray drift and its measurement. In Matthews, G.A. and Hislop, E.C. (eds.) *Application Technology for Crop Protection*, CAB International.

Miller, P.C.H. and Hadfield, D.J. [1989] A simulation of spray drift from hydraulic nozzles. *J Agric. Eng. Res.* **42**, 135-147.

Miller, P.C.H., Mawer, C.J. and Merritt, C.R. [1989] Wind tunnel studies of the spray drift from two types of agricultural spray nozzle. *Aspects of Appl. Biol.* **21**, 237-238.

Perkins, R.J., Ghosh, S. and Phillips, J.C. [1991] In Johansson, A.V. and Alfredson, P.H. (eds.) *Advances in Turbulence 3*, 93-100, Springer-Verlag, Berlin.

Rutherford, I., Bell, G.J., Freer, J.B.S., Herrington, P.J. and Miller, P.C.H. [1989] An evaluation of chemical application systems. *Proc. British Crop Protection Conf.-Weeds*, 601-613.

Sankal, S.V., Inenaga, A. and Bachalo, W.D. [1992] Trajectory dependent scattering in phase-Doppler anemometry: minimising and eliminating sizing error. Proceedings 6th International Symposium of Application of Laser Technology to Fluid Mechanics, Lisbon, Portugal.

Tropea, C., Xu, T.-H., Onofri, F., Grenhan, G., Haugen, P. and Stiegelmeier, M. [1995] Dual mode phase-Doppler anemometer. Proceedings of 4th Conference on Optical Particle Sizing, Nuremburg, Germany.

Western, N.M., Hislop, E.C., Herrington, P.J. and Jones, E.I. [1989] Comparative drift measurements for BCPC reference nozzles and for an Airtec twin fluid nozzle under controlled conditions. *Proc. British Crop Protection Conf.-Weeds*, 641-648.

Western, N.M. and Hislop, E.C. [1991] Drift of charged and uncharged droplets from an experimental air assisted sprayer. *British Crop Protection Monograph no. 46: Air-assisted Spraying in Crop Protection,* 69-77.

Figures

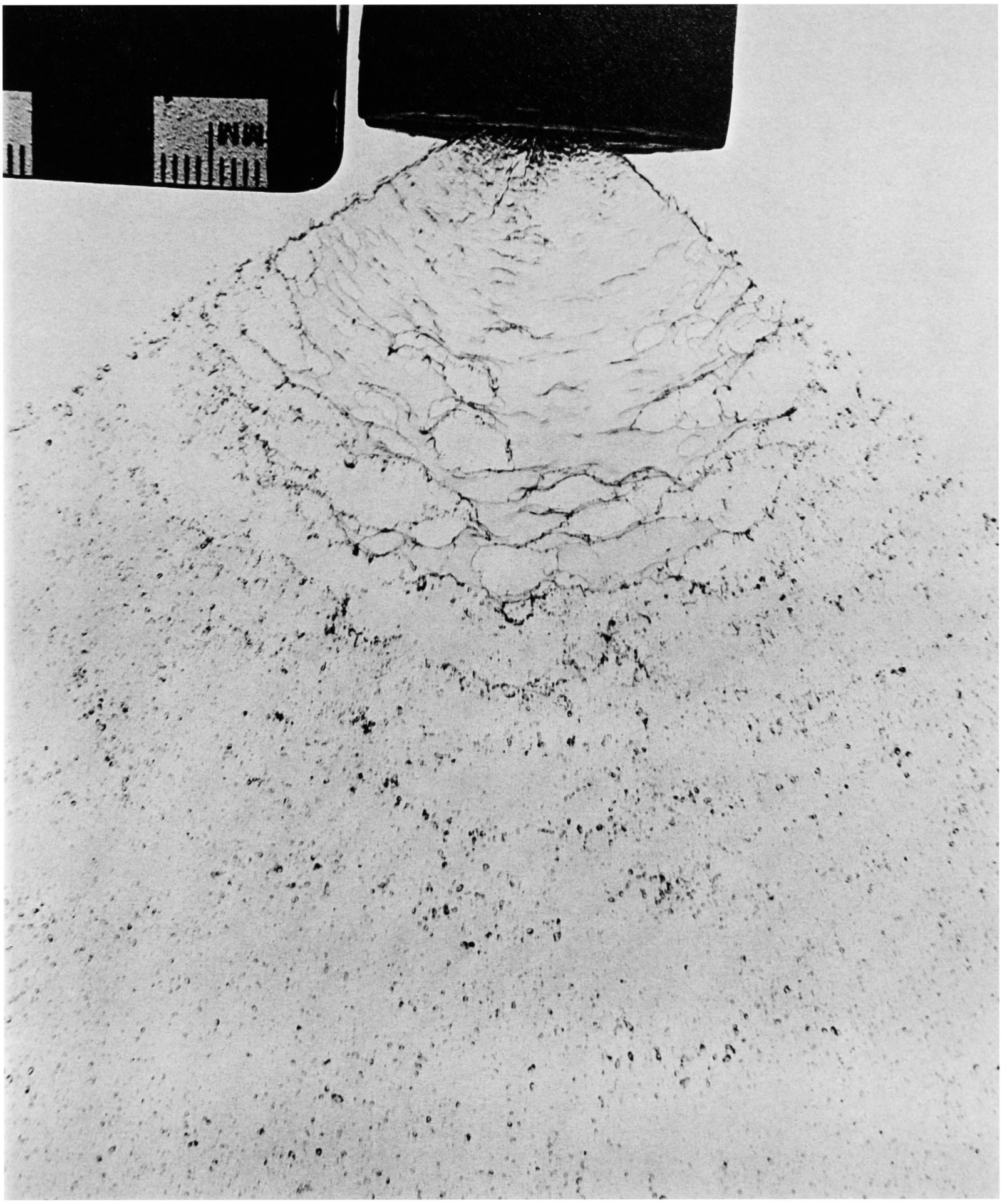

1. The disintegration of a liquid sheet issuing from a 110° flat-fan nozzle supplied at 1.6 L/min and 3.0 bar pressure, photographed with a flash duration of 0.1 ms. The width of the nozzle housing is 36 mm (Courtesy Silsoe Research Institute).

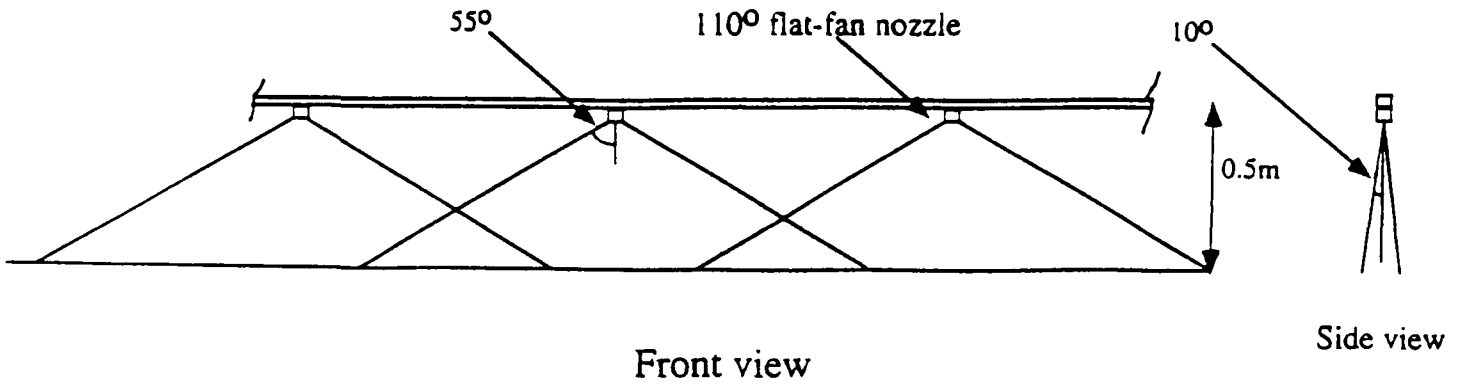

2. The arrangement of flat-fan sprays used experimentally, based on typical agricultural configuration. In plan, the nozzles are positioned such that the spray major axis is offset 5^o to the boom axis.

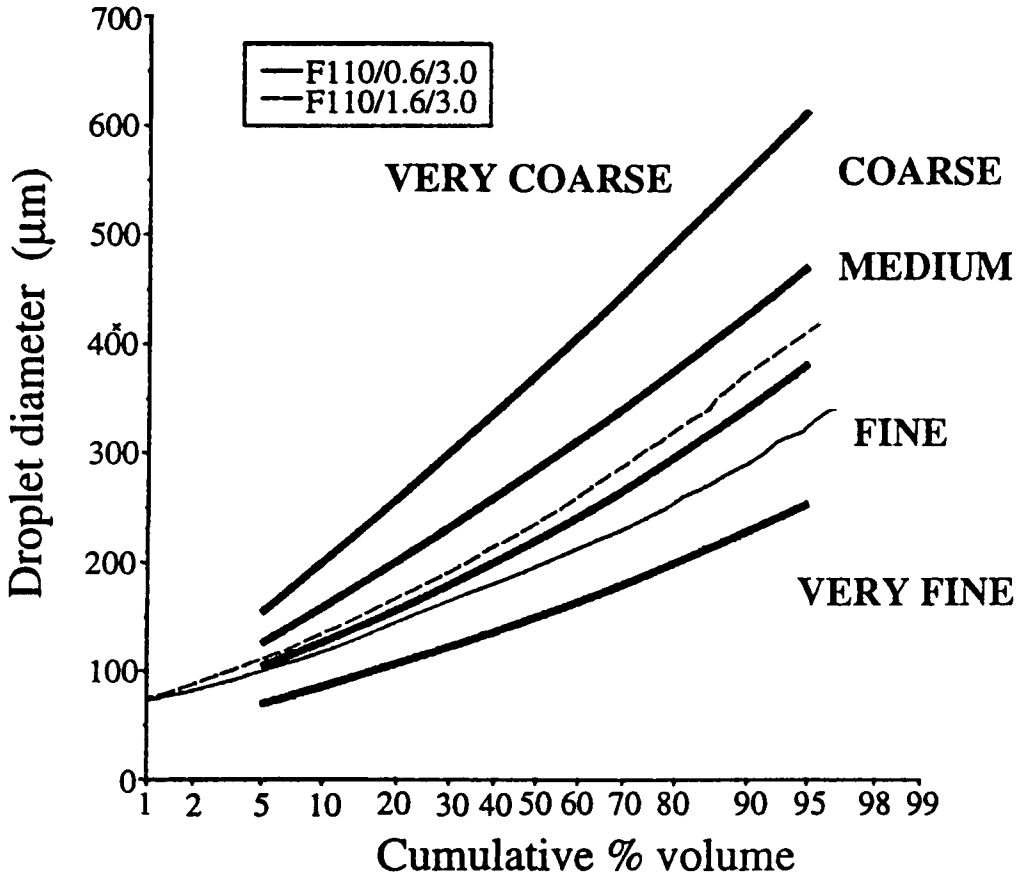

3. The reference grid based on cumulative size distribution for classifying agricultural spray nozzles (Doble et al., 1985) also showing the characterisations of the nozzles used in the experiments, denoted as F110/0.6/3.0 (110^o flat-fan nozzle supplied at 0.6 L/min and 3.0 bar pressure) for the fine spray and F110/1.6/3.0 (110^o flat-fan nozzle supplied at 1.6 L/min and 3.0 bar pressure) for the medium spray.

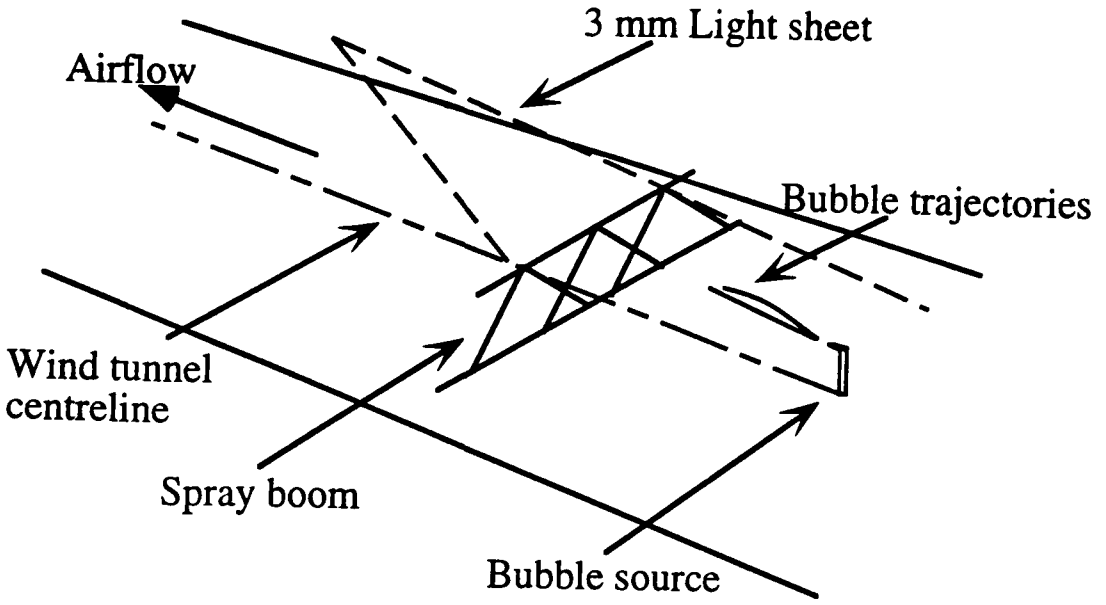

(a)

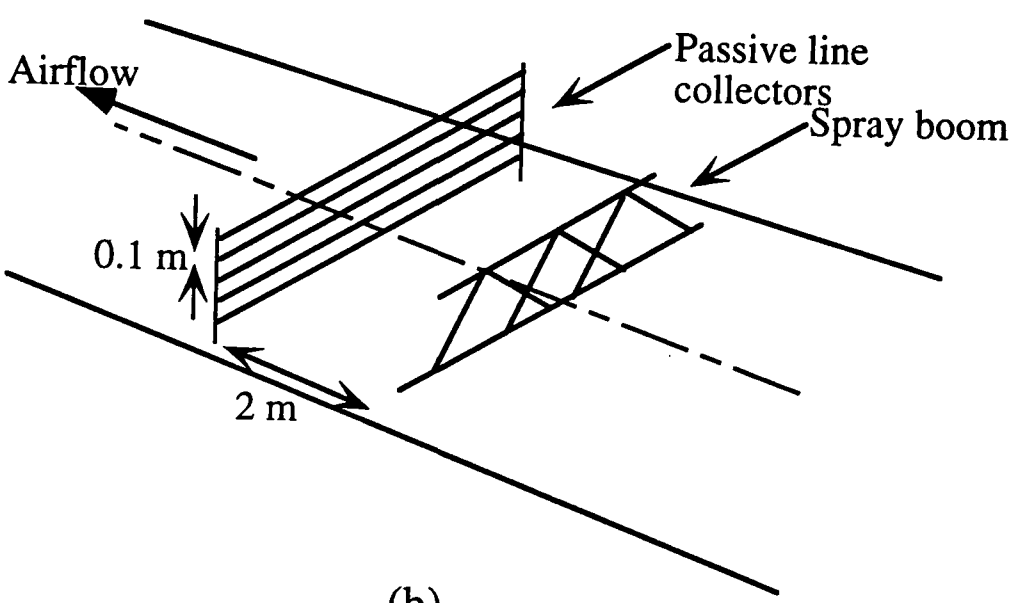

(b)

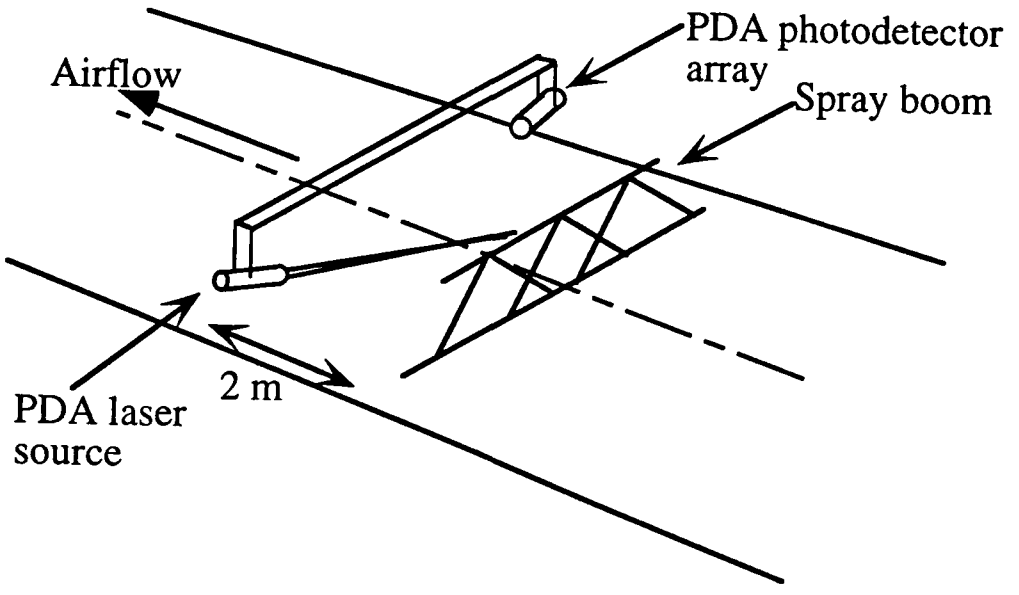

(c)

4. Schematic diagram showing arrangement of the experimental equipment. a. Flow visualisation experiments. b. Passive line collectors for airborne flux measurements. c. Phase-Doppler analyser.

Fig 5a

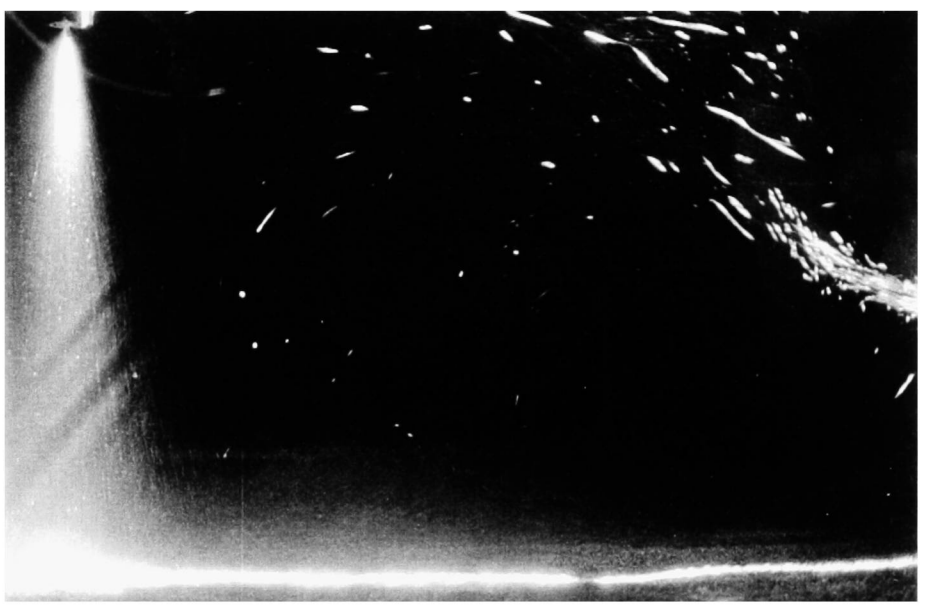

Fig 5b

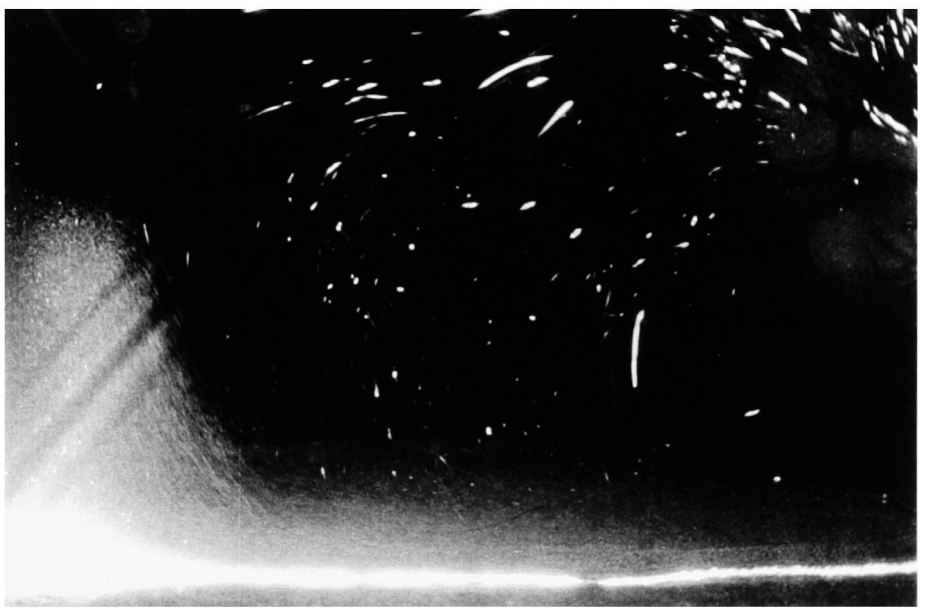

Fig 5c

5. Visualisation of the interaction of fine sprays with weak (0.75 m s^{-1}) cross flow a. Tracer release position 0.4 m above the floor on the boom centreline. b. Tracer release position 0.2 m above the floor on the boom centreline. c. Tracer release position 0.2 m above the floor on the midplane between adjoining sprays.

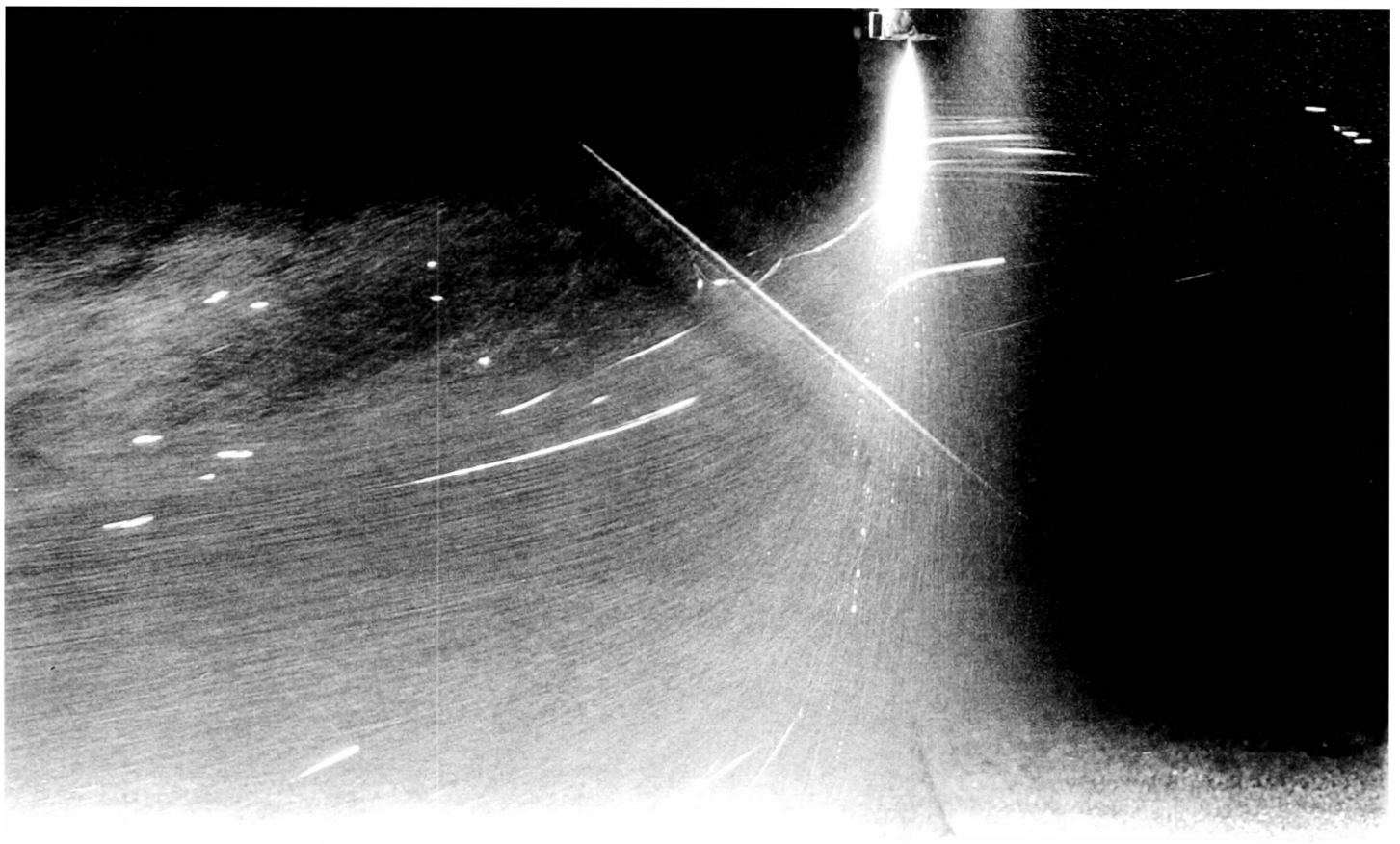

Fig 6a

Fig 6b

6. Visualisation of the interaction of fine sprays with moderate (3.0 m s^{-1}) cross flow a. Tracer release position 0.4 m above the floor on the boom centreline. b. Tracer release position 0.2 m above the floor on the boom centreline.

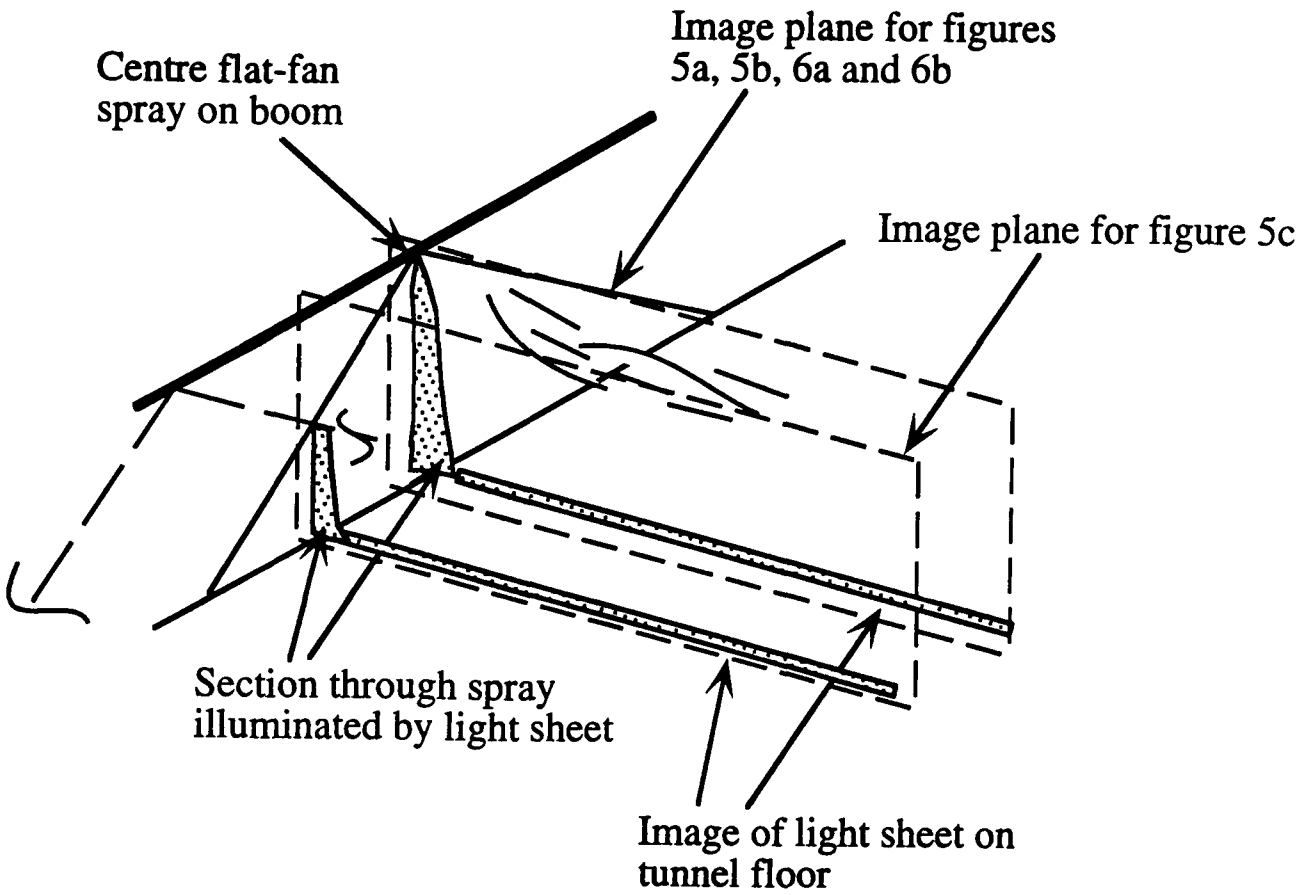

7. Schematic diagram of the image plane reproduced in figures 5 and 6. This includes the spray centreline for figures 5a, 5b, 6a and 6b, and includes the midplane between adjoining sprays for figure 5c. The height of the boom is 0.5 m.

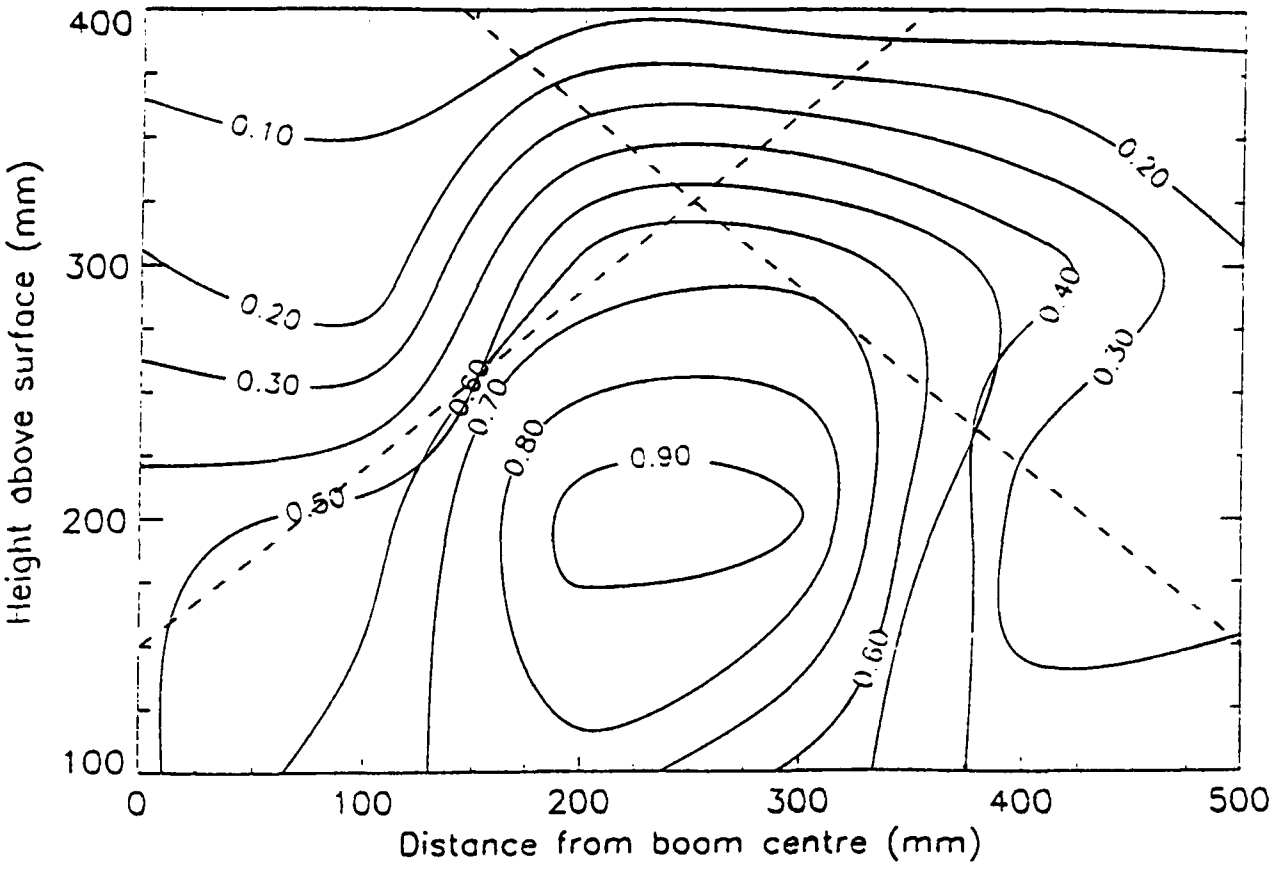

8. Airborne spray volume flux 2 m downwind of the boom of fine nozzles in weak cross flow (μL/cm^2 s) calculated as collector deposition. Dashed lines show the superimposed position of the edge loci of the undistorted spray fans.

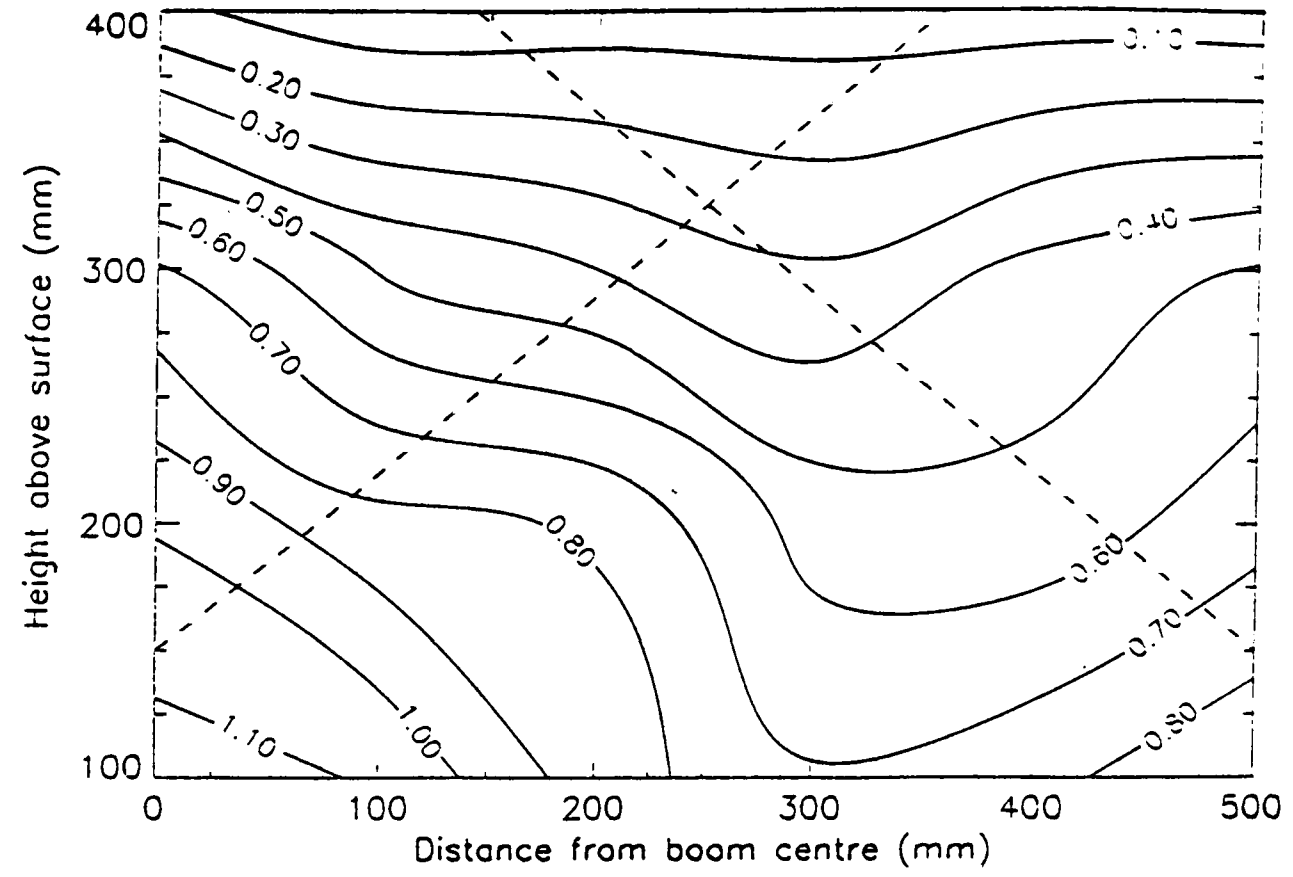

9. Airborne spray volume flux 2 m downwind of the boom of fine nozzles in moderate cross flow (μL/cm^2 s) calculated as collector deposition. Dashed lines show the superimposed position of the edge loci of the undistorted spray fans.

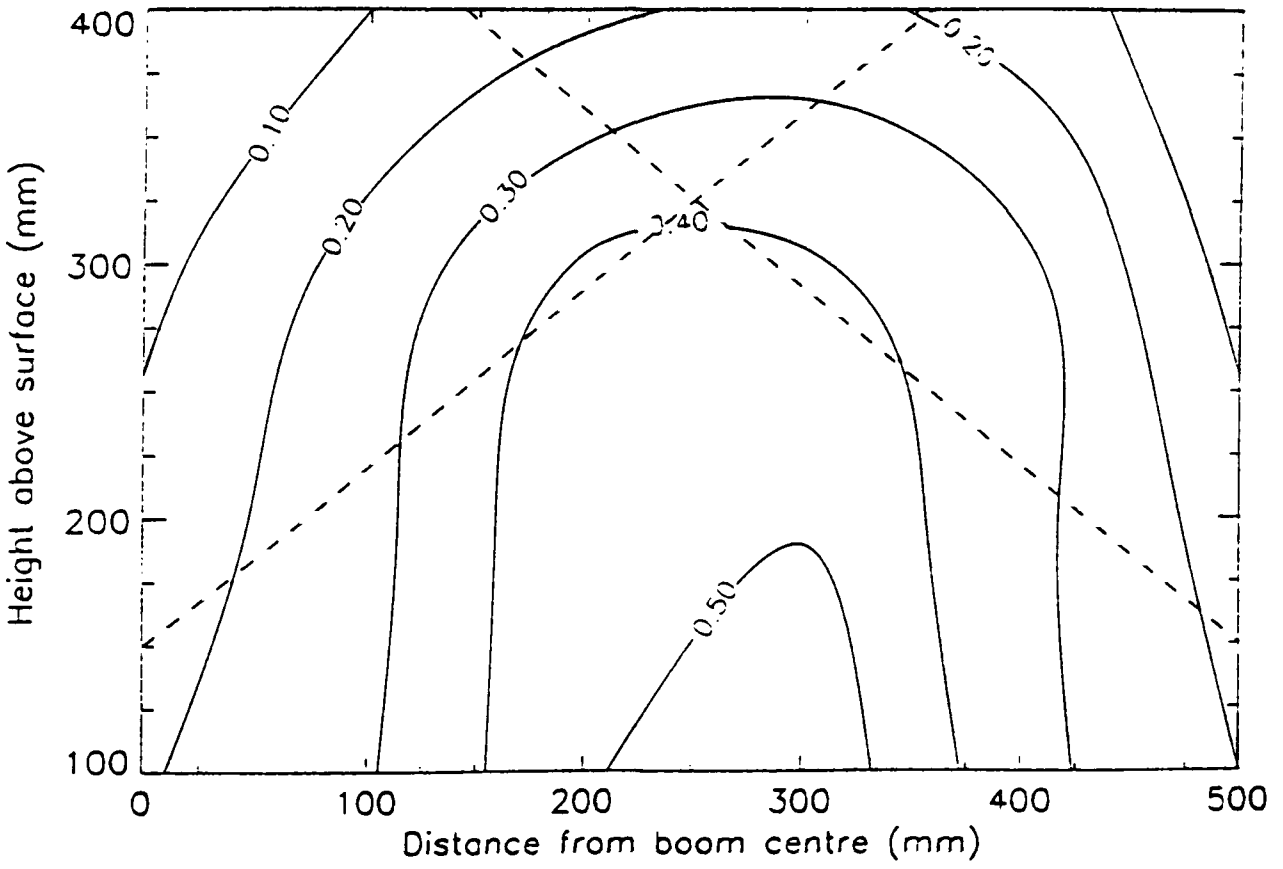

10. Airborne spray volume flux 2 m downwind of the boom of medium nozzles in weak cross flow (μL/cm^2 s) calculated as collector deposition. Dashed lines show the superimposed position of the edge loci of the undistorted spray fans.

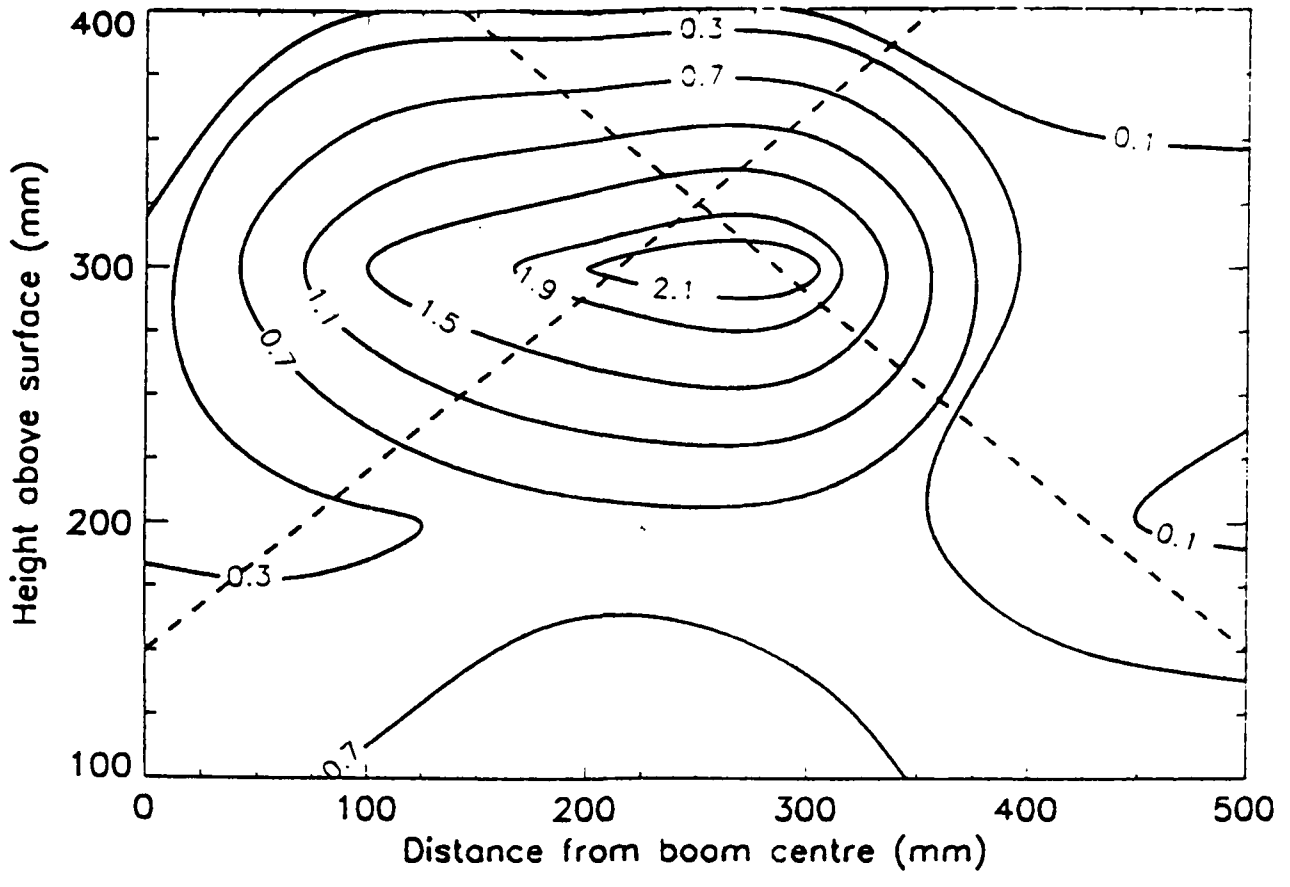

11. Airborne spray volume flux 2 m downwind of the boom of fine nozzles in weak cross flow (μL/cm^2 s) measured using PDA. Dashed lines show the superimposed position of the edge loci of the undistorted spray fans.

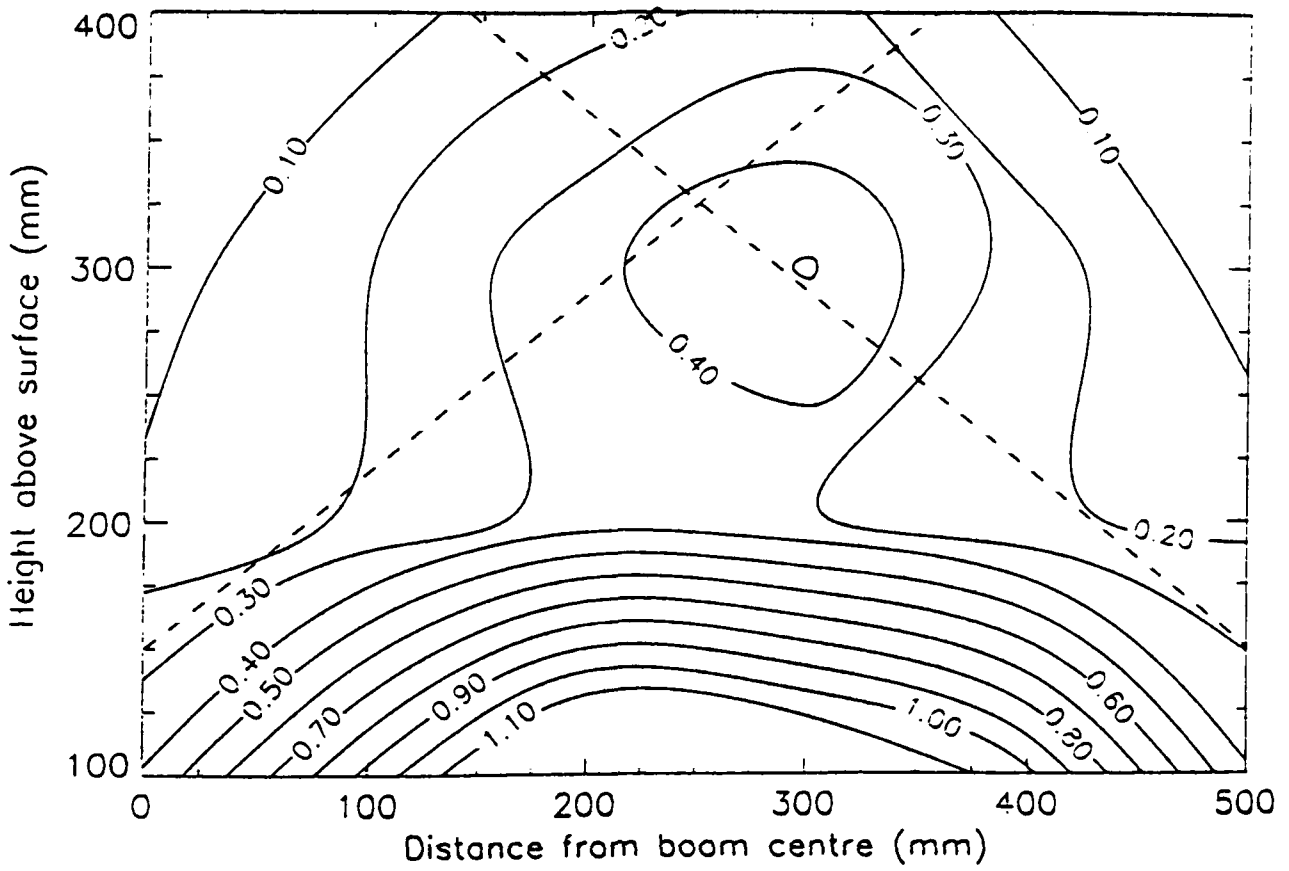

12. Airborne spray volume flux 2 m downwind of the boom of medium nozzles in weak cross flow (μL/cm^2 s) measured using PDA. Dashed lines show the superimposed position of the edge loci of the undistorted spray fans.

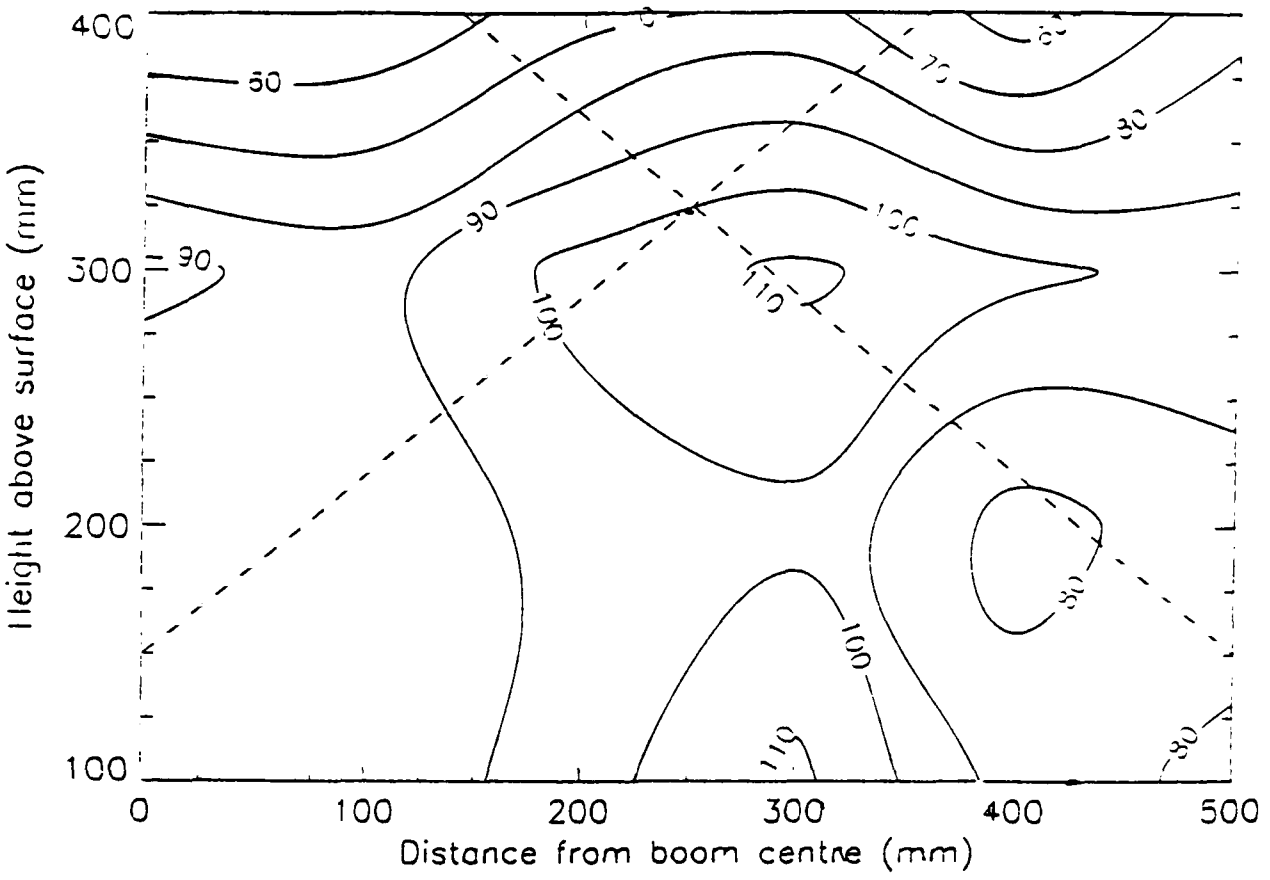

13. Airborne droplet volume median diameter 2 m downwind of the boom of fine nozzles in weak cross flow (μm) measured using PDA. Dashed lines show the superimposed position of the edge loci of the undistorted spray fans.

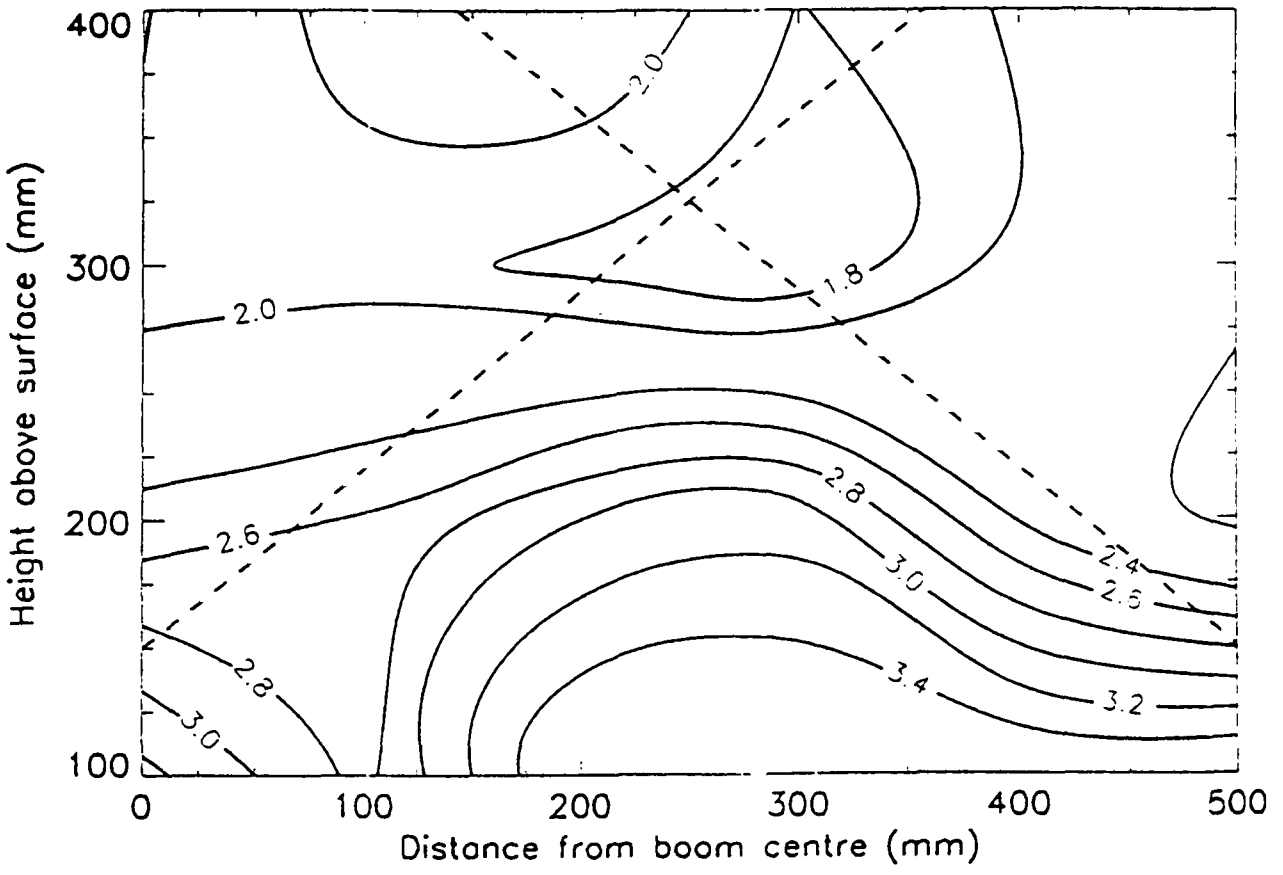

14. Streamwise velocity of 45-55 μm droplets (used to represent streamwise air velocity) 2 m downwind of the boom of fine nozzles in weak cross flow (m s^{-1}) measured using PDA. Dashed lines show the superimposed position of the edge loci of the undistorted spray fans.

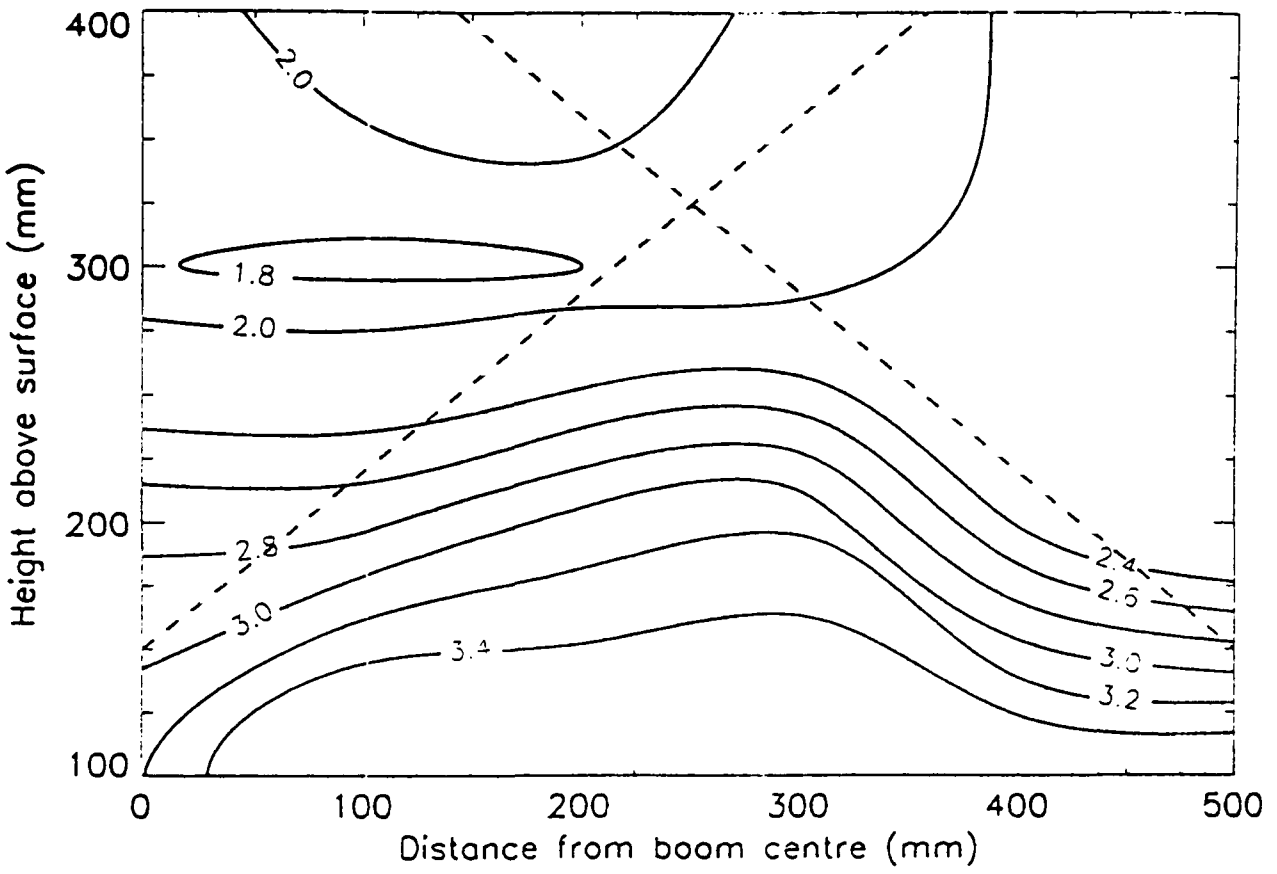

15. Streamwise velocity of 95-105 μm droplets (typical of drifting droplet sizes) 2 m downwind of the boom of fine nozzles in weak cross flow (m s^{-1}) measured using PDA. Dashed lines show the superimposed position of the edge loci of the undistorted spray fans.

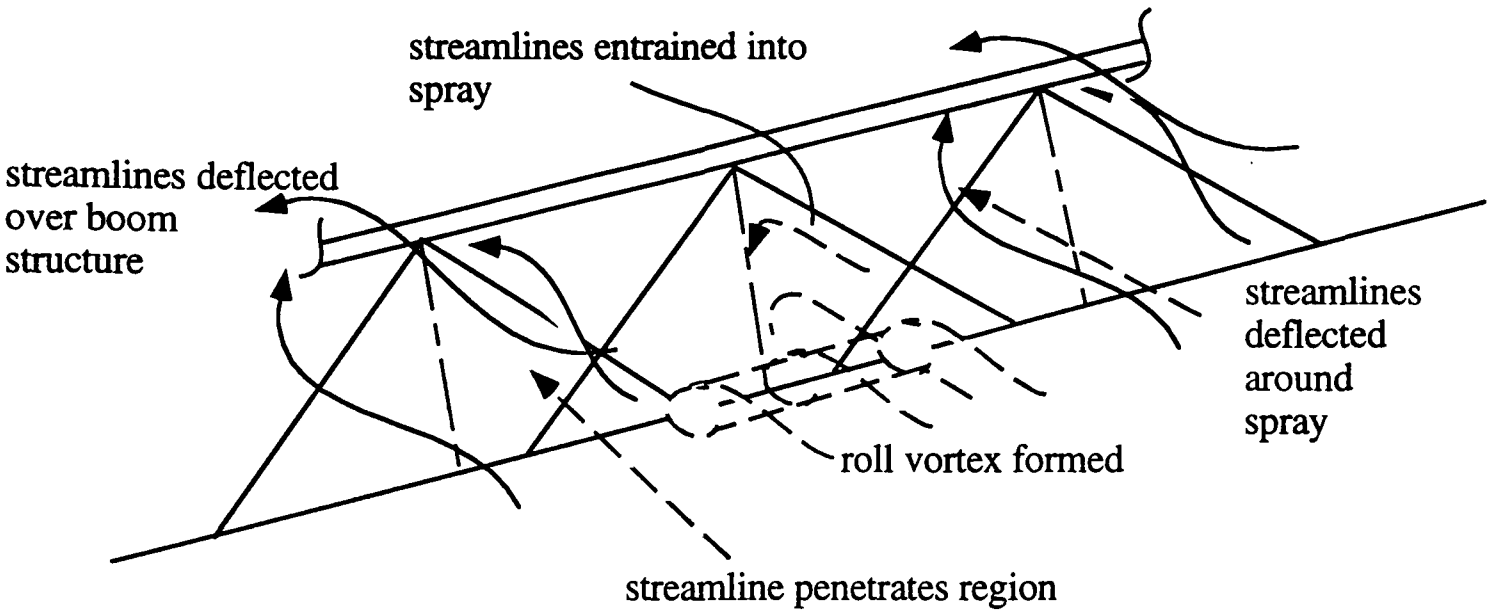

(a)

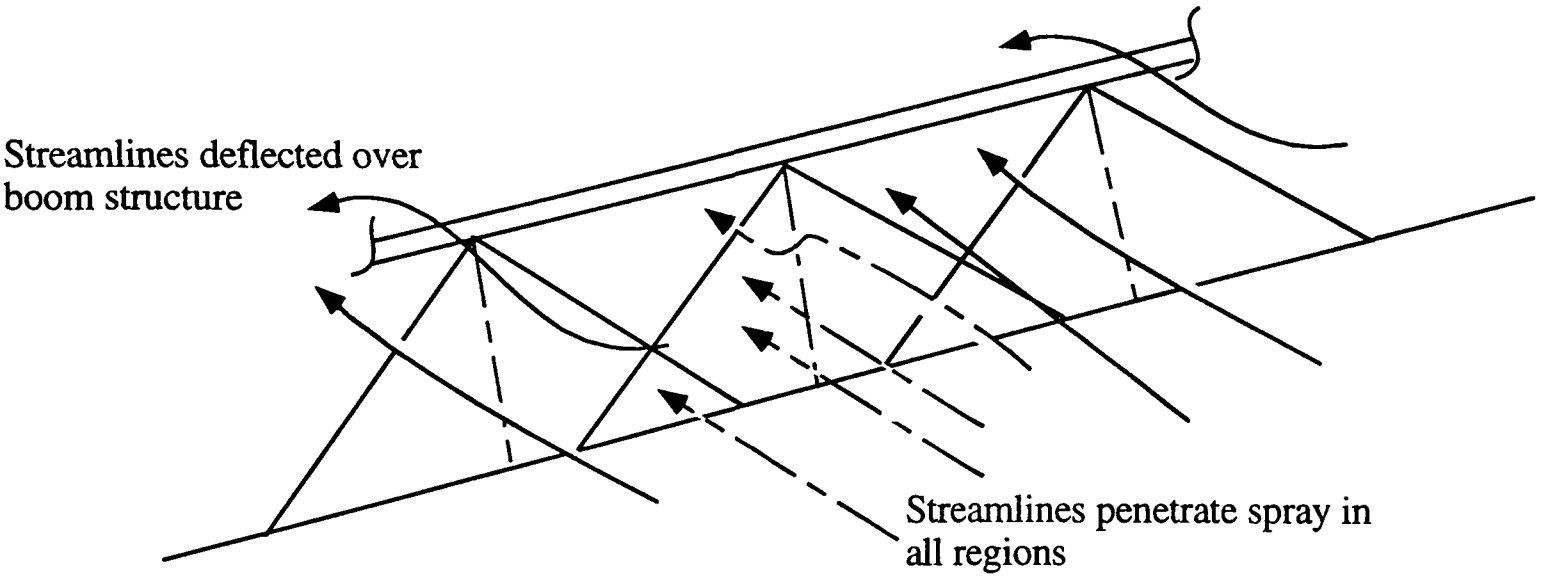

(b)

16. Summary schematic diagrams for the visualisation of flow around typical agricultural spray booms: (a) weak cross flow conditions; (b) moderate cross flow conditions.

CHAPTER 6. DISCUSSION OF FINDINGS AND IMPLICATIONS

In this chapter, mechanisms of droplet transport in the spray near-field suggested by the present experimental investigation are briefly discussed. Recent studies extending the present study are briefly reviewed, and implications for numerical simulation of spray drift are presented.

1. Methodology

The aim of this study was to identify the mechanism of droplet removal from an agricultural spray by the wind or spraying vehicle motion, and thus to lead the development of numerical simulations of this process. Previous study of this problem has been restricted to making observations of downwind deposition, either using conventional spraying equipment in the field or single nozzles in the wind tunnel. Field experiments are expensive and tend to yield low quality data due to present inability to characterise the effects of localised wind veering and the role of the plant canopy as a compliant boundary (recall chapter 1). They are thus inappropriate as a means of identifying key mechanisms of droplet transport. Previous wind tunnel experiments have lacked any coherent verification, in that no published experimental studies reconcile field and wind tunnel measurements of spray drift, or attempt to reproduce field cross flow conditions.

The methodology here has attempted to rationalise these discrepancies in a combined approach to spray drift measurement. The baseline for this study was the fundamental role of air entrainment controlling deflection of single-phase jets, and by analogy, droplet dispersion from liquid sprays. Reviewed studies of the behaviour of air jets in cross flows identified requirements for wind tunnel simulations, later shown to be capable of reproducing field drift observations. Creation of a realistic wind tunnel environment enabled application of novel experimental techniques (in present context) to provide a detailed description of the drift field downwind of the spray boom. These techniques have significant overheads in terms of time requirements for setting up and equipment tuning, significant data requirements to establish meaningful statistics and relatively long analysis times. The methodology of the wind tunnel studies has been to identify flow regimes and initial and characteristic conditions to reduce the range of experimental measurements required.

2. Mechanisms of Small Droplet Transport

Field, wind tunnel and numerical simulation studies reviewed in chapter 1 suggest that the droplet size fraction measured as downwind drift has a maximum volume median diameter of about 100 μm. In this study of the mechanism of droplet dispersion from agricultural sprays, the transport of small (diameter <100 μm) droplets has been investigated within typical agricultural sprays and in the spray near-field (up to 2 m downwind of the spray). Initial entrainment of air occurs due to the motion of the coherent liquid sheet issuing from the nozzle, due to aerodynamic drag which causes sheet breakup. At a distance from the nozzle comparable to the aerodynamic stopping distance of the VMD-sized droplet, the centreline entrained air velocity starts to decrease linearly with distance from the nozzle. At a distance from the nozzle approximately twice this, the velocity of small droplets has relaxed to the entrained air velocity. Thus, for typical agricultural spraying configurations, the cross flow samples the spray as an air jet passively transporting small droplets over most of the region between the spray nozzle and the plant canopy top. These observations were made in still air conditions in order to accurately position the PDA measuring volume within the symmetrical spray. It is noted here that spray flexure is likely to occur under cross flow conditions, as observed in the study of single-phase jets in cross flow. However, asymmetries resulting from this interaction are not calculable *a priori*, so a still air study must be made initially. The use of phase-Doppler anemometry is not common in concentrated two-phase flows, and the flow seeding using 50 μm diameter droplets to measure airflows represents the best compromise between data rate and droplet aerodynamic response time.

The maximum entrainment velocity into the spray (about 2.5 m s^{-1} for an agricultural flat-fan spray) characterises its interaction with the cross flow, as a measure of the initial conditions of entrained airflow establishment. Under weak cross flow (defined by a cross flow velocity less than this threshold value) the spray acts on the cross flow as a momentum sink, and no underflow is observed. Drifting droplets originate from the edges of the spray fan, as a consequence of low entrainment velocity and accelerated cross flow in this region. Under moderate cross flow (defined by a cross flow velocity greater than this threshold value) the cross flow passed through the spray fan, showing slight perturbation in regions of highest entrainment velocity. The spray thus presents a porous resistance to the approach flow.

The cross flow does not simply remove droplets from regions where its velocity is greater than the local air velocity within the spray. A complex interaction between the spray entrained

air and cross flow velocity fields is observed, akin to the interaction of a single-phase air jet with a cross flow. Field observations indicate a systematic increase of airborne spray volume with windspeed, which suggests that greater areas of the spray become porous to the cross flow as its velocity increases. It may be that the effective cross flow velocity must reach a threshold value (by acceleration around regions of the spray it cannot pass through) in order for the spray to become locally porous. Under conditions typical of agricultural spraying, small droplets are passively transported downwind of the boom by the accelerated weak cross flow or the unperturbed moderate cross flow.

The wind tunnel studies which identified these transport mechanisms for small droplets were carried out in uniform cross flow. Mean shear can be neglected, as comparative measurements using two mean velocity profiles show only weak dependence on the form of mean velocity profile. This is also consistent with the entrained air velocity field within the spray controlling dispersion. Vertical velocity gradients within the spray entrained air field are in any case greater than those within the cross flow, also suggesting that entrained air velocity field must control small droplet transport. In this case, the effect of upstream turbulence is negligible, as previously shown by Coelho and Hunt [1989] for axisymmetric air jets in cross flows (recall chapter 1). The greatest discrepancy observed in comparative field and wind tunnel studies is due to the action of the plant canopy as a compliant, rather than fully rigid boundary. Correct simulation of flow in this region should improve matching of field and wind tunnel measurements, although further fundamental investigation of the flow in this region is required to provide full characterisation (recall chapter 1). However, the comparative study conducted here suggests that under wind tunnel conditions representative of agricultural spraying adequate agreement may be achieved using a rigid boundary in wind tunnel experiments. Windflow interaction with the compliant plant canopy is likely to generate turbulent eddies at the boundary, which may control droplet deposition onto the crop in the spray near- and far-fields. The timescale for transient eddy trapping of small droplets identified in numerical simulations [Chung and Troutt, 1988] has been experimentally verified here in an analogue study of particle dispersion in an air jet.

3. Recent Extensions of the Present Study

The interaction of entrained air and cross flow velocity fields controlling droplet dispersion identified here clearly depends on equipment geometry, the orientation of the spray to the cross flow and the arrangement of sprays on a boom. These two latter aspects have been further characterised in recent studies by Smith and Miller [1994] and Miller et al. [1997]. Smith and

Miller measured airborne spray volume downwind of a single static nozzle with major axis oriented between angles of 0^o (parallel) to 90^o (perpendicular) to cross flow direction in an eiffel-type 1.5 m $\times$ 2 m wind tunnel (described in chapter 2). They used the same sampling configuration as used here in chapter 3, and examined weak cross flow conditions. Their results show that averaged airborne spray volume 2 m downwind of the nozzle depends strongly on nozzle orientation (figure 1). Their results support the concept of the spray providing a porous resistance to the cross flow, with greatest drift observed in the perpendicular orientation, where the spray provides the greatest spanwise resistance to the cross flow. The simple trend of increasing airborne spray volume with windspeed produced by a single static nozzle aligned parallel to cross flow direction (chapter 3) can be explained by the spanwise decrease of entrained air across the spray minor axis (chapter 4). Smith and Miller [1994] identify Gaussian profiles of entrained air across the spray minor axis, thus the streamlined spray becomes progressively more porous from its edge towards the centreline with increasing cross flow velocity.

A recent study by Miller et al. [1997] extends the study of a boom of sprays arranged perpendicular to cross flow direction presented in chapter 5. Using an identical equipment configuration to that employed in chapter 5, they reproduced the downwind spatial distributions of airborne spray volume (figure 2) obtained here, and made detailed comparison with the behaviour of a single nozzle. By spraying tracer dye from the central nozzle and water from the outer nozzles, they measured airborne spray volume downwind of a single nozzle with and without adjacent sprays present (figure 2). Their results show that downwind airborne spray volume is enhanced by the presence of adjacent sprays on the boom, presumably as a consequence of local acceleration of the cross flow around regions of high entrained air velocity within the spray identified in chapter 5.

4. Implications for Numerical Modelling

It is clear that previous formulations of numerical models of spray drift are questionable, based on incomplete and untested field and wind tunnel experiments. New experimental evidence presented here shows that when arranged conventionally on a boom, agricultural sprays show spanwise variation of porosity to a cross flow, which is not reproduced in any existing models. A first attempt at modelling the structure of axisymmetric and flat-fan sprays is offered by Ghosh and Hunt [1997] guided by the experimental study presented here. Results from their models

broadly reproduce the behaviour shown here, and further development of their models is desirable to investigate the increase of porosity with increasing cross flow velocity suggested by the experimental data, and local enhancement of porosity by adjacent sprays on a boom as observed by Miller et al. [1997].

As an intermediate stage, it is possible to use the experimental data presented in chapter 5 as empirical input to far-field dispersion models. Under weak cross flow conditions, observations of accelerated flow supporting a shear layer in which there is a high small droplet concentration provide significantly different input conditions from those predicted using trajectory models which do not incorporate spray structure. Experimental observations under weak and moderate cross flow provide input into far-field models to determine the effect on dispersion of increased vehicle forward speed, a desirable future development.

5. Further Work

Whilst further experimental study of increase of spray porosity with increasing cross flow velocity is feasible by extending the study presented in chapter 5 to a range of cross flow conditions between weak and moderate cross flow, it is suggested that primary effort should be directed at improving the performance of realistic numerical models, based on the platform provided by Ghosh and Hunt [1997]. The concept of the spray as a porous resistance to the cross flow clearly depends on spraying equipment geometry; to implement equipment classification and testing protocols such as that suggested by Legg and Miller [1990] requires development of a general model of spray structure which is applicable to current and novel spray configurations. This model must be capable of reproducing the spatial variation of entrained air produced by a liquid spray from a variety of nozzle configurations, and modelling the complex interactions between entrained air and cross flow identified above.

In order to test future numerical models, a more complete description of droplet transport in the spray near-field is required, in addition to detailed characterisation of spray porosity to the cross flow. This can only be achieved by measurement of entrained air velocity within the spray in a cross flow, and cross flow velocity immediately upstream of the spray, which is significantly modified from uniform approach flow due to blockage by the spray. Near-field characterisation must also extend to sprays within the wake of the spraying vehicle. The expectation is that blockage of the approach flow by the spray will again control dispersion, although generation of turbulent eddies of a discreet range of length scales in the wake may generate different patterns of spray porosity to those for sprays on the boom ends. Phase-Doppler anemometry using suitable

seeding for airflow provides a viable technique for these measurements, resolving the entrained airflow to vertical component velocity and cross flow to horizontal component velocity, although interaction between the airflow velocity fields will not be fully revealed until 2 or 3-dimensional velocity measurements are made.

To realistically model droplet deposition onto the plant canopy, a more complete characterisation of the effect of the canopy as a compliant boundary is required. Whilst adequate approximation using a rigid boundary can be achieved for the near-field (recall chapter 3), further investigation is required to determine to what extent coupling between the atmospheric wind and the plant canopy elements and the resulting generation of turbulent eddies controls droplet deposition further downwind.

6. Conclusions

1. The role of entrained air within the spray fan providing the controlling resistance to droplet dispersion by a cross flow has been identified. As a consequence of this mechanism, individual spray geometry, spray arrangement on a conventional agricultural boom and orientation of the spray to the cross flow direction influence downwind airborne spray volume. Later studies [Smith and Miller, 1994; Miller et al., 1997] confirm these observations.

2. A first attempt at modelling spray structure guided by this study [Ghosh and Hunt, 1997] broadly reproduces the experimental observations. Further testing of this model is required to elucidate the relationship between spray porosity and cross flow velocity and the effect of adjacent sprays on the boom.

3. It is clear that the problem of spray drift minimisation is complex, showing strong dependence on equipment geometry and configuration. Identification of the essential mechanism of droplet dispersion is only the first stage in spray drift mitigation. Results obtained in this study provide a framework for further experimental study, and the basis for development of numerical models of spray drift.

References

Chung, J.N. and Troutt, T.R. [1988] Simulations of particle dispersion in an axisymmetric jet. *J. Fluid Mech.* **186**, 199-222.

Coelho, S.L.V., and Hunt, J.C.R. [1989] The dynamics of the near-field of strong jets in crossflows. *J. Fluid Mech.* **200**, 95-120.

Ghosh, S. and Hunt, J.C.R. [1997] Numerical simulation of sprays in cross flows. Submitted to *J. Fluid Mech.*

Legg, B.J. and Miller, P.C.H. [1990] Drift assessment using measurements and mathematical models. *Paper 901593 presented to the American Society of Agricultural Engineers, Winter Meeting, Chicago.*

Miller, P.C.H., Ganzelmeier, H., Smith, R.W. and Herbst, A. [1997] Measurements of the downwind airborne spray characteristics from hydraulic flat-fan nozzles operating in a wind tunnel. Submitted to *Crop Prot.*

Smith, R.W. and Miller, P.C.H. [1994] Drift predictions in the near nozzle region of a flat fan spray. *J. Agric. Eng. Res.* **59**, 111-120.

Figures

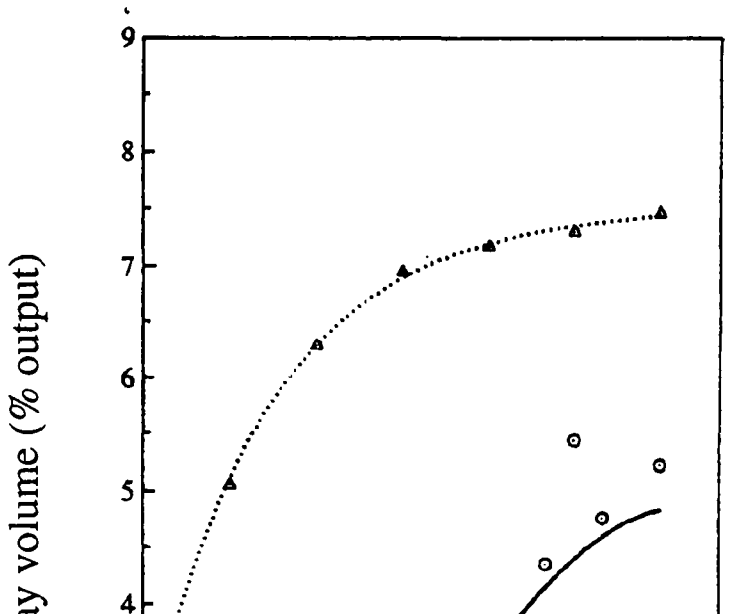

1. Averaged airborne spray volume 2 m downwind of a single nozzle at a range of spray major axis-cross flow orientations (after Smith and Miller, 1994). Circles denote wind tunnel measurements, triangles denote model predictions.

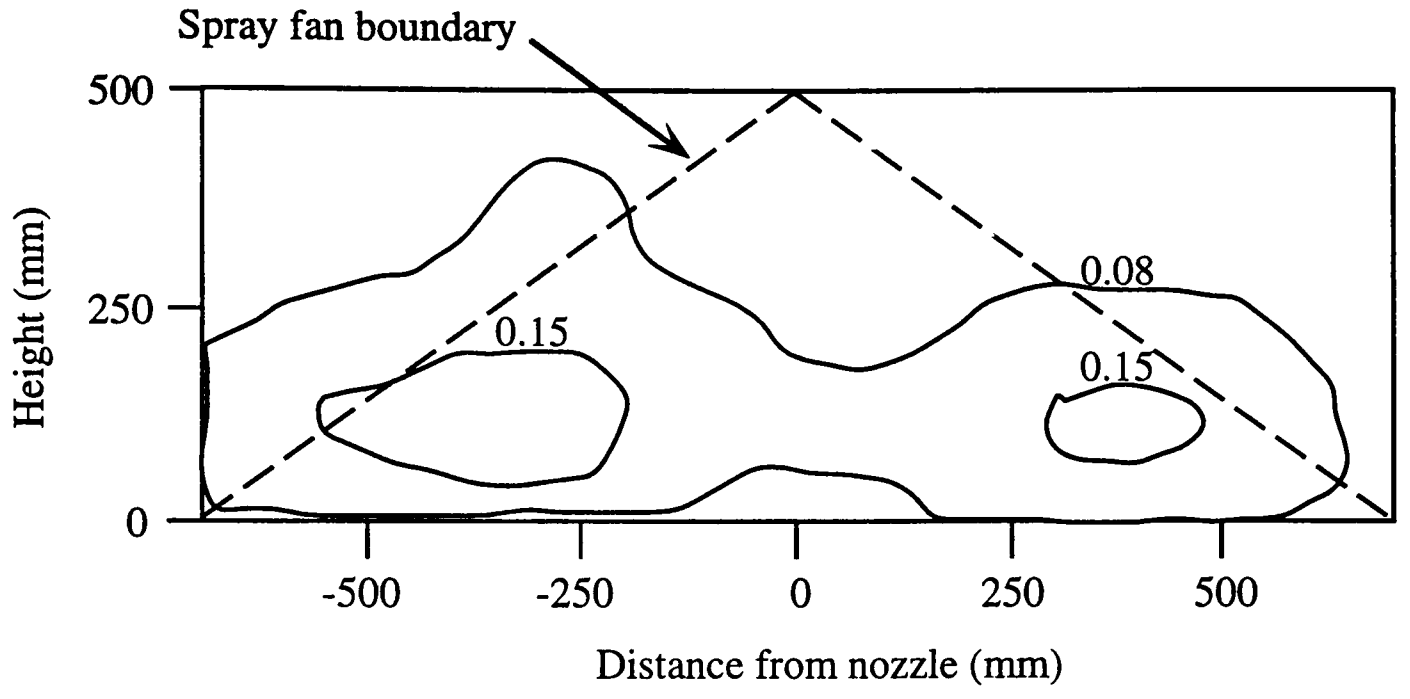

(a) Deposition from single nozzle

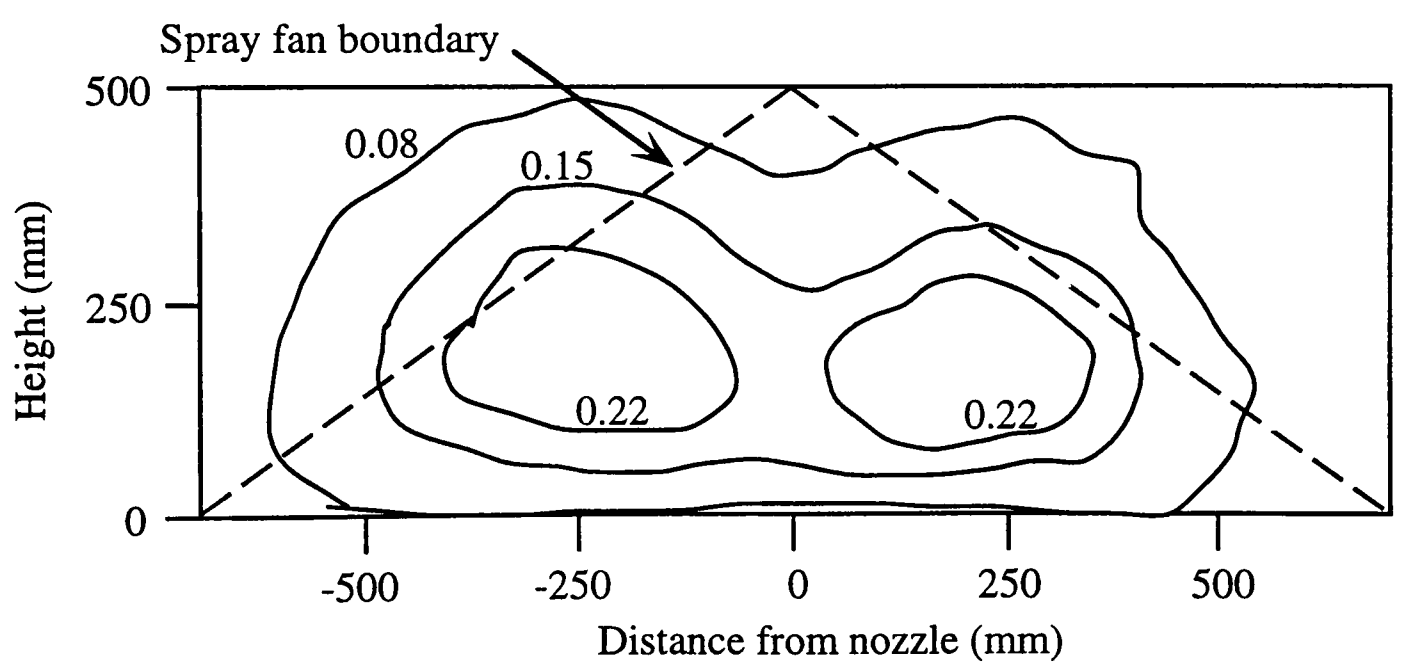

(b) Deposition from central nozzle on boom

2. Airborne spray volume 2 m downwind of a single nozzle and the central nozzle of a boom of sprays (after Miller et al., 1997). Contours show airborne spray volume flux as % nozzle output.

References

Andreopoulis, J. and Rodi, W. [1984] Experimental investigation of jets in a crossflow. *J. Fluid Mech.* **138**, 93-127.

Anon [1975] ESDU Item 75001 Characteristics of atmospheric turbulence near the ground III: variation in space and time for strong winds (neutral atmosphere). *Wind Engineering sub-series I.* Engineering Sciences Data Unit, London.

Anon [1978] ESDU 82026 (superceeds 72026) Characteristics of the wind speed in the lower layers of the atmosphere: Strong winds (neutral atmosphere). ESD item 82026, E.S.D.U.

Anon [1985] *Physics Students Guide 1 - Nuffield Advance Science.* Longman, U.K.

Anon [1990] Pesticides: code of practice for the safe use of pesticides on farms and holdings. Part III of the Food and Environmental Protection Act, 1985. HMSO, London.

Armitt, J., and Counihan, J. [1968] The simulation of the atmospheric boundary layer in a wind tunnel. *Atmos. Env.*, **2**, 49-71.

Bachalo, M.D. and Houser, W.J. 1984. Phase/Doppler spray analyser for simultaneous measurements of droplet size and velocity distributions. *Optical Eng.* **23**, 583-590.

Blackadar, A.K. and Tennekes, H.A. [1968] Asymptotic similarity in neutral barotropic planetary boundary layers. *J. Atmos. Sci.* **25**, 1015-1020.

Bradbury, L.J.S. [1965] The structure of a self-preserving turbulent plane jet. *J. Fluid Mech.* **23**, 31-64.

Brenn, G., Dominik, J., Durst, F., Tropea, C. and Xu, T.-H. [1995] Phase-Doppler arrangements with minimised Gaussian Beam effect and slit effect. Proc. 20th Anniversary Meeting of Phase-Doppler Anemometry, Erlangen, Germany.

Broadwell, J.E. and Briedenthal, R.E. [1984] Structure and mixing of a transverse jet in incompressible flow. *J. Fluid Mech.* **148**, 405-412.

Briffa, F.E.J. and Dombrowski, N. [1966] Entrainment of air into a liquid spray. *A.I.Ch.E. Jnl.* **43**, 708-717.

Busch, N.E. [1973] The surface boundary layer (part 1). *Bound. Layer Meteor.* **4**, 213-240.

Byass, J.B. and Lake, J.R. [1977] Spray drift from a tractor powered field sprayer. *Pesticide Science* **8**, 117-126.

Chandrasekhar, S. [1961] *Hydrodynamic and Hydromagnetic Stability.* Clarendon Press, Oxford.

Chung, J.N. and Troutt, T.R. [1988] Simulations of particle dispersion in an axisymmetric jet. *J. Fluid Mech.* **186**, 199-222.

Cionco, R.M. [1972] Intensity of turbulence within canopies with simple and complex roughness elements. *Bound. Layer Meteor.* **2**, 453-465.

Clark, C.J. and Dombrowski, N. [1972] Aerodynamic instability and disintegration of inviscid liquid sheets. *Proc. Roy. Soc. Lond. A.* **329**, 467-478.

Clift, R., Grace, J.R. and Weber, M.E. [1978] *Bubbles, Drops and Particles.* Academic Press, London.

Coelho, S.L.V., and Hunt, J.C.R. [1989] The dynamics of the near-field of strong jets in crossflows. *J. Fluid Mech.* **200**, 95-120.

Cook, N.J. [1978] Wind tunnel simulation of the atmospheric boundary layer by roughness, barrier and mixing device methods. *J. Wind Eng. Ind. Aero.* **3**, 157-176.

Cook, R.J. [1996] The potential impact of buffer zones in agricultural practice. In *Buffer Zones - Their Processes and Potential in Water Protection*, Samara Pub. Ltd., 12-13.

Corrsin, S. [1963] Estimation of the relation between Eulerian and Lagrangian scales in large Reynolds number turbulence. *J. Atmos. Sci.* **20**, 115-119.

Counihan, J. [1969] An improved method of simulating an atmospheric boundary layer in a wind tunnel. *Atmos. Env.*, **3**, 197-214.

Doble, S.J., Matthews, G.A., Rutherford, I. and Southcombe, E. [1985] A system for classifying hydraulic nozzles and other atomisers into catagories of spray quality. *Proc. British Crop Protection Conference*, 1125.

Dombrowski, N. and Johns, W.R. [1963] The aerodynamic instability and disintegration of liquid sheets. *Chem. Eng. Sci.*, **18** 203-214.

Douglas, J.F., Gasiorek, J.M. and Swaffield, J.A. [1993] *Fluid Mechanics.* 3rd ed., Longman, U.K.

Durst, F., Tropea, C. and Xu, T.-H. [1994] The slit effect in phase-Doppler anemometry. Proc 2nd International Conference on Fluid Dynamics Measurement and its Application, Beijing, China.

Elliott, J.G. and Wilson, B.J.(eds.) [1983] The influence of weather on the efficiency and safety of pesticide application. The drift of herbicides. *British Crop Protection Council Occasional Publication No.3.*

Ghosh, S., Phillips, J.C. and Perkins R.J. [1991] Modelling the flow in droplet driven sprays. In Johansson, A.V. and Alfredson, P.H. (eds.) *Advances in Turbulence 3*, 405-414, Springer-Verlag, Berlin.

Ghosh, S. and Hunt, J.C.R. [1994] Induced air velocity within droplet driven sprays. *Proc. Roy. Soc. Lond. A* **444**, 105-127.

Ghosh, S. and Hunt, J.C.R. [1997] Spray jets in a cross flow. Submitted to *J. Fluid Mech.*

Gilbert, A.J. and Bell, G.J. [1988] Evaluation of drift hazards arising from pesticide spray application. *Aspects of Appl. Biol.* **17**, 363-375.

Hinze, J.O. [1955] Fundamentals of the hydrodynamic mechanism of splitting in dispersion processes. *A.I.Ch. E. Jnl.* **1**, 289-295.

Hislop, E.C. [1987] Can we define and achieve optimum pesticide deposits? *Aspects of Appl. Biol.* **14**, 153-172.

Hobson, P.A., Miller, P.C.H., Walklate, P.J., Tuck, C.R. and Western, N.M. [1993] Spray drift from hydraulic spray nozzles: the use of a computer simulation model to examine

factors influencing drift. *J. Agric. Eng. Res.* **54**, 293-305.

Hunt, J.C.R. and Nalpanis, P. [1985] Saltating and suspended particles over flat and sloping surfaces. I. Modelling concepts. Proc. International Workshop on the Physics of Blown Sand, Aarhus, Denmark.

Irwin, H.P.A.H. [1981] The design of spires for wind simulation. *J. Wind Eng. Ind. Aero.* **7**, 361-366.

Jackson, P.S. [1981] On the displacement height in the logarithmic velocity profile. *J. Fluid Mech.* **111**, 15-25.

Lane, W.R. [1951] Shatter of drops in streams of air. *Ind Eng. Chem.* **43**, 1312-1317.

Lawson, T.V. [1980] *Wind Effects on Buildings. Part 1: Design Applications.* Applied Science Publishers, U.K.

Lee, S.Y. and Tankin, R.S. [1984] Study of a liquid spray (water) in a non-condensable environment (air). *Int. Jnl. Heat and Mass Trans.* **27**, 351-361.

Legg, B.J. [1983] Movement of plant pathogens in the crop canopy. *Phil. Trans. Roy. Soc. Lond. B* **302**, 559-574.

Legg, B.J. and Raupach, M.R. [1982] Markov-chain simulation of particle dispersion in inhomogeneous flows: mean drift induced by a gradient in Eulerian velocity variances. *Bound. Layer Met.* **24**, 3-13.

Legg, B.J. and Miller, P.C.H. [1990] Drift assessment using measurements and mathematical models. Paper 901593 presented to *The American Society of Agricultural Engineers* Winter Meeting, Chicago.

Lefebvre, A.H. [1980] Airblast atomization. *Prog. Energy Combust. Sci.* **6**, 233-261.

List, E.J. [1982] Turbulent jets and plumes. *Ann. Rev. Fluid Mech.* **14**, 189-212.

Lloyd, A.R.J. [1967] The generation of shear flow in a wind tunnel. *Q. J. Roy. Met. Soc.* **93**, 79-96.

Luhar, A.K. and Britter, R.E. [1989] A random walk model for dispersion in inhomogeneous turbulence in a convective boundary layer. *Atmos. Env.* **23**, 1911-1924.

Maskell, E.C. [1963] A theory of the blockage effects on bluff bodies and stalled wings in a closed wind tunnel. *A.R.C. R & M,* **3400**, HMSO, London.

May, K.R. and Clifford, R. [1967] The impact of aerosol particles on cylinders, spheres, ribbons and discs. *Annals of Occupational Hygiene* **10**, 83-95.

Miller, P.C.H. [1988] Engineering aspects of spray drift control. *Aspects of Applied Biology*, **17**, 377-384.

Miller, P.C.H. [1993] Spray drift and its measurement. In Matthews, G.A. and Hislop, E.C. (eds.) *Application Technology for Crop Protection*, CAB International.

Miller, P.C.H. and Hadfield, D.J. [1989] A simulation of spray drift from hydraulic nozzles. *J Agric. Eng. Res.* **42**, 135-147.

Miller, P.C.H., Mawer, C.J. and Merritt, C.R. [1989] Wind tunnel studies of the spray drift from two types of agricultural spray nozzle. *Aspects of Appl. Biol.* **21**, 237-238.

Miller, P.C.H., Butler Ellis, M.C. and Tuck C.R. [1996] Entrained air and droplet velocities produced by agricultural flat-fan nozzles. *Atomization and Sprays*, **6**, 693-707.

Miller, P.C.H., Ganzelmeier, H., Smith, R.W. and Herbst, A. [1997] Measurements of the downwind airborne spray characteristics from hydraulic flat-fan nozzles operating in a wind tunnel. Submitted to *Crop Prot.*

Morton, B.R., Taylor, G.I. and Turner, J.S. [1956] Turbulent gravitational convection from maintained and instantaneous sources. *Proc. Roy. Soc. Lond. A.* **234**, 1-23.

Moussa, Z.M., Trischka, J.W. and Eskinazi, S. [1977] The near field in the mixing of a round jet with a cross stream. *J. Fluid Mech.* **80**, 49-80.

Mulhearn, P.J. and Finnigan, J.J. [1978] Turbulent flow over a very rough, random surface. *Bound. Layer Meteor.* **15**, 109-132.

Nation, H.J. [1978] Logistics of spraying with reduced volume of spray and higher vehicle speeds. *Proc. British Crop Protection Conf.-Weeds*, 641-647.

Nieuwstadt, F.T.M., and Van Dop, H. [1982] *Atmospheric Turbulence and Air Pollution Modelling.* D.Reidel, Dordrecht.

Nishi, A. and Miyagi, H. [1995] Computer-controlled wind-tunnel for wind-engineering applications. *J. Wind Eng. Ind. Aero.* **54**, 493-504.

Oke, T.R. [1978] *Boundary Layer Climates.* Methuen, London.

Owen, P.R. and Zienkiewicz, H.K. [1957] The production of shear flow in a wind tunnel. *J. Fluid Mech.* **2**, 521-531.

Pankhurst, R.C. and Holder, D.W. [1952] *Wind Tunnel Technique.* Pitman, London.

Parkin, C.S. and Merritt, C.R. [1988] The measurement and prediction of spray drift. *Aspects of Applied Biology*, **17**, 351-362.

Parkin, C.S., Gilbert, A.J., Southcombe, E.S.E. and Marshall, C.J. [1994] British Crop Protection Council scheme for the classification of pesticide application equipment by hazard. *Crop Protection* **13**, 281-285.

Perkins, R.J. and Hunt, J.C.R. [1986] Particle Transport in Turbulent Shear Flows. *Report to SERC.*

Perkins, R.J., Ghosh, S. and Phillips, J.C. [1991] In Johansson, A.V. and Alfredson, P.H. (eds.) *Advances in Turbulence 3*, 93-100, Springer-Verlag, Berlin.

Plate, E.J. [1971] *Aerodynamic characteristics of atmospheric boundary layers.* U.S. Atomic Energy Commission, AEC critical review series.

Plate, E.J.(ed.) [1982] *Engineering Meteorology.* Elsevier, Amsterdam.

Rajaratnam, N. [1976] *Turbulent Jets.* Elsevier, London.

Raupach, M.R., Thom, A.S. and Edwards, I. [1980] A wind tunnel study of turbulent flow close to regularly arrayed rough surfaces. *Boundary-Layer Meteorology* **18**, 373-379.

Raupach, M.R. and Thom, A.S. [1981] Turbulence in and above plant canopies. *Ann. Rev. Fluid Mech.* **13**, 97-129.

Rutherford, I., Bell, G.J., Freer, J.B.S., Herrington, P.J. and Miller, P.C.H. [1989] An evaluation of chemical application systems. *Proc. British Crop Protection Conf.-Weeds*, 601-613.

Sankal, S.V., Inenaga, A. and Bachalo, W.D. [1992] Trajectory dependent scattering in phase-Doppler anemometry: minimising and eliminating sizing error. Proceedings 6th International Symposium of Application of Laser Technology to Fluid Mechanics, Lisbon, Portugal.

Schlichting, H. [1968] *Boundary-Layer Theory.* 6th ed. McGraw-Hill, New York.

Seniger, I., Mulhearn, P.J., Bradley, E.F. and Finnigan J.J. [1976] Turbulent flow in a model plant canopy. *Bound. Layer Meteor.* **10**, 423-453.

Sharpe, R.B. [1974]. Spray deposit measurement by fluorescence. *Pesticide Science* **5**, 197-209.

Shaw, R.H., Silversides, R.H. and Thurtell, G.W. [1974] Some observations of turbulence and turbulent transport within and above plant canopies. *Bound. Layer Meteor.* **5**, 429-449.

Smith, R.W. and Miller, P.C.H. [1994] Drift predictions in the near nozzle region of a flat fan spray. *J. Agric. Eng. Res.* **59**, 111-120.

Stull, R.B. [1988] *Boundary-Layer Meteorology.* Kluwer, Dordrecht.

Tennekes, H. and Lumley, J.L. [1972] *A First Course in Turbulence.* M.I.T. Press, Cambridge, Massachusetts.

Teunissen, H.W. [1975] Simulation of the planetary boundary layer in a multiple jet wind tunnel. *Atmos. Env.* **9**, 154-174.

Thompson, N. and Ley, A.J. [1983] Estimating spray drift using a random-walk model of evaporating drops. *J. Agric. Engng. Res.* **28**, 419-435.

Townsend, A.A. [1976] *The Structure of Turbulent Shear Flow* (2nd ed.) Cambridge University Press.

Tropea, C., Xu, T.-H., Onofri, F., Grenhan, G., Haugen, P. and Stiegelmeier, M. [1995] Dual mode phase-Doppler anemometer. Proceedings of 4th Conference on Optical Particle Sizing, Nuremburg, Germany.

van Dop, H., Nieuwstadt, F.T.M. and Hunt, J.C.R. [1985] Random walk models for particle displacements in inhomogeneous unsteady turbulent flows. *Phys. Fluids* **28**, 1639-1653.

Walklate, P.J. [1987] A random-walk model for dispersion of heavy particles in turbulent airflow. *Bound. Layer Met.* **39**, 175-190.

Wells, M.R. and Stock, D.E. [1983] The effects of crossing trajectories on the dispersion of particles in turbulent flow. *J. Fluid Mech.* **136**, 31-63.

Western, N.M., Hislop, E.C., Herrington, P.J. and Jones, E.I. [1989] Comparative drift measurements for BCPC reference nozzles and for an Airtec twin fluid nozzle under controlled

conditions. *Proc. British Crop Protection Conf.-Weeds*, 641-648.

Western, N.M. and Hislop, E.C. [1991] Drift of charged and uncharged droplets from an experimental air assisted sprayer. *British Crop Protection Monograph no. 46: Air-assisted Spraying in Crop Protection,* 69-77.

White, F. [1979] *Fluid Mechanics.* McGraw-Hill Kogakusha, Tokyo.

Yarin, A.L. [1993] *Free Liquid Jets and Films: Hydrodynamics and Rheology.* Longman Scientific and Technical.

Young, B.W. [1991] A method for assessing the drift potential of hydraulic nozzle spray clouds and the effect of air assistance. *British Crop Protection Monograph no. 46: Air-assisted Spraying in Crop Protection,* 77-86.

Yule, A.J. [1980] Investigations of eddy coherence in jet flows. In *The Role of Coherent Structures in Modelling Turbulence and Mixing* (ed. J.Jiminez), 188-207, Springer-Verlag, Berlin.